

THE FORMATION AND REACTIVITY OF

SOME TRANSITION METAL NITRIDES

A Thesis presented for the Research Degree of

DOCTOR OF PHILOSOPHY

of the

COUNCIL FOR NATIONAL ACADEMIC AWARDS

London

by

IRSHAD ALI

Department of Chemistry,

Plymouth Polytechnic,

PLYMOUTH, Devon

May, 1970

PLYMOUTH POLYTECHNIC LEARNING RESOURCES CENTRE	
Locn. ACCR. No.	5. 5 1218 <del>IHS 6 (b)</del>
CLASS No.	T 546.711 ALI

Cont'd no. X700427251

## A C K N O W L E D G M E N T S

The author wishes to express his sincere gratitude to Dr. D. R. Glasson for his supervision, guidance and encouragement throughout the course of this work.

He is grateful to Dr. A. B. Meggy, Head of Chemistry Department, Plymouth Polytechnic, for the use of facilities and the supply of materials. His thanks are also due to the Polytechnic Governors for the award of a Research Assistantship.

Further acknowledgement is made to the following: Margaret Sheppard for her technical assistance; lecturers of the Chemistry Department for their help and useful discussions; the Polytechnic Library Staff for their co-operation and to Miss Vivienne Colwill, who typed the manuscript.

1944

1945

1946

1947

1948

1949

1950

1951

## A B S T R A C T

The formation of transition metal nitrides is reviewed critically with special reference to newer production methods and fabrication techniques. Crystal structures and types of bonding are discussed in relation to those of other nitrides and refractory hard metals generally, cf., borides, carbides and silicides.

Information so far available on the sintering of materials is summarised. For nitrides (as with borides and carbides), the sintering is influenced by additives and impurities such as oxides formed by partial hydrolysis and oxidation. Resistance to oxidation is increased by sintering and hot-pressing the refractories. The kinetics and products of oxidation of nitrides so far studied depend mainly on the intrinsic reactivity of the material and available surface at which oxidation can occur.

In the present research, changes in phase composition, surface area, crystallite and aggregate sizes are correlated with oxidation time and temperature conditions for nitrides of some transition metals, viz., Ti, Zr, V, Nb, Ta, Cr and Mo. Kinetics and rates of oxidation are influenced by the crystallite and aggregate sizes of the nitrides, by differences in type of crystal structure and in molecular volume of the oxide products. Sintering of the newly-formed oxide is an additional factor.

The nitrides were milled to increase their surface activity and to examine changes in the microstructure caused by the comminution. The milled nitrides apparently have greater surface heterogeneity and tend initially to give linear rather than parabolic oxidation rates until sufficient oxide of rational crystallite size composition is formed to give stable oxide layers. The sintering of the oxides is controlled by surface diffusion promoting grain-boundary penetration at lower temperatures (above about  $\frac{1}{2}$  m.p. oxide in K) and crystal lattice diffusion at higher temperatures (above the Tammann Temperature, about  $\frac{1}{2}$  m.p. oxide in K). Comparison of the oxidation of nitrided and free metals indicates that oxide sintering is inhibited sometimes by removal of nitrogen but accelerated occasionally by the remaining metal.

# C O N T E N T S

<u>Chapter</u>	<u>Page</u>
<b>I <u>Introductory Survey and Review</u></b>	
1.1 Classification of Nitrides .. .. .	2
1.2 Transition Metal Nitrides .. .. .	9
1.3 Relationship between Bonding and Crystal Structure of Binary Compounds .. .. .	14
1.3.1 Hagg's Rule of Radius Ratio Limit .. .. .	14
1.3.2 Pauling-Rundle Theory .. .. .	15
1.3.3 Application of Band Theory .. .. .	16
1.3.4 Ubbelohde - Samsonov Theory .. .. .	18
1.4 Relationship between Bonding and Crystal Structure of Ternary Compounds .. .. .	21
1.5 Production of Nitrides .. .. .	21
1.5.1 Methods of Production .. .. .	21
1.5.2 Thermodynamics of Nitride Production .. .. .	25
1.6 Kinetics of Metal Nitridation .. .. .	29
1.6.1 Rate of Nitridation .. .. .	29
1.6.2 Factors Affecting the Rate of Reaction .. .. .	30
1.6.3 Ionic Diffusion : Parabolic Relationship .. .. .	35
1.6.4 Linear Growth Rate .. .. .	36
1.6.5 Nature of Nitride Scale .. .. .	37
1.6.6 Kinetic Studies of Nitride Formation with Ammonia. .. .. .	41
1.6.7 Effect of Gas Pressure on Nitridation Kinetics. .. .. .	41
1.7 Reactivity of Nitrides .. .. .	42
1.7.1 Sintering of Nitrides .. .. .	43
1.7.2 Oxidation and Hydrolysis of Nitrides .. .. .	47
1.8 Titanium Nitride .. .. .	49
1.8.1 Formation .. .. .	49
1.8.2 The System Titanium-Nitrogen .. .. .	51
1.9 Zirconium Nitride .. .. .	52
1.9.1 Formation .. .. .	52
1.9.2 The System Zirconium-Nitrogen .. .. .	53
1.10 Vanadium Nitride .. .. .	54
1.10.1 Formation .. .. .	54
1.10.2 The System Vanadium-Nitrogen .. .. .	55
1.11 Niobium Nitride .. .. .	56
1.11.1 Formation .. .. .	56
1.11.2 The System Niobium-Nitrogen .. .. .	57

# C O N T E N T S

<u>Chapter</u>	<u>Page</u>
I	
1.12 Tantalum Nitride .. .. .	57
1.12.1 Formation .. .. .	57
1.12.2 The System Tantalum-Nitrogen .. .. .	59
1.13 Chromium Nitride .. .. .	59
1.13.1 Formation .. .. .	59
1.13.2 The System Chromium-Nitrogen .. .. .	60
1.14 Molybdenum Nitride .. .. .	61
1.14.1 Formation .. .. .	61
1.14.2 The System Molybdenum-Nitrogen .. .. .	62
II <u>Experimental Techniques</u>	
2.1 X-Ray Diffraction .. .. .	64
2.1.1 Theory of X-ray Diffraction .. .. .	64
2.1.2 X-ray Generators .. .. .	64
2.1.3 Debye-Scherrer Powder Diffraction Camera .. .. .	67
2.1.4 The Counter Diffractometer .. .. .	68
2.1.5 X-ray Line Broadening .. .. .	71
2.1.5(a) Broadening due to Small Crystallite size. .. .. .	71
2.1.5(b) Broadening due to Lattice Distortion .. .. .	72
2.1.6 Measurement of Intrinsic Broadening .. .. .	72
2.1.7 The Interpretation of Intrinsic Broadening .. .. .	74
2.2 Electron Microscopy and Diffraction .. .. .	75
2.2.1 Theory of Electron Microscopy and Diffraction .. .. .	75
2.2.2 The Equipment .. .. .	79
2.2.3 Preparation of Samples .. .. .	80
2.2.4 The Replica Technique and Shadow casting .. .. .	82
2.3 Optical Microscopy .. .. .	83
2.4 Surface Area Measurement by Gas Sorption .. .. .	83
2.4.1 B.E.T. Procedure .. .. .	84
2.4.2 The Apparatus .. .. .	87
2.4.3 Measurement of Sorption Isotherms .. .. .	87
2.5 Thermoanalytical Techniques : .. .. .	89
2.5.1 Thermal Balance .. .. .	89
2.5.2 High Temperature Vacuum Furnace .. .. .	91
2.5.3 Analysis of Materials .. .. .	93
2.6 Ball-Milling .. .. .	95
2.7 Computation .. .. .	96

# C O N T E N T S

<u>Chapter</u>	<u>Page</u>
<u>III. Titanium and Zirconium Nitrides</u>	
3.1 Titanium Nitride .. .. .	97
3.1.1 Nitridation of Titanium .. .. .	97
3.1.1(a) Compactness of Titanium Nitride Films	115
3.1.2 Milling of Titanium Nitride .. .. .	117
3.1.3 Oxidation of Titanium Nitride .. .. .	121
3.1.3(a) Comparison with oxidation of Titanium metal. .. .. .	122
3.1.3(b) Comparison with oxidation of Titanium Boride and Carbide. .. .. .	128
3.2 Zirconium Nitride .. .. .	130
3.2.1 Nitridation of Zirconium .. .. .	130
3.2.2 Milling of Zirconium Nitride .. .. .	131
3.2.3 Oxidation of Zirconium Nitride .. .. .	136
<u>IV. Vanadium, Niobium and Tantalum Nitrides</u>	
4.1 Vanadium Nitride .. .. .	145
4.1.1 Nitridation of Vanadium .. .. .	145
4.1.2 Milling of Vanadium Nitride .. .. .	145
4.1.3 Oxidation of Vanadium Nitride .. .. .	151
4.2 Niobium Nitride .. .. .	156
4.2.1 Nitridation of Niobium .. .. .	156
4.2.2 Milling of Niobium Nitride .. .. .	157
4.2.3 Oxidation of Niobium Nitride .. .. .	161
4.2.3(a) Comparison with oxidation of Niobium metal. .. .. .	168
4.3 Tantalum Nitride .. .. .	170
4.3.1. Nitridation of Tantalum .. .. .	170
4.3.2 Milling of Tantalum Nitride .. .. .	171
4.3.3 Oxidation of Tantalum Nitride .. .. .	176
4.3.3(a) Comparison with oxidation of Tantalum Metal. .. .. .	181
4.3.3(b) Oxidation of Tantalum and its Nitride at higher temperatures .. .. .	183
<u>V. Chromium and Molybdenum Nitrides</u>	
5.1 Chromium Nitride .. .. .	185
5.1.1 Nitridation of Chromium .. .. .	185
5.1.2 Milling of Chromium Nitride .. .. .	187
5.1.3 Oxidation of Chromium Nitride .. .. .	192
5.1.3(a) Comparison with Oxidation of Chromium Metal. .. .. .	194



# C O N T E N T S

<u>Chapter</u>	<u>Page</u>
V. 5.2 Molybdenum Nitride .. .. .	209
5.2.1 Nitridation of Molybdenum .. .. .	209
5.2.2 Milling of Molybdenum Nitride .. .. .	210
5.2.3 Oxidation of Molybdenum Nitride .. .. .	217
5.2.3(a) Comparison with Oxidation of Molybdenum Metal. .. .. .	222
VI. <u>Concluding Summary</u> .. .. .	226
REFERENCES .. .. .	230-245
APPENDICES .. .. .	246-251

Chapter I  
INTRODUCTORY SURVEY AND REVIEW

Nitrides are the nitrogen compounds formed generally at elevated temperatures when nitrogen reacts with other elements especially the more electropositive elements.

Transition elements such as those of sub groups IVA, VA, and VIA of the Periodic Table, form nitrides which have high melting points and great hardness approaching that of diamond (Whittemore, 1968). Hence they are termed refractory materials. They also possess most of the properties of metals and alloys. Thus, they exhibit thermal and electrical conductivities of the same order of magnitude as pure metals. These also show metallic lustre. The term 'hard metals' is often applied to these compounds together with the borides, carbides and silicides of the metals (Schwarzkopf, 1950; Schwarzkopf & Kieffer, 1953, pp 3-5; Hagg 1953).

The above mentioned properties of the transition metal nitrides cause them to be of considerable technological importance. Nitrides of metals belonging to the IV A and V A subgroups of the Periodic Table have been important in high melting point cermets (Schwarzkopf & Kieffer, 1953). High melting points in combination with good non-scaling properties make these materials useful for rocket technology and jet propulsion. The reaction chambers of jet engines are lined with these refractory materials. The demands on these materials in respect of thermal shock resistance are particularly severe, owing to the high rates of temperature change, which can hardly be reproduced in testing (Kingery, 1955 ; Buessem, 1955). The blades of gas turbines are also covered with coatings of these materials. The refractory nitrides exhibit their greatest refractoriness in nitrogen atmospheres (Bradshaw, et.al., 1958). High electrical

conductivity and low reactivity towards normally corrosive chemicals permits their application in fused salt electrolysis.

Nitriding is extensively used for hardening steel surfaces. During the process, atomic nitrogen is adsorbed from either a gaseous or liquid (salt) carrier and subsequently into the base metal. The case is quite hard and acquires excellent wear resistance and galling properties. Presently, devices like gears, pinions, shafts, clutches, piston rings etc., are hardened by this technique. (Leeming; 1964),

In the past, studies have been mainly confined to the direct oxidation of metals, and oxides have been applied extensively as refractory materials. The formation and reactivity of oxides has therefore been studied in depth (e.g. Glasson, 1956, 1958 a-b, 1960 a-b, 1963 a-b, 1967; Glasson & Sheppard, 1968). Similar studies on transition metal Nitrides have been less extensive. Recently some nitrides of elements in groups II, III, & IV of the Periodic Table have been investigated (Jayaweera, 1969). In this thesis, selected nitrides of metals belonging to sub-groups IV A, V A and VI A of the Periodic Table have been studied with respect to their production, sintering and oxidation. Since nitridation of metals followed by oxidation constitutes indirect corrosion, comparisons have been made with the oxidation behaviour of the corresponding metals.

### 1.1 Classification of Nitrides.

Nitrides are categorised generally as ionic, covalent and interstitial (or metallic) depending on the nature of their bonding (Brown, 1964, P.150; Moore, 1948). The atomic number of nitrogen is 7 and its electronic configuration in the ground state is, therefore  $1s^2, 2s^2, 2p^3$ ; the three 2p electrons occupy different space orbitals in accordance with Hund's Rule of Maximum Multiplicity.

There are three possible ways in which nitrogen may acquire electronic stability, (a) as in ionic compounds, it may form the nitride ion,  $N^{3-}$ ; (b) It may form covalent compounds by the overlapping of its singly occupied orbitals with similar orbitals of other atoms, and (c) in the interstitial nitrides, the small nitrogen atoms (radius  $0.92\text{\AA}$ ) occupy some or all of the octahedral interstices in the metallic lattices, which are generally close-packed.

There seems to be no need for a rigorous classification, in view of the fact that their bonding is heterodesmic i.e. a combination of metallic as well as ionic and covalent forces, of which one type may predominate depending on the crystal structure. However, convenient classification depending on their properties can be made as follows (Jayaweera, 1969).

Readily hydrolysable nitrides forming ammonia are considered ionic. These are typified by lithium in group I ( $Li_3N$ ) and the alkaline-earth metals in group II ( $M_3N_2$ ). The formation of nitrides by the other alkali metals in group I is restricted by crystal structure conditions. Whether elements are capable of forming stable nitrides is indicated by comparing heats of formation (Kcal. per equiv.) of corresponding oxides and fluorides (Van Arkel, 1956), which are more stable than the nitrides, their standard free energies varying similarly with temperatures (Glasson & Jayaweera 1968). Since the radii of  $F^-$ ,  $O^{2-}$  and  $N^{3-}$  are similar, variations in heats of formation will depend mainly on the charge of the negative ion. The electron affinities,  $E$ , and crystal energies,  $U$ , will be affected.  $E$  is expected to predominate in compounds with large positive ions of low charge, so that the heat of formation decreases with increasing negative ion charge; e.g.  $LiF$ ,  $Li_2O$  and  $Li_3N$  have

heats of formation of 146, 71 and 15 kcal. per equiv. respectively. The sharper decrease from NaF (Juza et. al., 1959) to Na<sub>2</sub>O (Samsonov, 1965) suggests a very low value for Na<sub>3</sub>N, which is evidently unstable at room temperature and has so far not been prepared in the pure condition. The Madelung constant is significant in that it is unfavourable for Li<sub>3</sub>N and high for the fluoride. Thus, the decrease in heat of formation from fluoride to nitride is much greater than in the group III series AlF<sub>3</sub> (Stadelmaier & Tong, 1961), Al<sub>2</sub>O<sub>3</sub> (Mott, 1958) and AlN (Guilland & Wyart, 1947), where the nitride has the higher Madelung constant, compared with that of Li<sub>3</sub>N. Comparison of the molecular susceptibilities of Mg, Zn and Cd nitrides shows that the polarising action of the metal ion decreases from Mg to Zn to Cd (Croato, et.al. 1951).

Elements with high ionic charge and small ionic radius tend to form covalent nitrides e.g. B, Al, Ga in group III and Si, Sn, in group IV of the Periodic Table.

Interstitial nitrides are formed mainly by transition metals. These are generally nitrogen deficient, nonstoichiometric compounds, which retain most of the properties of the parent metal. Although non-metal vacancies occur in large numbers in these nitrides, there is evidence for metal vacancies in TiN (A. Brager, 1939 Straumuis; et.al. 1967) and NbN (G. Brauer, 1964). Most of these compounds crystallize in either cubic close-packed or hexagonally close-packed structure, or in a slight modification of one of these. There are variations in the number of nitrogen-occupied sites and their type (octahedral or tetrahedral). Hence these compounds have certain homogeneity ranges. UN is an extreme example, having the stoichiometric composition. This may be ascribed to the large radius (1.42Å) of the uranium atom, giving rise to large interstitial

sites, thereby facilitating their occupation by nitrogen atoms. The composition of interstitial nitrides with a narrow range of homogeneity is not determined by the metal valency, in contrast to some transition metal oxides, also having narrow homogeneity ranges.

### 1.2 Transition Metal Nitrides

These materials form one of three fundamental classes of refractory compounds;

- (1) Compounds of metals with non-metals, such as borides, carbides, nitrides, oxides, silicides, phosphides and sulphides;
- (2) Compounds of non-metals with each other, such as carbides, nitrides, sulphides and phosphides of boron and silicon, and also alloys of B and Si;
- (3) Compounds of metals with each other, generally known as intermetallic compounds.

The nature of the chemical bond between the components of these compounds is predominantly metallic or covalent with a small proportion of ionic bond. These types of bond are established mainly by transition metals with non-metals having ionisation potentials sufficiently low to avoid exclusive ionic bond formation. These bonds are also formed between two non-metals and certain metals with each other. The metallic components of refractory compounds include elements of the subgroups III A to VII A, group VIII, lanthanides, actinides and aluminium. The non-metallic components include light non-metals of the short periods (B, C, N, O, Si, P, S). The chemical bond in the lattices of these compounds (in addition to the s- and p- electrons of the metallic and non-metallic components respectively) is formed also by the electrons of the deeper incomplete d- and f- levels of the transition metals. Isolated

atoms of metals of group II, the alkaline-earth metals, do not have any electrons in the  $d$ - and  $f$ - shells. But in compounds with non-metals, energy states corresponding to these shells may occur (Shaffer & Samsonov, 1964; Samsonov, 1964; Samsonov, 1965).

Nitrides have correspondingly greater proportions of ionic bond, because of the higher ionisation potential of nitrogen compared with the other non-metal refractory components. This is more evident in nitrides of metals having a low acceptor capacity (Mo, W, Re), while the nitrides of Nb, Ta and Cr show a combination of metallic and ionic bond, with the latter predominating. Decreasing the nitrogen content of the nitride phases, within their homogeneity ranges strengthens the metal to metal bonds and weakens the bonds of metal to nitrogen. Fairly wide gaps in the lattice energy states become possible and determine the semi-conductor properties of nitrides having N- deficient lattices.

The proportion of ionic bond in metal oxides having high acceptor characteristics (Ti, Zr, Hf, V) is rather less than in the corresponding nitrides, because oxygen has a lower ionisation potential than nitrogen. These differences will be more pronounced for the lower oxides.

The second class of refractory compounds includes boron and silicon nitrides (Thompson & Wood, 1963; Popper & Ruddlesden, 1957; Hardie & Jack, 1957; Gill & Spence, 1962). Their bond character is also heterodesmic, but with covalent bond predominating. They have semi-conductor properties as well as high electrical resistance at room temperature. Generally, their structure consists of layer chain or skeletal structural groups or patterns, and they either melt with decomposition or decompose before reaching the melting point .

Three typical elements of groups II and III, namely Be, Mg and Al are intermediate in their ability to form refractory metal-like and

non-metallic compounds. Fairly refractory semi-conductors are given with non-metals (Shaffer & Samsonov, 1964). Thus borides of Be, Mg and Al and also AlN. These three metals also can form intermetallic compounds.

### 1.3 Relationship Between Bonding and Crystal Structure of Binary Compounds

An account of some of the attempts to explain the bonding and crystal structure characteristics of refractory compounds is included in the following subsections. The nitrides of metals of the first transition series are reviewed by Juza (1966).

#### 1.3.1 Hagg's Rule of Radius Ratio Limit

According to Hagg (1930, 1931 a-b, 1953), binary interstitial compounds of the transition elements had simple or "normal" structures when the radius ratio,  $r_x : r_m$  of the non-metal and metal atoms was less than 0.59:1 with the non-metal atoms occupying the interstices of the original metal lattice. When the radius ratio exceeds this figure, the structures become more complicated, but still retain metallic characteristics. Higher non-metallic concentrations increase the unit cell dimensions of the interstitial phases, effectively making the radius ratio less favourable for normal structures. It has been indicated that the limiting radius ratio rule is valid only for carbides, the nitrides generally having lower radius ratios (Schwarzkopf & Kieffer, 1953).

Usually, the metal atoms in the interstitial compounds are arranged differently from the original metal lattices. The non-metal atoms occupy those interstices where they can remain in contact with the metal atoms. The face-centred cubic, close-packed hexagonal and body-centred cubic lattices have two types of interstices, tetrahedral and octahedral with co-ordination numbers of 4 and 6 respectively.



The octahedral hole is perfectly regular in the two close-packed structures (face-centred cubic and close-packed hexagonal) but has tetragonal symmetry in the body-centred cubic structure. The only interstices of the simple hexagonal unit cell are the large octahedral (6-fold co-ordinated) sites at the centres of trigonal prisms of metal atoms.

In the interstitial structures, not all of the holes of one type are necessarily occupied, so that many homogeneous phases show wide composition ranges. Nevertheless, homogeneity ranges of phases often approximate to some simple stoichiometric composition corresponding to the occupation of a definite fraction of the number of available interstices. In the cubic close-packed lattice, the large octahedral sites are occupied only if the radius ratio exceeds 0.41:1. Many mononitrides and monocarbides (MX-type) have radius ratios within the range 0.41 - 0.59:1, and have rock-salt structures irrespective of whether the parent metal has a cubic close-packed structure or not (Rundle, 1948).

### 1.3.2. Pauling-Rundle Theory

Rundle (1948) suggested that the metal to non-metal bonding is octahedral, with six equal bonds being directed from the non-metal towards the corners of an octahedron. He applied Pauling's basic concept of resonance of four covalent N- or C- bonds amongst the six positions (Pauling, 1938, 1940, 1947, 1948, 1949; Pauling and Ewing, 1948). The concept of half bonds is introduced, where an electron pair in an atomic orbital is used to form two bonds.

In Rundle's theory the non-metal atom can achieve an octahedral arrangement in two ways: (i) two equivalent sp hybrid orbitals form electron pair bonds and hybridize with four half-bonds given by the two remaining p orbitals.

(ii) the three 2p orbitals form six half-bonds, and an electron pair occupies the 2s orbital. In each case, the resulting six bonds have an octahedral arrangement, which exemplifies the rock-salt structure of the compounds. The directional nature of the bonds explains the brittleness and hardness of these materials.

Rundle also points out that there is a marked increase in metal-metal distances, when refractory interstitial compounds are formed. This observed increase indicates a weakening of the metal-metal bonds. Therefore, electrons are drawn away from the metal-metal bonds and utilized for the formation of metal to non-metal bonds. The high melting points of these interstitial phases, therefore, can be ascribed to the high strengths of the metal-nonmetal bonds.

A critical appraisal of the Pauling's theory of metals has been made by Hume-Rothery (1949). He has also criticised Rundle's theory. Hume-Rothery (1953) has argued that the occupation of the octahedral sites by the non-metal would be equally valid in a hexagonally closed-packed lattice. The face-centred cubic structure, however, has been adopted because in this structure, the metal too has mutually perpendicular covalent bonds directed to its six neighbouring non-metal atoms, a situation not present in the hexagonal structure. (In the latter, the octahedral sites around a metal atom form a triangular prism).

### 1.3.3 Application of Band Theory

The band theory of metals has been applied by Bilz (1958) and Denker (1968) to elucidate the electronic states for refractory materials. Thus, metallic character is expected to develop with increased electron occupation of the d-band in the series SiN, TiN, VN. This is supported by nuclear magnetic resonance measurements on ScN and VN (Kume & Yamagishi, 1964). However, the expected increase in metallic character is not supplemented by the trend in electrical conductivities (Nemchenko et.al. 1962).

Goodenough (1963, pp. 266-267) has termed nitrides with a rock-salt structure as "ionic compounds with metallic conductivity", and in particular related to the oxides. The bond is partly ionic because of the electro-negativity difference between the metal and nitrogen, and also partly covalent. According to Goodenough (1960), in the metallic bond in transition metals and their compounds, the electron distribution between localised and more delocalised bonding states is determined by a critical interatomic distance of  $2.9\overset{\circ}{\text{A}}$ . Above this separation the electrons are localised, but below it they are present as "collective" electrons. Electrical conductivity is associated with partial filling of the  $t_{2g}$  bands by collective electrons, and is limited to compounds where the metal-metal distances are less than  $2.9\overset{\circ}{\text{A}}$ . Nitrides possessing rock-salt structure are formed only if three or less  $d$ -electrons are available in the formally trivalent cation, when the  $e_g$  - orbitals are empty and the  $t_{2g}$  - orbitals are either half or less than half filled. Great electronegativity differences produce a large forbidden zone, with the bonding electrons belonging mainly to the nitrogen sub-lattice. Thus, in case of ScN, the bonding  $s$ - and  $p$ -  $e_g$  - electrons are predominantly on the nitrogen. Decreasing electronegativity differences confer a stronger  $e_g$  character on the bonding electrons. Increasing covalent bond character may lead to cation-anion-cation interaction, e.g. CrN. Special bonding relationships intermediate between the two extremes exist for  $\text{CrN}$  (rock-salt lattice). Transition from cubic to orthorhombic symmetry is associated with localisation of the covalent bond and accords with changes in magnetic properties (Goodenough, 1960, p.1442). Nitrides of the Perovskite type,  $M_4N$  ( $M = \text{Fe}$  or  $\text{Mn}$ ) are classified by Goodenough (1963) as interstitial alloys, where the metal-nonmetal bond is predominant i.e. N is

probably present as a neutral atom. This agrees with Kuriyama's determination of the N atomic scattering factor in  $Mn_4N$ , showing nitrogen to be present as  $N^0$  or  $N^{1-}$  (Kuriyama, et.al. 1963). These results conflict with Elliott's (1963) determinations for  $Fe_4N$ , which indicate  $N^{3-}$  as the probable species. Mekata (1962) based his qualitative band scheme for  $\underline{E} - Mn_4N$  on neutron diffraction study. It is a modification of Goodenough's scheme for cubic face-centred manganese, differing in the energetic arrangement of the  $e_g$ - and  $t_{2g}$ - bands relative to one another.

#### 1.3.4 Ubbelohde-Samsonov Theory

Ubbelohde (1932, 1937) presented evidence for the interstitial dissolution of hydrogen in palladium, tantalum and titanium. He assumes that hydrogen dissolves in the form of atoms which are subsequently ionized, and the electrons of dissolved hydrogen go into the vacant levels of the  $d$ - band of the transition metal. Thus, the metal is the acceptor and hydrogen the donor. Umanskii (1943) extended this to carbides and nitrides. This is expected, because the ionization potentials of carbon and nitrogen are of the same order as that of hydrogen. Further support for this theory is provided by Seith & Kubaschewski (1935) and Prosvirin (1937) who demonstrated the ionic character of dissolved carbon and nitrogen in iron. Kiessling (1950) makes a similar conclusion from a study of borides. He has suggested that the ability of the non-metal to donate electrons increases in the order, O, N, C, B, Si (Kiessling, 1954, 1959). The importance of bond lengths has also been emphasized by Kiessling (1957). One of the prime requirements for metallic bond formation is that the metal atoms should not be too far apart.

This explains why small non-metal atoms only may form interstitial compounds with transition metals.

Further development by Samsonov (1953a, 1956 a-c, 1964 b, 1965), implied that the bonding between the transition metal and the non-metal in refractory compounds is essentially metallic in character. Similar theory has been described by Neshpor (1964) and Samsonov & Neshpor (1958, 1959). This involves transfer of non-metal valency electrons into the electron cloud of the compound, at least partially filling the electron-defect of the metal atoms. The additional forces of the donor-acceptor interaction greatly strengthen the interatomic bond. Thus, Jack (1948) and Clarke & Jack (1951) interpret the structure of iron, cobalt and nickel nitrides, carbides and carbonitrides on the basis of electron transfer from the interstitial C and N atom to the metal lattice.

The degree of participation in the bond (of incomplete d- and f- electron levels) and the distribution of electron concentration in the crystal lattice is expressed by the quantity  $1/N_n$ , termed by Samsonov as "acceptor ability". In this expression, N is the principal quantum number of the incomplete shell of d- or f- electrons and n is the number of such electrons. A high acceptor ability favours a high electron concentration in the crystal lattice, i.e. greater metallic character. Decreasing acceptor ability causes corresponding decreases in electrical conductivity (Schaffer & Samsonov, 1964), heat of formation, lattice energy and hardness (Sarkisov, 1947; Sarkisov, 1954; Baughan, 1959; Shulishova, 1962).

The essentially metallic character of the interatomic bond is comparable with the Hume-Rothery electron phases, the nature of the crystal structure depending on the electron concentration (Kiessling,

1954, 1958; Robins, 1958). Increasing concentration produces a sequence of crystal lattices, viz., body-centred cubic, base-centred hexagonal, face-centred cubic, simple hexagonal, for similar atomic radii ratios,  $x : m$ , where  $X = B, Si, C, N$ . The face-centred cubic lattice, most characteristic of group IVA and VA metal carbides and nitrides corresponds to an electron concentration of 5.5 to 6 electrons per atom. Nevertheless, formation of crystal structures characteristic for metal compounds does not necessarily arise from the transitional nature of their atomic components. Thus, nitrides of rare-earth metals are mainly ionic (Jandell, 1956; Klemm & Winkelmann, 1956), yet crystallise in face-centred cubic (rock-salt) lattice, similar to monoborides and monocarbides of group IV and V transition metals having metallic properties.

Weiner and Berger (1955) demonstrated that the occupation of incomplete  $d$ -shells of the metal atoms by electrons donated from the non-metal atoms reduced the magnetic moment. Results for Fe, Co and Ni nitrides suggested donation of about three electrons by each nitrogen atom. The nitrogen was regarded as a positive ion or as forming a covalent bond by interaction of the  $p$ - electrons of N with the unpaired  $d$ - electrons of the nearest neighbour atom.

There have been only limited studies of the energy spectrum of electrons in metallic compounds. These include an approximate quantum mechanical analysis of the electron structure of the interstitial phases TiC and TiN (Bilz, 1958) and investigations of the X-ray spectra of Ti, V, Nb, and Cr nitrides (Vanysh'teyn & Vag'li'yev, 1957; Vanysh'teyn & Zhurakovskiy, 1958, 1959; Nemnonov & Men'shikov, 1959; Korsunskiy & Genkin, 1958; Karal'nik et al., 1959). The latter are interpreted by the

splitting of the  $3d$ - level into  $t_{2g}$ - and  $e_g$ - levels by the crystal field in the octahedral environment.

#### 1.4 Relationship between Bonding & Crystal Structure of Ternary Compounds

The ternary compounds so far examined have been classified by Juza (1966) and their properties are summarised by Glasson & Jayaweera (1968, pp. 70-71) in relation to what is known of their crystal structures.

#### 1.5 Production of Nitrides

##### 1.5.1 Methods of Production

There are a number of diverse methods available for preparing metallic nitrides. This is due mainly to great differences in thermal stability, associated in turn with heats of formation. Nitrides can be prepared by heating the elements in a nitrogen, ammonia or nitrogen and hydrogen atmosphere (Mellor, 1927, p.97; Soliman, 1951; Juza, 1966; Brown, 1964). Variations of these methods include heating the metal amalgams, e.g., Ca, Ba, Mn and Fe, or the metal oxide and aluminium or magnesium, e.g. Ce, La, Nd, Pr and U, or the metal oxides and carbon, e.g. Mg, and Si. Sometimes, however, heating metal carbides in nitrogen produces carbonitrides such as cyanides and cyanamides, e.g. in the case of Ti, Hf (Portnoi & Levinskii, 1963), Ca, Sr, Ba (Cochet, 1931). An advantage of using ammonia (or nitrogen and hydrogen mixtures) over nitrogen is that the reaction is carried out in a reducing atmosphere and thus the formation of oxide impurities is kept to the minimum. Oxygen must be scrupulously avoided since it cannot be eliminated from the nitride phase (Farr, 1968). Nitrides may be obtained also by decomposing suitable

metal amides, e.g. Co (Schmitz-Dumont, 1956) and Ni (Watt & Davies, 1948). The reaction between a metal oxide and ammonia to form the nitride is the reversal of the hydrolysis of the nitride. Thus, mercury nitride (Glasson, 1949) and gallium nitride (Lorenz & Binkowski, 1962) are formed in this manner.

Transition metal nitrides are produced generally by the action of nitrogen or ammonia on the respective metals or their hydrides, oxides or halides. A classical method for preparing transition metal nitrides is the reaction of metallic oxides, e.g.  $TiO_2$ , with nitrogen in presence of Carbon. This process was used by Friederich and Sittig (1925) but did not lead to pure products. Very pure carbide-free nitrides are best obtained by heating the metal powders under very pure nitrogen or ammonia. Nitridation of metals by nitrogen or ammonia gas has become more important with the increased availability of high purity metals. Besides conventional heating techniques, high frequency induction heating has been employed in transition metal nitride production. In the ionitriding process an electric glow discharge is utilised in splitting up molecular nitrogen (Beisswenger, 1958; Bernhard Berghaus, 1961; Laplauche, 1963; Sterling and Swann, 1965; Sterling et.al., 1966).

The decomposition of metal amides or imides, may be used as means of obtaining nitrides. Other preparative methods include heating an ammonium metallate in ammonia, the action of cyanogen gas or dinitrogen trioxide on the metal, the reaction between a metal salt in liquid ammonia and a reducing metal, and by double decomposition with another nitride.

Molten salt bath nitriding is used widely industrially to obtain



thin protective nitride coatings. The bath usually contains a cyanide or cyanate of an alkali metal reacting with a transition metal or one of its alloys, e.g., Fe and its alloys. Vapour phase deposition is one of the widely used methods of industrial nitridation (Campbell et.al., 1949, 1952; Powell et.al., 1966). This process involves the use of a volatile metal salt such as the chloride with ammonia or nitrogen and hydrogen. A thin and uniform coating of nitride on machine parts is produced by this method, which is especially employed with transition metal nitrides. An exploding wire technique also has been described (Joncich et.al., 1966).

The more stable nitrides e.g., Ti, Zr, Hf, V and Ta, may be deposited directly on heated surfaces from gaseous mixtures of suitable volatile metal halides and nitrogen and hydrogen (Van Arkel & de Boer, 1925; Agte & Moers, 1931; Becker, 1933; Van Arkel, 1934; Pollard & Woodward, 1948; Münster & Ruppert, 1953; Münster, 1957). This method is preferred, particularly when metal surface nitridation slows down considerably after formation of a thin skin of nitride. Several hours are required for coatings of more than one or two mm thickness, unless much higher temperatures are used to ensure adequate diffusion across the nitride layer. Small TiN crystallites have been obtained in the cooled anode cavities, when  $TiCl_4$  is introduced into the nitrogen-argon stream of a plasma burner (Stokes & Knipe, 1960; Opfermann, 1964). Hydrogen is not required, since the elements are ionised in the plasma beam.

A summary of transition metal nitride production methods is given in Table 1.1, which also includes a selection of references to methods of producing these compounds:-

Table 1.1 Methods of Transition Metal Nitride Production

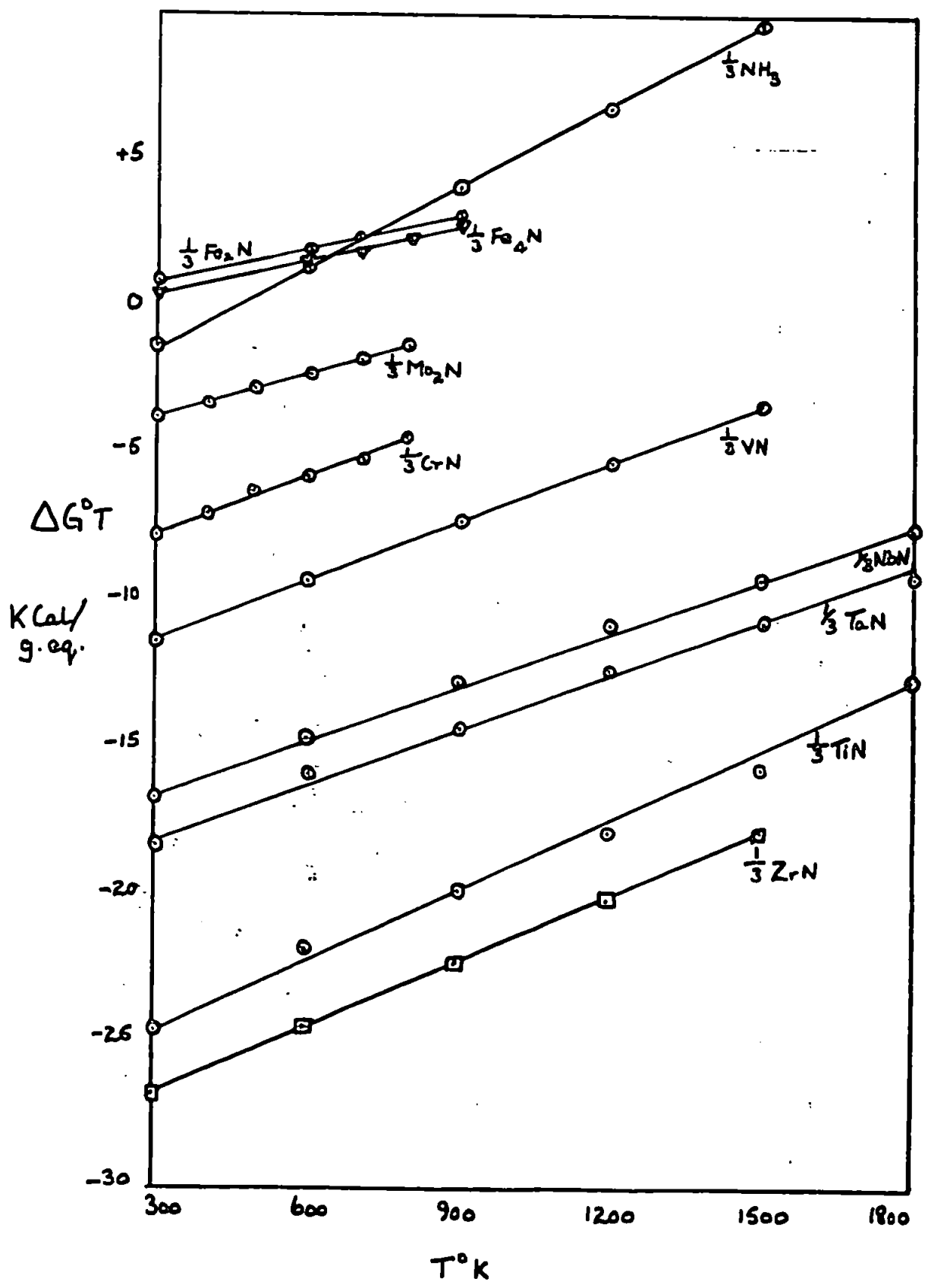
METHOD	METALS NITRIDED	REFERENCES
1) Action of Nitrogen (or Air) on:-		
(a) Metal	Ti, Zr, Y, U,  Cr, Mn, rare  earth metals, Ta, V, Fe, Th, Co, Sc Zr	(Samsonov et.al., 1959 b, 1961a) Kirchevskii & Khazanova (1950); Lyntaya & Samsonov (1964); Campbell et.al., (1949); Evans (1965)
(b) Oxide		
(c) Oxide & Al or Mg	Ce, La, Nb, U, Zr	
(d) Oxide & Carbon	Si, Ti, V, Sc	Lyntaya & Samsonov (1964)
(e) Hydride	Ti, Si, V, U, Pu	Kempton et. al., (1957); Anselin & Pascard (1963)
(f) Boride	Cr, Fe	Samsonov (1964 a, pp. 312-19)
2) Action of Ammonia or nitrogen & hydrogen mixture on:-		
(a) metal	Ti, Ni, Ce, La, Ga Si, Nb, Mn, Fe, Mo, W U, Cr, Co.	Neugebauer et.al., (1959) Moreau & Phillipot (1963); Septier et.al., (1952); Deeley (1964)
(b) oxide	Ti, In, W, Cu, Nb Ga	Neugebauer et.al., (1959) Lyntaya & Samsonov (1964); Lorentz & Binkowski (1962);
(c) boride	Cr, Fe, W.	Kiessling & Liu (1951)
(d) hydride	Si	Sterling & Swann (1965); Sterling et.al. (1966)
(e) Metal salt & reducing metal with liquid ammonia	Ga, In, Tl, Fe, Co, Ni, Ru, Rh, Pd Os, Ir, Pt	Schneider et.al. (1963)
(f) Ammonium metallate	Nb, Ta, U, Cr, Fe, Re, W.	Samsonov et.al. (1961a); Funk & Boehland (1964); Hahn & Konrad (1951); Neugebauer et.al. (1951)
3) Action of cyanides & cyanates on metal (or alloy)	Fe and its alloys:	Mitchell & Dawes (1964); Minkevich (1964); Albrecht & Mueller (1963);

### 1.5.2 Thermodynamics of Nitride Production

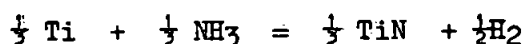
Although the extensive thermodynamic properties such as enthalpy and free energy of elements and their compounds cannot be measured absolutely, it is possible to estimate relative changes in these properties when a chemical reaction takes place. The standard free energy change  $\Delta G^{\circ}$ , for a particular reaction affords a direct quantitative measure of the extent to which the reaction may proceed.

The stability of the nitrides and their production at various temperatures are related to their standard free energies of formation,  $\Delta G^{\circ}_T$  (Margrave & Sthapitanonda, 1955). If data is compiled for the reactions of some of the transition elements with nitrogen, the relative affinities of these elements can be ascertained by plotting the standard free energy change per gram equivalent of the element as a function of temperature (in oK). This graphical method of presentation, the Ellingham diagram (1944), readily indicates the feasibility of a reaction over a particular temperature range and also the compatibility of materials at high temperatures. The more negative values of standard free energies indicate stabler compounds. In Fig.1.1, the values of  $\Delta G^{\circ}_T$  are compared for a selection of transition metal nitrides on an Ellingham diagram, using data compiled by Wicks & Block (1963); see also Pearson & Ende (1953) and Olette & Ancy-Moret (1963). Nitrides of transition metals belonging to group IV and V have the greatest stability. This progressively decreases for nitrides in the lower groups and for transition metals in groups VI to VIII. The iron nitrides,  $Fe_2N$  and  $Fe_4N$  are relatively unstable, having positive  $\Delta G^{\circ}_T$  values for a fairly wide temperature range. By comparison, ammonia is less stable than most nitrides.

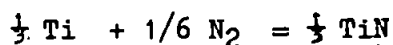
Figure 1.1. Free Energy of Formation of Nitrides



From Figure 1.1 the standard free energy changes for the reaction of metal with ammonia ( to form the nitride and hydrogen ) can also be compared for different metals. Thus for titanium nitride, the value of  $G_T^0$  for the reaction,



is the difference between the values for the reactions:-



Hence the difference between the graphs for  $\frac{1}{2} \text{TiN}$  and  $\frac{1}{2} \text{NH}_3$  in Figure 1.1 indicates the relative ease of nitride formation from the metal + ammonia, when the materials are in their standard states. From the thermochemical data, it is evident that all the metal nitrides can be formed from the metal and ammonia, except  $\text{Fe}_2\text{N}$  and  $\text{Fe}_4\text{N}$ , at lower temperatures. However, although energetically possible, these reactions may be kinetically unfavourable, as thermodynamics does not give any information regarding the rate of the processes under consideration. This applies especially to solid state reactions, where the number of variable factors is high, e.g., solubility of the gases in the various solid phases, formation of binary and ternary compounds, adherence of compound layer on to the metal. The last of these factors is important in the kinetics of the reaction as discussed later in section 1.6.2.

A plot of free energy data for the oxidation of some transition metal nitrides is presented in Figure 1.2, which shows that the oxidation products are appreciably stabler than the corresponding nitrides, especially at low temperatures.

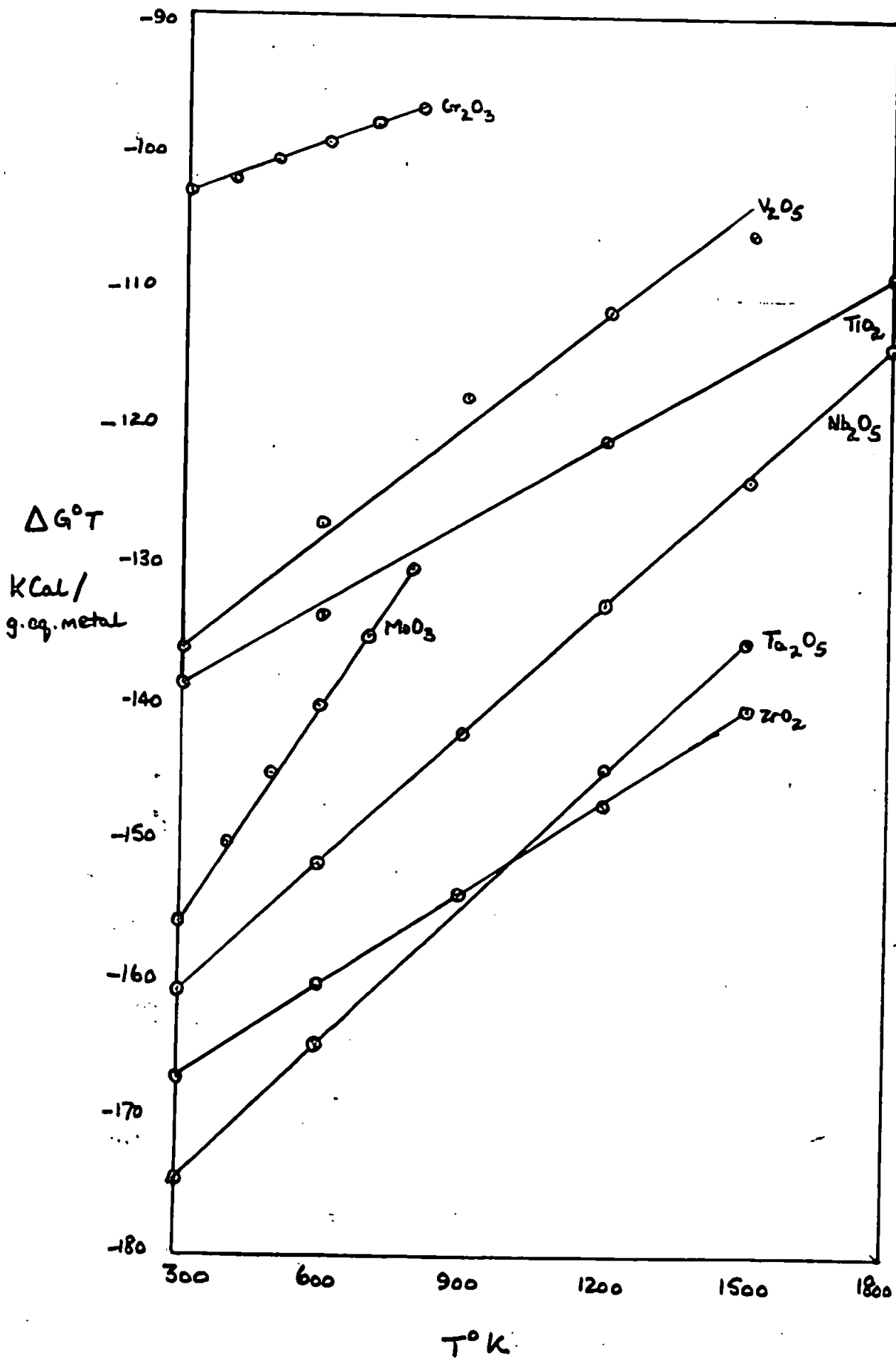


Fig 2.2. FREE ENERGY CHANGE FOR THE OXIDATION OF NITRIDES

## 1.6 Kinetics of Metal Nitridation

### 1.6.1 Rate of Nitridation

Nitridation rates are expected to conform to the same principles as applied for metal oxidations (Kubaschewski & Hopkins, 1962). A number of relationships are known which relate the extent of nitridation (or oxidation) with reaction time. They give the weight increase per unit surface area,  $m$ , as a function of time,  $t$ .

The simplest relationship which is the linear one, namely,

$$m = K't$$

where  $K'$  is a constant. Since the weight increase per unit area is proportional to the thickness of the nitride (or oxide) film,  $y$ , and this in turn is proportional to the decrease in thickness of the metal,  $x$ , the above equation can be written as,

$$y = Kt$$

Where  $K$  is a constant.

The parabolic law, generally encountered at higher temperatures can be stated as follows:

$$y^2 = Kt + C$$

It gives a straight line when the square of the weight gain is plotted against time; a non-zero value of constant  $C$  implies an initial induction period. Factors causing slight deviations from the parabolic rate law in the earlier reaction stages are probably similar to those encountered in metal oxidations (Gulbransen & Andrew, 1951), viz., decreases in surface heterogeneity and specific surface as the reaction proceeds, impurity concentrations, changes in local surface temperatures caused by the heat of reaction, solubility effects and possible changes in nitride composition.

Other relationships described are, cubic, logarithmic and inverse logarithmic. A single nitridation curve may have combinations of two or more of the above relationships, e.g., the nitridation of a metal or alloy may begin parabolically and continue linearly. This is termed a parilinear relationship.

#### 1.6.2 Factors Affecting the Rate of Reaction

In the direct nitridation of metals a nitride layer is formed between the metal and its gaseous environment. The reactants have to pass through this barrier if the reaction is to continue and the nitride layer to grow. The overall rate of a reaction may be influenced by one or more of the following type of rates:-

- 1) the rate of supply of reacting gas to the outer surface of the nitride layer.
- 2) the rate of transport of reacting species through the nitride layer.
- 3) the rate of reaction between metal and nitrogen forming nitride.

Each of the above rates is governed by factors such as temperature, external gas pressure, defects in the nitride structure, etc. The slowest of the above rates is the rate-determining step.

The mechanical stability of the nitride layer is important in determining rate and extent of nitridation. The strength of the layer on the metal depends on the differences in molecular volume and type of crystal lattice of the product layer compared with the original metal (Pilling & Bedworth, 1923), and also on the rate of nitride sintering. Higher temperatures enhance sintering, i.e., they promote recrystallisation of newly formed nitride, but also increase evaporation



of the metal below the nitride layer. This is exemplified by electropolished magnesium in very pure nitrogen (Gregg & Bickley, 1966), at 10 cm mercury pressure above 500°. Such evaporation is usually absent in the nitridation of transition metals as they have very high evaporation temperatures. (Table 1.2)

Table 1.3 summarises molecular volume and crystal lattice changes accompanying nitridation of some of the transition elements. The calculations are based on X-ray data compiled by Taylor & Kagle (1963), and checked experimentally, densities being deduced from metal and nitride crystal structures existent at temperatures normally used for nitridation. Volume changes are expressed as fractions of the original metal volume, allowing for weight increases during nitridation, expansions and contractions are indicated by + and - signs respectively. In Table 1.4 these changes are recorded for conversion of the nitrides to their corresponding stable oxides. Where small decreases in unit cell size are caused by sintering of the newly-formed nitride or oxide, the lowest limiting value is recorded.

Table 1.2 Evaporation Temperatures  
of some Transition Metals

Metal	Evaporation Temperature *	
	°C	K
Titanium	1703	1980
Zirconium	2397	2670
Vanadium (1)	1945	2118
Niobium	2500 (M.P.) p = 1.85 <sup>at</sup>	2773 (M.P.)
Tantalum	2996 (M.P.) p = 5.0 <sup>at</sup>	3269 (M.P.)
Chromium	1392	1665
Molybdenum (1)	2577	2850
Tungsten	3334	3607

\* The evaporation temperature is taken as the temperature at which a vapour pressure of 0.01 torr or 10<sup>-2</sup> is attained.

(1) indicates that the material is liquid at the specified temperature.

Notes. (1) Data reproduced from Powell, Oxley & Blocher, Jr., 1966, pp. 224-25.

(2) Unlike the above transition metals, magnesium readily undergoes evaporation due to its lower evaporation temperature, i.e., 442°C.

Table 1.3 Fractional Volume and  
Crystal Lattice Changes on Nitridation

Nitride	Fractional Volume Change	Element		Nitride	
		Crystal Lattice	Lattice Constants in Å	Crystal Lattice	Lattice Constants in Å
Ti V*	+0.05	b.c.c. <sup>(β)</sup>	a = 3.30	Cubic NaCl	a = 4.24
	+0.08	h.c.p. <sup>(α)</sup>	a = 2.95 c = 4.68		
ZrN*	0.00	b.c.c. <sup>(β)</sup>	a = 3.60	Cubic NaCl	a = 4.56
	+0.02	h.c.p. <sup>(α)</sup>	a = 3.23 c = 5.15		
VN	+0.27	b.c.c.	a = 3.03	cubic NaCl	a = 4.28
NbN(β)	+0.18	b.c.c.	a = 3.30	hexagonal	a = 2.97 c = 5.53
TaN(β)	+ 0.26	b.c.c.	a = 3.31	hexagonal	a = 5.19 c = 2.91
C <sub>3</sub> N	+0.49	b.c.c.	a = 2.88	Cubic, NaCl	a = 4.15
Cr <sub>2</sub> N	+0.21	b.c.c.	a = 2.88	hexagonal	a = 4.76
MoN (β)	+0.21	b.c.c.	a = 3.15	superlatc. hexagonal	c = 4.44 a = 5.72
Mo <sub>2</sub> N*	+0.09	b.c.c.	a = 3.15	super-la ttice	c = 5.61
Mo <sub>2</sub> N*	+0.09	b.c.c.	a = 3.15	cubic, NaCl	a = 4.16
WN (β)	+1.16	b.c.c.	a = 3.17	hexagonal	a = 2.89 c = 2.83
W <sub>2</sub> N (β)	+0.39	b.c.c.	a = 3.17	cubic NaCl	a = 4.13

\* low temperature form

b.c.c. = body-centred cube

h.c.p. = hexagonal close-packed

Table 1.4 Fractional Volume and  
Crystal Lattice Changes on Oxidation of Nitride

Nitride	Fractional Volume Change	Nitride		Oxide	
		Crystal Lattice	Lattice Constants in Å	Crystal Lattice	Lattice Constants in Å
TiN	+0.649	Cubic, NaCl	a = 4.24	tetragonal (rutile)	a = 4.59 c = 2.96
ZrN	+0.518	Cubic, NaCl	a = 4.56	Monoclinic (ZrO <sub>2</sub> )	a = 5.14 b = 5.20 c = 5.3107 β = 99° 14'
VN	+1.272	Cubic, NaCl	a = 4.28	Orthorhombic (V <sub>2</sub> O <sub>5</sub> )	a = 11.52 b = 3.56 c = 4.37
NbN(E)	+1.375	hexagonal	a = 2.97 c = 5.53	Monoclinic (Nb <sub>2</sub> O <sub>5</sub> )	a = 21.34 b = 3.816 c = 19.47
TaN(E)	+0.986	hexagonal	a = 5.19 c = 2.91	Orthorhombic (Ta <sub>2</sub> O <sub>5</sub> )	a = 6.19 b = 44.02 c = 3.90
CrN	+0.354	Cubic NaCl	a = 4.15	Hexagonal (Cr <sub>2</sub> O <sub>3</sub> )	a = 4.95 c = 13.58
Cr <sub>2</sub> N	+0.597	hexagonal superlattice	a = 4.76 c = 4.44		
MoN(δ)	1.606	hexagonal superlattice	a = 5.72 c = 5.61	orthorhombic (MoO <sub>3</sub> )	a = 13.85 b = 3.69 c = 3.96
Mo <sub>2</sub> N	1.839	cubic, NaCl	a = 4.16		

### 1.6.3 Ionic Diffusion: Parabolic Relationship

At higher temperature ranges (above 500°C), the diffusion of the reacting species through the nitride layer involves the movement of cations from the metal-nitride interface towards the nitride-chemisorbed nitrogen interface. Anion diffusion is slower because of larger size, but is not always important. Simultaneous movement of anions and cations also is known to be significant in some mechanisms of reactions.

Cation migration is possible because of vacant cation lattice sites in the nitride layer. Such migration is favoured therefore by a high degree of nonstoichiometry and a large number of cation defects in the nitride lattice. The overall effect is, therefore, a flow of cation vacancies through the nitride layer towards the metal-nitride interface or cations in the opposite direction, i.e., an electric current through the nitride layer. Cabrera & Mott (1948), present a thin film theory, which stipulates that the ions move under the potential difference set up between the anions and cations on the respective interfaces. The cations are formed by the migration of electrons through the film by the "tunnel effect" followed by reaction with gas molecules adsorbed on the outer surface of the film. (tunnel effect is a quantum mechanical phenomenon which predicts a finite chance that an electron can pass through a thin film of an insulator without requiring appreciable activation energy). The accumulation of vacancies at the nitride-metal interface leads to the formation of cavities.

Many nitridation and oxidation processes follow the parabolic

law. A simplified derivation of the law is described by Chilton (1968: p.5). If ion (or electron) migration is the rate determining step, the reaction rate, i.e., the rate of growth of product layer, is proportional to the conductance of the layer, or inversely proportional to its thickness,  $y$ . Therefore,

$$\frac{dy}{dt} = \frac{k}{y}$$

Rearranging and integrating the above equation,

$$y^2 = 2kt + C$$

Where  $k$  and  $C$  are constants.

In a parabolic process the driving force for the reaction is two-fold. Firstly, there is a concentration gradient across the film and secondly, there is an electric potential gradient. These factors are responsible for diffusion and migration across the film respectively. The concentration gradient in the film produces a difference in chemical potential across the film which in turn results in the necessary free energy change for diffusion to occur.

#### 1.6.4 Linear Growth Rate

The derivation of the parabolic law described above assumes that the product layer remains adhered to the metal during the course of the reaction and keeps it completely protected from the reacting gas. This is not the case when stresses generated within the layer are large enough to cause its breakdown when its thickness reaches certain critical value, or if the specific surface of the product layer is less than that of the metal originally. The mechanical stability of this layer depends on the molecular volume changes accompanying the reaction. Larger volume changes, enhance quicker splitting of the layer.

Film rupture exposes fresh metal surface to the reacting gas, and the resulting reaction may follow a new parabolic rate. More nitride is then produced in contact with the metal and after a similar time interval, disruption of the film again takes place. When film breakdown takes place at frequent intervals the number of parabolas increases and their size decreases. The resulting curve then approximates to a straight line, i.e. corresponds to a linear rate process (Jayaweera, 1969).

A simplified derivation of linear rate law is as follows. In the absence of a coherent nitride layer, the metal is continuously exposed to the reacting gas and the reaction rate is independent of the decrease in the thickness of the metal,  $y$ , under a given set of conditions. Therefore,

$$\frac{dy}{dt} = k$$

Whence,

$$y = kt + c$$

Where  $k$  and  $c$  are constants.

Unlike the parabolic and logarithmic rate equations, for which the rate of reaction decreases with time, the rate of linear reaction is constant with time and is thus independent of the amount of gas or metal previously consumed in the reaction. If the nitridation is linear, ionic migration cannot be the rate determining step, instead the surface or phase boundary process is rate-determining.

A comprehensive account of reaction rates applicable to thin films are summarised by Kubschewski & Hopkins (1962, p.71).

#### 1.6.5 Nature of Nitride Scale

For the formation of thick oxide (or nitride) layers, Wagner (1933)

has provided a satisfactory theory (Jubaschewski & Hopkins, 1962, p.84). According to this theory, the mechanism is controlled by diffusion due to a concentration gradient. The parabolic rate law applies when the scale is uniform in thickness.

Formation of non-uniform (i.e. porous or cracked) scales depends partly on the pilling-Bedworth Rule, which is probably less significant if the scales grow by outward migration of matter (Vermilyea, 1957). It is more important when diffusion is from the surface towards the metal-scale interface. Fractional volume changes are comparatively small for the formation of the group IV A metal nitrides, TiN, and ZrN (Table 1.3). Hence, titanium nitride films flake much less than those of the oxidised metal (fractional volume change for rutile, TiO<sub>2</sub>, formation is 0.73), as found by various workers (Carpenter & Reavell, 1948; Gulbransen & Andrew, 1949; Richardson & Grant, 1954; Wasilewski & Kehl, 1954). Both nitrogen and oxygen are involved in the scaling of zirconium in air. The two-layered scale ultimately formed consists of an outer white or buff scale (ZrO<sub>2</sub>) and an inner black scale (consisting of ZrO<sub>2</sub>, ZrN and possibly N). The white scale predominates below 1050° and the black above that temperature (Phalnikar & Baldwin, 1952). Similarly, vanadium, niobium and tantalum in group VA, form oxides of exceptionally large volume ratios (fractional volume changes of 2.19, 1.68 and 1.50 for their pentoxides) compared with the nitrides (Table 1.3). The resultant extensive rupturing of the oxide films changes the kinetics from parabolic to approximately linear at lower temperatures, 500-700°, for Nb (Argent & Phelps, 1960; Hurlen et.al., 1959; Kofstad & Kjollesdal, 1961; Cathcart et.al., 1958), and Ta (Gebhart & Seghezzi, 1959; Peterson, et.al., 1954; Cathcart et.al., 1960).



If the scale becomes coherent and protective, the reaction may practically be stopped, even when the scale is completely detached from the metal surface, e.g., 'asymptotic' oxidation of niobium at 1250°C, ( Kubaschewski Schneider, 1949).

The group IV A and V A metals nitride much more slowly than they oxidise at corresponding temperatures (Gulbransen & Andrew, 1950). Rates of nitrogen diffusion through  $\alpha$ - and  $\beta$ -Ti and TiN indicate that the nitridations are controlled ultimately by diffusion through titanium and the surface nitride layer (Wasilewski & Kehl, 1954). The initial controlling process is more likely diffusion through  $\alpha$ -Ti. Likewise, the low activation energies for nitrogen diffusion in  $\beta$ -Zr compared with those for the nitridation ( Gulbransen & Andrew, 1949), indicate that the rate of solution in the  $\beta$ -phase is not the rate-determining factor (Mallet et.al., 1954). Nitridations of the other group IV A and V A metals are similar. The nitride films make the reaction rates practically insensitive to nitrogen gas pressure variations, and the film thickness is governed by the rate of nitride formation and the rate of dissolution of nitrogen in the metal (Duwez & Odell, 1950; Gulbransen & Andrew, 1949<sup>c</sup>, 1950; Ang, 1953).

The M-N systems with M = V, Nb and Ta are very similar for low N-contents, but differ for high N-contents. The solubilities of nitrogen in the metal lattices are only about 2 atomic-per cent (Brauer & Jander, 1952). The interstitial structure type, M<sub>2</sub>N, is common for the three M-N systems (Hahn, 1949; Schönberg, 1954; Epelbaum & Ormont, 1947; Rostoker & Yamamoto, 1947; Brauer & Zapp, 1953). The metal atoms are

hexagonally close-packed and the N atoms are in one of the two metal atom octahedral voids of the unit cell. This phase has a comparatively broad homogeneity range with the upper phase limit closely corresponding to the composition,  $M_2N$ . The  $NbN_{0.8-0.9}$  and  $TaN_{0.8-0.9}$  phases are isomorphous, but there is no analogous V-N phase reported. The  $\epsilon$  phase in the Nb-N system (Table 1.3) represents the transitional state between the atomic arrangements in the  $\gamma$ - and  $\delta$ - phases (Schönberg, 1954).

Nitridation of uranium is more complicated. Reaction rates with nitrogen (1 atm., pressure) measured volumetrically indicate parabolic nitridation with some deviations initially and after the period of parabolic kinetics (Mallett & Gerd, 1955). The surface nitride formed at temperatures between  $550^\circ$  and  $750^\circ$  is mainly  $UN_2$  (probably deficient in nitrogen); at higher temperatures, viz.,  $775-900^\circ$ , the three nitrides, UN,  $U_2N_3$  and  $UN_2$  form a rather roughened scale surface. The region between UN and  $U_2N_3$  consists of two phases, but that between  $U_2N_3$  and  $UN_2$  is a homogeneous solid solution; the crystal structure changes from a distorted ( $U_2N_3$ ) to a true fluorite-type ( $UN_2$ ), Table 1.3. This has been reported by Rundle et.al., (1948). However, Vaughan (1956), regards  $U_2N_3$  as being isomorphous with  $Th_2N_3$  and suggests it is polymorphic (two forms). Reaction between nitrogen and uranium or thorium films has been followed by surface potential studies (Rivière, 1968). At higher nitrogen pressures, rapid variations in the rates of change in potential with time are associated with the formation of higher nitrides at the surfaces.

### 1.6.6 Kinetic studies of Nitride Formation with Ammonia

The kinetics of metal nitridation with ammonia has been studied by comparatively few workers, and mainly relates to metal catalysts for nitrogen fixation. Metallic chromium, molybdenum and tungsten do not react appreciably with nitrogen at 900°C under ordinary pressures (Duparc, et.al., 1930; Neumann, et.al., 1931). They readily react with ammonia, even at lower temperatures (700-900°C) giving single or mixed nitrides, MN & M<sub>2</sub>N (Table 1.3), where M = Cr (Blix, 1929; Eriksson, 1934; Korolev, 1953), Mo (Sieverts & Zapf, 1936; Ghosh, 1952) or W (Häg, 1930; Laffitte & Grandadam, 1935; Kiessling & Liu, 1951; Kiessling & Peterson, 1954; Schönberg, 1954). Heats of decomposition of Cr<sub>2</sub>N and Fe<sub>4</sub>N to saturated solid solutions compared with enthalpies of formation, indicate heat absorptions of about 5000 calories per g. atom of nitrogen, dissolving in either of the two body-centred cubic solvents. This accords with the similar electronic distributions of Cr and Fe about the N atoms. The much lower stability of Fe<sub>4</sub>N compared with Cr<sub>2</sub>N derives from the smaller radii of the octahedral sites available for N atoms (1.89Å in Fe, compared with 2.13Å in Cr). Nitridation kinetics of iron have been discussed by Glasson & Jayaweera (1968, p.72).

### 1.6.7 Effect of Gas Pressure on Nitridation Kinetics

Much information of theoretical and potential practical interest can be obtained from studies of the kinetics of the uptake of gases by the metal surface as a function of temperature as well as gas pressure. When the rate-determining step involves the dissociation of the attacking diatomic gas (nitrogen or oxygen), the reaction rate

is expected to be proportional to the square root of the gas pressure. The rate-determining step in this case is the direct reaction at the solid-gas interface.

When gases dissolve in metals, Henry's Law is obeyed; also the molecules of the gas split up into atoms (or ions) on dissociation. Hence, the solubility of a diatomic gas in a metal would also be expected to vary as the square root of gas pressure. The diffusion of gaseous atoms through a metal also requires a square root relationship with pressure when the metal surface is directly exposed to the gas (Barrer, 1941, p.146). The effect of nitrogen pressure on the rate of gas dissolution has been investigated by Gulbransen and Andrew (1949), who report that although a slight increase in reaction rate with increasing  $N_2$ - pressure was observed, the effect was not proportional to the square root of the pressure. Wasilewski and Kehl (1954) on the other hand, found that a reduction in  $N_2$ - pressure causes a slight increase in rate of uptake. Richardson and Grant (1954) measured changes in  $N_2$ - pressure occurring with time when a titanium specimen was nitrided at temperatures in the range 787-1014°C in a closed vessel containing nitrogen at initial pressures between 150-380 mmHg. All three groups of workers agree that the rate of dissolution of nitrogen is much less rapid than that of oxygen.

### 1.7 Reactivity of Nitrides

A general account of active solids together with references to the original literature are described by Gregg (1951, 1958) and Gregg & Sing (1967).

The reactivity of solids is influenced by a number of factors, of which particle size is a significant one. An increase in activity is generally ascribed to an increase in the specific surface (i.e., the surface area per unit mass) of the substance and quite often, to imperfections in the lattice itself. A substance consisting of small particles possesses high surface energy. Also lattice imperfections represent a high level of 'bulk' potential energy. Thus an active solid is in a meta-stable state and tends to go back spontaneously to a more stable state of lower energy content. This loss of activity takes place (usually very slowly) on mere standing at room temperature, and is called "ageing". Ageing results in the formation of large crystallites with less imperfections. It is enhanced by increasing temperature, as increased thermal agitation of the constituent atoms or ions facilitate their movement into positions of minimum potential energy.

#### 1.7.1 Sintering of Nitrides

In its broadest sense, sintering, includes all the processes employed to produce adhesion or consolidation of the materials of refractory nature. In the narrower, technical sense, it may be defined as the mechanism whereby a single pure material consolidates under the influence of temperature, pressure and time less than that sufficient to cause complete breakdown of molecular structure i.e., melting. Theories of sintering have been developed by Kingery (1960), Hüttig (1941), Coble (1961, 1964), Kuczynski (1961), White (1962, 1965) and Fedorchenko & Skorokhod (1967).

At present there is much more information available on the sintering

of oxides which is expected to resemble that of nitrides. The chemical reactivity of nitrides is controlled considerably by the extent to which they have been sintered during their formation and any subsequent calcination. Sintering is enhanced by compacting the powdered nitride e.g., Be, La, Ti, Th, U and Ta, before calcining in vacuo to prevent possible oxidation or hydrolysis (Chiotti, 1952). It is also affected by low melting additives (Glasson, 1967), but these may cause serious reductions in optical and mechanical properties. However, TiN is extremely brittle and may be sintered with a metal such as cobalt to give a satisfactory cermet, or may be used as a surface coating (Munster, 1957). The thermodynamics of the sintering of TiN in the presence of carbon (Blum, 1962) and the defect structure and bonding of ZrN containing excess nitrogen have been described (Straumanis et.al., 1962). The micro-hardness of vanadium and chromium nitrides varies with bonding changes during progressive metal nitriding and subsequent sintering (Samsonov & Verkhoglyalova, 1962); the lower nitrides,  $V_3N$  and  $Cr_2N$  are harder than VN and CrN. Besides nitride formation, introduction of nitrogen into metallic chromium increases brittleness by locally distorting the metal lattice (Weaver, 1957).

Sintering is enhanced by high pressure e.g., hot pressing which often extensively densifies materials (Schwarzkopf & Kieffer, 1953; Spriggs & Atterass, 1966), giving almost theoretical densities for some oxides such as CaO, MgO, and  $Al_2O_3$  (Rice, 1969). But a prerequisite is the production of finely divided material with suitable particle size range. The gas producing contaminants such as carbonates and hydroxides delay the extent of sintering. Hence, often, vacuum hot pressing is preferred (Fulrath, 1969). These factors are

important in ceramic fabrication science (Cooper, 1969). Nitride sintering is also influenced by partial nitride hydrolysis or oxidation, or both, forming oxide impurities. When BN is purified at higher temperatures to reduce oxide content, the increased particle size makes subsequent hot pressing more difficult (Ruddlesden, 1962).

The rate of sintering of a solid markedly increases within a narrow range of temperature near  $0.5T_m^{\circ}\text{K}$ , where  $T_m^{\circ}\text{K}$  is the melting point of the solid (Hüttig, 1941). At this temperature, called the Tammann temperature, vacancies in the solid are no longer "frozen", so that ionic migration through the bulk of the solid (i.e. "lattice" or "volume" diffusion) sharply increases. At lower temperatures eg., in the region of about  $0.3 T_m^{\circ}\text{K}$ , "surface" diffusion along grain and crystallite boundaries is the more important factor.

There are two overlapping stages in sintering which can be distinguished. The first stage is characterized by the formation and growth of contact areas between adjacent powder particles. During the second stage, the material is densified and the pore volume decreased. The driving force in both stages of sintering is recognised to be the surface free energy. The energy required for sintering is supplied by the decrease of surface areas or by the replacement of interfaces of high energy by those of lower energy (e.g. grain boundaries). The surface free energy is sufficient to account for sintering, provided a suitable mechanism is available for the transport of atoms involved in the consolidation of powder compacts. The following five possible mechanisms are likely in the case of homogeneous materials:-

- i) Evaporation followed by condensation
- ii) Surface diffusion
- iii) Volume diffusion

iv) Viscous flow (characterized by a linear relationship between strain rate and stress).

v) Plastic flow (characterized by the existence of a yield stress ).

Frenkel (1965) made the first attempt to develop a quantitative theory, assuming that <sup>with</sup> both crystalline and amorphous powders, viscous flow would occur under the variation influence of the capillary forces associated with the curved surfaces of the pores with time. The viscosity may be represented by the equation:-

$$\eta = K T / D \omega_0$$

where,

$\eta$  = viscosity

D = coefficient of self diffusion

T = absolute temperature

K = constant

$\omega_0$  = atomic volume.

The mechanism of deformation of solids by viscous flow and the rate of diffusion in the deformation of crystalline solids was evolved further by Schaler & Wulff (1948), Natarro (1948) and Herring (1950).

Methods of preparing finely divided materials (active solids) include grinding, calcination, sublimation and precipitation. In the first case, the mechanical breaking up of the particles is opposed to some extent by the tendency of the fine particles to adhere together under joint influence of surface forces and the mechanical pressure of the mill. This effect is more pronounced if the grinding is carried out for longer periods (Jones, 1970).



Calcination is based on chemical reactions of the type:-



e.g., the decomposition of hydroxides and carbonates (Gregg, 1953; Glasson, 1956, 1958a, 1961b, 1963a; Glasson and Sheppard 1968).

The specific surface of B is considerably greater than that of A if the two solid phases possess different lattices and if there is a large volume change between them, c.f., Pilling & Bedworth (1923) rule for metal oxidations.

Sublimation and precipitation are 'condensation' methods of preparing active solids, whereas grinding and calcination are 'fragmentation' methods. The preparation of evaporated metal films is an example of a sublimation method, and is generally carried out under high vacuum. Films of calcium, magnesium, zinc and cadmium have been investigated by Jayaweera (1969) and chromium and nickel by Maude (1970).

In the present work, ball-milling has been used to produce activated materials and the enhanced reactivity has been determined with respect to increased surface area and oxidation behaviour.

#### 1.7.2 Oxidation and Hydrolysis of Nitrides

The chemical reactivities of refractory nitrides have been summarised by Shaffer (1964) and Samsonov (1964), those of Ti, Zr, Nb and Ta have been investigated by Popova & Kabannik(1960). These workers have studied action of water, aqueous acids and alkalies. TaN appears to be the most stable to the attack of different reagents, and ZrN the least. In nitride production, usually oxygen must be avoided, for it prevents nitrogen from reacting with the clean metal surfaces.

The transition metal nitrides are less readily hydrolysed, but some of them, e.g., those of Ti, Zr, Hf, Th, V, Nb, Ta, Cr, Mo, W, and U are converted to oxides on calcining in air. The oxidation rate depends mainly on two factors, (a) the intrinsic reactivity of the material itself and (b) the available surface for oxidation to occur. Thorium mononitride oxidises rapidly and quantitatively in moist air at room temperature even in ingot form, but powdered uranium, titanium and zirconium mono-nitrides are quite stable at 100°C in boiling water (Dell, et.al., 1966). UN powder ignites in dry oxygen at about 300°, but W<sub>2</sub>N, Mo<sub>2</sub>N and CrN have an increasing oxidation stability (Dell, et.al., 1966).

The only interstitial nitride oxidations that have been studied in any detail are those of TiN (Munster & Schlamp 1957; Glasson & Jayaweera, 1968) and UN (Dell, et.al., 1966). They illustrate factors to consider and problems to be encountered in further investigations of other transition metal nitride oxidations. Although, the corrosion resistance of surface layers of these nitrides is good, the scaling resistance in air (or oxygen) is poor.

In this thesis the author has studied and compared the oxidation behaviour of some of the nitrides of transition elements in groups IVA, VA and VIA. Changes in phase composition and crystal structure for oxidation of these nitrides have been investigated by X-ray, optical and electron-micrographic methods. Surface area determinations have been made by gas sorption and correlated with changes in crystal structure and crystallite size on oxidation. Similar studies of the effect of milling of the nitrides on their oxidation rates and sintering characteristics have been carried out. The average crystallite sizes of the milled

nitrides have been estimated from X-ray line or peak-broadening (Glasson, 1964). Certain metal powders have been further oxidised and compared with the oxidation behaviour of the corresponding nitride, in a similar manner.

In the following sections of this chapter a summarised account of the studies made by other workers on formation of the above nitrides is presented.

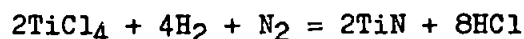
## 1.8 Titanium Nitride, TiN

### 1.8.1 Formation

Mellor (1927, p.117) and Brown (1964, p. 167) have summarised various methods of production of titanium nitride. A review of these methods also has been given by Jayaweera (1969). Agte & Moers (1931) have produced the nitride by heating Ti-metal powder under very pure nitrogen in molybdenum boats in a porcelain tube furnace. This method of direct combination of elements has been adopted at temperatures ranging from 400 to 1200°C (Ehrlich, 1949; Chiotti, 1952; Cuthill, et.al., 1960; Clair, 1960; Arai, et.al., 1962). Metal nitridation by ammonia or mixtures of hydrogen + nitrogen has been employed (Chiotti, 1952; Wyatt & Grant, 1954, 1957; Samsonov et.al., 1961a; Sato & Yamane, 1955). Alexander (1949) has patented a method which consists of reducing titanium dioxide to the metal and subsequent nitridation.

Another widely used method of titanium nitride production is the vapour phase deposition from a mixture of titanium chloride and ammonia or nitrogen and hydrogen mixture. Thus Hughes & Harris (1957) have patented a method whereby anhydrous  $\text{NH}_3$  gas and  $\text{TiCl}_4$  vapour

react to form TiN with a uniform particle size less than  $1 \mu\text{m}$ . This method was first evolved by van Arkel and de Boer (1925), with the mixtures in contact with heated tungsten filaments. Aivazov & Melekin (1967) have crystallised TiN from the gaseous phases according to the reaction.



They have claimed that at  $1400^\circ\text{C}$ , favourable conditions exist for the growth of  $3 \times 3 \text{ mm}$  crystals. Suchet (1960) has reported the formation of a nitride of titanium having composition,  $\text{Ti}_3\text{N}_4$ , by passing a high frequency discharge through the mixture of vapours. Niederhause (1962) has been able to produce the nitride via the formation of an intermediate ammoniated complex. The complex formation has been avoided by Ruppert & Scwedler (1958, 1959) by using high enough temperature preferably between the range  $900-1200^\circ\text{C}$ . According to Brager (1939) there are two forms of the intermediate complex,  $\Delta$  - and  $\underline{\Delta}$  -  $\text{TiCl}_4 \cdot 4\text{NH}_3$ . The thermodynamics of the reactions has been discussed by Münster & Ruppert (1953) and Münster et.al., (1956).

There are two prime reasons for the widespread use of vapour deposition process in industry. Firstly that a uniformly thin coating of nitride can be prepared on the surface of an object, regardless of its shape. Secondly, the reaction can be controlled accurately. In this way mechanical and other properties of articles have been improved by coating them with titanium nitride and other refractory materials. (Münster & Weber, 1958; Löhberg et.al., 1958).

Titanium carbide reacts with nitrogen forming nitride. Zelikman

& Govorits (1950), have reported formation of TiC-TiN solid solutions at 1300-1800°C during the reaction. They have also remarked that a nitrogen pressure greater than 1 atmosphere is necessary for complete nitridation of the carbide. Portnoi & Levinskii (1963) also report the formation of solid solutions of TiC-TiN at 1500°C, but the product obtained had carbide impurity. However, when metallic titanium is heated with a mixture of carbon and nitrogen, only the nitride is obtained, Umezu (1931) and Samsonov & Petrash (1955) have obtained similar results, when they heated titanium oxides with carbon in the presence of nitrogen. These observations can be explained by the greater diffusion rate of nitrogen than of carbon. Blum (1962) claims that sintering of titanium nitride is possible on a graphite support without being attacked.

Starting materials for other production methods of titanium nitride include the hydride, sulphide and reduced titanium halides (Foster, 1952; Duwez & Odell, 1950; Jacobson, 1954; National Lead Co., 1956).

### 1.8.2 The System Titanium-Nitrogen

A comprehensive account of the titanium-nitrogen phase diagram studies is given by Brown (1964, p.168). McQuillan & McQuillan (1956) have also discussed this system. It is well known that at 882.5°C pure Ti-metal undergoes an allotropic phase transformation from a hexagonal close-packed  $\alpha$ -structure (stable at low temperatures) to a cubic body-centred  $\beta$ -phase, which persists

up to the melting point of the metal, i.e.  $1668 \pm 5^{\circ}\text{C}$  (this uncertainty is due to the possibility of dissociation as  $\text{N}_2$  gas). In this respect the behaviour of titanium is similar to that of zirconium (transformation temperature,  $865^{\circ}\text{C}$ ).

Ehrlich (1949), who carried out X-ray investigations on this system, concluded from his results that at room temperature only the  $\alpha$ -Ti solid solution and the nitride, TiN, existed in the composition range up to 50 atomic % nitrogen. This was confirmed by a more detailed investigation by Palty et.al., (1954), who concluded that both the  $\alpha$ -phase and TiN have wide ranges of homogeneity. They also demonstrated the existence (at a composition of about 26 atomic % nitrogen), of a second compound,  $\beta$ -TiN formed at a temperature between  $1000$ - $1100^{\circ}\text{C}$ . The crystal structure of the  $\beta$ -phase has been found to have a tetragonal lattice (Palty et.al., 1954). Holmberg (1962) assigns the formula,  $\text{Ti}_2\text{N}$ , to the compound he prepared, and considers that his phase is the one designated as the  $\beta$ -nitride by Palty et.al. (1954). Olson (1967) reports the preparation of a compound with formula,  $\text{Ti}_3\text{N}_4$ .

Although titanium nitride phase is usually described as TiN, it has a fairly wide range of homogeneity around the stoichiometric composition (Münster & Sagel, 1953), varying between  $\text{TiN}_{0.42}$  (Ehrlich, 1949) and  $\text{Ti}_{0.6}\text{N}$  (Holmberg, 1962). However, Schwarzkopf and Kieffer (1953, p.230) consider that the only stable nitride of titanium existing is TiN

## 1.9 Zirconium Nitride, ZrN

### 1.9.1 Formation

Zirconium nitride can be produced by methods similar to those

for titanium nitride (Mellor 1927, p.120; Brown 1964, p.177). In the formation of this compound from the elements, temperatures varying from 700 to 2000° have been used (Agte and Moers, 1931; Clausing, 1932; Fujiwara, 1950; Chiotti, 1952; Clair, 1960; Samsonov et.al., 1961a; Hough, 1962; Salibekov et.al., 1964). The metal has been nitrided also by ammonia gas (Chiotti, 1952; Wyatt & Grant, 1957), when the reaction rate is correspondingly lower (Samsonov et.al., 1961a).

The Van Arkel-de Boer (1925) method of vapour deposition of the nitride from the chloride can be used also (Moers, 1931; Campbell et.al., 1949). The production of zirconium nitride has been effected by using other starting materials such as bromide, hydride, and oxide (Foster 1952; Duwez & Odell, 1950; Alexander, 1949b; Schneider et.al., 1963). Zirconium, like titanium, reacts preferentially with nitrogen rather than with carbon, owing to the greater diffusion rate of the former (Portnoi & Levinskii, 1963). Blum (1962), reported that ZrN, unlike TiN, is attacked by carbon at higher temperatures and forms the carbide.

### 1.9.2 The System Zirconium-Nitrogen

A summary of the phase diagram studies of the Zr-N system has been presented by Brown (1964, p.178); see also Domagala et. al., (1956) and Farr (1968). Two forms of metallic zirconium are reported; an  $\alpha$ -form having a hexagonal close-packed structure, stable up to 865, transforms to a  $\beta$ -form with a cubic body-centred structure above this temperature. Metallic zirconium forms a solid solution with nitrogen up to an atomic percentage of 20 (de Boer &

& Fast, 1936; Jeffe & Campbell, 1948). Above this limit, the nitride phase is precipitated. The absorption of nitrogen, like that of oxygen, raises the transformation temperature (865°C) of the metal. Ishii (1943) & Ishii & Wada (1943) reported the existence of two modifications of ZrN, but this has not been confirmed by other researchers. The homogeneity range of ZrN varies from nitrogen-deficient  $ZrN_{0.46}$  at 1985°C to ZrN below 600°C.

### 1.10 Vanadium Nitride, VN

#### 1.10.1 Formation

A summary of production methods of vanadium nitride is given by Mellor (1927, p.124) and Brown (1964, p.185).

Vanadium nitride is difficult to produce by heating mixtures of vanadium pentoxide ( $V_2O_5$ ) and carbon in a nitrogen current because at temperatures below 1200°C, the nitride is transformed to carbide in the presence of carbon. Friederich and Sittig (1925) were able to prepare a product containing 78.3% V, 21.1% N and 0.5%  $SiO_2$  (theoretical values for VN; 78.45% V and 21.55% N).

Pure vanadium nitride has been prepared by reaction of ammonium vanadate with ammonia at 900–1100°C (Epelbaum & Ormont, 1946, 1947; Epelbaum & Brager, 1940; Juza, 1945). Direct nitridation of pure vanadium metal powder in a nitrogen current has been employed by Duwez & Odell (1950) and Hahn (1949). The latter has also obtained a product of lower nitrogen content, i.e.  $V_3N$ , by sintering vanadium nitride with metallic vanadium powder in sealed quartz tubes for 24 hours at 1000–1100°C.



The van Arkel method of deposition of vanadium nitride from  $\text{VCl}_4\text{-N}_2\text{-H}_2$  vapour mixtures on tungsten wires at a temperature range of  $1400\text{-}1600^\circ\text{C}$  was used by Moers (1931). The fine crystalline coatings had a brownish-grey colour. Campbell and coworkers (1949) employed, for the same vapour mixtures, deposition temperatures of  $1100\text{-}1600^\circ\text{C}$ , while Pollard and Fowles (1952) reported for the continuous deposition an optimum temperature of  $1540\text{-}1570^\circ\text{C}$ .

#### 1.10.2 The System Vanadium-Nitrogen

This system has been thoroughly investigated by Hahn (1949) and confirmed by Schönberg (1954). The solid solubility of nitrogen in vanadium has been found by Rostoker & Yamamoto (1953) to be at least 3.5 atomic % nitrogen above  $900^\circ\text{C}$ . According to Hahn (1949) the nitride has a wide homogeneity range extending from  $\text{VN}_{1.0}$  to  $\text{VN}_{0.71}$ . The stoichiometric phase ( $\gamma$ -VN) has been well established and its thermodynamic characteristics determined by Sato (1938), King (1949) and Brewer et al., (1950). Epelbaum & Ormont (1947), have extended the upper limit of this phase to  $\text{VN}_{1.04}$ . Besides  $\gamma$ -Vn (Cubic, NaCl) phase, there exists only one other nitride phase ( $\beta$ -phase, hexagonal), which likewise has a wide homogeneity range. Between  $\text{VN}_{0.43}$  -  $\text{VN}_{0.37}$  (10.5% - 9.3% N) the hexagonal phase alone exists, which is less stable than the cubic one.

Brauer & Schnell (1964) have re-examined the published data on the phases of the Vanadium-Nitrogen system. Hosoya & Co-workers (1968) have also studied this system using a powder of almost stoichiometric VN.

## 1.11 Niobium Nitride, NbN

### 1.11.1 Formation

A summarised account of various methods used in preparation of niobium nitride is given by Mellor (1927, p.125) and Brown (1964, p.189).

Pure niobium nitride can be prepared without difficulties by nitriding niobium metal powder with nitrogen at 1200°C (Duwez & Odell, 1950; Brauer, 1940; Brauer, et.al., 1952, 1953). Using a continuous flow method, crystalline niobium nitride can be deposited from  $\text{NbCl}_5$  vapour in the presence of  $\text{N}_2 + \text{H}_2$  mixtures on a heated tungsten filament. With an optimum filament temperature of 1340-1360°C, small silver-grey crystals are obtained (Pollard & Fowles, 1952).

Kroll and Bacon (1947) patented a method which involves separation of powdered pentoxides of Nb and Ta by nitriding at 500-800°C with ammonia or at a little below 900°C, with  $\text{N}_2 + \text{H}_2$  mixture. Niobium nitride is produced if the reaction proceeds quickly, but very little or no tantalum nitride is formed. Meerson et.al., (1966) have prepared the nitride also from its pentoxide.

If a compressed mixture of equimolecular proportions of niobium nitride and niobium metal is heated at 1700°C for 15 minutes, the pale-grey heminitride ( $\text{Nb}_2\text{N}$ ) is obtained. This substance is also formed if niobium wire is heated in ammonia at 1400-1800°C. (Septier, et.al., 1952).

### 1.11.2 The System, Niobium-Nitrogen

The solubility of nitrogen in the niobium lattice is very small; thus Brauer & Jander (1952) found that up to about 2 atomic-% nitrogen would dissolve, giving the so called  $\alpha$ -phase. A  $\beta$ -phase corresponding to the composition range  $\text{NbN}_{0.40} - \text{NbN}_{0.50}$  (i.e.,  $\text{Nb}_2\text{N}$ ) was found to be of the common 'interstitial' structural type with the metal atoms hexagonally close-packed (Epelbaum & Ormont, 1948). A phase which is the richest in nitrogen (called  $\delta$ -phase by Schönberg) has the composition  $\text{NbN}_{1.00}$  and possesses a hexagonal lattice. A nitride of the formula  $\text{Nb}_3\text{N}_5$  has been reported way back in 1907 by Muthmann, et.al., but has not been confirmed.

Solid solubility studies have also been made on this system by Taylor & Doyle (1967), and phase transformations investigated by van Torn & Thomas (1964). The niobium-nitrogen constitution diagram has been examined from 1100 to 1450°C at 1 atmosphere nitrogen pressure (Guard, et.al., 1967). The phase diagram studies of this system have also been conducted by Elliot & Komjathy (1960).

### 1.12 Tantalum Nitride, TaN

#### 1.12.1 Formation

Mellor (1927, p.126) and Brown (1964, p.192) have summarised methods of production of tantalum nitride. The nitride, TaN, can be prepared by causing tantalum metal to react with nitrogen or ammonia; Chiotti (1952) treated tantalum metal powder with ammonia for 18 hours at 900°C, and even this procedure does not give complete conversion to the mononitride.

When the powdered pentoxide reacts with ammonia at 500–800°C or with N<sub>2</sub> + H<sub>2</sub> mixture at about 900°C, little or no TaN is formed (Bagnall, 1957). Agte & Moers (1931) mixed the pentoxide with lampblack and then caused the mixture to react with nitrogen at 2300°C.

The vapour phase deposition of tantalum nitride (TaN) from TaCl<sub>5</sub> vapour, nitrogen and hydrogen on a heated tungsten filament is reported (Agte & Moers, 1931). The deposition is difficult below 1600°C, because Ta metal is deposited in the presence of hydrogen. According to Agte & Moers (1931), it is best to work with pure nitrogen and to use filament temperatures as high as about 2,500–2,800°C. A patent method based on this principle is reported (CIBA, Ltd., 1966).

Highly nitrated films of tantalum have been prepared by cathodically sputtering high-purity tantalum in a pure nitrogen atmosphere (Coyne & Tauber, 1968). Rairden (1968) synthesized thin film of tantalum nitride on soda-lime glass substrates by the reactive evaporation process, i.e., the film was deposited by evaporation of tantalum from an electron-beam heated source in a nitrogen atmosphere at pressures of 10<sup>-4</sup> - 10<sup>-3</sup> torr. Another vacuum deposition method is given by Gaydou (1967). Goon (1969) has described preparation of TaN powder by hydriding Ta, milling to a fine powder, dehydriding and then nitriding under conditions to avoid sintering. Preparation of TaN by means of a nitrogen plasma jet has been reported (Matsumoto & Hayakawa, 1966). The red nitride 'Ta<sub>3</sub>N<sub>5</sub>' has been prepared from pure Ta<sub>2</sub>O<sub>5</sub> and extra pure gaseous ammonia

at 860-920°C in the presence of titanium shavings as oxygen getter (Brauer & Weidlein, 1965).

#### 1.12.2 The System, Tantalum-Nitrogen

In this system the existence of the compound TaN with hexagonal close-packed structure appeared well established. Chiotti(1952), however, presented evidence indicating that the structure attributed to TaN is actually that of Ta<sub>2</sub>N. The same conclusion has also been reached by Rundle (1948) from theoretical considerations. The 'Ta<sub>2</sub>N' phase has a homogeneity range of TaN<sub>0.5</sub> - TaN<sub>0.41</sub>, while the 'TaN' phase has a homogeneity range of TaN to TaN<sub>0.99</sub>.

Investigations pertaining to the solubility of nitrogen in tantalum has been carried out by Griffiths & Pryde (1967), Osthagen & Kofstad (1963) & Bakish (1958). The equilibrium studies in the system tantalum-nitrogen have been reported by Gebhardt et.al., (1961) and U.S. Air Force Technological Division in 1966.

#### 1.13 Chromium Nitride, CrN

##### 1.13.1 Formation

Preparative methods have been described briefly by Mellor (1927, p.126) and Brown (1964, p.197).

Chromium nitride (CrN), can be prepared by the direct combination of nitrogen and chromium at 900°C and 25 atmospheres, (Neumann, et.al., 1931; Duparc et.al., 1930). Kiessling & Liu (1951) report the formation of Cr<sub>2</sub>N as well as CrN by reaction of chromium borides with dry ammonia. At 735°C only CrN is obtained;

between 800° and 1100°C both nitrides are formed whilst at 1,180°C, only Cr<sub>2</sub>N is formed. Arkharov et al., (1959) confirm that nitridation of chromium below 1030° produces layers of the two different phases, a thicker inner layer of Cr<sub>2</sub>N and a thinner outer layer of CrN.

De Gelis (1966) has been able to prepare the nitride by the action of ammonia on chromium (III) chloride. The latter, in finely divided state, is heated to above 500°C under vacuum and ammonia is added from a reservoir to maintain 1 atmospheric pressure. Another method patented by Gooding & Parratt (1965) involves sintering of chromium metal powder in hydrogen atmosphere for 24 hours and then nitriding in a furnace with nitrogen, also for 24 hours at an optimum temperature range of 1400-1450°C.

The formation of textured chromium nitride layers on chromium (produced in vacuo by condensation on Mo-plates from the vapour phase) has been studied by Vasyutinskii et al., (1962). The hemi-nitride (Cr<sub>2</sub>N) has been obtained also by treating chromium metal powder with nitrogen and hydrogen gas mixture in the temperature range 1100-1310°C (Schwerdtfeger, 1967).

#### 1.13.2 The System, Chromium-Nitrogen

The two nitrides of chromium, Cr<sub>2</sub>N and CrN are now well-established compounds. Blix (1929) has made an X-ray study of a series of chromium-nitrogen products which had been prepared by heating electrolytic chromium in a stream of ammonia at 900°C. He concluded from his work that the solid solubility of nitrogen in chromium can

be only low. According to Brick & Creevy (1940), liquid chromium dissolves at atmospheric pressure 4 per cent by weight of nitrogen. Blix (1929) also revealed the existence of two intermediate phases in the system. In one of these, corresponding to  $\text{Cr}_2\text{N}$ , the nitrogen atoms have random interstitial positions in the hexagonal close-packed Cr-lattice. Eriksson (1934) observes that this hexagonal phase ( $\text{Cr}_2\text{N}$ ) has a "super-structure" with a volume three times that of the close-packed hexagonal lattice. The other phase reported by Blix (1929) corresponds to CrN and has the cubic sodium chloride structure.

The equilibrium studies on the system Cr-Cr<sub>2</sub>N-CrN have been performed by Mills (1967). He has reported that Cr<sub>2</sub>N and CrN both exhibit a homogeneity range; the upper limit of Cr<sub>2</sub>N is 11.35 weight %N, which is less than the stoichiometric value of 11.87 weight % nitrogen. The lower limit varies from 10.45 wt % N at 950° to 8.7 wt. % N at 1200°C.

#### 1.14 Molybdenum Nitride, MoN

##### 1.14.1 Formation

Mellor (1927, p.128) and Brown (1964, p.200) have summarised the various production methods used to obtain molybdenum nitride. The reaction between molybdenum and nitrogen proceeds at a correspondingly lower rate than the one between chromium and nitrogen. Henderson & Galletly (1908) reported that by reaction of metallic molybdenum with ammonia at 850°C, only a small portion of the metal is transformed into nitride. An X-ray investigation of the products of the action of nitrogen on molybdenum at

temperatures between 400°C - 1000°C showed no indication of nitride formation (Ghosh, 1952). Hägg (1930) nitrated very pure molybdenum for 4 hours in a porcelain tube furnace with ammonia between 400-725°C. The amount of nitrogen in the product ranged from 0.77 weight-% to 7.15 weight-% or 5.1 atomic-% to 34.6 atomic-%, respectively.

By carrying out the nitrating reaction for periods up to 120 hours at 700°C, Hägg (1930) was able to obtain products with nitrogen contents of up to 48 atomic-%.

A patent method for obtaining molybdenum nitride consists of passing anhydrous ammonia on heated finely-powdered molybdenum oxide (Oswald, 1950). Molybdenum plate and wire annealed at 1400°C absorb only very small quantities of nitrogen between 900 and 1200°C (Sieverts & Zapf, 1936). Unannealed molybdenum wire, however, absorbs much greater quantities of nitrogen. Sieverts & Zapf (1936) also report that on cooling unannealed molybdenum wire that has dissolved nitrogen at higher temperatures, a nitride phase separates; this can be demonstrated microscopically and by X-rays.

Matsumoto (1966) prepared Mo<sub>2</sub>N by the nitrogen plasma jet in a 40% yield. The maximum surface temperature of Mo was 2900°C.

#### 1.14.2 The System, Molybdenum-Nitrogen

A phase diagram of the molybdenum-nitrogen system constructed by Hägg has been reproduced by Brown (1964, p.202). Hägg (1930) based his investigations on X-ray measurements on the products obtained by treatment of the pure metal powder with ammonia at



temperatures from  $400^{\circ}\text{C}$  to  $725^{\circ}\text{C}$  for periods of up to two days.

He has reported four phases:—

- (i)  $\alpha$ - phase representing the solubility of nitrogen in molybdenum which is very small.
- (ii)  $\beta$  - phase, which is stable only above  $600^{\circ}\text{C}$ . The homogeneity range lies at about 28 atomic % of nitrogen. The metal atoms form a face-centred tetragonal lattice. Hägg could not ascertain the positions of the nitrogen atoms.
- (iii)  $\gamma$  -phase at temperatures below  $600$ - $700^{\circ}\text{C}$ . This phase has a narrow homogeneity range in the region of 33 atomic % N, corresponding to formula  $\text{Mo}_2\text{N}$ . The metal atoms form a face-centred cubic lattice
- (iv)  $\delta$  - phase which exists at about 50 atomic % of nitrogen, corresponding to the formula  $\text{MoN}$ . The metal atoms form a single hexagonal lattice; the weak extra lines in the X-ray diagram indicate the existence of a super-lattice. According to Pauling et.al., (1952), the distance of  $2.16\text{\AA}$  between molybdenum and nitrogen atoms in this phase agrees with the assumption of half-bonds.

The work of Hägg has been confirmed in all respects by Schönberg (1954). He has found that the  $\delta$  - phase is a super-structure containing 8 MoN molecules. It is also suggested that in this phase the non-metal atoms are situated at the centres of trigonal prisms (largest interstices) of metal atoms.

## CHAPTER II

### EXPERIMENTAL TECHNIQUES

The experimental techniques employed in this work, including the principles underlying them and a description of the relevant apparatus, are described briefly in this chapter.

#### 2.1 X-ray Diffraction

An extensive account of the theory and practice of X-ray diffraction techniques is given by Peiser and Coworkers. (1960, pp. 27-322).

##### 2.1.1. Theory of X-ray Diffraction

A crystal consists of a regular three dimensional network of atoms in space. Points having identical surroundings in the structure are called lattice points, and a collection of such points in space form the crystal lattice. If the neighbouring lattice points are joined together, the unit cell is obtained. It is the smallest repeating unit of the structure. In general the unit cell is a parallelepiped, but in some cases, depending on the symmetry of the crystal, it can have more regular shape, e.g., a rectangular box, or in the extreme case, a cube. The shape of the unit cell is completely described by the length of its three edges or axes and the angles between them. By convention, the axes are named  $x$ ,  $y$ ,  $z$  or  $a$ ,  $b$ ,  $c$  and the angles  $\alpha$ ,  $\beta$ ,  $\gamma$ . The angle between  $y$  and  $z$  is  $\alpha$ , and so on.

Crystals have been classified into seven classes depending on their symmetry. The unit cell dimensions of a crystal obey some relationships according to the crystal class. These relationships are presented in Table 2.1

TABLE 2.1 Classification of Crystals

Crystal Class	Conditions Limiting Cell Dimensions	Minimum Symmetry
Triclinic	$a \neq b \neq c$ ; $\alpha \neq \beta \neq \gamma \neq 90^\circ$	-
Monoclinic	$a \neq b = c$ ; $\alpha = \gamma = 90^\circ \neq \beta$	one 2-fold axis or one plane of symmetry
Orthorhombic	$a \neq b \neq c$ ; $\alpha = \beta = \gamma = 90^\circ$	Two perpendicular 2-fold axes or two perpendicular planes of symmetry
Tetragonal	$a = b \neq c$ ; $\alpha = \beta = \gamma = 90^\circ$	one 4-fold axis
Hexagonal	$a = b \neq c$ ; $\alpha = \beta = 90^\circ, \gamma = 120^\circ$	one 6-fold axis
Trigonal	$a = b = c$ ; $\alpha = \beta = \gamma \neq 90^\circ$	one 3-fold axis
Cubic	$a = b = c$ ; $\alpha = \beta = \gamma = 90^\circ$	Four 3-fold axes

It is possible to draw various sets of parallel planes through the lattice points of a crystal. Each set of parallel planes is identified by a set of three integers, namely, the Miller indices,  $\underline{h}$ ,  $\underline{k}$ ,  $\underline{l}$ , corresponding to the three axes  $\underline{a}$ ,  $\underline{b}$ ,  $\underline{c}$ , respectively. The index  $\underline{h}$  is the reciprocal of the fractional value of the intercept made by the set of planes on the  $\underline{a}$  axis, and so on.

When an incident beam of X-rays impinge on a crystal, they are scattered by the atoms. Since the scattered radiation results from the acceleration and deceleration of electrons set in motion by the X-rays, it has the same wave-length as the incident X-rays. This fact plus the regularity of the pattern of atoms in a crystal, permits the crystal lattice to act as a three dimensional diffraction grating.

A diffracted beam emerges from a particular set of lattice planes when their scattering is in phase. This is governed by Bragg's Law:

$$\lambda = 2 d \sin \theta$$

Where,  $\lambda$  = Wavelength of X-rays

$d$  = interplanar spacing

and  $\theta$  = angle of incidence = angle of diffraction

$d$  is related to the unit cell dimensions of the crystal and the Miller indices of the set of planes. Hence, the measurement of Bragg angles can lead to the determination of lattice parameters.

When the crystal is large, i.e., there are a large number of lattice planes in each set, the diffracted beam appears at a sharp angle. However, with appreciably small crystals, diffraction takes place over a range of Bragg angle. The X-ray line broadening provides information on crystallite size.

If a single crystal of a substance is rotated in a beam of monochromatic X-rays, the diffraction pattern forms a series of spots on a photographic film. However, if the sample is in the form of a powder with the crystallites in random orientation, the diffracted beams lie along the surfaces of a set of coaxial cones. The pattern can then be recorded photographically in a powder camera, or by scanning with a radiation detector, (e.g., Geiger counter) moving continuously around the diffractometer table.

The distribution with respect to Bragg angles and intensities of the diffracted beams is characteristic of a particular structure and can be used therefore as a means of identification. The X-ray

powder diffraction patterns of most of the crystalline substances are recorded in the A.S.T.M. to which reference can be made to identify "unknown" substances. The powder pattern of a mixture of crystalline substances consists of the superimposed patterns of the individual structures. Thus, the method can be used to identify the different components of a mixture also.

### 2.1.2. X-ray Generators

Two X-ray generators of different designs were used for the diffraction experiments, namely, (a) a Solus-Schall unit connected to a sealed tube containing the filament and target, (b) a Raymax 60 generator manufactured by Newton Victor Limited, with interchangeable target and replaceable filament and kept continuously pumped by an oil diffusion pump coupled to a rotary pump. A sealed tube generator has a more stable X-ray output than a continuously pumped one. The radiation used was the well-known Copper  $K_{\alpha}$ , wavelength  $1.542\text{\AA}$ . This was obtained by having a copper target and a nickel filter to remove the  $k_{\beta}$  component.

### 2.1.3. Debye-Scherrer Powder Diffraction Camera

The phase compositions of crystalline samples were investigated by recording their powder diffraction patterns in two ways, (1) by a photographic method, and (2) by using an X-ray diffractometer with attached counter and ratemeter.

For the photographic method of recording diffraction data, a Debye-Scherrer camera, of 9 cm diameter and manufactured by Unicam Instruments Ltd., was used. The strip of film was mounted according to the Van Arkel Method. The specimen for X-ray investigation was

prepared by loosely filling a glass capillary tube - about 0.5 mm in diameter and 1 cm. in length - with the crystalline powder, and sealing both ends of the capillary tube with an adhesive. The sample was mounted vertically along the camera axis and necessary alignment was made by means of two push-pull screws set at right angles to each other. The specimen was rotated about the camera axis consequently bringing each set of lattice planes of every crystallite to a diffracting position several times during an exposure. In this way, variations in the incident X-ray intensity were accounted. To avoid the scattering of X-rays by air the camera was evacuated by having it continuously pumped during the exposures which varied up to several hours. The powder camera was used in conjunction with the Raymax-60 generating unit.

Kodirex X-ray films were used in the powder camera. After exposure the film was developed for 5 minutes at 20°C in Kodak D-196 developer, rinsed with water, fixed in Kodak FX-40 fixer, washed in running water for  $\frac{1}{2}$  hour and hung up to dry. The fixing time was twice the time required for the milkiness on the film to disappear. This was usually about 5-6 minutes. The films were examined and measured on an illuminated screen fitted with a scale. The intensities of the powder diffraction lines were visually compared.

#### 2.1.4. The Counter Diffractometer

The counter diffractometer gives a direct, simple and accurate measurement of Bragg angles of the various reflections in the powder

diffraction patterns. This method was used extensively in this work as it has the added advantage of rapid determination and interpretation of interplanar spacings. A Solus Schall X-ray diffractometer fitted with a Geiger counter and connected to a Panax ratemeter and an Elliot chart recorder was used. The diffractometer works on the focussing principle described by Bragg & Brentano. The diameter of the diffractometer is 50 cm.

The sample for examination was prepared by pouring a suspension of the crystalline powder in acetone onto a glass slide. Generally it was necessary to mix an adhesive with the suspension to ensure the adherence of the powder to the glass slide when the organic solvent evaporated. The glass slide containing the flat specimen was mounted vertically at the centre of the diffractometer on a circular specimen table and rotated at half the speed of the detector. The X-rays, generated in a sealed tube unit, passed through a collimator diaphragm on to the specimen. The reflected X-rays from the sample are incident on the counter diaphragm. The intensity of the diffracted radiation as a function of the diffracting angle,  $\theta$ , was given by the chart recorder coupled to the associated rate-meter. The full chart deflection could be made equal to 2,000 10,000 or 40,000 counts per minute to accommodate the traces of the peaks. To give reasonably smooth traces, a time constant of 25 seconds was used for the most expanded scale (2,000 c.p.m) and 5 seconds for the other two scales. Since the peaks are recorded at different times by the diffractometer, it is necessary to have a stable incident beam of X-radiation. Hence the sealed-off tube type generator with a copper target was used with the diffractometer. It was necessary

to use nickel filter to remove  $K_{\alpha 2}$  component, for obtaining monochromatic radiation. The tube was operated at a rating of 30 KV and 10 ma. The Elliot chart recorder could be operated at either 3 inches per hour or at 30 inches per hour and records the line intensities. Both the specimen and the counter could be rotated in a clockwise or anti-clockwise direction by means of a geared electric motor having three available speeds of  $\frac{1}{3}$ , 1 and 2 angular degrees per minute. The phase composition studies of all the specimens were carried out at one angular degree per minute whilst all line-broadening investigations were made at  $\frac{1}{3}$  of an angular degree per minute. The recordings of the diffracted radiation were used for two purposes. Firstly, to qualitatively analyse the original nitride samples and their oxidation products for their phase composition. Secondly, to estimate the amount of line-broadening by measuring the intensity and breadth of the reflections of the appropriate samples i.e., ball milled nitrides. The measurements on these specimens were made as follows. The best smooth line was drawn through the statistically fluctuating pattern recorded on the chart. In order to obtain the intensity of a particular peak, the mean background level on either side of the peak was subtracted from the intensity at the maximum peak height. The breadth of the peak was measured at half-maximum intensity. This measurement was carried out, with a ruler, to a precision of about 5 per cent of the breadth.



### 2.1.5 X-ray Line Broadening

The lines or peaks in a diffraction pattern are always broadened due to instrumental causes (e.g. the finite slit-width of a counter diffractometer). In addition, there may occur an intrinsic broadening, i.e., a broadening associated with small crystallite size or crystal lattice strain of the sample. The ground nitride samples gave such intrinsically broadened lines. A discussion of the causes of line broadening has therefore been included.

#### 2.1.5(a) Broadening due to small crystallite size

If the linear dimensions of the crystallites in a specimen fall below about  $1000\text{\AA}$ , appreciable intrinsic broadening of the lines will result. The mean crystalline dimension ( $D$ ) normal to the diffraction planes is related to the intrinsic broadening ( $\beta$ ) by the Scherrer equation (1918),

$$D = \frac{K \lambda}{\cos \theta}$$

Where,  $K$  = the Scherrer constant, approximately equal to unity.

$\lambda$  = the wave length of the X-rays

and  $\theta$  = the reflecting or "Bragg" angle (Peiser et.al. 1955, p.413)

The value of  $K$  depends on the way the line width  $\beta$  is measured (integral breadth or breadth at half-maximum intensity). The shape and size distribution factors for the crystallites, as well as the shape and breadth of the diffraction profile affect the value of  $K$ . In view of the fact that little is usually known about these factors, the absolute accuracy with which one can calculate the crystallite

dimensions cannot be expected to exceed the range of 25 to 50 per cent. For this reason the value of D is often called the apparent crystallite size. The relative values of D, particularly for a related series of specimens, will in general be reliable to appreciably greater extent.

According to the recommendation by Kug and Alexander (1954), the widespread practice of putting K equal to unity has been adopted in the present work. This has been claimed to provide an easy comparison of the most published investigations in this field.

#### 2.1.5(b) Broadening due to Lattice Distortion

The mean lattice distortion or lattice strain ( $\epsilon$ ) normal to the diffracting planes is related to the intrinsic broadening ( $\beta$ ) by the relation.

$$\epsilon = \beta \cot \theta$$

The broadening is caused by variations in the dimensions of the unit cell. The strain distribution factor will affect the shape and breadth of the diffraction profile. There is little information available about such a factor and thus the absolute accuracy with which the strain can be calculated will be poor. The value of  $\epsilon$  is often termed as the apparent strain component. There is also an inherent difficulty in separating the instrumental from the intrinsic line broadening which adds a further amount of uncertainty to the value of  $\epsilon$ . The same difficulty arises in the determination of D.

#### 2.1.6. Measurement of Intrinsic Broadening:-

The experimentally measured line breadth has to be corrected

twice in order to obtain the intrinsic broadening. A correction has to be made because the diffracted radiation is not monochromatic, but consists of an  $\alpha$ -doublet ( $K-\alpha_1$  and  $K-\alpha_2$ ). Instrumental broadening has also to be corrected for. Unfortunately the amounts of broadening due to various factors such as non-monochromatic, instrumental and intrinsic ones are not linearly additive. A graphical method due to Jones (1938) has been used to effect the separations. The curves are reproduced in Appendix 1 and can be used to calculate the intrinsic broadening due to the single radiation,  $K-\alpha_1$ . The symbols shown in the Appendix have the following meanings.

Radiation	Observed Breadth	Instrumental Breadth	Intrinsic Broadening
$K-\alpha_1$	B	b	$\beta$
$K-\alpha$ doublet	$B_0$	$b_0$	$\beta_0$

The angular separation,  $\Delta$ , of the  $K-\alpha_1$  and  $K-\alpha_2$  radiations is calculated using the expression, whose derivation is given in Appendix 2.

$$\Delta = \frac{360}{\lambda} \frac{\lambda \alpha_2 - \lambda \alpha_1}{\lambda_{\text{average}}} \tan \theta_{\text{average}} = C \tan \theta$$

The value of C for copper  $K-\alpha$  radiation is 0.285.

The intrinsic line broadening of the milled nitride samples were determined by comparing their X-ray powder line profiles with those of the original nitrides. The broadening of the latter samples was assumed to be entirely due to instrumental factors. This assumption is reasonable in view of the conditions of production of the nitride. At the temperatures of formation ( $> 1200^\circ\text{C}$  in most cases)

the nitride crystallites are extensively annealed and therefore free of strain. Also, because these temperatures are well above the respective Tammann temperatures of the compounds, sintering is expected to be extensive. This is confirmed by electron and optical microscopic examination of the samples and also by surface area determination by gas sorption. The surface areas of these samples were found to be mostly below  $11 \text{ m}^2 \text{ g}^{-1}$ . Further confirmation of the above assumption was made by comparing the X-ray line profiles of the nitride samples with those of the cleavage plane (2022 reflection) of a single calcite crystal. The 2022 reflection at  $14^\circ 43'$  was used mainly to standardize the diffractometer settings for each nitride.

The curve of  $\beta/B$  against  $b/B$  was derived by Jones (1938) using the function:

$$1/(1 + K^2 x^2)$$

where,  $K = \text{a constant}$

and,  $x = \text{the angular distance from the top of the peak.}$

This function describes the intensity distribution across the diffraction line obtained under ideal conditions of no instrumental broadening. The evidence available so far (Jones, 1938, 1950) suggests that this function is the best one to describe the intrinsic diffraction profile where an even distribution of crystallite sizes or strains is present. In applying the Jones' Method of correction, it was assumed that there was such a distribution of crystallite sizes or strains in the milled material.

#### 2.1.7. The Interpretation of Intrinsic Broadening

During milling, either a strained lattice or very small crystallites

or both may be produced. These in turn may give rise to intrinsic line broadening. In theory, it should be possible to distinguish between these two possible causes of broadening since:-

$\Delta \lambda / \lambda \approx \delta$  - for small crystallite broadening.

and  $\Delta \lambda / \lambda \approx \epsilon \tan \theta$  - for lattice strain broadening.

Klug and Alexander<sup>(1954)</sup> have pointed out that the task of matching the experimental data requires a precise technique and high accuracy. Further discussion of this method of separating the causes of intrinsic line broadening will be dealt with in subsequent chapters.

## 2.2 Electron Microscopy and Diffraction

Comprehensive accounts of the theory and practice of electron microscopy and diffraction are given by Hirsch et.al., (1965), Kay (1965) and Zworykin et.al., (1945).

### 2.2.1. Theory of Electron Microscopy & Diffraction

A beam of electrons possesses wave properties similar to those of a beam of electromagnetic radiation, the wavelength being given by the de Broglie relationship:

$$\lambda = \frac{h}{p} = \frac{h}{mv} \quad \dots \dots \dots \dots (i)$$

Where,

$\lambda$  = wavelength

$h$  = planck's constant

$m$  = mass of an electron

$v$  = velocity of electron

and  $p$  = momentum of the electron

If the accelerating potential difference is  $V$ , the energy,  $E$ , of an electron is given by;

$$E = \frac{1}{2} mv^2 = Ve \quad \dots \dots \dots \dots (ii)$$

Where,  $e$  = electron charge

Combining equations (i) and (ii) and eliminating  $V$ , it follows;

$$\lambda = \frac{h}{\sqrt{2 \text{ meV}}} \quad \dots \quad \dots \quad \dots \quad \text{(iii)}$$

A relativistic correction has to be applied to equation (iii) to account for the variation in the mass of the electron with velocity, which itself depends on the voltage. In practice, however, the wavelength if required, is determined by recording the diffraction pattern of a substance with known unit cell dimensions. This enables a single factor, the camera constant,  $L\lambda$ , to be calculated, where  $L$  is the effective camera length. If the same instrument, is used at the same accelerating voltage, then  $L\lambda$  remains constant. At an accelerating voltage of 100 kilovolts, the wavelength of an electronic beam is  $0.037\text{\AA}$ .

As mentioned earlier, in view of the fact that electron beams possess wave properties, they can be used in a magnifying instrument with electromagnetic fields as lenses, just as light waves are used in the optical microscope with glass lenses. The theoretical limit of resolution of a microscope is half the wavelength of the radiation used. For the electron microscope this is about  $0.02\text{\AA}$  whilst for an optical microscope it is about  $2000\text{\AA}$ . The shorter wave length of electrons enables a much greater resolution to be achieved on the electron microscope, although this is still very far from the theoretical limit.

The construction of an electron microscope, is in principle, similar to that of the optical microscope, Figure 2.1. It consists of a cathode,  $C$ , which provides a source of illuminating electrons.

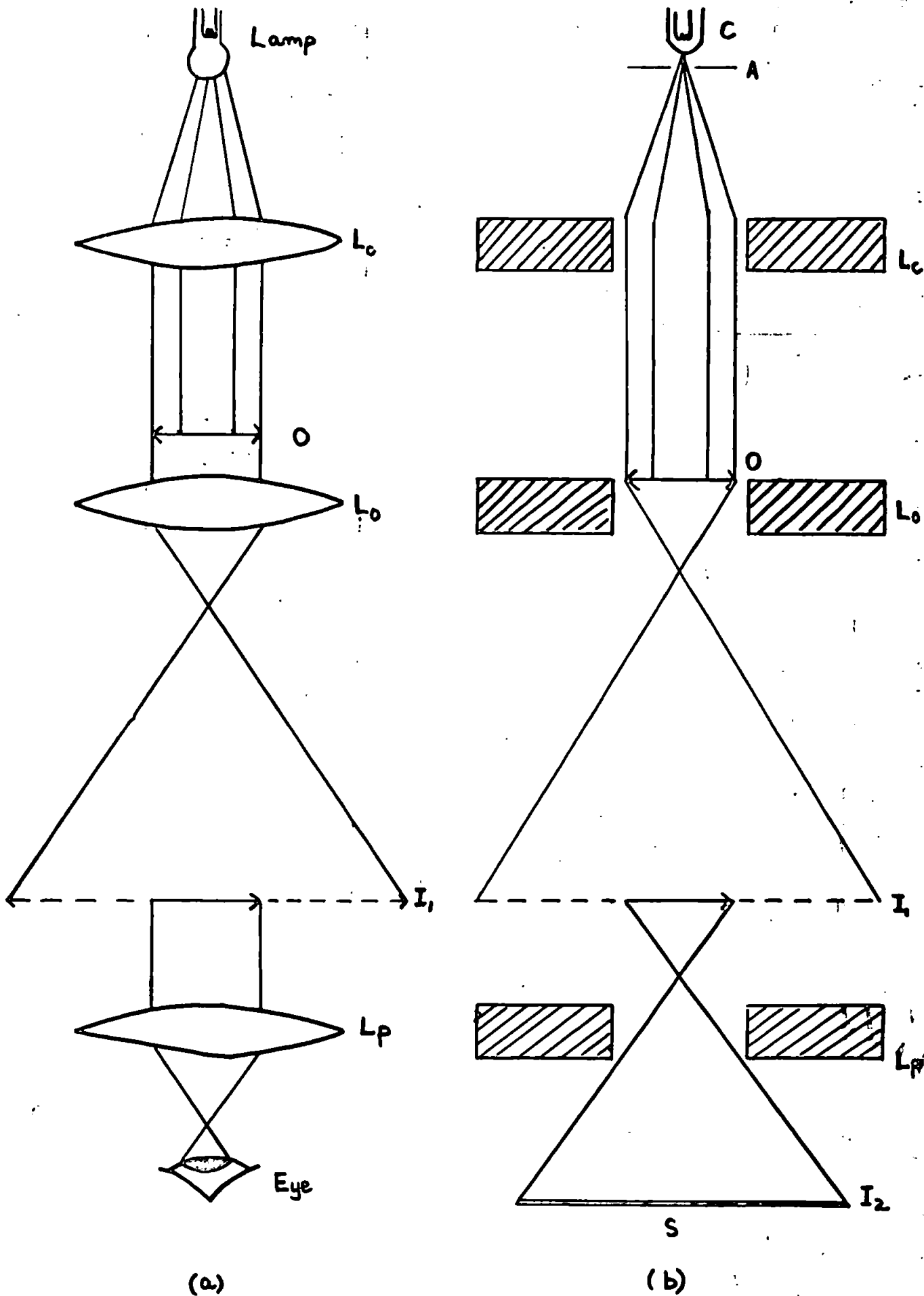


Fig-2:1. Diagrammatic analogy between (a) optical and (b) electron microscopes

A high voltage struck between C and the anode A, accelerates the electrons, which pass through a small hole in A. The condenser lense, Lc, converges the electron beam on to the specimen, O, situated in the magnetic field of the objective lens, Lo. An image, I<sub>1</sub> is formed due to magnification by the objective lens. This is followed by further magnification by the projector lens, Lp, to form a final image, I<sub>2</sub> on a screen, S. The microscope, used in this work and described in the next section, consists of two more lenses (not shown in the figure), namely a diffraction lens and an intermediate lens, placed between the objective and the projector. The intermediate lens enables a high overall magnification to be reached without the magnifications of the individual lenses having to be excessively large. It also helps to keep the length of the instrument short and to attain easily a continuously varying magnification within wide limits. The diffraction lens is energised only when diffraction patterns or low magnifications are required off the sample.

The energy of electrons is reduced when they are scattered readily on collision with gas molecules. Hence, the instrument is operated at a sufficiently low pressure (about  $10^{-6}$  mm Hg). Focussing is achieved by the variation of the strengths of the magnetic fields by changing the currents generating them. A phosphor screen is provided at the end of the tube to align and select a suitable part of the image, and the magnified image can also be recorded on to a 35 mm photographic film held in a camera within the instrument.

Electron diffraction by a crystal is similar in principle to that of X-ray diffraction, but it differs in certain respects. Because of their electrical charge, electrons are heavily scattered



by solid materials, and therefore the depth of the penetration of the electrons is relatively small (say, a few hundred  $\text{\AA}$ ). Hence only very thin crystals (of few hundred  $\text{\AA}$  thickness) can be used in contrast to X-rays which penetrate deeply and yield information about the bulk properties. The diffraction pattern of a single crystal consists of "reflections" from a plane of reciprocal lattice points. In this case, electrons, because of their very short wavelengths differ from X-rays. Nevertheless for a polycrystalline specimen in random orientation, the diffraction pattern consists of the typical concentric powder rings, provided the sample is sufficiently thin.

#### 2.2.2. The Equipment

In the present work, direct transmission and diffraction micrographs of powdered materials and transmission micrograph surface replicas of sintered refractory materials were obtained, using a Philips E.M.100B model electron microscope (Van Dorsten, Nieuwdoorn & Verhoeff, 1950). The instrument has a resolution of 25 $\text{\AA}$ , under normal operating conditions. The pumping system of the microscope consists of a prevacuum rotary pump, a mercury diffusion pump and an oil diffusion pump. The magnification is varied by adjusting the currents to the electromagnetic lenses. There are also control knobs provided for focussing and for moving the sample holder so that different regions of the grid can be observed. An image of a section of the sample is thrown on the fluorescent screen in front of the observer. The magnification of the image is determined by reading a scale and then reference is made

to standard tables. When a diffraction micrograph is required an exclusive area of the sample is selected by means of diffraction selection diaphragms; the diffraction lens is switched on and the intermediate lens switched off. Diffraction micrographs require longer exposures because of their lower intensity, whilst transmission micrographs are exposed up to a few seconds according to the brightness of the image. The microscope was usually operated at 80 KV.

Specimens were supported by thin films of carbon lying over copper grids. The carbon films were prepared in a "Speedivac" High Vacuum Coating Unit 12E6 model, manufactured by Edwards High Vacuum Ltd. The unit consists of a glass work chamber sealed with an L section Viton A gasket, evacuated by an oil diffusion pump backed by a rotary pump. Low vacuum in the work area inside the chamber was registered by a Pirani gauge and the high vacuum by a Penning gauge. The ultimate vacuum obtainable with this unit was  $3 \times 10^{-5}$  torr. The electrical supplies to the carbon electrodes and tungsten filaments were provided by a 10V, 60 amp source, the current being regulated as necessary by means of controls.

### 2.2.3. Preparation of Samples

Samples of the crystalline powders for microscopic examination were made by dispersing the particles on a carbon film supported on a copper grid. The thickness of the carbon film was roughly  $200\text{\AA}$ . A copper grid consists of a 3 mm diameter and a mesh of square windows  $100\ \mu\text{m}$  across.

The substrate used for depositing the carbon film was freshly cleaved high quality mica available from "Mica and Miconite Supplies

Ltd." The dimensions of the mica plates were 2 x 1 inches. A thin film of carbon was deposited on to the mica substrate placed inside the workchamber by striking an electric arc between two spectrographically pure carbon electrodes. The carbon electrodes were of  $\frac{1}{4}$ " diameter. The arc voltage was 10 volts and the current 60 amperes. The arc was struck in about 8 intermittent bursts, in order to cool the carbon electrodes. Each burst consisted of approximately three seconds duration. The pressure inside the chamber was of the order of  $3 \times 10^{-5}$  torr.

The carbon film was floated off on distilled water by carefully dipping the mica substrate at an angle of about  $45^{\circ}$ . This operation stripped the carbon film off the mica due to the surface tension of the water. It was facilitated by trimming the mica sheet around its edges after deposition of the film and contaminating the mica sheet by breathing heavily on to it before deposition.

A section of the floating carbon film was picked up by a copper grid. The grid carrying the film was transferred to a vertical cylindrical holder and held in position with a cylindrical cap. The latter had an open end, hence exposing the grid. Micro-crystalline samples, for direct transmission were prepared by suspending the powder in distilled water or an organic solvent which remained inert. The particles were well dispersed by means of an ultrasonic dispersion unit. A drop of the suspension was placed on the copper grid carrying the film, and evaporated to dryness under an infra-red lamp. Finally the sample was transferred into a microscope grid holder, which was inserted in the instrument.

#### 2.2.4. The Replica Technique and Shadow Casting

The principle of the replica technique involves the transfer of a surface topography of a solid body to a thin film which may be observed by transmission electron microscopy. The detail of a surface may be sharpened by shadowing with a heavy metal which absorbs electrons strongly. Where the surface detail was of particular interest; carbon replicas with a shadow casting of palladium metal were prepared as follows:

A little amount of a polystyrene polymer was melted on a glass slide, which was held over a bunsen burner, until the polymer is melted. The appropriate surface of the sintered sample is pressed into the clear melt and allowed to cool, when it solidified. The sintered sample surface thus transferred its features and impressions on to the solidified polymer, which was fixed inside the vacuum unit and a carbon film was deposited on it, as described above. The film replica so produced was then shadowed i.e. coated with a film of palladium placed inside a helical tungsten filament. On passing a heavy current through the filament, the thin palladium metal wire evaporated and struck the film replica obliquely. In this manner, the surface structure was highlighted. The polymer was dissolved away, using 1:2 dichloroethylene. The film was picked up on a copper grid, dried under infra-red lamp and the specimen was ready for examination, under the electron microscope.

Before each evaporation operation with the filament, the latter was "flashed" i.e., its temperature was raised to remove dirt etc., by passing slightly higher current through it than was subsequently used for metal evaporation.

On completion of a set of exposures the film camera was removed from the microscope, and developed in a fine grain developer to give optimum contrast. Prints were made from the "negative" on to Kodak bromide paper noting the magnification factor of the enlargement from its negative. In this manner magnifications of over 70,000 times the original size were obtained.

### 2.3 Optical Microscopy

The determination of particle sizes of specimens was carried out by a Polarising Microscope (Manufactured by Vickers Ltd.) This is the only method in which direct observation can be made of the particle size, (B.S. 3406, 1963). Examination of the samples under reflected light, using a high power objective (magnification x 40) gave an approximate estimation of single crystallite and aggregate sizes and shapes. A graticule (as described in B.S. 3625, 1963) was mounted in the eye piece (magnification x 10). The magnified image formed by the high power objective in the plane of the graticule was viewed through the eye-piece. The total magnification obtained was x 400. Reference open circles, closed circles and the rectangles inscribed on the graticule were matched with particles having approximately the same area. The dimensions of the graticule were calibrated by means of a stage micrometer.

### 2.4 Surface Area Measurement by Gas Sorption

A most important quantity to be determined in this investigation is the specific surface (i.e. the surface area per unit mass). The amount of gas adsorbed on a solid depends on the specific surface of the solid. The mean particle size of a specimen can readily be calculated from its specific surface. Thus by

measuring the true extent of the surface of the solid under consideration, the changes in particle size produced by milling or sintering can be followed. A general account of the technique is given by Gregg & Sing (1967). Refer also de Boer (1969) and Joy (1969) & British Standards 4359 Part I (1969).

#### 2.4 1. BET Procedure

To determine the specific surface of a solid from the nitrogen sorption data, the well-known and widely used method due to Brunauer, Emmett & Teller (1938) has been used. Although the method is open to several criticisms, it is the one very often used when comparing the specific surfaces of a series of related solids.

The B.E.T. equation is usually expressed in the linear form,

$$\frac{p}{x(p_0 - p)} = \frac{C}{x_m C} \cdot \frac{p}{p_0} + \frac{1}{x_m C}$$

where,

$p$  = pressure of adsorbate vapour in equilibrium with adsorbent.

$p_0$  = saturated vapour pressure of vapour adsorbed.

$x$  = amount of vapour adsorbed, ( $g.g^{-1}$ , or c.c.  $g^{-1}$ )

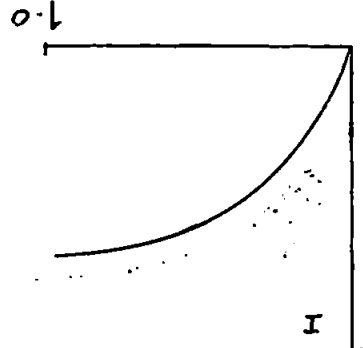
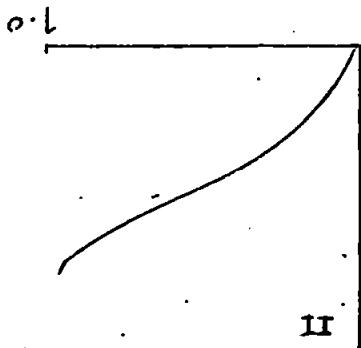
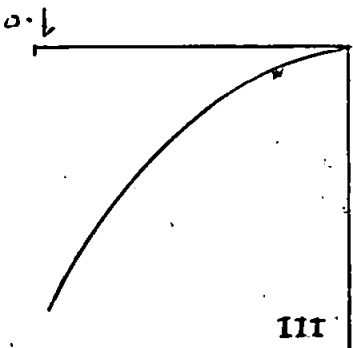
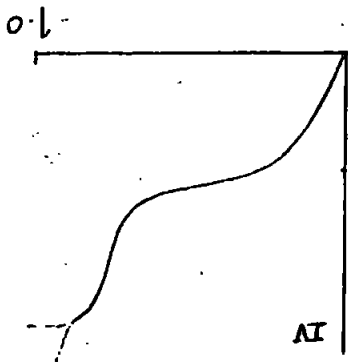
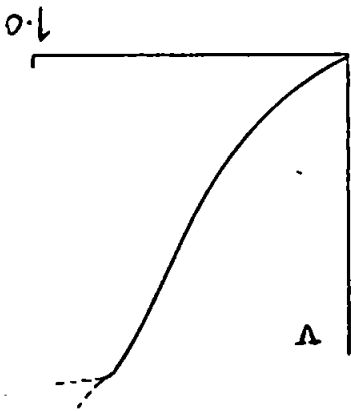
$x_m$  = capacity of filled monolayer, ( $g.g^{-1}$  or c.c.  $g^{-1}$ )

$C$  = a constant, related to the heat of adsorption

There are five principal types of adsorption isotherms as illustrated in Figure 2.2. The type II isotherms give the best agreement with the BET equation over limited ranges of relative vapour pressure (Gregg, 1961 pp.31, 56). Thus a plot of  $\frac{p}{x(p_0 - p)}$

BET Classification  
Five Types of Adsorption Isotherms in the

Relative Pressure ( $P/P_0$ ) →



Amount adsorbed →

Figure 2.2

against  $p/p_0$  results in a straight line of slope  $\frac{C-1}{x_m C}$  and

intercept  $\frac{1}{x_m C}$ . Elimination of  $C$  from these two expressions gives

$x_m$ . The region of relative vapour pressure ( $p/p_0$ ) over which a straight line is obtained is not very great. For a type II isotherm, the values of  $p/p_0$  varies between the limits 0.05 to about 0.3. The adsorbate vapour can be measured either gravimetrically or volumetrically (Gregg & Sing, 1967, p.310)

The specific surface,  $S_g$ , is related to  $x_m$  by the equation:-

$$S = \frac{x_m}{M} \cdot N \cdot A_m$$

where,

$M$  = molecular weight of adsorbate,

$N$  = Avogadro number,

$A_m$  = cross sectional area of an adsorbate molecule in a completed monolayer.

If the specific surface ( $S_g$ ) of a powder is known, the average crystallite size,  $\bar{r}$  assuming that all the particles are spherical can be easily determined.

$$S_g = \frac{4\pi(\bar{r}/2)^2 \cdot n}{4/3\pi(\bar{r}/2)^3 \cdot n \rho} = \frac{6}{\bar{r} \rho}$$

where,  $n$  = number of particles per gram of solid

and  $\rho$  = the density of the solid (adsorbent).

The assumption that all the particles are cubic leads to the



same expression, similar relationships can be derived for plate and needle-shaped crystallite powders.

#### 2.4 The Apparatus

The sorption balance used in this work is based on one designed by Gregg (1946, 1955). The balance arms are made of glass and supported on sapphire needles set into a glass cradle. One arm of the balance supports buckets for the sample and counterweights the other arm either a solenoid or magnet enclosed in glass and surrounded by an external solenoid. The whole assembly is encased in glass and connected to a system of evacuation pumps, gauges and gas reservoirs. The balance used for low temperature nitrogen adsorption as described by Glasson (1956) and B.S. 4359, Part I (1969) and is shown in Figure (2.3).

The current in the external solenoid is varied to obtain the null point, which is observed by noting the position of a horizontal metal pointer attached to the balance arm against a similar fixed pointer. The instrument is calibrated by measuring the current required to observe the null point for known weight.

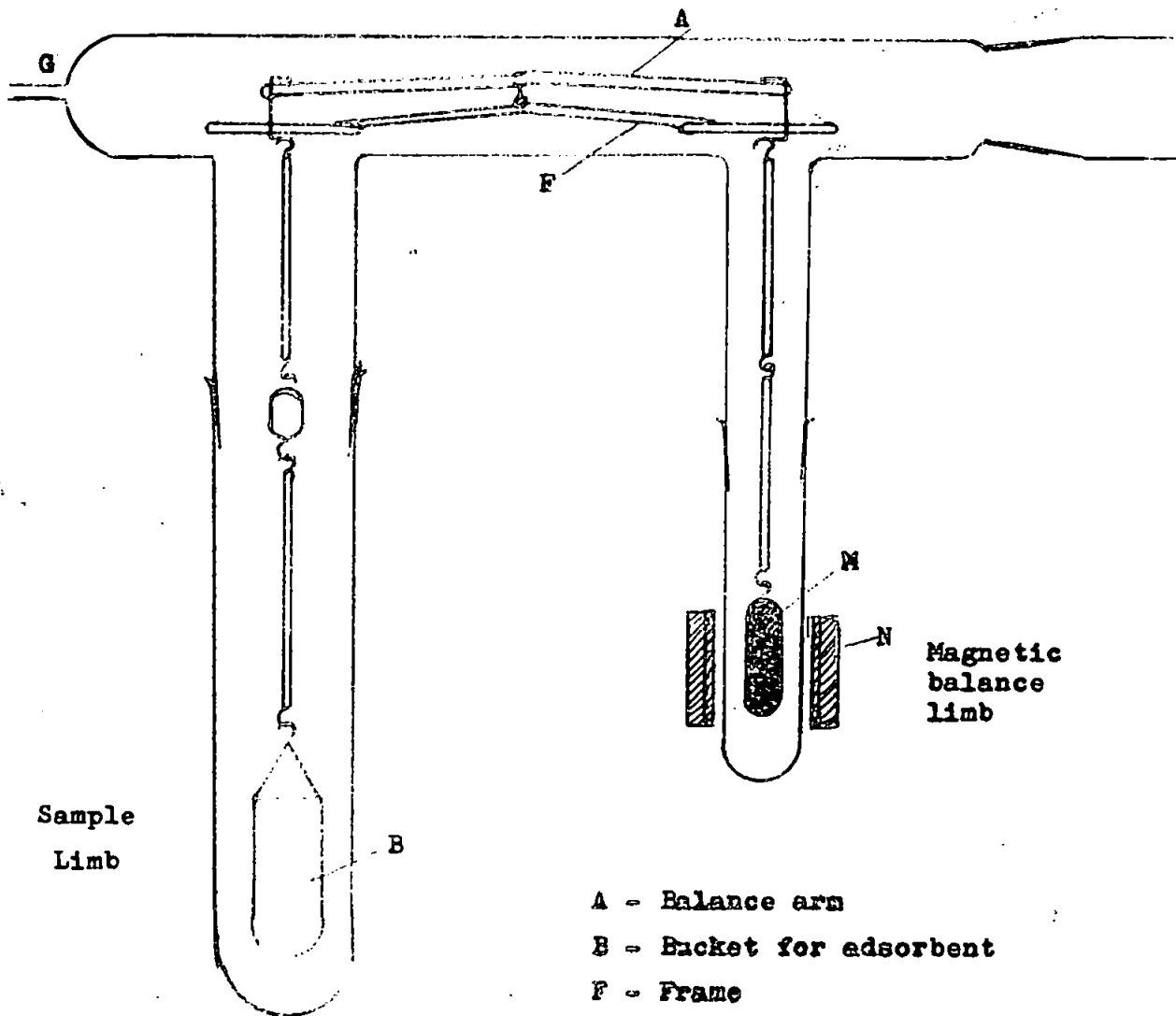
#### 2.4.3. Measurement of Sorption Isotherms

The samples for which specific surfaces were to be determined, were placed in the specimen bucket and outgassed to remove physically adsorbed vapour. This was usually carried out at 200°C by surrounding the balance limb with a furnace (Glasson, 1964a).

The adsorbate was nitrogen gas (supplied by BOC Ltd.). Boiling liquid oxygen contained in a Dewar flask was used as a coolant, so that the isotherms were measured at  $-183^{\circ}\text{C}$ . The weight of the sample

Figure 2.3.

The gas sorption balance



Magnetic  
balance  
limb

Sample  
Limb

- A - Balance arm
- B - Bucket for adsorbent
- F - Frame
- G - Connection to gas handling system
- M - Permanent magnet or solenoid
- N - Solenoid

was determined in vacuo, and doses of nitrogen were introduced into the system. Simultaneous readings of sample weight and nitrogen gas pressure were taken after equilibrium was reached. To obtain the desorption branch of the isotherm (if necessary), increments of the nitrogen vapour were pumped away and the changes in the weight of the sample again followed.

All the weight changes had to be corrected for buoyancies of the samples and their containers. These were determined from experiments using materials of known X-ray density and negligible surface area.

## 2.5 Thermoanalytical Techniques

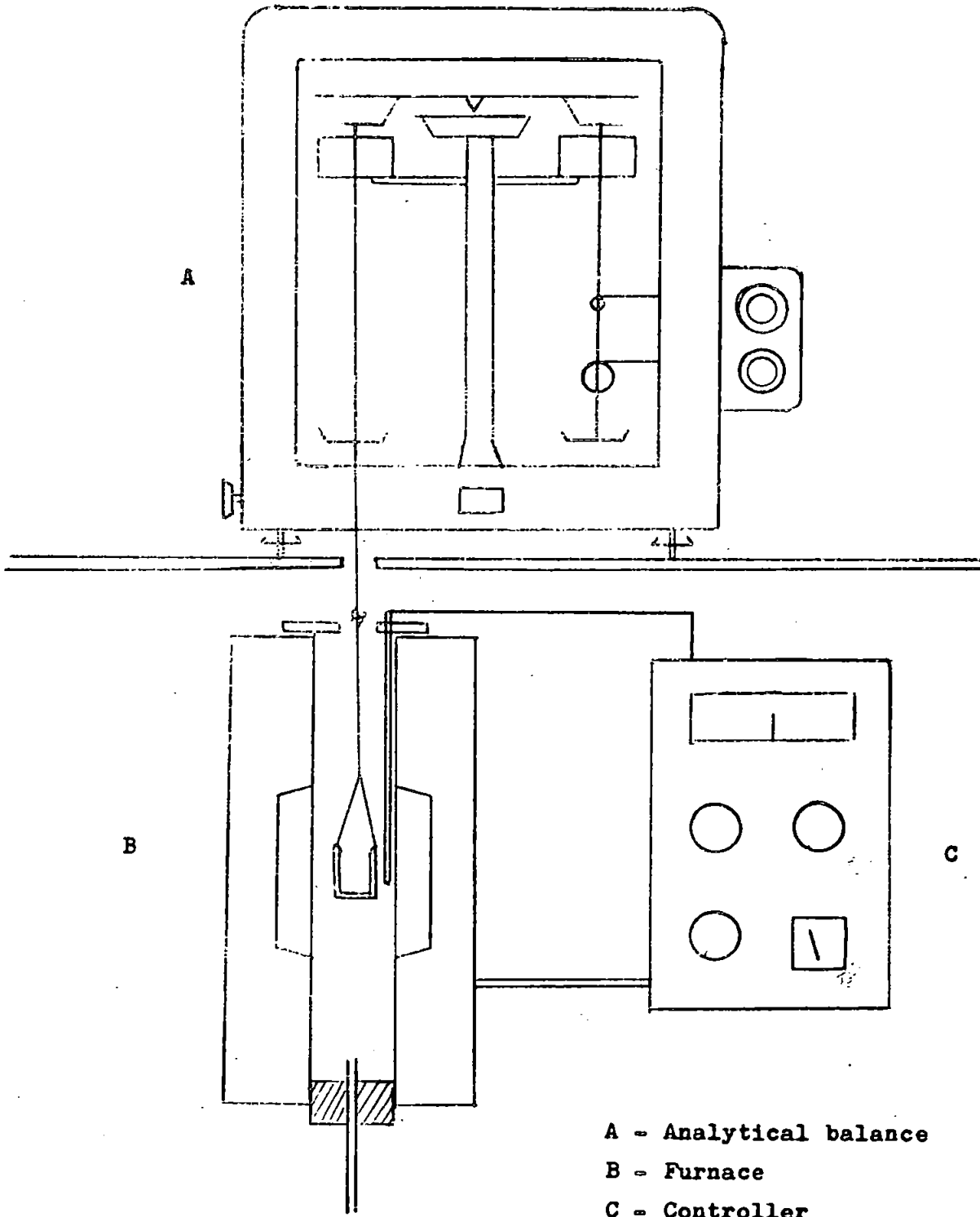
The technique of thermogravimetric analysis at a series of fixed temperatures in air has been used extensively in this work as a tool for the detailed analysis of thermal reactions involving fine particles (Gregg & Sing, 1952; Gregg & Wheatley, 1955; Gregg & Packer, 1955). In this technique the weight gain or loss of a sample can be continuously followed over a period of time while the temperature is maintained constant.

### 2.5.1. Thermal Balances

The thermal balance usually consists of a modified single or double pan analytical balance (Gregg & Winsor, 1945). In the present investigation, a Stanton-Redcroft Model A 49, balance was used, which could detect a weight change of  $10^{-4}$  gram. One pan of the balance was furnished, on its underside, with a hook carrying a length of nichrome wire. The wire passed through a hole in the balance shelf and supported a sample bucket, made of silica

Figure 2.4.

Thermal gravimetric analysis apparatus



which was suspended in an electric furnace. The temperature in the vicinity of the sample was measured using a chromel-alumel thermocouple placed close to the sample bucket and attached to a milli-volt meter. (Baird and Tatlock-Resilia). The general arrangement is shown in Figure 2.4.

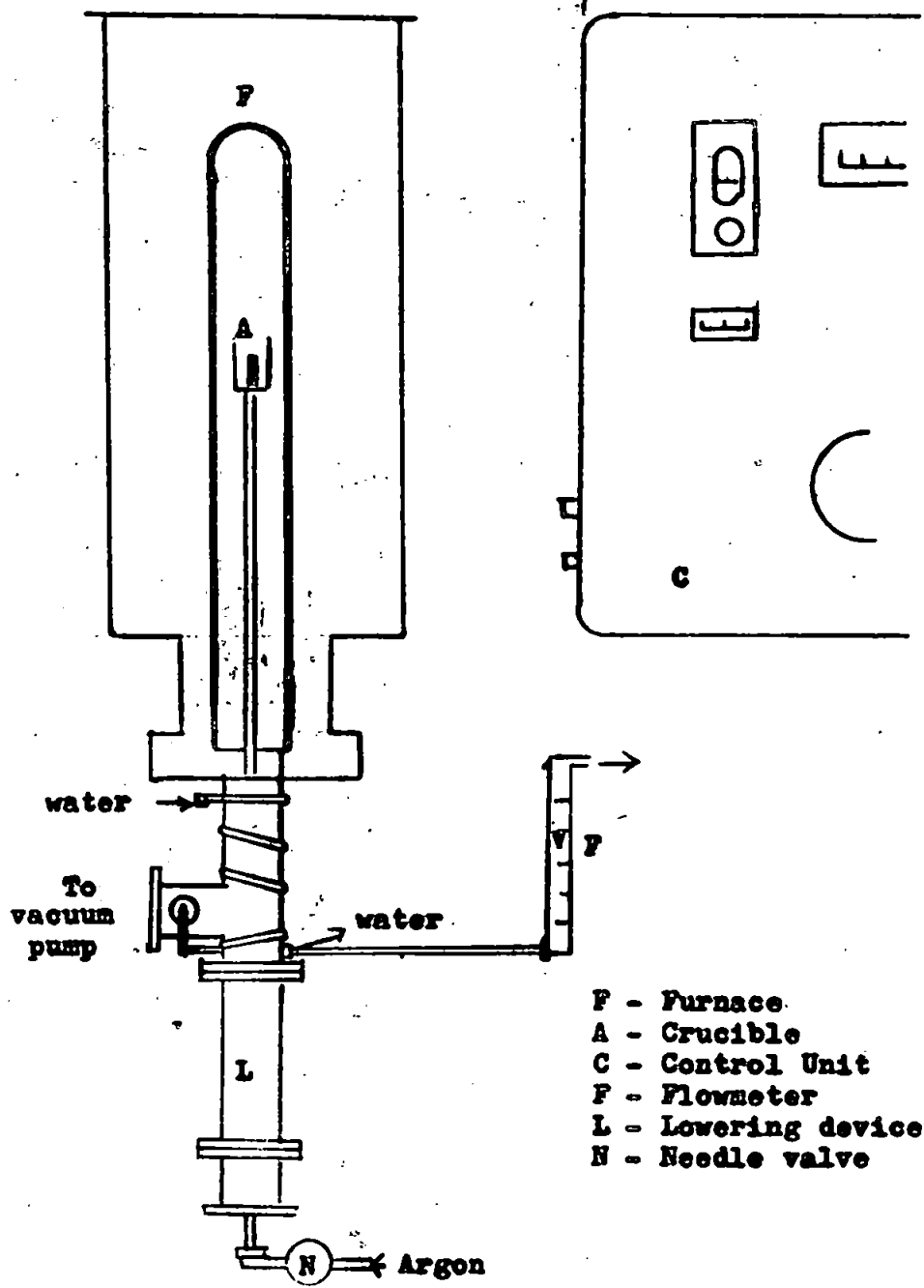
The main kinetic study was carried out by determination of the weight gain on 1 gram of a sample. The furnace is pre-stabilised at the required temperature, and the sample is introduced into it. The weight of the sample was recorded at known intervals of time. Samples of unmilled and milled nitrides were studied at a series of suitable fixed temperatures. The weight gains of the specimen were plotted against the corresponding time to provide oxidation rates from these isotherms.

Newkirk (1960) has shown that changes in the buoyancy of the sample and the bucket and the convection currents inside the furnace can cause apparent weight changes. This effect is more pronounced in dynamic thermogravimetry i.e. the one in which the sample is heated under a continuous rate of increase of temperature. In case of isothermal weight-change determination (or static thermogravimetry) this effect has been assumed to be negligible.

#### 2.5.2 High Temperature Vacuum Furnace

The metals Research High Temperature Laboratory Furnace comprises a fully sealed element assembly housed in a water cooled case containing alumina insulating powder. The element assembly consists of an impervious alumina sheath, having a molybdenum element wound externally and placed concentrically inside a larger sheath of the same material. The sheaths are joined by a water-cooled metal

Figure 2.5. High temperature Laboratory Furnace  
(Metals Research, Type PCA10)



header, which completes the assembly and seals the annular space through which the hydrogen is passed to protect the molybdenum winding. A W/W-Re thermocouple is positioned in the annular space close to the centre of the furnace winding.

A complete displacement of air from the interior of the furnace is ensured by passing hydrogen gas at least for an hour before the power supply is switched on. This gas flow is maintained until the furnace is completely cold after a run, otherwise contraction of the gas in the furnace on cooling will permit air to be drawn into the element assembly with consequent oxidation of the element. The flow rate of nitrogen gas, used for nitriding the Ti-base alloys, was controlled by a gas flow meter.

A schematic illustration of this furnace is presented in Figure 2.5.

### 2.5.3 Analysis of Materials

The nitrogen content of the more ionic and readily hydrolysable nitrides may be determined by the Kjeldahl method. This process involves three stages: (i) Dissolution of the sample in an acid solution to convert nitrides into ammonium salts, followed by addition of alkali to liberate ammonia (ii) separation of ammonia by distillation and (iii) determination of ammonia by standard volumetric or colorimetric methods. The first stage is very difficult for the majority of interstitial nitrides. These are extremely stable and temperatures above 1600°C are required for decomposition. In such cases, alkali fusion methods are recommended (Passer, et.al, 1962). The sample is fused with sodium hydroxide in a Pyrex-glass test tube and the ammonia evolved is swept by a slow stream of argon through

a trap into a solution of boric acid and titrated with hydrochloric acid. The argon is passed through a bubbler containing water to ensure that sufficient water is present for complete reaction.

This method affords a rapid determination of nitrogen in the more covalent nitrides such as boron, aluminium and silicon nitrides. It is applicable also to some of the interstitial nitrides where the corresponding metal oxides are sufficiently amphoteric. The resultant sodium salts, for example, Na-zirconate, may not be readily soluble in water and require acidification by hydrochloric acid before the hydrous metal oxide can be precipitated by ammonia at a suitable pH (Britton, 1955). Elwell & Wood (1961) have also recommended Kjeldahl distillation method for some nitrides. At the concentration levels of 0-100 ppm, a spectrophotometric finish appears to be preferable to the titrimetric finish used at higher concentration levels. Orsage (1964) describe vacuum or inert gas fusion method, in which case nitrogen is evaluated by "difference". The present state of this analysis is less satisfactory. Moreover, many nitrides may resist vacuum extraction; on the other hand occluded or free nitrogen eludes the Kjeldahl analysis, Sloman et.al., (1951) reported that several combinations of nitrogen may co-exist in a sample and there is no known method which will ensure their destruction with high temperatures or their transformation into ammonium ions for their chemical analysis.

Several methods have been described for the determination of nitrogen in boron and silicon nitrides. (Bennett & Lindop, 1958; Cosgrove & Shears, 1960; Kriege, 1959). But these methods are lengthy and require considerable manipulative skill and are of doubtful



accuracy when applied to highly refractory materials. Bennett and Lindop's oxidising fusion method requires several hours even for boron nitride which yields a readily fusible oxide,  $B_2O_3$ , m pt.  $450^{\circ}C$ . Techniques of gas analysis in metals, including interstitial nitrides have been reviewed by James (1964). A tube furnace oxidation method has also been described (Meyer et.al., 1967).

The Dumas method, where the sample is mixed with cupric oxide or lead oxide (Tsuchiya, 1959) and heated in a current of pure  $CO_2$ , is generally unsuitable where the nitride becomes surrounded by impermeable oxide layers e.g. vanadium nitride (Gerschbacher, 1947). Thus, atmospheric oxidation at high temperatures (up to  $1200^{\circ}C$ ) has proved more effective, preferably at temperatures permitting diffusion of nitrogen and oxygen through the surrounding oxide layers. In cases where the oxidation is not quantitative, dissolution of the oxide and further oxidation by either alkaline fusion with sodium hydroxide or acidic fusion with potassium bisulphate is suitable.

#### 2.6 Ball Milling

Ball milling is a simple method of reducing the particle size of a solid material. The mills used were cylindrical drums containing porcelain balls. Each pot had radiused ends to present a smooth interior surface free from corners and crevices. The open end cover was secured by a quick-release bar and screw. The pots were of 2.5 l capacity and contained the same number of balls of three different sizes (36 of 18.7 mm diameter; 81 of 12.6 mm diameter and 180 of 9.5 mm diameter).

In the tumbling motion within the mill, wearing of the surfaces of the mill may occur, depending on the properties of the porcelain. This is described by the makers, the Pascall Engineering Company,

as being a hard, dense, non-porous ceramic material which is in a vitreous condition after firing to over 1200°C. In view of its high resistance to abrasion and chemical inertness, the makers claim that it is useful when absence of contamination is required. The porcelain is, however, lacking in ductility and susceptible to breakage under violent impact.

Although the nitrides milled were hard materials (Mohs' hardness up to 9), nevertheless no fragments of porcelain were detected in the X-ray traces of the milled samples. The milling times, however, were 10 hours or less. The ball-milling was carried out under standard conditions, i.e. a constant ratio of sample weight to number and sizes of the porcelain balls was maintained. Besides the same porcelain pot was used for a particular nitride for different lengths of time.

### 2.7 Computation

The IBM programme for computing specific surfaces by the B.E.T. method was that devised by P. O'Neill and Denise Harris (Plymouth Polytechnic) and is given in Appendix.

## CHAPTER III

### TITANIUM AND ZIRCONIUM NITRIDES

#### 3.1 Titanium Nitride

##### 3.1.1 Nitridation of Titanium

The titanium-nitrogen system and its thermodynamics have been described in Chapter I. Yet reactions which are thermodynamically feasible are not necessarily kinetically favourable, especially where solids are concerned. Here, the rates depend not only on the intrinsic reactivity of the material concerned, but also on the available surface or interface at which reaction can occur.

The reaction of titanium with nitrogen at atmospheric pressure is considerably slower than that with oxygen at corresponding temperatures (Bradford, et.al., 1949). The rate obeys essentially a parabolic law in the temperature range 550-850°C. over times of up to two hours. Gulbransen and Andrew (1949a & b) find that the rate constant in this temperature range is:-

$$k_p = 3.8 \times 10^{-5} \exp.(-36,300/RT) \text{ g}^2 \text{ cm}^{-4} \text{ s}^{-1}$$

Nitridation at higher temperatures will be more complicated crystallographically since alpha-titanium transforms to beta-titanium at 882.5°C. In this work, therefore, crystal changes have been studied in the formation of titanium nitride layers on substrates of titanium and some of its alloys.

Titanium, one of the lightest of the transition elements, has other desirable properties such as resistance to corrosion, strength and toughness. In the pure state it exists as alpha-hexagonal phase, but commercially pure titanium is essentially a dilute alloy of titanium with oxygen, nitrogen and carbon. According to

McQuillan & McQuillan (1956) and Sabroff et.al. (1968), it is convenient to divide commercial titanium alloys into three classes:-

(a) the alpha-phase alloys, consisting of elements which stabilize the alpha-phase in titanium, namely O, N, C and a number of non-transitional elements, e.g., Al, Sn, Some of these alloys may have a small amount of the beta-form "frozen" in the structure at room temperature and are known as 'near' or 'super' alpha alloys,

(b) the mixed alpha-beta alloys, contain additional elements which stabilize the beta-phase to such an extent that the microstructure, at room temperature, consists of a mixture of the alpha and beta phases. The addition of Transition elements, such as Fe, Cr, Mo and V, stabilizes the beta-phase. These alloys are very important because it is possible to control their mechanical properties by precipitation-hardening,

(c) the beta-phase alloys, are all of beta-form at room temperature and contain a large proportion of beta-stabilizing elements, e.g., Mo, Cr and V. These have limited applicability since they are not weldable, but sheet forms can be aged up to an ultimate tensile strength of 131,000 lb/in<sup>2</sup> (Crossley & Kessler, 1954).

The alloys are produced commercially as cylindrical ingots by vacuum arc-melting in consumable-electrode furnaces (Sabroff et.al., 1968).

The occurrence of an allotropic transformation in pure titanium controls the type of structures which can be produced by the heat-treatment of titanium-rich alloys. Phase diagrams of the binary alloy systems are illustrated schematically in Figure 3.1 (McQuillan & McQuillan, 1956).

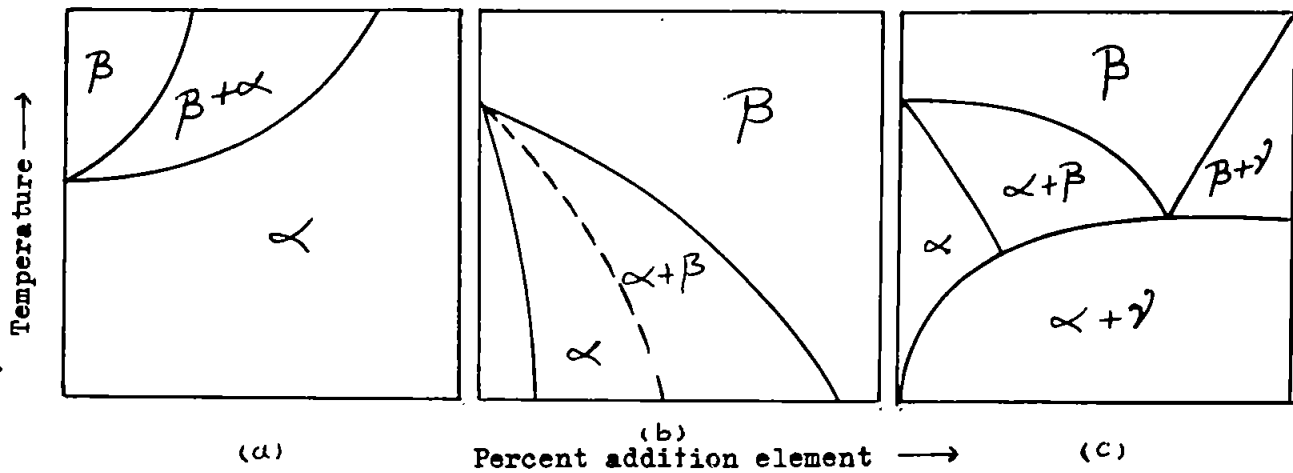


Figure 3.1 Major Types of Phase diagrams  
for Ti-rich binary systems

The binary systems of titanium with the elements oxygen, nitrogen, carbon and the industrially important addition element aluminium, are of the alpha-phase stabilizing type shown in Figure 3.1(a). Transition elements, on the other hand, all appear to give rise to diagrams of either type (b) or type (c). The beta-phase containing more than a critical concentration of addition element can be retained in an unstable condition at room temperature by rapidly quenching from the beta-phase field. Figure 3.1(c) represents also the systems of titanium with copper, silver and gold. The gamma-phase is said to exist on the titanium-rich side of the TiCu composition (47-50 at % copper) and is body-centred tetragonal (McQuillan & McQuillan, 1956 p.206).

The phase compositions of commercially available titanium (I.M.I. Limited) are presented in Table 3.1. Boride coating of these alloys has been described by Jones (1970) and in the present work four of these, i.e. I.M.I., 130, 230, 318 and 205, have been subjected to nitridation at various temperatures.

TABLE 3.1

The Composition and phases of commercially available titanium  
(Imperial Metal Industries (Kynoch) Limited)

I.M.I.	B.S. SPECIFICATIONS	COMPOSITION	PHASE	CLASS	DENSITY g/cm <sup>3</sup>	REMARKS
130	_____	Commercially pure	Alpha	I	4.51	become successively mechanically stronger
160	TA, 7, 8, 9	Commercially pure	Alpha	I	4.51	
230	TA, 21, 22, 23, 24	Ti - 2.5 Cu	Alpha	I	4.56	Ductile, medium strength
314	_____	Ti-4Al - 4Mn	Alpha-beta	III(2)	---	_____
315	_____	Ti-2Al-2Mn	Alpha-beta	III(2)	4.51	Low strength
317	TA, 14, 15, 16, 17	Ti-5Al-2.55n	Alpha-beta	III(1)	4.46	Medium strength
318	TA, 10, 11, 12, 13 28	Ti-6Al-4V	Alpha-beta	III(2)	4.42	Medium strength
205	_____	Ti - 15Mo	Beta	II	---	High Strength

(100)

The alloys were sectioned by a diamond grit wheel (Bullock Diamond Products Ltd.) and polished. Specimens, about 1 c.m. in diameter, in fused alumina crucibles (Thermal Syndicate Ltd.), were put in a high temperature vacuum furnace (Metals Research, Type PCA10, described in Chapter II, section, 2.52). For vacuum and inert atmospheres (argon) a small amount of titanium hydride ( $TiH_2$ ) was placed in the furnace to getter any residual oxygen or nitrogen in the system. For nitridation, specimens were heated at temperatures between  $750-1400^\circ C$ , using nitrogen flow rates of 100-125 ml/min. Subsequently, the samples were cooled slowly to allow the titanium phases to equilibrate. The coatings were examined by X-ray diffraction and by electron microscopy of replicas. Approximate thicknesses of the nitrided layers were estimated from weight increases and surface areas of the initial metal samples (Table 3.2; Replicas in Plates 3.1 & 3.2).

On partial nitridation of the alpha-titanium (Figure 3.2 a) at  $1000^\circ C$  for four hour and eight hour periods (gas flow rate 125 ml/min) only  $TiN$  corresponding to the stoichiometric composition was formed. The remaining alpha-Ti showed a small lattice expansion along the a-axis ( $2.95$  to  $2.97^\circ A$ ) and contraction along the c-axis ( $4.68$  to  $4.58^\circ A$ ), i.e., the (002) spacing decreased from  $2.34$  to  $2.29^\circ A$  and passed through the value  $2.31^\circ A$ , which coincides with the main spacing of beta-titanium (110-spacing). Therefore any beta-Ti formed at  $1000^\circ C$  has been nitrided, for no other beta-Ti peaks were detected, i.e.  $TiN$  and  $\alpha$ -Ti accounted for all the peaks (Fig. 3.2(b) & (c)). The decreased 002 spacing ( $2.29^\circ A$ ) is approximately that recorded in the literature for main peak of the so called  $\epsilon$ - $TiN$ , but two other main peaks for the latter were not observed as they would have been masked by  $TiN$  and

(102)

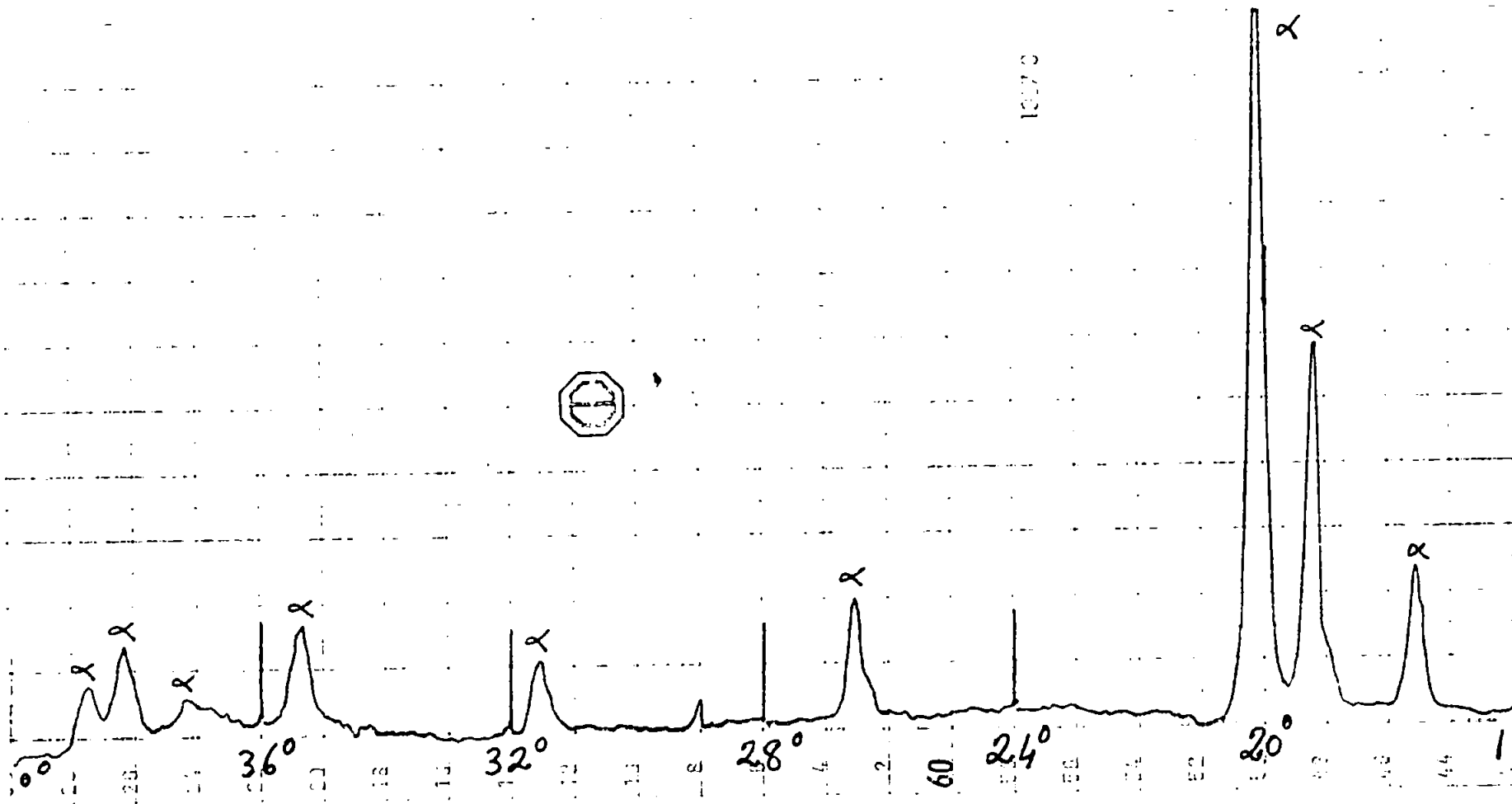


Fig. 3.2 (a) :- X-ray Diffractometer Trace of I.M.I. (130) [Commercially Pure  $\alpha$ -Ti].



1  $\mu$ m



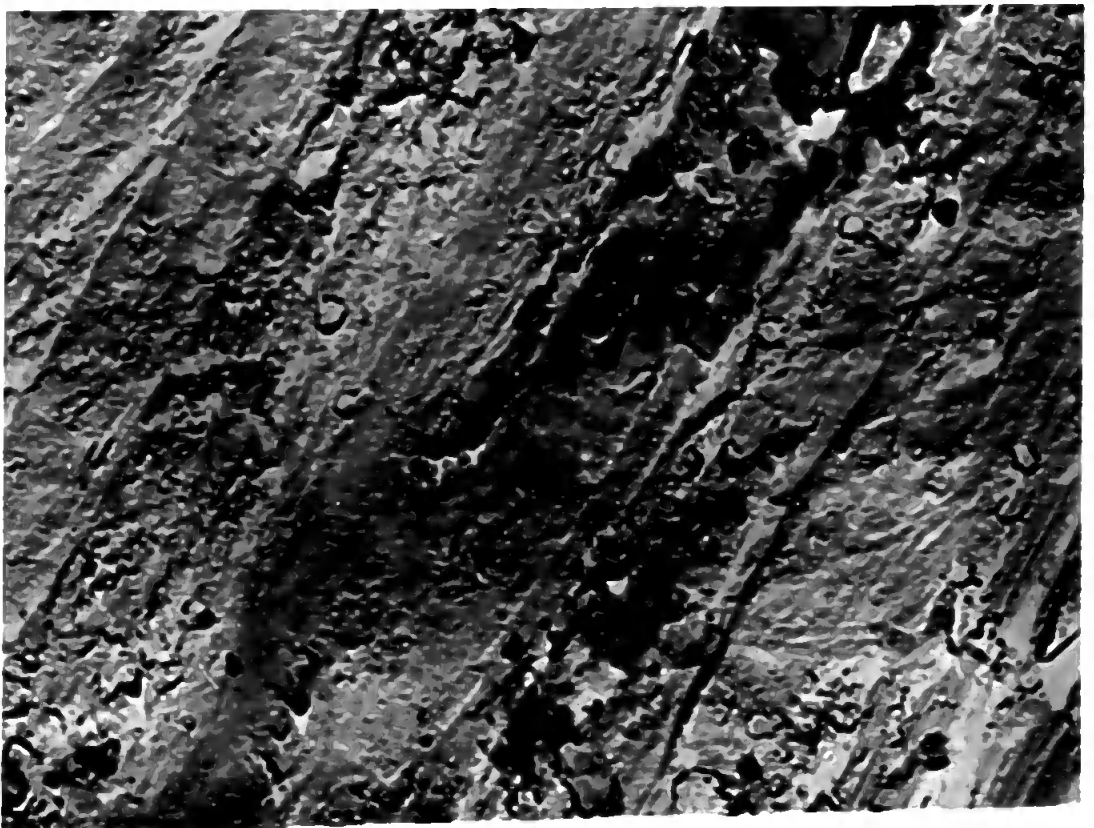
PLATE 3.1(a) I.M.I. 130 Nitride Coated for 8h at 1000°C.

Magnification x20,000

Page(107)

PLATE 3.1(b) I.M.I. 130 Untreated

1  $\mu$ m



1  $\mu\text{m}$



PLATE 3.2(a) I.M.I. 205 Nitride Coated for 8h at 1030°C.

Magnification x20,000

Page(108)

PLATE 3.2(b) I.M.I. 205 Untreated

1  $\mu\text{m}$



alpha-Ti peaks.

In Figures 3.2, 3.3, 3.4 and 3.5 the X-ray diffractometer patterns of the alloys along with those of the corresponding nitrided samples are presented for comparison.

There was no appreciable nitridation of alpha-Ti (130) at 750°C in half hour implying that the alpha-phase remained stable during this time interval. When the nitridation of alpha-Ti (130) was carried out at higher temperatures (2h at 1200°C + 1 h at 1400°C), there was complete conversion to TiN in the top layer and the (111) reflection became the most prominent instead of the (220) as was observed at lower temperatures (e.g. 1000°C), where development of crystallinity may not have been complete. Figures 3.2(c) and 3.2(d) illustrate this observation. In accordance with the findings of Bradford, et.al., (1949), traces of oxygen resulted in rutile formation which predominated over nitridation even at the lower temperatures (900-1000°C). At 900°C (Figure 3.2(e)), i.e. just above the alpha-beta transformation temperature, the X-ray trace shows peaks for both the alpha-Ti (002) c-spacing at 2.34Å and the 2.29Å spacing. This again suggests some dissolution of nitrogen in the original alpha-Ti to slightly distort its lattice, before further nitridation and formation of well-defined crystalline TiN. The relative thickness of this interfacial zone between unchanged alpha-Ti and TiN depends on temperature, and is probably greater at lower temperatures when the nitrogen diffusion is slower. The beta-Ti alloy, stabilised with 15 Mo [Figure 3.3(a)] gives a mixture of rutile (TiO<sub>2</sub>) and TiN in the presence of small amounts of oxygen (Figure 3.3(b)). However, it nitrifies completely to TiN at 1400°C

(011)

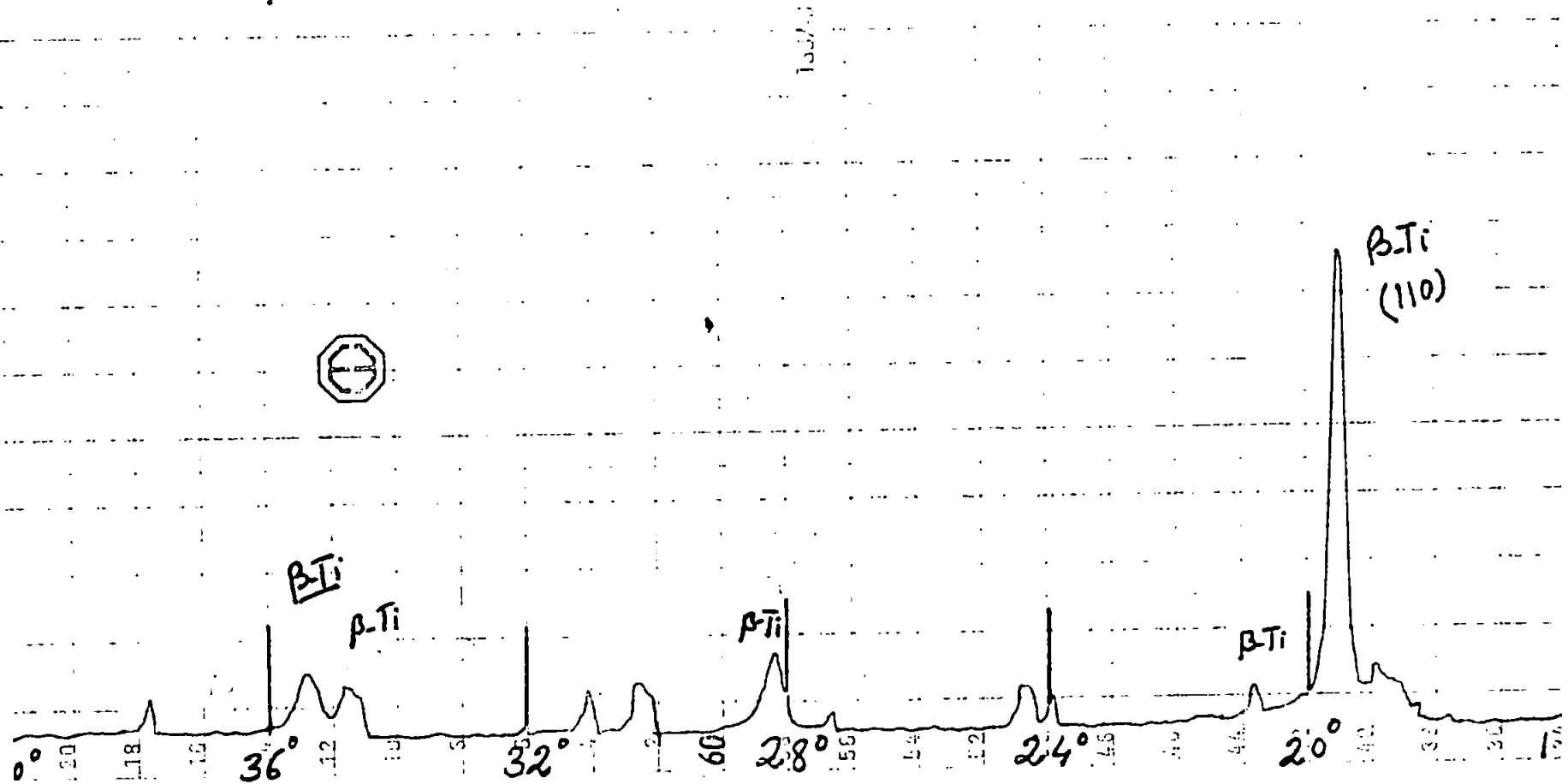
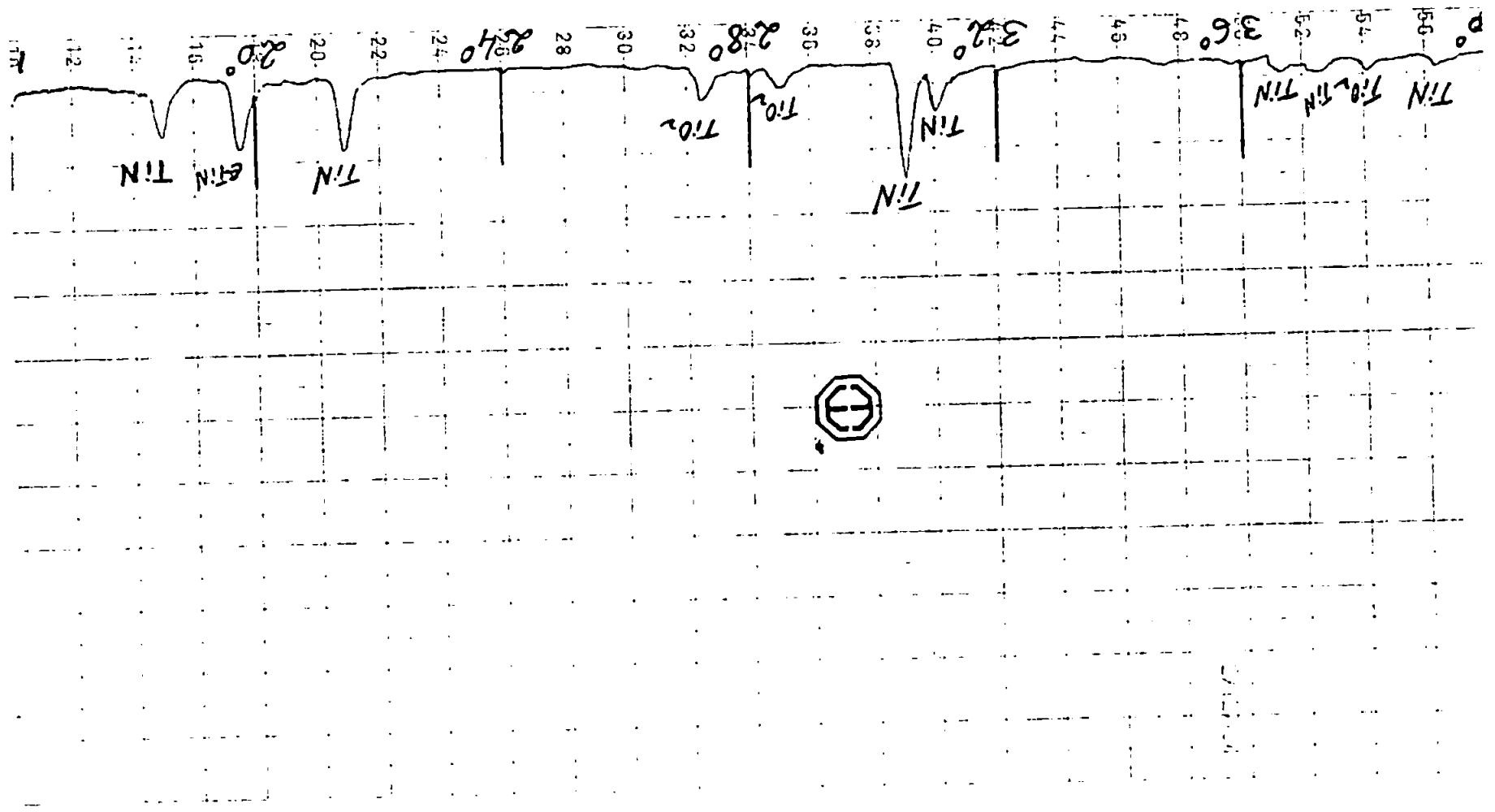


Fig. 3.3(a) :- X-ray Diffractometer Trace of I.M.I. (205) [Ti+15Mo].

Fig. 3.3(b) :- I.M.I. 205 (B-Ti)<sub>2</sub> Nitrided for 8h at 1000°C



(111)

within 1 hour in the top layer (Figure 3.3 (c)). The X-ray trace again shows a further peak for a  $2.29\overset{\circ}{\text{A}}$  spacing (corresponding to  $\beta$ -TiN) replacing the original main peak for the (110)-spacing of beta-Ti ( $2.31\overset{\circ}{\text{A}}$ ). Comparison of Figures 3.3(a) and 3.3(b) illustrates this observation. Electron micrographs of replicas of the original and nitrated surfaces of alpha-Ti (230) and  $\beta$ -Ti (205) are presented in Plates 3.1 & 3.2.

Similar results are obtained on nitriding alpha-Ti (230) alloy (with 2.5 cu). The X-ray diffractometer trace on the original is shown in Figure 3.4. The mixed alpha-beta-Ti (318) alloy (with 6Al + 4V) also nitrates completely near the surface to TiN at high temperatures (2 hours at  $1200^{\circ}\text{C}$  + 1 hour at  $1400^{\circ}\text{C}$ ), giving a trace similar to that shown in Figure 3.3 (c). The diffractometer trace of the original material is illustrated in Figure 3.5.

### 3.1.1(a) Compactness of Titanium Nitride Films

The titanium nitride films all strongly adhered to the metal surface for wide ranges of thickness and temperatures of formation. The thicknesses calculated from weight gains on nitridation are shown in Table 3.2.

By analogy with general theories of metal oxide formation (Evans, 1968), it would be expected that at higher temperatures good adhesion of the nitride layer would be facilitated by lattice diffusion. This explanation is applicable only above the Tamman temperature (above  $700^{\circ}\text{C}$  for Ti and  $1330^{\circ}\text{C}$  for TiN). At lower temperatures (above about  $375^{\circ}\text{C}$  for Ti and  $795^{\circ}\text{C}$  for the nitride), the adhesion may be

TABLE 3.2

Thicknesses of TiN formed at different temperatures

I.M.I. Alloy	Nitridation Temperatures & Time	Nitride film thickness, $\mu\text{m}$
230(Ti + 2.5 cu)	(i) 1000°C, 8 h	23
	(ii) 1200°C, 2 h + 1400°C, 1 h	51
t30 (commercially pure alpha-Ti)	(i) 1000°C, 8 h	13
	(ii) 1200°C, 2 h + 1400°C, 1 h	22
205 (Ti + 15Mo)	(i) 1000°C, 8 h	10
	(ii) 1200°C, 2 h + 1400°C, 1 h	41

caused by 'keying - in' through grain boundary penetration ( Tylecote, 1960) where surface diffusion is operative.

Interlocking or adherence may be produced by solution of nitrogen in the metallic phase followed by nucleation of internal platelets when the nitrogen concentration exceeds a saturation value (0.9 at % at 1000°C & 4.5 at % at 1560°C). Alternatively, there may be interlocking by nitridation at the walls of crevices or by penetration along dislocations and grain boundaries. In these typical cases, where there is an increase in volume on nitridation (Table 1.3, Chapter I), any nitride formed at the metal-nitride interface is likely to produce compression. This tends to keep the internally formed nitride pressed against the metal, reducing the risk of poor adhesion due to possible cavity-formation. Thus, the Pilling-Bedworth rule is probably more important for scales where there is anion diffusion from the surface to the metal-scale interface

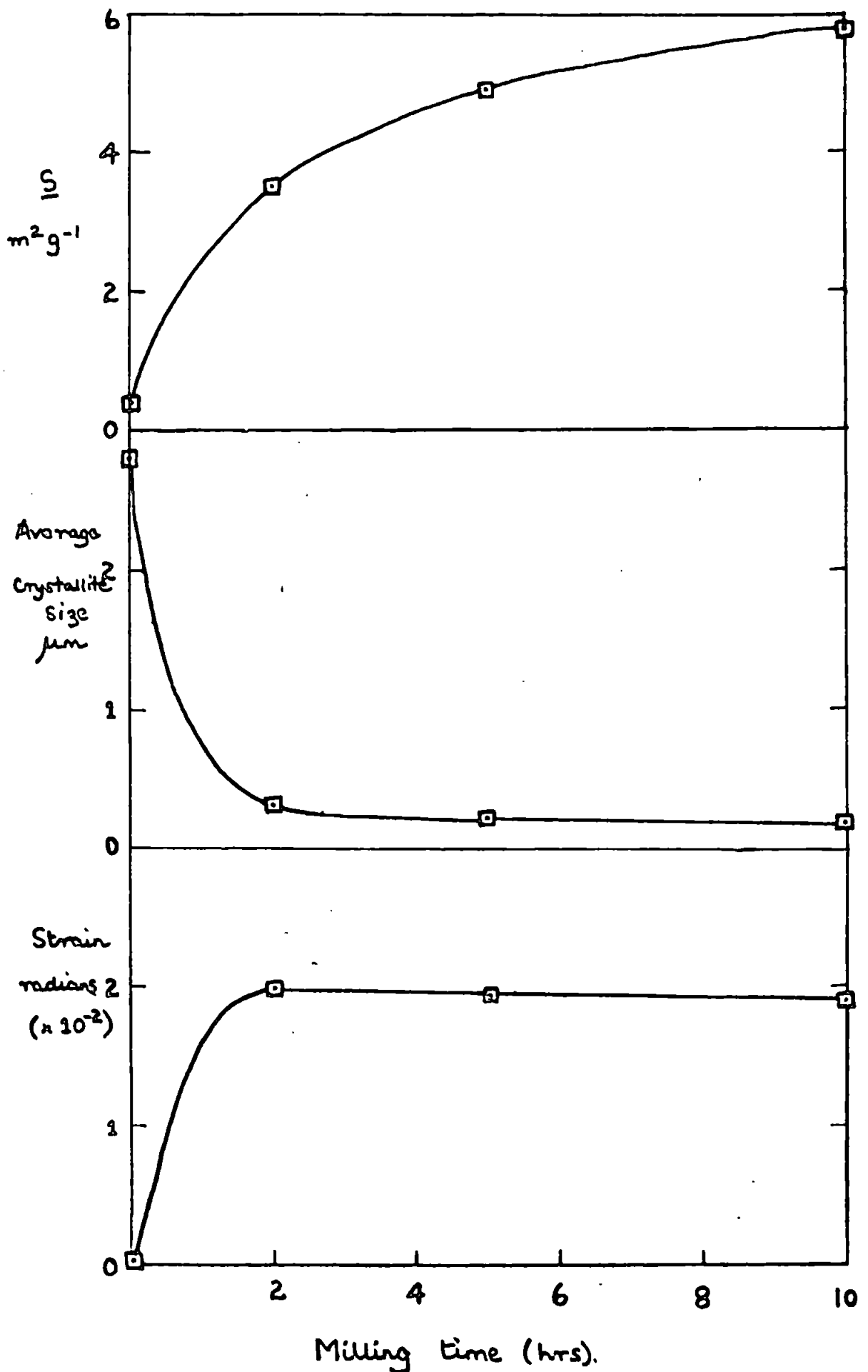
compared with scales that grow by outward migration of matter as observed by Vermilyea (1957). In the present work, cation diffusion for titanium is feasible at temperatures above  $700^{\circ}\text{C}$  which explains the stability and larger grain sizes of the nitride films formed at  $1000^{\circ}\text{C}$  &  $1200^{\circ}\text{C}$  +  $1400^{\circ}\text{C}$ .

### 3.1.2. Milling of Titanium Nitride

The high temperatures required for the production of nitrides cause sintering to the extent that samples generally have specific surfaces of below  $1\text{ m}^2\text{g}^{-1}$ , and average crystallite sizes (equivalent spherical diameters) of over  $2\text{ }\mu\text{m}$ . Thus, samples of titanium nitride were milled to increase their surface activity and to examine changes in microstructure caused by the comminution. When 6 g samples were milled (under conditions described in Chapter II, Section 2.6), the specific surface progressively increased as shown in Figure 3.6a. Electron micrographs showed that the original nitride consisted of single crystals and aggregates of about  $0.5\text{--}5\text{ }\mu\text{m}$  size (Plate 3.3). The micrographs of milled (2h and 10h) and oxidised samples are also presented (Plates 3.4, 3.5 and 3.6). The single crystals were fractured during the earlier stages of the milling and the fragments were incorporated into the aggregates which remained approximately the same size throughout the milling. Thus, the average crystallite size (Figure 3.6b), decreased rapidly at first and later slowly when the crystallites became of submicron size. This is in accordance with the findings of Bradshaw (1951) and Hüttig (1957), who found that if aggregation and attrition processes proceed at equal rates, 'a grinding equilibrium' would be set up. Then the specific surface or the average crystallite size, will remain



FIG. 3.6: MILLING OF TITANIUM NITRIDE



1  $\mu$ m

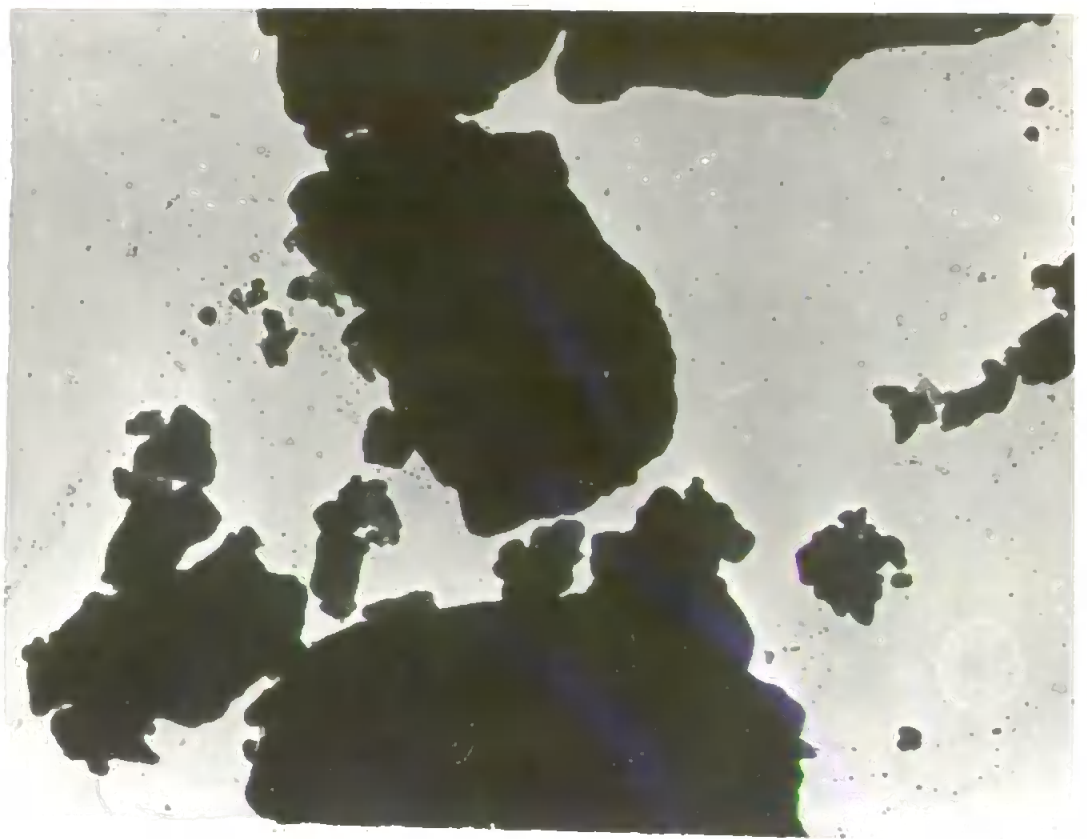


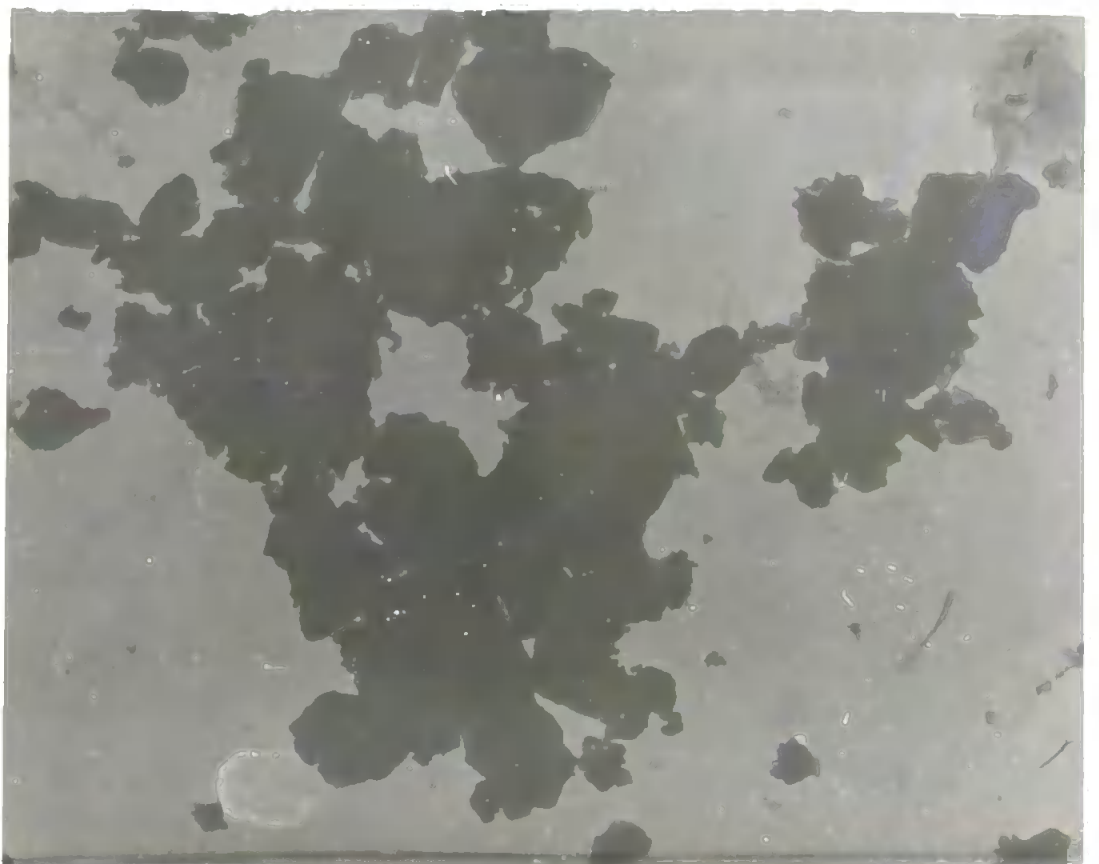
PLATE 3.3 Titanium Nitride, Untreated

Magnification x 20,000

Page (119)

PLATE 3.4 Titanium Nitride, Ball-Milled for 2 hours.

1  $\mu$ m



1  $\mu$ m

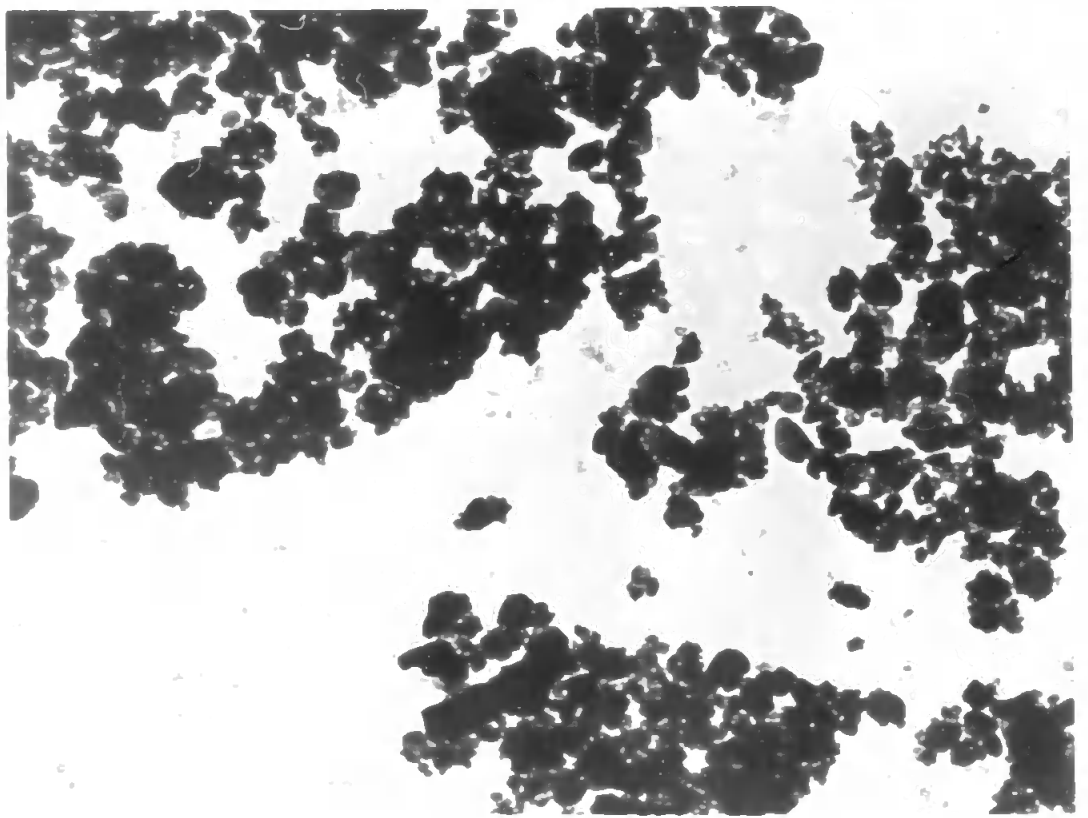


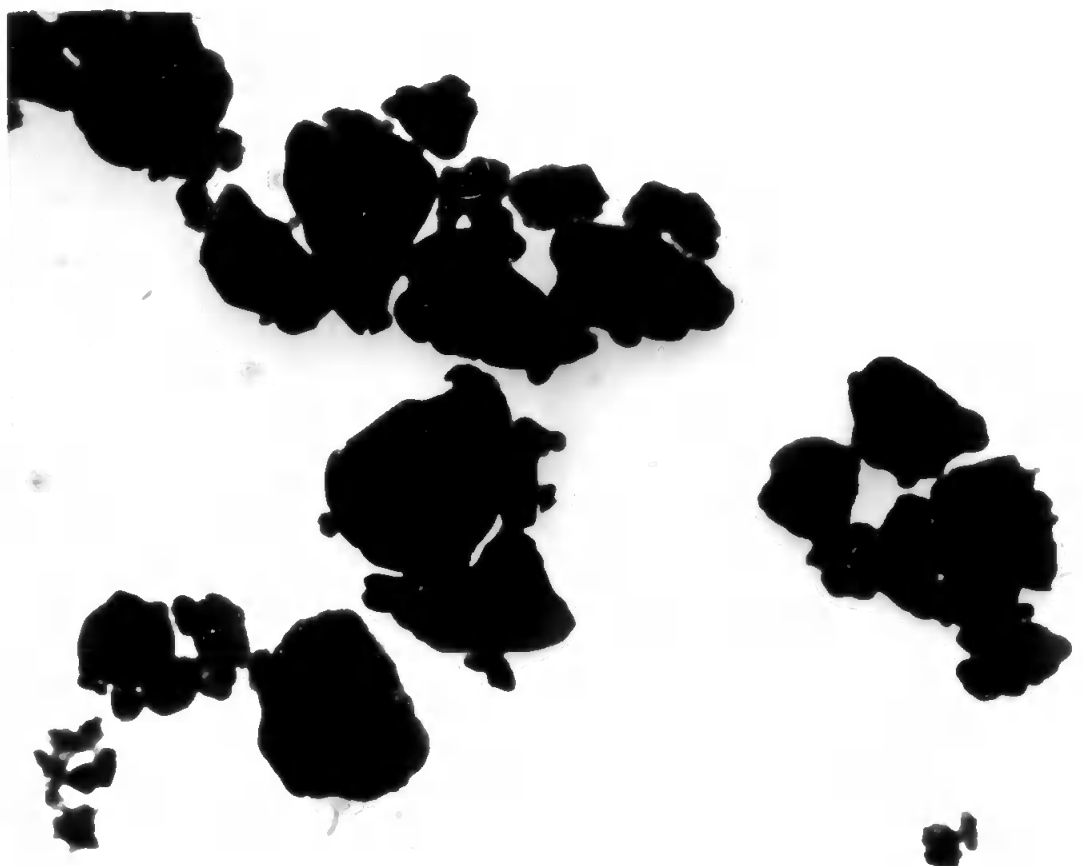
PLATE 3.5 Titanium Nitride, Ball-Milled for 10 hours

Magnification x 20,000

Page (120)

PLATE 3.6 Titanium Nitride, Oxidised in Air at 600°C for 5 hours

1  $\mu$ m



practically constant. Prolonged milling may favour the tendency of the finest particles to adhere to one another, and thus causing a slight reduction in specific surface after a maximum has been reached.

(Gregg, 1961, p.300) Such a process has been found to occur in the ball milling of Kaolinite (Gregg et.al., 1954), graphite (Hickman, 1959) and molybdenum disulphide (Braithwaite, 1959).

The milling caused strain to be set up within the crystallites, so that there was X-ray line (or peak)- broadening. Table 3.1 shows the half-peak widths of the (111) and (200) reflections.

TABLE 3.3

Lattice Strain in Milled TiN Samples

Titanium Nitride	Half-peak widths (2 ) in Minutes for Reflections		Strain (radians) (Using (200) reflections.
	TiN (111)	TiN (200)	
Unmilled	14	14	-
Milled, 2 h	32	36	$1.99 \times 10^{-2}$
Milled, 5 h	34	36	$1.94 \times 10^{-2}$
Milled, 10 h	35	36	$1.90 \times 10^{-2}$

The strain was calculated from the half-peak width of the (200) X-ray reflection (Section 2.1.5), after allowing for broadening due to crystallite size. Figure 3.6(c) illustrates the development of strain which occurred mainly during the first two hours milling when the single crystals were fractured and incorporated into the aggregates. Subsequently, the strain remained practically constant.

### 3.1.3 Oxidation of Titanium Nitride

Variations in phase composition, surface areas, crystallite and aggregate sizes during the oxidation of the unmilled titanium nitride

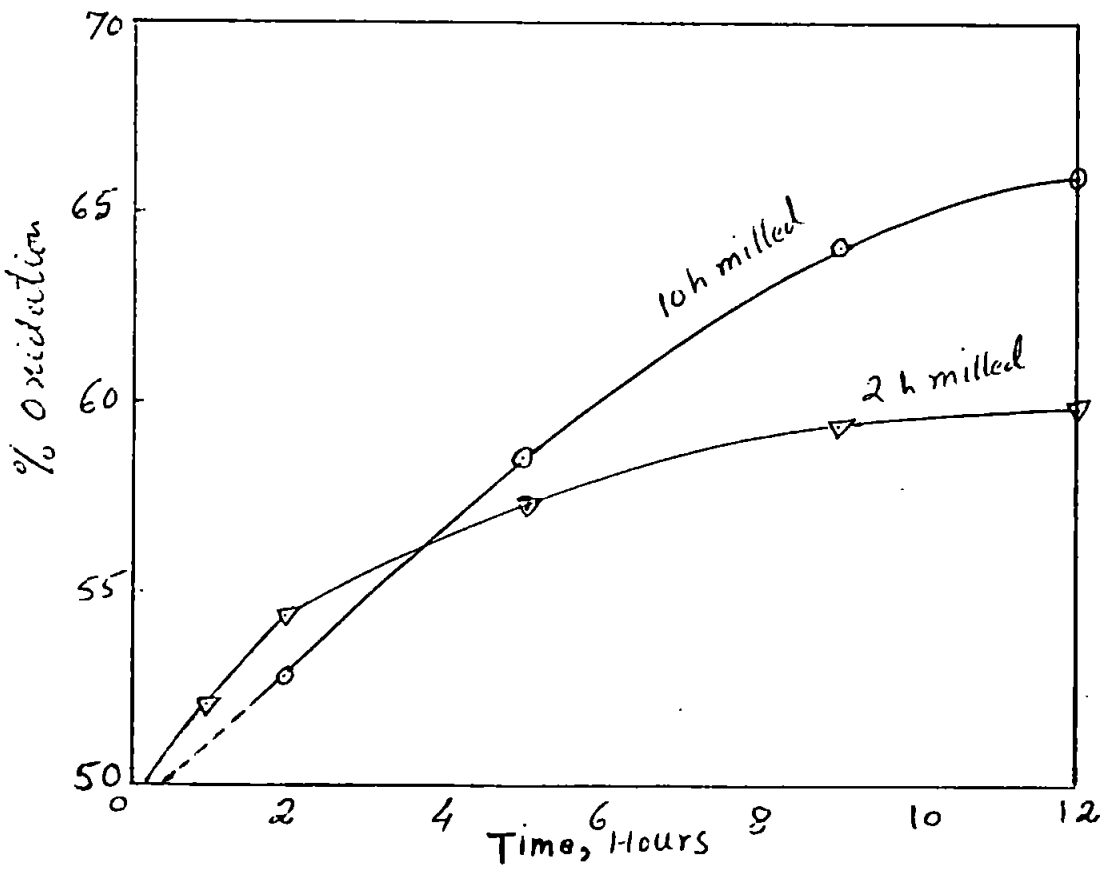
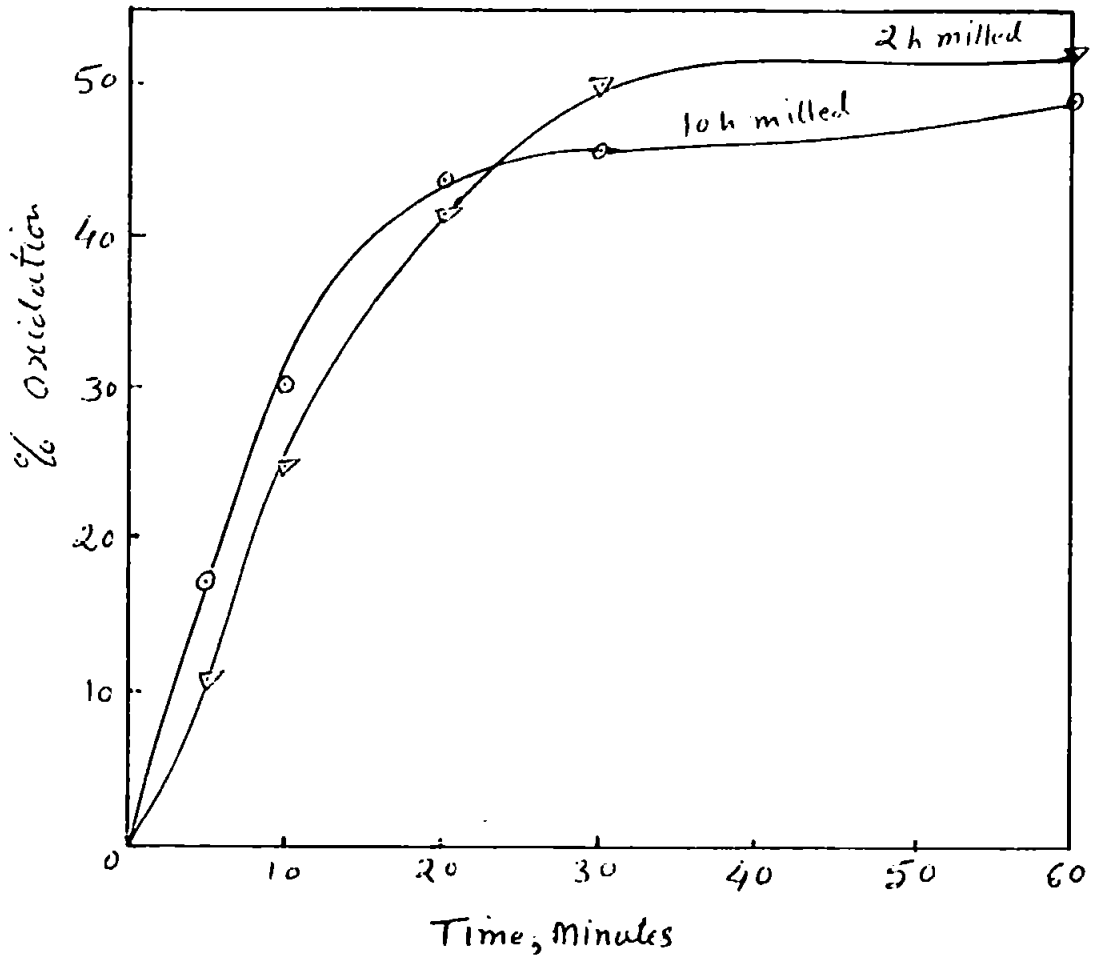
have been described in an earlier paper covering the preliminary part of the present investigation (See Appendix 4). Crystallites of rutile,  $TiO_2$ , split off from the remaining titanium nitride before they sinter, and inhibit further oxidation. Accordingly studies of oxidation rates on milled TiN at  $450^\circ C$  (Figure 3.7) show that the reaction proceeds readily until there is sufficient titanium dioxide of rational crystallite size composition for sintering to form surface films through which normal gaseous diffusion cannot easily occur. As before (Glasson & Jayaweera, 1969), this corresponds to about 50% conversion of the nitride.

The oxidation rates for the longer-milled (10 h) and more finely-divided sample are slightly greater than for the shorter (2 h) milled sample. The curve for the latter is slightly sigmoidal indicating initial nucleation. The later part of the oxidation is somewhat parabolic. This temperature ( $450^\circ C$ ) is just sufficiently high for sintering of the titanium dioxide by surface diffusion ( $\frac{1}{3}$  m.p. in K;  $TiO_2 = 460^\circ C$ ). It would appear that the oxide film is not sufficiently strong to prevent some scaling in the final stages when the oxidation rate becomes nearly linear. At  $600^\circ$  and  $700^\circ C$  (Figs. 3.8 & 3.9) the initial rates are also practically linear and later become parabolic, as found before (Glasson & Jayaweera, 1969) for unmilled TiN. However, there is little difference in oxidation rates at  $600^\circ$  and  $700^\circ C$  and this is ascribed to the more rapid sintering of the titanium dioxide at these higher temperatures, c.f., negative temperature coefficient found for oxidation of certain metals such as niobium (Argent & Phelps, 1960; Aylmore, et.al., 1960).

### 3.1.3 (a) Comparison with oxidation of Titanium Metal

For the oxidation of titanium, Jenkins (1955) and Wallwork & Jenkins (1958; 1959) have suggested a similar mechanism to

Figure 3.7: Oxidation Isotherms for Milled TiN in air at 450°C.



account for paralinear growth. Briefly, it involves the following stages:

- (i) The passage of oxygen to the metal-oxide interface through an essentially non-protective scale;
- (ii) The dissolution of oxygen in the metal phase, resulting in the nucleation and growth of oxide, on and just beneath the surface, simultaneously with the establishment of an oxygen diffusion gradient extending in depth as a function of time and temperature;
- (iii) The intermittent exfoliation of thin sections of the metal surface under the influence of the stresses developed by the nucleation and solution processes;
- (iv) The conversion of these thin layers to the highest oxide commensurate with the existing oxygen potential in the vicinity, followed by partial sintering of the layers into a porous and stratified scale. (See also Stringer, 1960).

Jenkins proposed that the parabolic region corresponds to the period when oxygen is taken into solid solution through the metal surface (Pemsler, 1958 on Zirconium) at a rate in excess of that required for the establishment of exfoliation conditions at that surface. The oxygen flux through the interface diminishes with time as the oxygen gradient penetrates deeper into the metal, and the paralinear transition is thought to occur when the flux just balances the demand made by the intermittent exfoliation process. Subsequently the oxygen absorption as measured experimentally is wholly attributable to the conversion of exfoliated metal surface layers to rutile scale. The extremely regular-layered structure of the scale

observed on titanium has been explained on this basis (Stringer, 1960; Wallwork & Jenkins, 1959). As required by the theory, the oxygen gradient in titanium does in fact reach a 'steady state', ceasing to extend in depth during the linear oxidation period. Further, if the scale is removed from the metal at this point and the specimen re-oxidised at the same temperature, the rate is approximately linear as before, indicating that the scale is not acting as a diffusion barrier in this instance.

A model that would account for linear followed by parabolic oxidation has been suggested earlier by Evans (1924), Fischbeck (1933) and Nöldge (1938). If the rate-determining reaction is a boundary effect at the beginning, and becomes diffusion-controlled in the later stages, the reaction may be considered as a flux of matter,  $J$ , which has to overcome a series of resistances, namely, the diffusion resistance  $R_d$  (the diffusion coefficient being taken to be independent of concentration) and the surface reactions  $R_1$  and  $R_2$  at the metal-film and film-gas boundaries. The driving force is as usual, a difference in concentration,  $\Delta c$ , at the two interfaces.

$$J = \text{const.} \frac{\Delta c}{R_d + R_1 + R_2}$$

If the flux of material is approximately constant, then,

$$J = d\xi/dt \quad R_d = a\xi, \quad R_1 + R_2 = b$$

and  $\text{const.} \Delta c = k$  where  $a, b, k$  are constants.

Hence, 
$$d\xi/dt = k/(a\xi + b)$$

and on integration,

$$a\xi^2 + 2b\xi = 2k \cdot t$$



or by combining the constants,

$$\xi^2 + K'_a = K'_b \cdot t,$$

the integration constant being zero if  $\xi = 0$  at  $t = 0$ .

This corresponds to a generalized parabolic law which involves the possibility that two different processes can be rate-determining during the progress of oxidation. The interface reaction governed by the term  $K'_a \xi$ , would be rate-determining in the initial stages of oxidation, and when the scale becomes thicker this term will become negligible, the square term governing the total reaction rate (Kubaschewski & Hopkins, 1962, p.99).

### 3.1.3(b) Comparison with Oxidation of Titanium Boride and Carbide

The oxidation mechanisms for these refractory hard metals  $TiB_2$  and  $TiC$  (Münster, 1959 and Samsonov & Golubeva, 1956) are essentially similar to those for titanium nitride and for the metal itself. Münster used platinum markers which were found at the scale surface after oxidation. Thus, the oxide-nitride interface moves away from the oxide-gas interface. In conjunction with the defect mechanism of rutile, this suggests that diffusion of oxygen ions ( $O^{2-}$ ) through the scale is rate-determining, at least in the parabolic stage of the oxidation; cf., diffusion of anion vacancies in the  $TiO_2$  (n-type conductor) which controls oxidation of titanium between  $600^\circ$  and  $700^\circ C$  and gives a similar energy of activation for coarser samples (Tylecote & Mitchell, 1960). The linear portion of the rate curve suggests that a phase boundary reaction may finally become rate-controlling. Probably, the atomic nitrogen diffuses from the metal to the outer scale surface where it then forms gaseous molecules, as in the decomposition of  $\alpha$ -iron nitride (Goodeve & Jack, 1948).

Small amounts of nitrogen are retained in the oxide layer, and some may have dissolved in the nitride phase (deficient in nitrogen) when freed by the oxidation reaction. The amount of nitrogen retained depends on the reaction rate, sintering temperature and changes in crystallite sizes of the materials. Thus, it becomes appreciable for the faster oxidations of titanium nitride above  $800^{\circ}\text{C}$  where sintering of the titanium dioxide is also rapid. The final product of composition  $\text{TiO}_2 \cdot \text{N}_{0.075}$  obtained at  $1000^{\circ}\text{C}$  resembles  $\text{UO}_3 \cdot \text{N}_{0.2-0.4}$  given when UN oxidises (Dell et.al., 1966); the latter is sensitive also to crystallite size variations and both the intermediate  $\text{U}_2\text{N}_3$  and  $\text{UO}_2$  are epitaxially orientated with respect to the UN.

The parabolic kinetics are modified by several factors contributing to the detailed shape of the initial rate curves of the oxidation isotherms (Gulbransen & Andrew, 1951) e.g., decreases in surface heterogeneity as the reaction proceeds, changes in specific surface or in local surface temperature due to heat of reaction, solubility effects, impurity concentrations, possible changes in oxide composition and electrical double layer effects. Hence, often the nitride oxidations do not immediately give parabolic kinetics, as found in the present work, and in the oxidation of AlN (Coles et. al., 1969). Before coherent oxide layers are formed, the free nitride surfaces remain exposed to the gas phase, so that the kinetics approach linearity. The subsequent parabolic kinetics may be replaced finally by approximately linear kinetics with abnormally slow rates where oxide sintering is extensive, often giving considerable variations in the energy of activation.

## 3.2 Zirconium Nitride

### 3.2.1. Nitridation of Zirconium

The zirconium-nitrogen system and its thermodynamics has been described in Chapter I. The kinetics of nitridation of zirconium has been investigated by various workers (Brown, 1964, p.179). Gulbransen & Andrew (1949a, c) report that the reaction is much slower than the corresponding one with oxygen or hydrogen. They observed that the rate is independent of nitrogen pressure in the temperature range 400-850°C, and ascribe this to the formation of a surface nitride layer. This observation was made also by Dravnieks (1950) at higher temperatures. From a study of the reaction at 900-1600°C, Mallet et.al., (1953, 1954) report the formation of a  $\beta$ -solid solution and a thin layer of  $\alpha$ -solid solution surrounded by zirconium nitride. The rate of diffusion of nitrogen into zirconium is much lower than that of oxygen. Near the transformation temperature (852°C) there is a marked increase in the absorption of both gases (Guldner & Wooten, 1948; Hayes & Roberson, 1949). Saliberkov et.al., (1964) studied the nitridation of zirconium at 1400-1700°. They observed the formation of an outer layer of nitride, a second layer of  $\alpha$ -solid solution, and a base mixture of  $\beta$ -solid solution with some  $\alpha$ -solid solution precipitated as a result of cooling. According to all the above workers the reaction rate is parabolic.

The following experimental results have been reported covering wide ranges of temperature, and these show that the rate of reaction of zirconium with nitrogen is strictly parabolic.

Nitrogen pressure = 0.1 atm., 400-825°C (Gulbransen & Andrew, 1949)

$$k_p = 5 \times 10^{-5} \exp(-39,200/RT) \text{ g}^2\text{cm}^{-4}\text{s}^{-1}$$

$$P_{N_2} = 10 - 300 \text{ mm Hg.}, 860-1045^\circ\text{C} \text{ (Dravnieks, 1950)}$$

$$k_p = 3.2 \times 10^{-3} \exp(-52,000/RT) \text{ g}^2\text{cm}^{-4}\text{s}^{-1}$$

$$P_{N_2} = 1 \text{ atm.}, 975-1640^\circ\text{C} \text{ (Mallet et.al., 1954)}$$

$$K_p = 7.8 \times 10^{-3} \exp(-48,000/RT) \text{ g}^2\text{cm}^{-4}\text{s}^{-1}$$

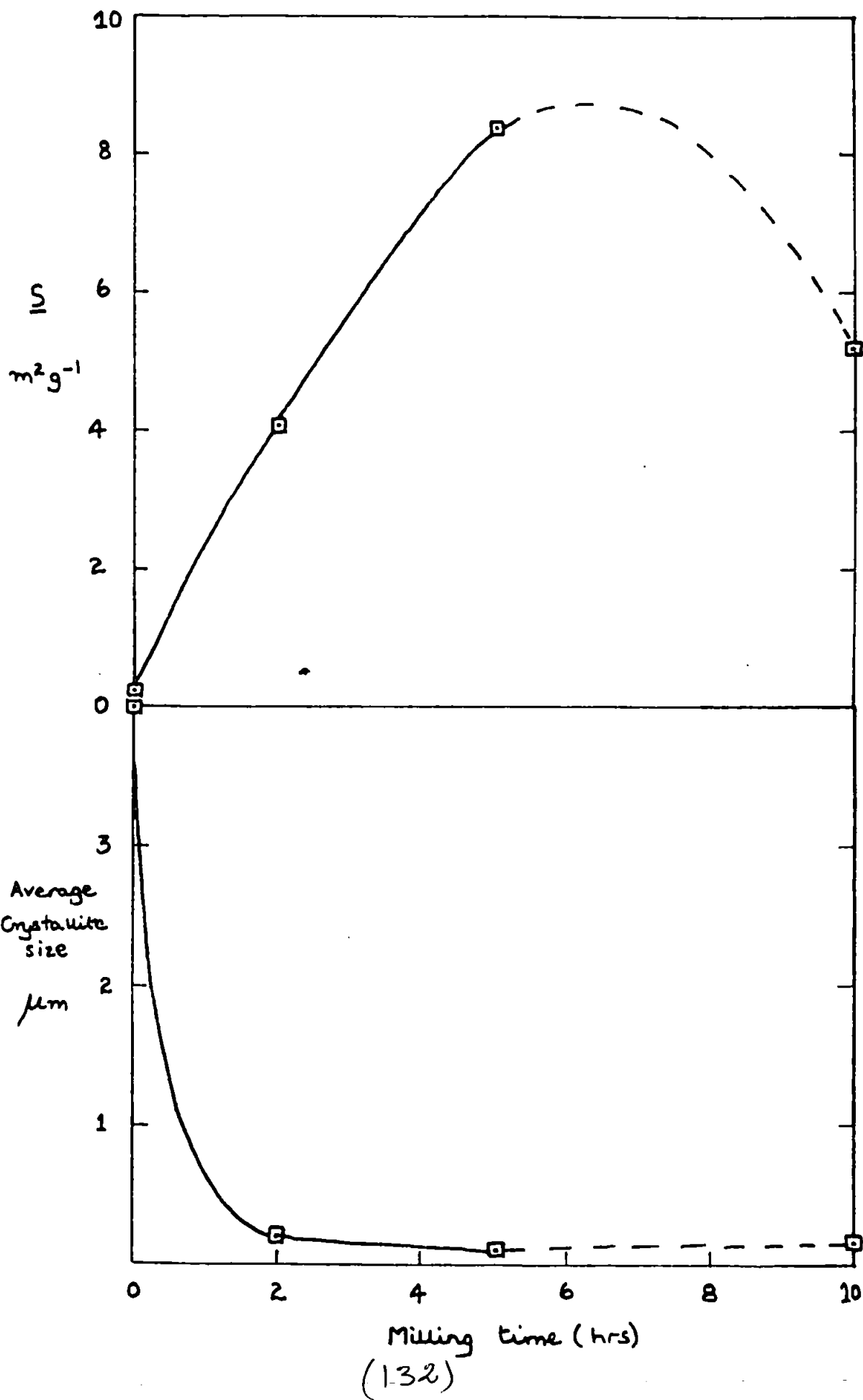
In the last equation the values of  $K_p$  are reduced somewhat, presumably because hafnium-free iodide-zirconium was used. Since the reaction rate is virtually independent of pressure (Dravnieks, 1950); and because of the applicability of the parabolic time relationship, oxidation is very probably diffusion-controlled by a scale consisting of an n-type semi-conductor.

Production of zirconium nitride from the tetrachloride vapour and nitrogen+hydrogen (Agte & Moers, 1931) and by heating the metal in nitrogen give samples of zirconium nitride showing homogeneity ranges from nearly stoichiometric ZrN (13.3 wt-%, 50 at-%N) at  $600^\circ\text{C}$  to lower nitrogen contents at temperatures up to  $1800^\circ\text{C}$ . Thus, typical samples of nitrided zirconium used in the present work contained only 10.32 wt-%, 42.8 at-%N and 9.29 wt-%, 40.0 at-% N.

### 3.2.2 Milling of Zirconium Nitride

The nitride samples sintered extensively during preparation, so that their specific surfaces were only about  $0.2 \text{ m}^2\text{g}^{-1}$ , and average crystallite sizes about  $4 \mu\text{m}$ . The sample containing 9.29 wt-% (40.0 at-%) nitrogen was milled to increase its surface activity and to examine changes in the microstructure caused by the comminution. 6g- portions of the zirconium nitride (69.1 wt-% ZrN + 30.1 wt-%Zr)

FIG. 3.10: MILLING OF ZIRCONIUM NITRIDE



were milled under standard conditions described in Section 2.6, Chapter II. The specific surface progressively increased ( Fig., 3.10(a)) during the first 5 hours milling, while the initial single crystals were fractured and incorporated into the aggregates. Thus, the average crystallite size decreased rapidly at first and later slowly when crystallites became of submicron size, similar to the behaviour of titanium nitride on milling. However, longer milling, 5 to 10 hours, appeared to give a considerable decrease in specific surface (from 8.2 to 5.2 m<sup>2</sup>g<sup>-1</sup>) and increase in average crystallite size (from 0.10 to 0.16 μm), as shown in Figure 3.10(b).

The milling caused strain to be set up within the crystallites so that there was X-ray line (or peak)-broadening as shown in Fig.3.11. These traces reveal that the metal present has been more extensively milled than the nitride. After 5 hours milling, the softer metal became difficult to remove from the balls of the mill, accounting for the lower specific surface and larger crystallites of the 10 hour milled sample (Figure 3.11.d) which was more representative of the nitride present. Nevertheless, the strain in the nitride crystallites increased progressively throughout the milling, as shown in Table 3.2.

TABLE 3.4

Lattice Strain in Milled ZrN Samples

Zirconium Nitride	Half-peak Widths (2θ) in Minutes for Reflections			Strain radians (using (200) reflections)
	ZrN(III)	ZrN(200)	α-Zr(101)	
Unmilled	23	19	30	-
Milled, 2h	24	22	32	2.53 x 10 <sup>-2</sup>
Milled, 5h	30	31	≈ 70	1.03 x 10 <sup>-2</sup>
Milled, 10h	44	40	≈ 70	1.88 x 10 <sup>-2</sup>

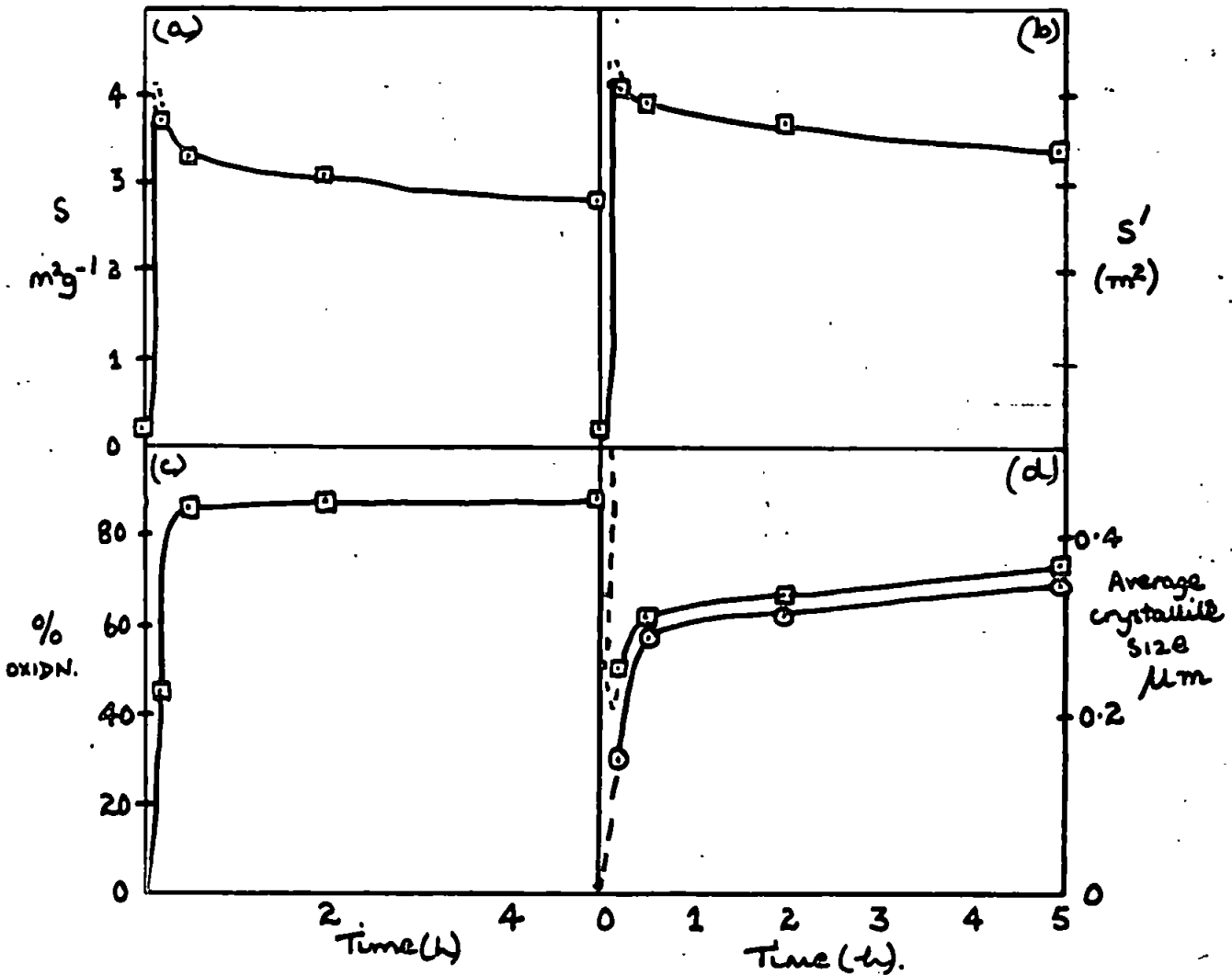
### 3.2.3 Oxidation of Zirconium Nitride

Changes in phase composition, surface area, crystallite and aggregate sizes during the oxidation of the unmilled zirconium nitride (10.32 wt %N, 42.8 at %N) have been described in an earlier paper covering the preliminary part of the present investigation (see Appendix 4). The zirconium nitride oxidation is complicated by formation of tetragonal  $ZrO_2$  at higher temperatures, particularly over  $1200^\circ$ , and monoclinic  $ZrO_2$  at lower temperatures. The nitride initially forms the so-called 'amorphous' cubic  $ZrO_2$ , notably between  $400^\circ$ - $600^\circ C$ , which may be stabilised somewhat by the remaining cubic  $ZrN$ . Subsequently there is a further fractional volume increase while formation of monoclinic  $ZrO_2$  is being completed.

When samples of zirconium nitride containing some free zirconium metal are calcined in air, the metal oxidises rapidly at temperatures of  $350^\circ$ - $400^\circ C$ . The nitride requires correspondingly higher oxidising temperatures, and initially forms the so-called 'amorphous' cubic  $ZrO_2$  (Mazdidasni & Lynch, 1964), notably between  $400^\circ$  and  $600^\circ C$  (cf. cubic  $ZrO_2$  from  $Zr$ -alkoxides decomposed in nitrogen at  $300^\circ$ - $400^\circ C$ , which may be stabilised somewhat by the remaining cubic  $ZrN$  in the present work). X-ray diffractometer traces show an additional reflection at  $2.94-95^\circ$ , some reinforcement of the  $2.54^\circ$  spacing and displacement and broadening of the  $1.81$  and  $1.54^\circ$  spacings of monoclinic  $ZrO_2$  towards the shorter distances of  $1.80$  and  $1.53^\circ$  of the cubic form. At higher temperatures ( $700$ - $1000^\circ C$ ), the additional reflection disappears and the main monoclinic  $ZrO_2$  reflections at  $3.16$  and  $2.84^\circ$  develop more rapidly. The conversion of cubic face-centred  $ZrN$  ( $a = 4.56^\circ$ ) to cubic face-centred  $ZrO_2$  ( $a = 5.09^\circ$ ) involves a fractional volume increase of 0.367 (of the initial

FIG. 3.12

OXIDATION OF UNMILLED ZIRCONIUM NITRIDE AT 500° IN AIR



OXIDATION OF MILLED ZIRCONIUM NITRIDE AT 400° IN AIR.

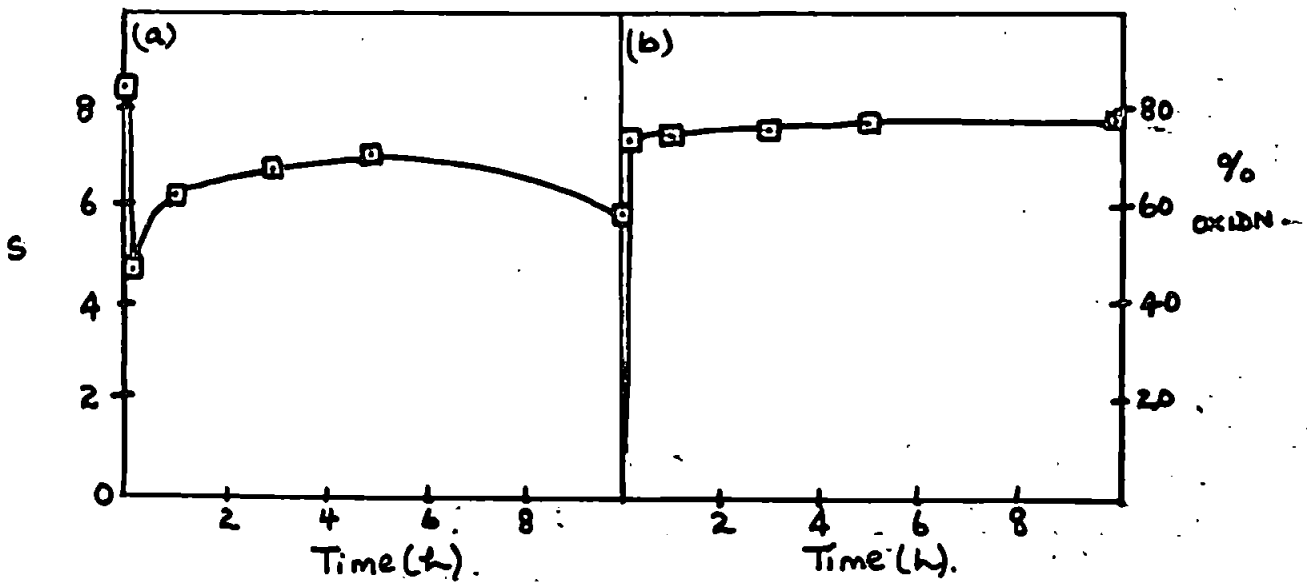


FIG. 3.13



volume) which further increases to 0.518 when formation of monoclinic  $ZrO_2$  is completed.

The nitride samples are completely oxidised to  $ZrO_2$  at temperatures above  $600^\circ C$  within reasonable lengths of time. X-ray diffractometer traces and powder photographs give no indications of any oxy-nitride being formed at temperatures between  $400^\circ$  to  $1000^\circ C$ . Variations in specific surface,  $S_s$ , actual surface area,  $S'$  (for 1 g. initial sample) and average crystallite size are shown in Figure 3.12, (a), (b), (d), for unmilled zirconium nitride samples, oxidised at  $500^\circ C$  in air. About  $\frac{3}{4}$  of the material is oxidised within half-hour (Figure 3.12 (c)). There is a considerable increase in specific surface and the actual surface area,  $S'$ . Thus, when the zirconia crystallises out from the nitride matrix, it evidently splits off to give smaller crystallites, which are mainly of sub-micron size, caused by changes in types of crystal lattice and by the volume increases given in the previous paragraph. Subsequently the oxidation becomes very slow and the specific surface decreases whilst the average crystallite size increases as the material slowly sinters. After the first stage most of the surface area is that of the oxide which then has an average crystallite size almost equal to that of the whole material. The oxide apparently forms impermeable layers around the remainder of the nitride through which normal gaseous diffusion cannot occur, since the oxidation is incomplete even after much longer heating. The high melting point of zirconium dioxide ( $2700^\circ C$ ) gives a Tammann temperature of about  $1210^\circ C$  (one-half of the m.p. in K) for appreciable lattice diffusion and a temperature of about  $720^\circ C$  (one-third of the m.p.), above which surface diffusion can be operative.

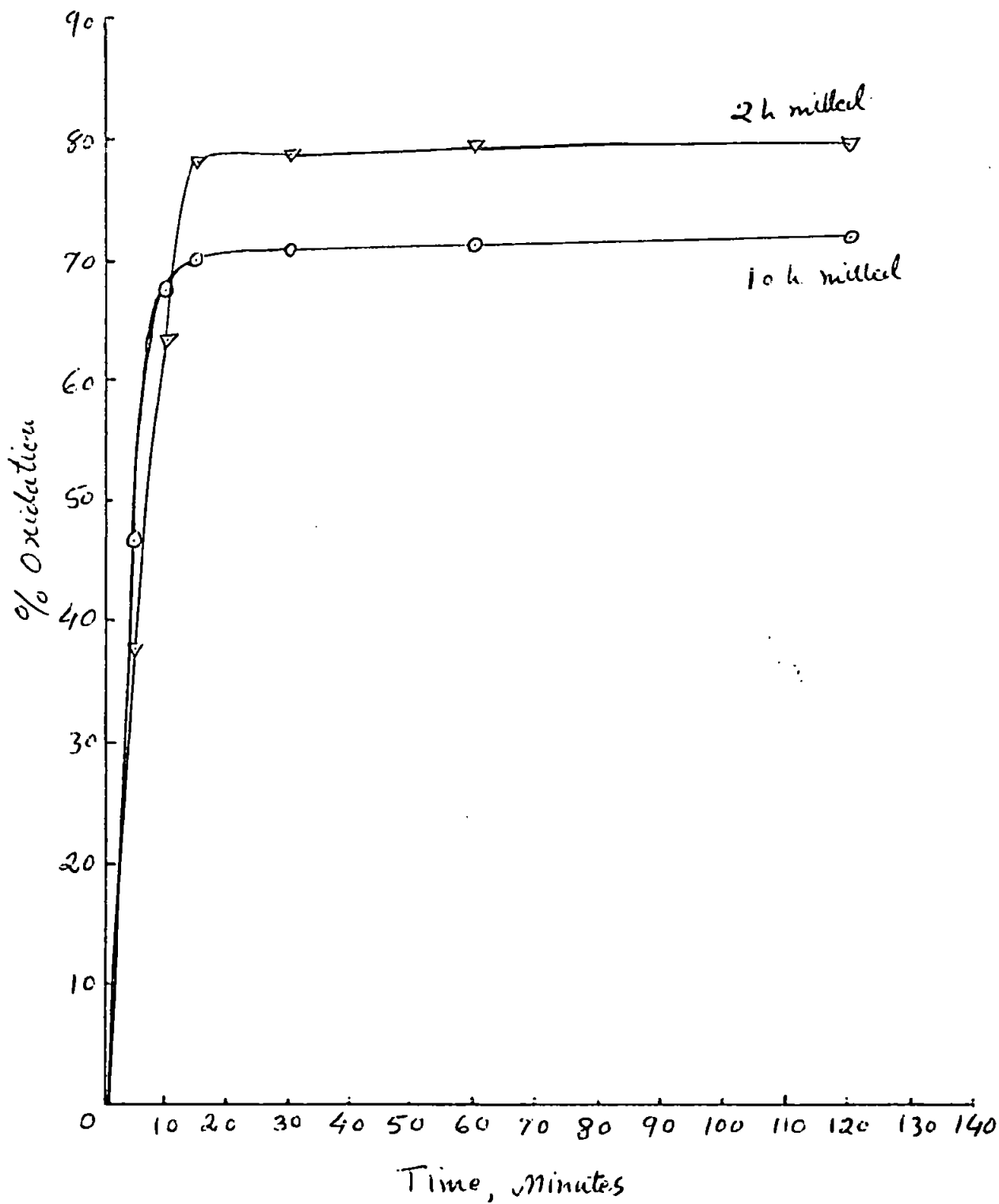
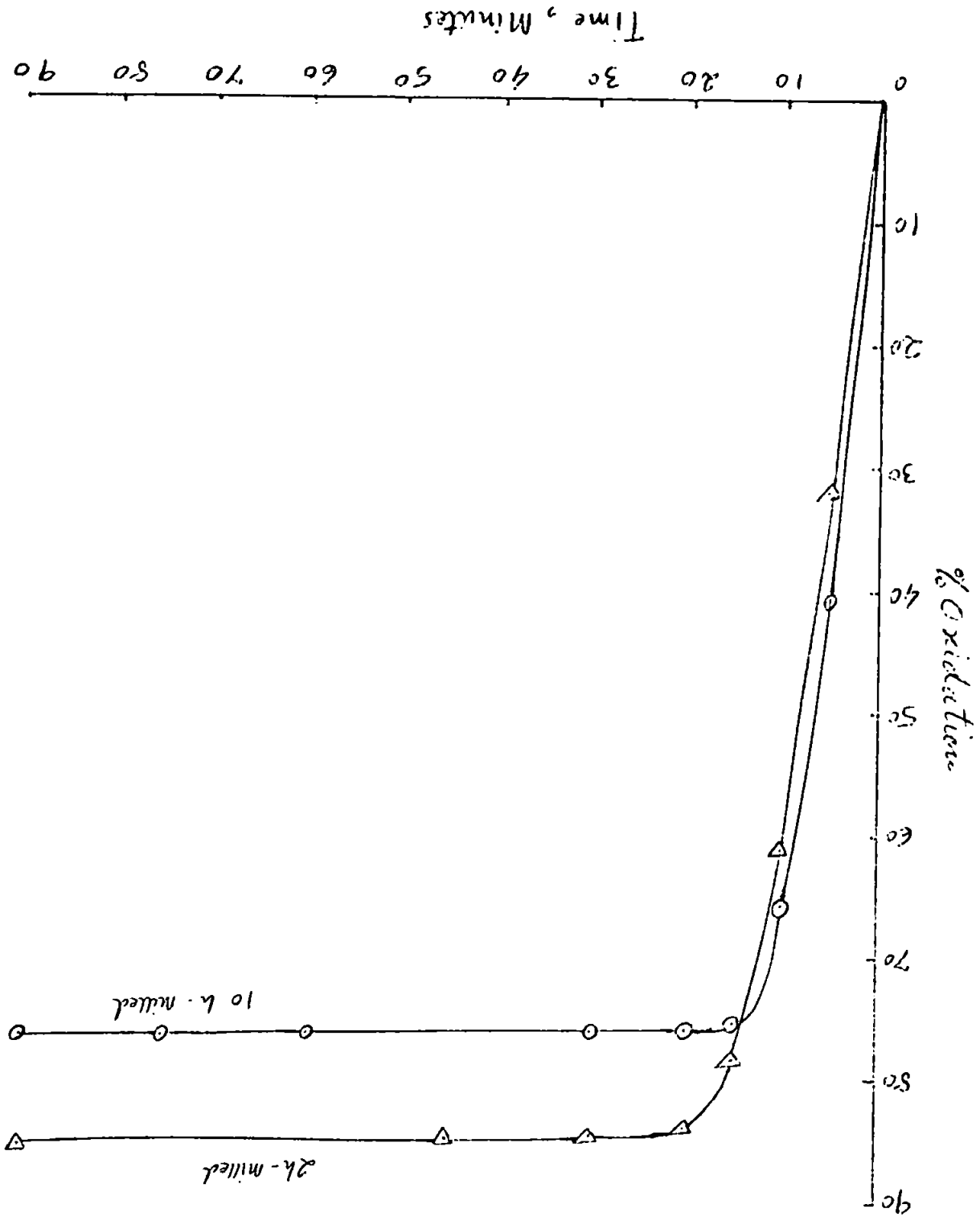


Figure 3.14(A): Oxidation Isotherms for milled zirconium Nitride in Air at 300°C.

(1710)

Figure 3(14b): Oxidation Isotherms for milled Zirconium Nitride in Air at 535°C.



Any sintering is probably given by grain boundary penetration, promoted by the presence of unoxidised metal (m.p. 1860°C), which can be effective above about  $\frac{1}{2}$  m.p. of zirconium metal (i.e. 440°C). This type of behaviour has been observed recently in the oxidation of Nickel and Chromium where more extensive oxide sintering gives good protective films (Maude, 1970).

Milled zirconium nitride (5 hours milled) oxidises rapidly even at lower temperatures, viz., 400°C. The very finely-divided Zr-metal present oxidises very rapidly (Figure 3.13 (b)), so that there is an initial decrease in surface. Later, the surface increases as more of the nitride is oxidised (Fig. 3.13(a)), but finally an impermeable oxide layer is formed which prevents further oxidation at this temperature. Similar oxidation behaviour is shown at 300°C, 435°C, and 540°C (Figs. 3.14 (a) (b) & (c)) for the samples that have been milled for 2 hours and 10 hours. The somewhat lower final amounts of oxidation for the milled samples are caused by the difficulties in complete removal of the zirconium metal component of the original nitride from the mill. This effect seems to be proportional to the milling time in the present case, and has been discussed in the previous section.

Electron micrographs of the unmilled, milled and oxidised zirconium nitride samples are presented in Plates 3.7, 3.8, 3.9 and 3.10.



A micrograph showing several large, dark, angular particles of zirconium nitride. The particles are irregular in shape and vary in size, with some appearing as large, flat plates and others as smaller, more rounded fragments. A scale bar in the upper left corner indicates a length of 2 micrometers.

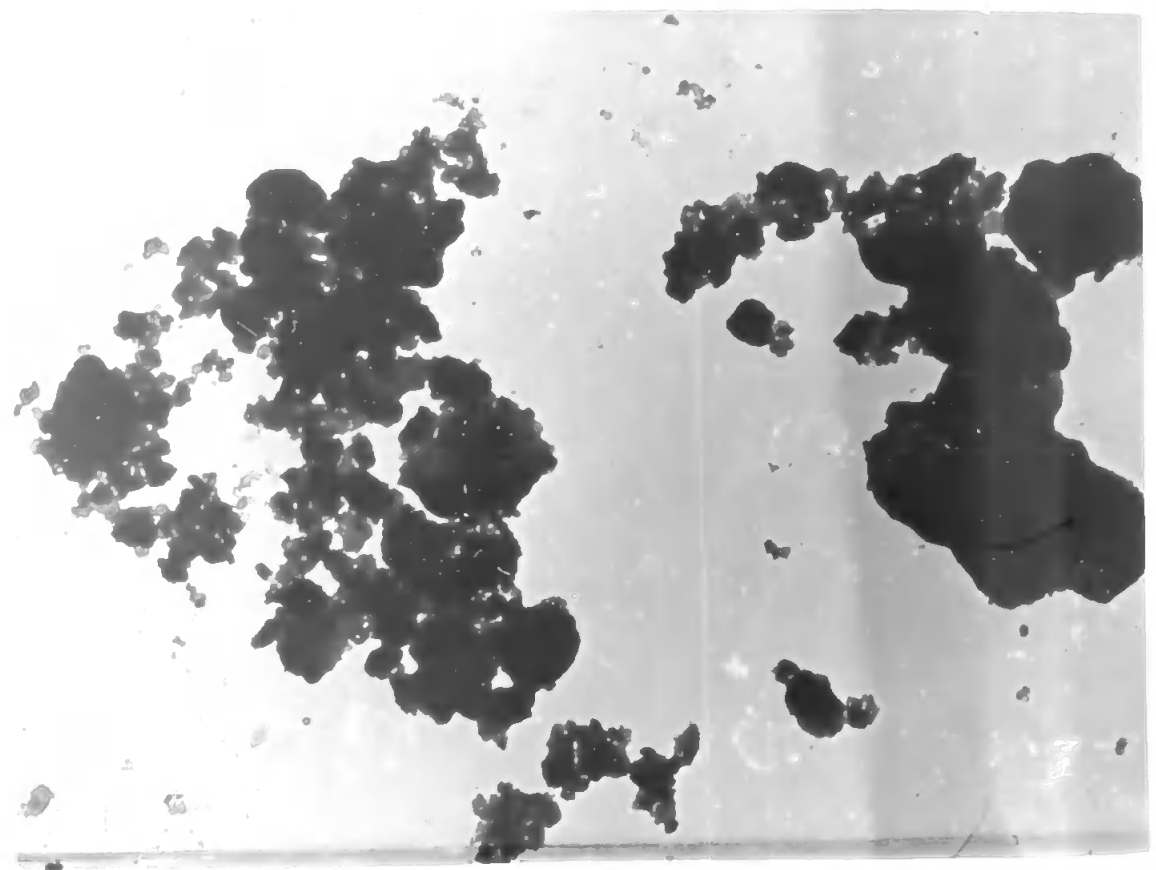
2  $\mu$ m

PLATE 3.7 Zirconium Nitride, Untreated

↑  
x 10,000  
Magnification x 20,000  
↓

Page (143)

PLATE 3.8 Zirconium Nitride, Ball-Milled for 2 hours.



A micrograph showing zirconium nitride particles after 2 hours of ball-milling. The particles are significantly smaller and more numerous than in the untreated sample. They appear as a dense, irregular cluster of small, dark, rounded particles. A scale bar in the lower left corner indicates a length of 1 micrometer.

1  $\mu$ m



PLATE 3.9 Zirconium Nitride, Ball-Milled for 10 hours

Magnification x 20,000

Page (144)

PLATE 3.10 Zirconium Nitride, Oxidised in Air at 450°C for 5 hours.



## CHAPTER IV

### VANADIUM, NIOBIUM AND TANTALUM NITRIDES

#### 4.1 VANADIUM NITRIDE

##### 4.1.1 Nitridation of Vanadium

The vanadium-nitrogen system and its thermodynamics have been described in Chapter I. As generally found for transition metal nitrides, the kinetics of formation depend not only on the intrinsic reactivity of the material concerned, but also on the available surface or interface at which reaction can occur.

The nitridation rate for vanadium is much less at a given temperature than for the corresponding oxidation, but it is similar to those for the reactions of nitrogen with niobium or tantalum. Likewise, the nitride films dissolve in these metals as fast as they are formed. Both, nitridation and oxidation of vanadium progress almost parabolically for temperature ranges of 600°-900°C and 400°-600°C respectively. The rate equations for  $p = 0.1$  atm. and  $t$  (Maximum) = 2 h (Gulbransen & Andrew, 1950) are as follows:

$$N_2 : K_p = 0.94 \times 10^{-5} \exp(-31,400/RT) \text{ g}^2\text{cm}^{-4}\text{s}^{-1}$$

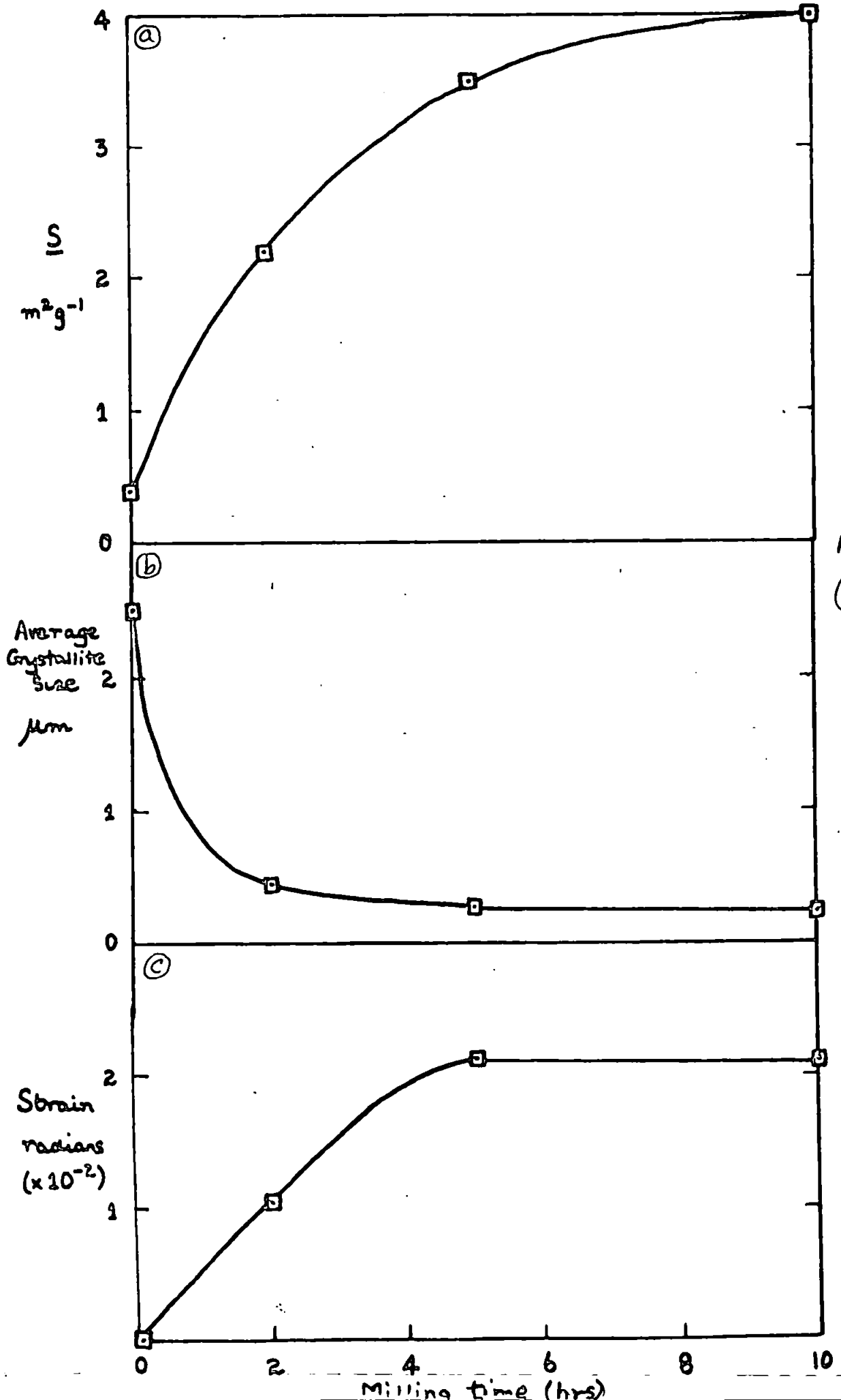
$$O_2 : K_p = 1.3 \times 10^{-3} \exp(-30,700/RT) \text{ g}^2\text{cm}^{-4}\text{s}^{-1}$$

Preliminary nitriding treatment was found to lower both the initial and ultimate oxidation rates.

##### 4.1.2 Milling of Vanadium Nitride

As with the nitrides of group IV (Ti, Zr), the high temperatures required for producing those of group V (V, Nb, Ta) cause sintering to the extent that samples generally have specific surfaces of below  $1 \text{ m}^2\text{g}^{-1}$ , and average crystallite sizes (equivalent spherical

FIG. 4.1: MILLING OF VANADIUM NITRIDE





diameters) of over  $2\ \mu\text{m}$ . Thus, samples of vanadium nitride, VN, were milled to increase their surface activity and to examine changes in microstructure caused by comminution. When 6g-samples were milled (under conditions described in Chapter II, Section 2.6), the specific surface progressively increased as shown in Fig. 4.1(a). Electron micrographs showed that the original nitride consisted of single crystals and aggregates of about  $0.4\text{--}8\ \mu\text{m}$  size (Plate 4.1). The single crystals were fractured during the earlier stages of the milling and the fragments were incorporated into the aggregates which remained approximately the same size throughout the milling. Thus, the average crystallite size (Fig. 4.1(b)), decreased rapidly at first and later slowly when the crystallites became of sub micron size. This behaviour is similar to that found for the milling of titanium nitride, TiN, described in Chapter III, Section 3.1.2. Electron micrographs of 2h and 10h milled samples are presented in Plates 4.2 and 4.3 respectively.

Again, the milling caused strain to be set up within the crystallites, so that there was X-ray line (or peak) - broadening. Table 4.1 shows the half-peak widths of the (111) and (200) reflections. The strain was calculated from the half-peak width of the (200) X-ray reflection (using Jones' Method, Chapter II, Section 2.1.5), after allowing for broadening due to crystallite size. Figure 4.1(c) illustrates the development of strain, which occurred mainly during the first two hours milling when the single crystals were fractured and incorporated into the aggregate. Subsequently the strain remained practically constant.

2  $\mu$ m

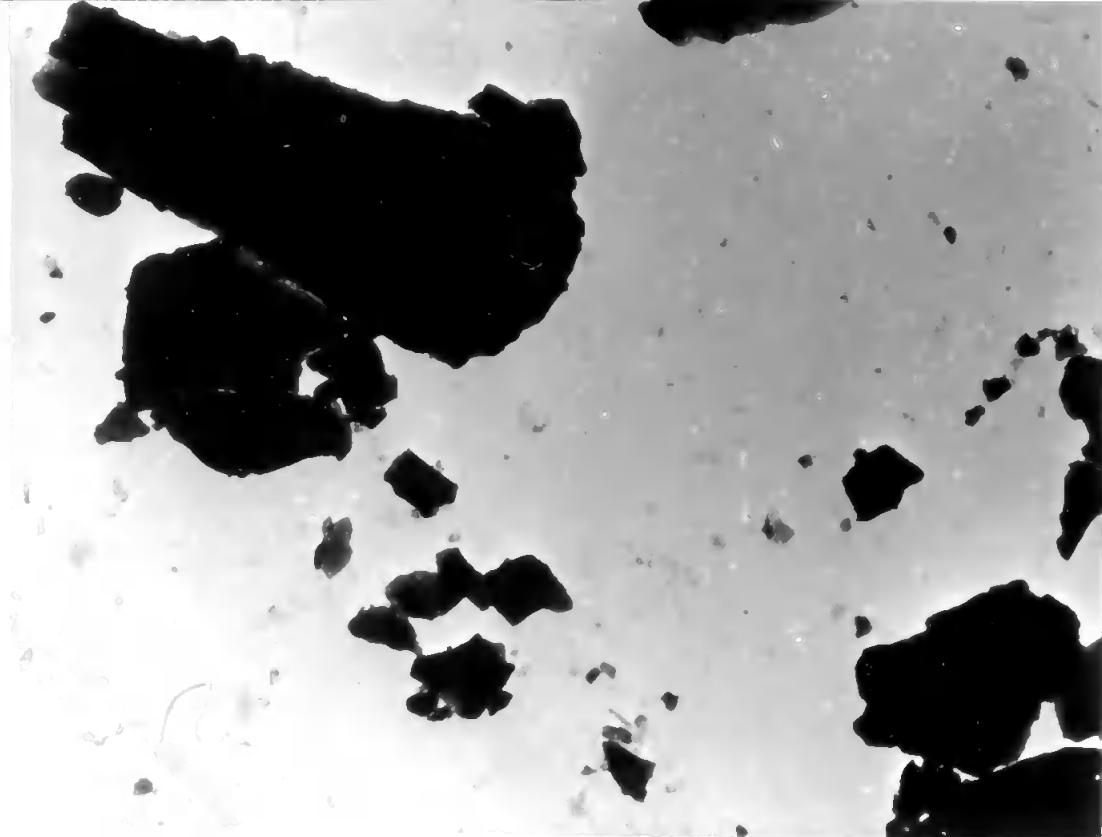


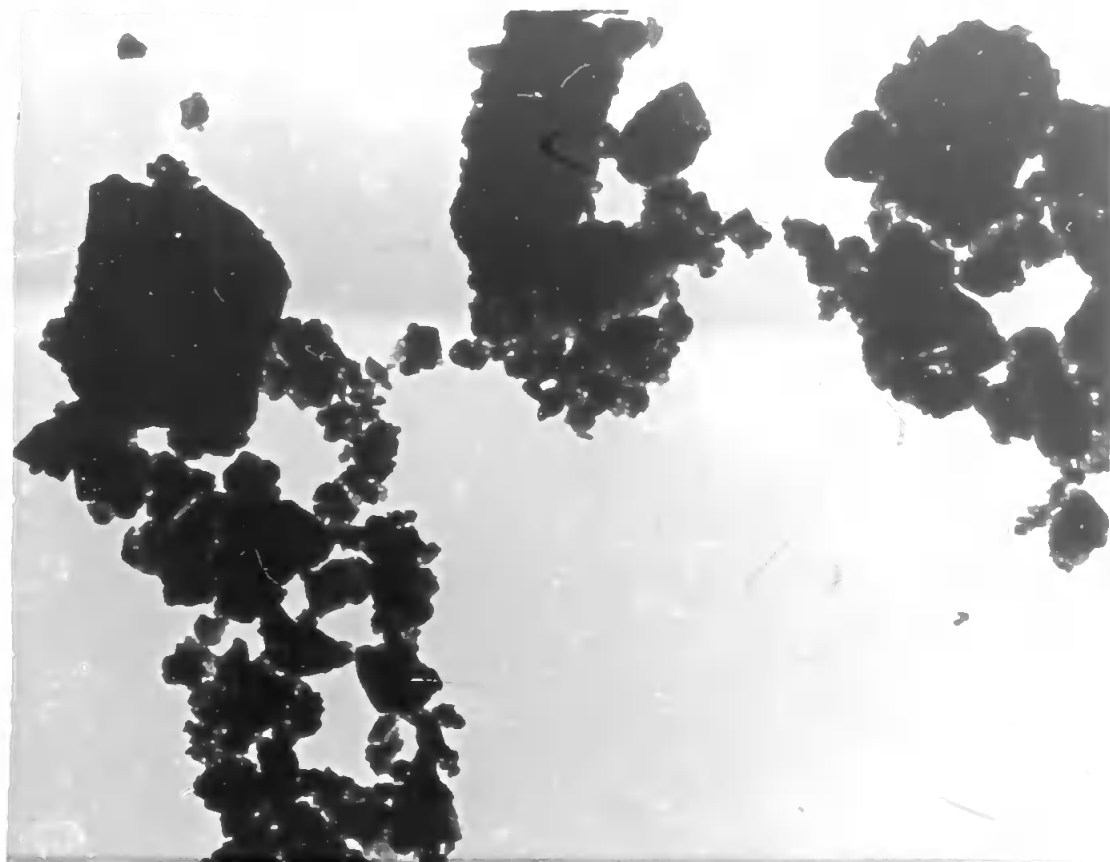
PLATE 4.1 Vanadium Nitride, Untreated.

Magnification:  $\times 10,000$   
 $\times 10,000$

Page (148)

PLATE 4.2 Vanadium Nitride, Ball-Milled for 2 hours.

1  $\mu$ m



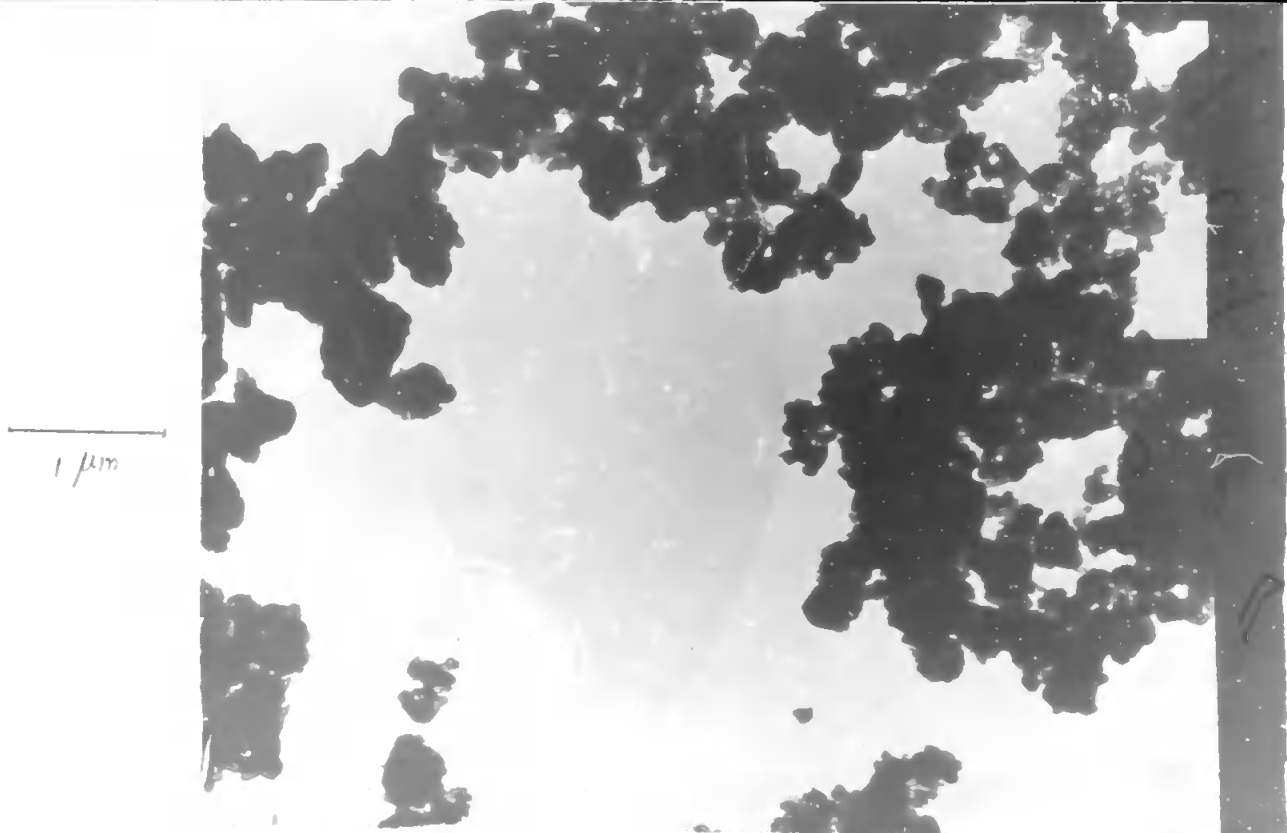


PLATE 4.3 Vanadium Nitride, Ball-Milled for 10 hours.

Magnification x 20,000

Page (119)

PLATE 4.3:1 Vanadium Nitride, Oxidised in Air at 500°C for 2 hours



1  $\mu$ m



PLATE 4.3:2 Vanadium Nitride, Untreated

Magnification  $\times$  20,000

Page (150)

PLATE 4.4 Vanadium Nitride, Oxidised in Air at 600°C for  $\frac{1}{2}$  hour.

1  $\mu$ m



TABLE 4.1

Lattice Strain in Milled VN Samples

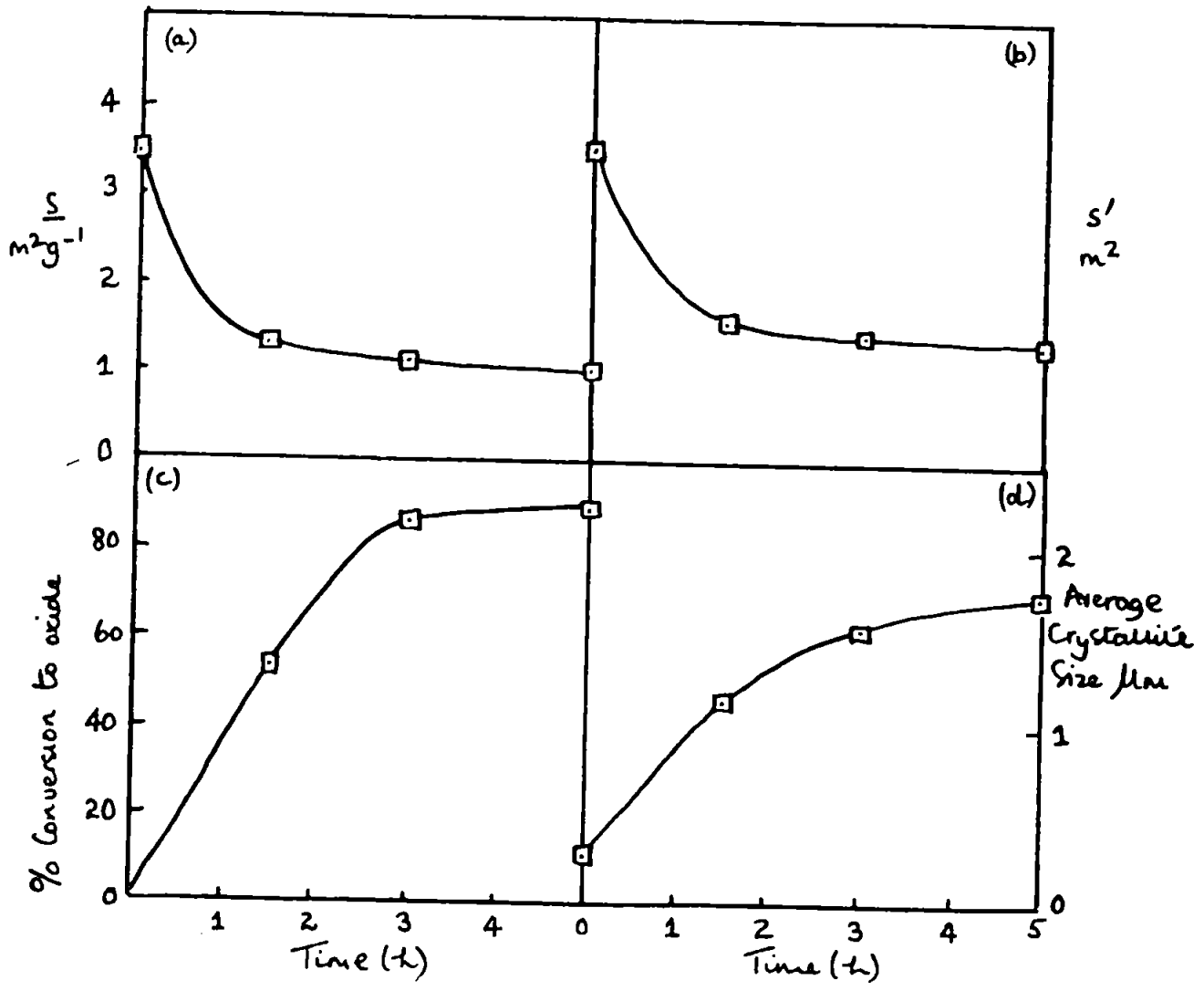
Vanadium Nitride	Half-Peak widths (2 $\theta$ ) in Minutes for Reflections		Strain (radians) (Using (200) reflections)
	VN 411	VN(200)	
Unmilled	17	18	-
Milled, 2h	30	32	$1.04 \times 10^{-2}$
Milled, 5h	40	42	$2.11 \times 10^{-2}$
Milled, 10h	40	42	$2.07 \times 10^{-2}$

4.1.3 Oxidation of Vanadium Nitride

Vanadium nitride, VN, is converted to vanadium pentoxide, V<sub>2</sub>O<sub>5</sub>, at 450°-650°C in air. X-ray diffractometer traces give no indications of any oxynitrides or lower oxides of vanadium being formed at these temperatures. Variations in specific surface,  $\underline{S}$ , actual surface area (for 1 g. initial sample),  $\underline{S}'$  and average crystallite size (equivalent spherical diameter) are shown in Figure 4.2 (a) & (b) for 5 hours-milled vanadium nitride oxidised at 550°C in air. About  $\frac{3}{4}$  of the material oxidises comparatively rapidly, while  $\underline{S}$  and  $\underline{S}'$  decrease considerably and the average crystallite size rapidly increases to above 1  $\mu$ m. Subsequently, the oxidation proceeds much more slowly with correspondingly smaller changes in the surface areas and average crystallite sizes. When the oxide crystallises out from the nitride matrix, the change in type of crystal lattice (cubic F-VN to orthorhombic V<sub>2</sub>O<sub>5</sub>) and large fractional volume increase (1.272 of the original volume), would be expected to produce considerable splitting away of oxide crystallites. However, the surface areas decrease since vanadium

FIGURE 4.2

OXIDATION OF MILLED VANADIUM NITRIDE AT 550° IN AIR



pentoxide sinters very readily at 550°C. This temperature is well above the Tammann temperature (ca.  $\frac{1}{2}$  m.p. in K) of about 200°C for vanadium pentoxide and close to its m.p. of 674°C, so that lattice diffusion can be extensive. Since the Tammann temperature of the nitride is very much higher (about 900°C), in the later stages of the oxidation, the nitride particles are surrounded by layers of oxide impermeable to normal gaseous diffusion. Thus, the initial approximately linear kinetics become parabolic being controlled by lattice diffusion through the oxide layer. This is demonstrated further by oxidation isotherms on 1 gram-samples of milled and unmilled vanadium nitride shown in Figures 4.3 and 4.4. The maximum oxidation rate is given at about 575°C for both the 2 hours and 10 hours milled samples. The rate at 650°C is considerably lower in each case apparently caused by more extensive sintering of the oxide impeding the oxidation, cf. negative temperature coefficients observed for oxidation rates of Niobium metal (Aylmore et.al., 1960; Argent & Phelps, 1960). Accordingly electron micrographs show that the initial irregular particles of unmilled or milled vanadium nitride ultimately give regular shaped V<sub>2</sub>O<sub>5</sub> particles on oxidation at 600°C (Plate 4.4)

## 4.2 NIOBIUM NITRIDE

### 4.2.1 Nitridation of Niobium

The niobium-nitrogen system and its thermodynamics have been described in Chapter I. Neumann et.al. (1934), Brewer et.al. (1950) and Armstrong (1949) have also given thermodynamic data on this nitride. The reaction between niobium and nitrogen mainly follows the parabolic rate law. At 700°C the rates are similar to those for the nitridation of titanium and tantalum, but correspondingly slower than

for zirconium. The data of Gulbransen and Andrew (1949 and 1950) deviate slightly from the parabolic law in the early reaction stages. These workers have measured the rate constant of the reaction of niobium metal with 0.1 atm. of nitrogen and is represented by:

$$\text{Nb} : 500 - 800^{\circ}\text{C} : K_p = 8 \times 10^{-8} \exp (-25,400/RT) \text{ g}^2\text{cm}^{-4}\text{s}^{-1}$$

However, by using the method of van Liempt (see Barrer, 1941), it has been shown that the parabolic rate law follows from consideration of direct diffusion of nitrogen into the metal. The negligible effect of pressure is similar to that found for the reaction of nitrogen with tantalum. In vacua of  $10^{-6}$  mm. Hg or lower the niobium-nitrogen product loses weight below  $605^{\circ}\text{C}$ , while at higher temperatures the metal acts as a 'getter' in a similar manner to tantalum and zirconium. The reaction apparently does not take place directly on the metal but rather through a film of nitride which hinders the pressure from exerting its normal influence on this type of reaction. The nitride film thickness is governed by the rate of formation and the rate of solution. The energy of activation for diffusion of nitrogen in niobium is 39,500 cal/mole (Ang, 1953).

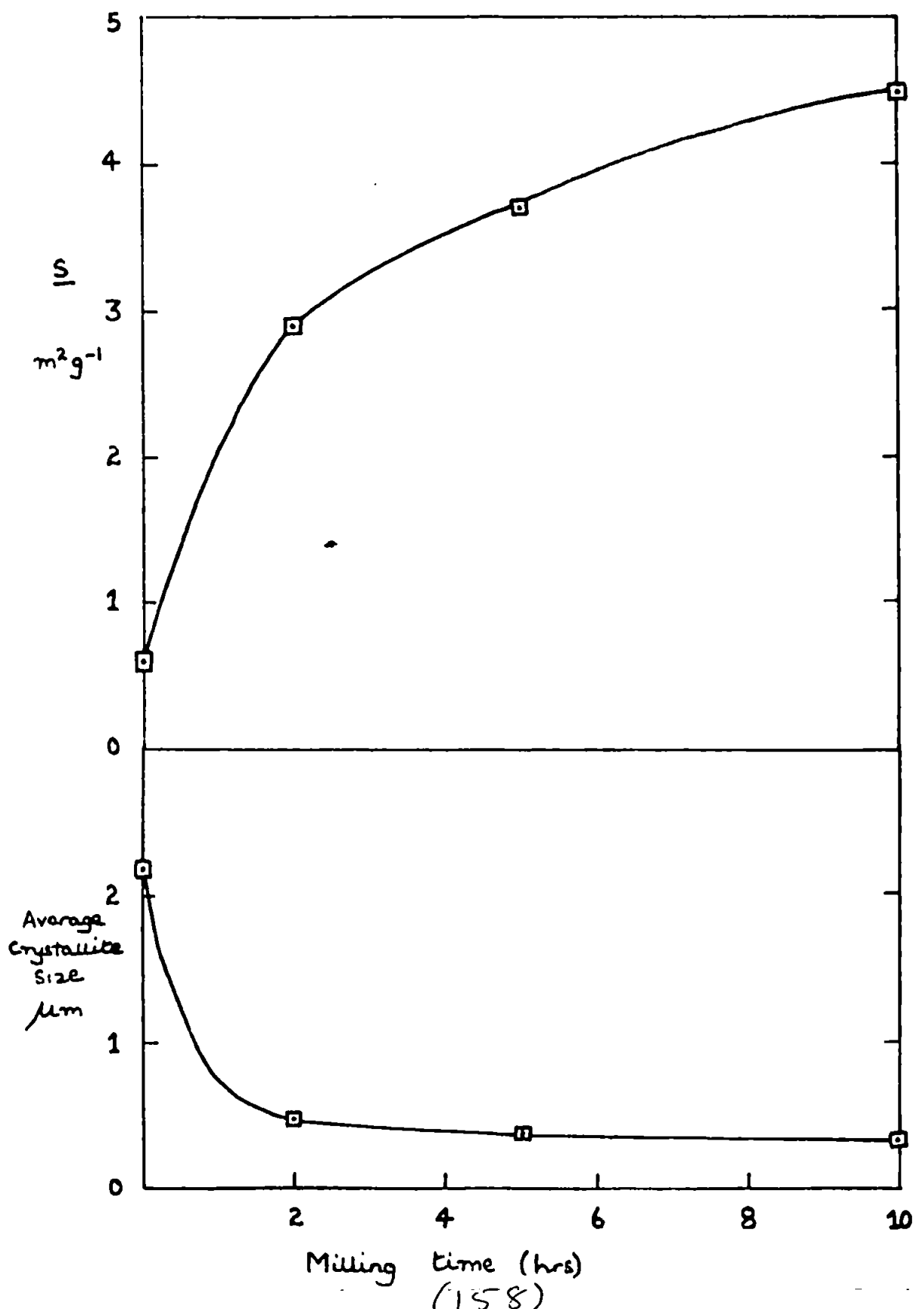
#### 4.2.2 Milling of Niobium Nitride

When 6g-samples of niobium nitride were milled (under conditions described in Chapter II, Section 2.6), the specific surface progressively increased as shown in Figure 4.5(a). The changes were of similar magnitude to those found for vanadium nitride, VN, under identical milling conditions, even though the niobium nitride sample was almost pure  $\xi$  - NbN (in which nitridation had been nearly complete giving  $\text{NbN}_{0.9}$  having a widely different crystal structure, viz., hexagonal,  $\gamma'$  - MoC (Bi), compared with the cubic F -type lattice for VN. Electron micrographs (Plates 4.5, 4.6, & 4.7) did not show any



FIGURE 4.5

MILLING OF NIOBIUM NITRIDE



1  $\mu$ m

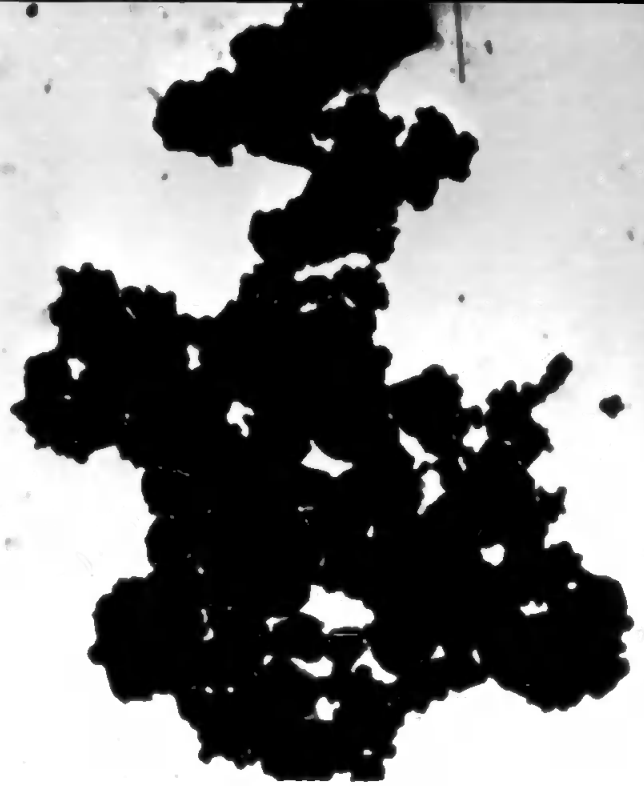


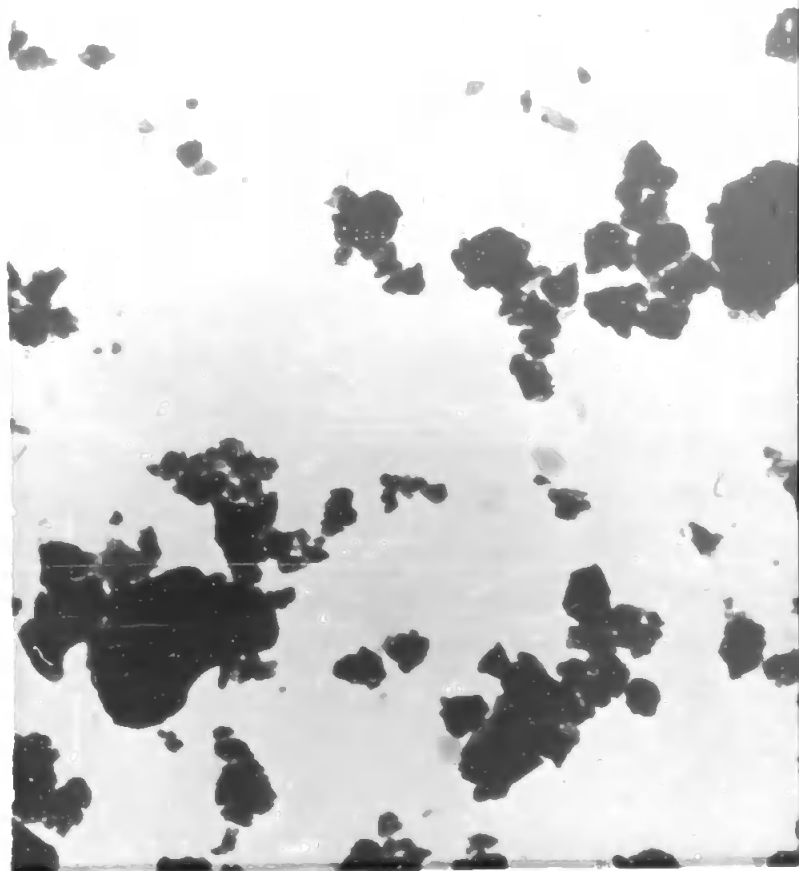
PLATE 4.5 Niobium Nitride, Ball-Milled for 2 hours

Magnification x 20,000

Page (159)

PLATE 4.6 Niobium Nitride, Ball-Milled for 10 hours

1  $\mu$ m



1  $\mu$ m



PLATE 4.7 Niobium Nitride, Untreated

Magnification x 80,000

Page (160)

PLATE 4.8 Niobium Nitride, Oxidised in Air at 800°C for 5 hours

1  $\mu$ m



well-defined hexagonal structures either in the original niobium nitride or in the milled material. Fracturing of single crystals in the earlier stages of the milling and their incorporation into the aggregates caused comparatively larger decreases in average crystallite size (Fig. 4.5 b) and production of more submicron-sized material. The strain set up in the crystallites caused X-ray line (or peak) - broadening of the several reflections associated with one or both of the  $a$ - and  $c$ - axes of the hexagonal lattice, but individual intensities and peak separations were insufficient for even approximate determination of strain perpendicular to the different crystal planes.

#### 4.2.3 Oxidation of Niobium Nitride

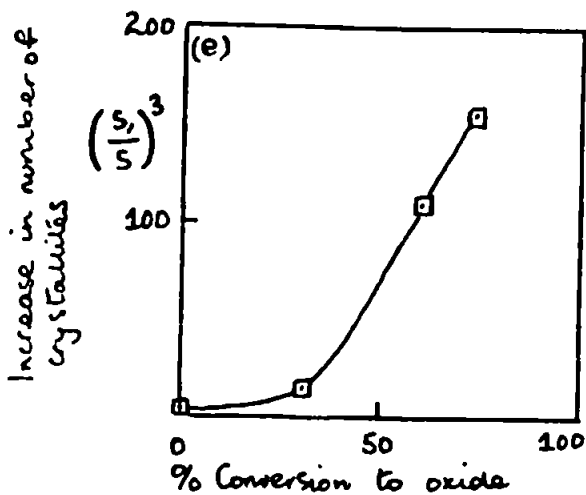
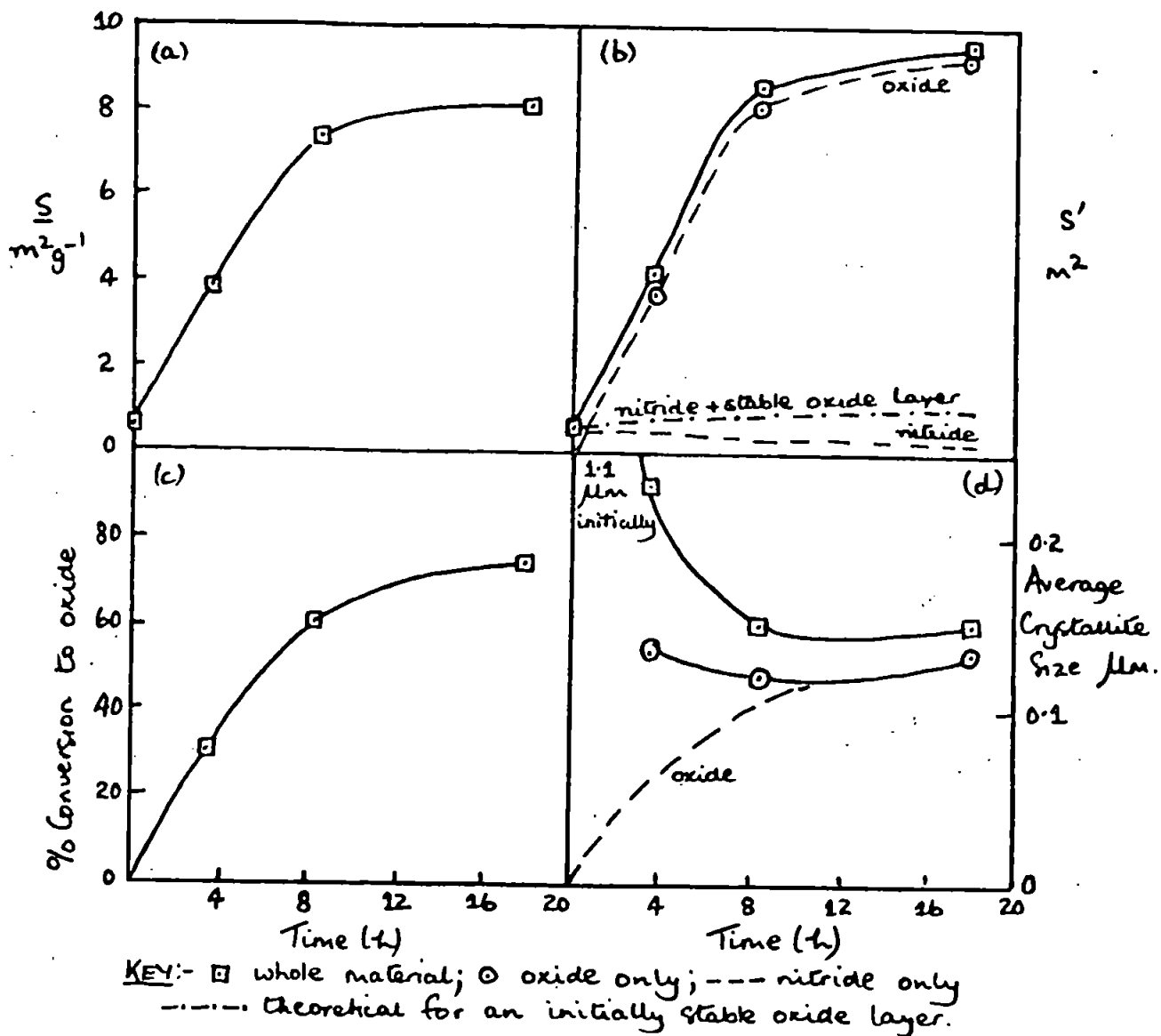
The niobium nitride  $\beta$ -NbN, is converted to  $\beta$ -niobium pentoxide, Nb<sub>2</sub>O<sub>5</sub>, at 300-600°C in air. X-ray diffractometer traces give no indications of any oxynitrides or lower oxides of niobium being formed at these temperatures; cf; Schonberg's (1954) initial oxynitride products formed by nitriding  $\beta$  or  $\gamma$ -NbN in steam and excess hydrogen at 700°C or by ammonia nitriding of niobium oxides or ammonium niobate (NbN<sub>0.9</sub>O<sub>0.1</sub> and NbN<sub>0.6</sub>O<sub>0.2-0.3</sub> having a cubic F-lattice).

Variations in specific surface  $S_p$ , actual surface area (for 1 g. initial sample),  $S_p^o$ , and average crystallite size are shown in Figures 4.6, and 4.7 for the atmospheric oxidation of unmilled and 5h -milled niobium nitride. These are compared with similar changes for the oxidation of niobium metal in Figure 4.8.

When the unmilled nitride is oxidised at 400°C in air,  $S_p$  increases considerably (Figure 4.6 a & c). Thus, when the niobium oxide crystallises out from the nitride matrix, it evidently splits off to give smaller crystallites. Any additional spalling at the oxide-nitride

FIG. 4:6:

OXIDATION OF UNMILLED NIOBIUM NITRIDE AT 400° IN AIR



interface when the samples were cooled for surface area determination was negligible by comparison, since the reheated samples proceeded to give oxidation rates similar to those of samples which had been continuously heated. Hence, the crystallite splitting results mainly from changes in type of crystal structure (hexagonal  $\gamma'$ -MoC (Bi) to  $\beta$ -monoclinic) and a volume increase of 1.37 of the original volume as the nitride is converted to the less dense oxide.

Changes in the actual surface area  $S'$  and in the average crystallite size of the remaining niobium nitride (assuming no appreciable sintering) and the niobium oxide,  $\beta$ -Nb<sub>2</sub>O<sub>5</sub>, are deduced from the surface area data and volume changes and are shown in Fig. 4.6 (b) and (d). These confirm the ultimate sintering of the oxide, and the larger crystallite sizes given in the first half of the oxidation (above the broken line in Figure 4.6 (d)) are caused probably by some of the newly-formed oxide not being detached from the nitride surface. This is similar to the behaviour of aluminium nitride on oxidation (Glasson et.al., 1969).

When there is sufficient oxide of rational crystallite composition, it tends to form a stable coating around the remaining nitride particles. Therefore, the surface area  $S'$ , in the earlier stage of the oxidation, increased much more rapidly (Fig. 4.6 (b)) than it would if a stable oxide layer had been formed throughout the oxidation. The experimental results lie well above the theoretical curve calculated from the formula for a continually stable oxide layer (Glasson, 1958), viz.,

$$S'/S = (1 + 1.37 x)^2$$

where,  $S$  = surface of product (oxide + remaining nitride)  
 $S$  = sp. surface of original ig- nitride.  
 and  $x$  = fraction of nitride oxidised.

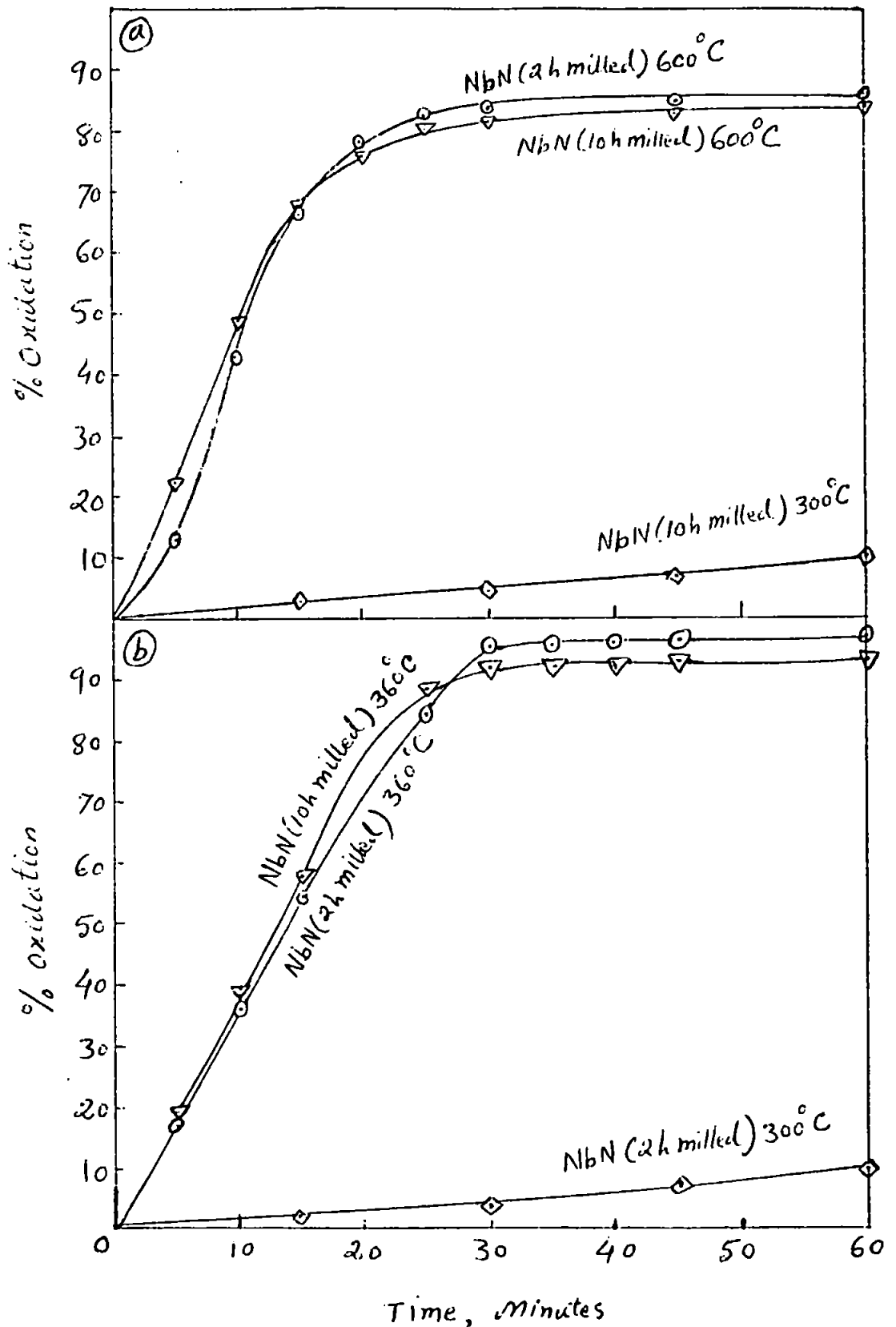


Figure 4.9: Oxidation Isotherms for milled Niobium Nitride.

This is confirmed by the increases in the number of crystallites calculated from  $(S_1/S)^3$ , where  $S_1 = S'/1.77$  i.e.  $S_1 = S/(2.37)^{1/3}$ , to allow for volume changes on oxidation (Figure 4.6(c)).

#### 4.2.3.1. Comparison with Oxidation of Niobium Metal

Similar behaviour to that of unmilled niobium nitride is shown by 5h-milled niobium nitride and niobium powder on oxidation in air at 300°C and 400°C respectively (Figures 4.7 and 4.8). The milled material apparently has greater surface heterogeneity and tends initially to give linear rather than parabolic oxidation rates (as discussed in Section 3.1.3 for titanium nitride and by Glasson et.al. (1969) for aluminium nitride oxidation). Further oxidation isotherms are compared in Figure 4.9 for the milled samples. The oxidation rates ultimately become almost linear with the formation of thicker oxide layers which are subject to cracking and partial detachment from the underlying metal or nitride because of the very large volume increases on oxidation. For oxide layers on larger metal samples (sheets), Kofstad (1960) has attributed similar behaviour to the formation of suboxides near the metal-oxide interface, but these lower oxides were not detected in the present work, involving oxidation of the metal powder.

For isothermal oxidations of 1g - portions of niobium nitride, a maximum rate was exhibited at about 360°C for both the 2h- and 10h- milled samples (Figure 4.9(b)). The rates at about 600°C are correspondingly lower, particularly in the later stages of the oxidation, probably due to the onset of sintering which tends to impede the oxidation process. This reversal of the temperature coefficient to negative values is similar to that found for oxidation



of milled titanium nitride in section 3.1.2 and niobium metal by Aylmore, Gregg and Jepson (1960). It has been ascribed to more extensive sintering of the oxide at the higher temperatures preventing normal gaseous diffusion. This is in accord with the Tammam temperature of  $\text{Nb}_2\text{O}_5$  ( $\frac{1}{2}$  m.p. in K) being about  $610^\circ\text{C}$ , when lattice diffusion becomes extensive. Sintering promoted by surface diffusion can become appreciable above about  $\frac{1}{3}$  m.p. in K, i.e.  $320^\circ\text{C}$ , which is approximately the temperature for the maximum oxidation rates for the milled nitride. At temperatures above  $600^\circ\text{C}$ , the oxidation rates for unmilled niobium nitride increase again with temperature, cf., rates at  $600^\circ$  and  $800^\circ\text{C}$  in Figure 4.10, as the lattice diffusion increases. The oxide crystallites obtained from the nitride at  $300^\circ\text{C}$  and  $400^\circ\text{C}$  are below  $0.2 \mu\text{m}$  average size (Figures 4.6 (d) and 4.7 (d)), but that obtained from the niobium metal at  $400^\circ\text{C}$  is correspondingly larger reaching average sizes of  $0.5-0.7 \mu\text{m}$ . (Figure 4.8 (d)) although the fractional volume increase is rather greater for the metal oxidation (1.68 compared with 1.37 for the nitride oxidation). Since the metal is comparatively high melting it would seem that the removal of nitrogen inhibits sintering of the oxide from the nitrified metal. In both cases, the porosity of the resulting oxides is low at all the temperatures studied. Adsorption hysteresis is only just detected in the most active samples. Hence, the increases in the numbers of crystallites are correspondingly much higher for the nitride oxidation than for the metal oxidation, cf., Figures 4.6(e) and 4.8 (e). Nevertheless, electron micrographs show rounding of the edges of the aggregates of oxide formed from the nitride at higher temperatures. (Plate 4.8)

### 4.3 TANTALUM NITRIDE

#### 4.3.1 Nitridation of Tantalum

The tantalum-nitrogen system and its thermodynamics have been described in Chapter I. Neumann et.al., (1934), Brewer et.al. (1950) and Armstrong (1949) have also determined thermodynamic data on this nitride. The reaction between tantalum and nitrogen mainly follows the parabolic rate law. At 700°C, the rates are similar to those for the nitridation of titanium and niobium, but correspondingly slower than for zirconium. The data of Gulbransen and Andrew (1949c, and 1950) deviate slightly from the parabolic law in the early reaction stages. These workers have measured the rate constant of the reaction of niobium metal with 0.1 atm. of nitrogen and is represented by:

$$\text{Ta ; } 600\text{--}850^{\circ}\text{C} : K_p = 1.4 \times 10^{-4} \exp (-39,400/RT) \text{ g}^2\text{cm}^{-4}\text{s}^{-1}$$

However, it is interesting to note that with the method of van Liempt the parabolic rate law could be deduced from consideration of direct diffusion of nitrogen into the metal. The negligible effect of pressure is similar to that found for the reaction of nitrogen with niobium. In a vacuum of  $10^{-5}$  or lower the tantalum-nitrogen product loses weight below 605°C, while at higher temperatures the metal acts as a 'getter' in a similar manner to niobium and zirconium. The reaction apparently does not take place directly on the metal but rather through a film of nitride which hinders the pressure from exerting its normal influence on this type of reaction. The nitride film thickness is governed by the rate of formation and the rate of solution of nitrogen.

The reaction between tantalum and nitrogen between the temperature range 800–1300°C has been investigated by Osthagen and Kofstad (1963). The total reaction at this temperature range involves both the dissolution of nitrogen in the metal and nitride formation. The

former process is predominant during the initial stages of the reaction. Formation of four different nitrides, namely,  $TaN_{0.05}$ ,  $Ta_2N$ ,  $TaN_{0.8-0.9}$  and  $TaN$ , has been reported; the relative amounts depending on experimental conditions. At temperatures below  $1000^\circ C$ , mainly  $Ta_2N$  is formed, while above this temperature  $TaN_{0.8-0.9}$  and  $TaN$  are the main reaction products.  $TaN_{0.05}$  is formed in traces at the nitride-metal surface. The X-ray diffraction and microhardness measurements show that an outer layer of tantalum metal is rapidly saturated with nitrogen. The nitrides adhere extremely well to the metal surface.

Superconducting properties of tantalum nitride thin film resistors have been critically evaluated by Gerstenberg & Hall (1964) and Berry et.al., (1964)

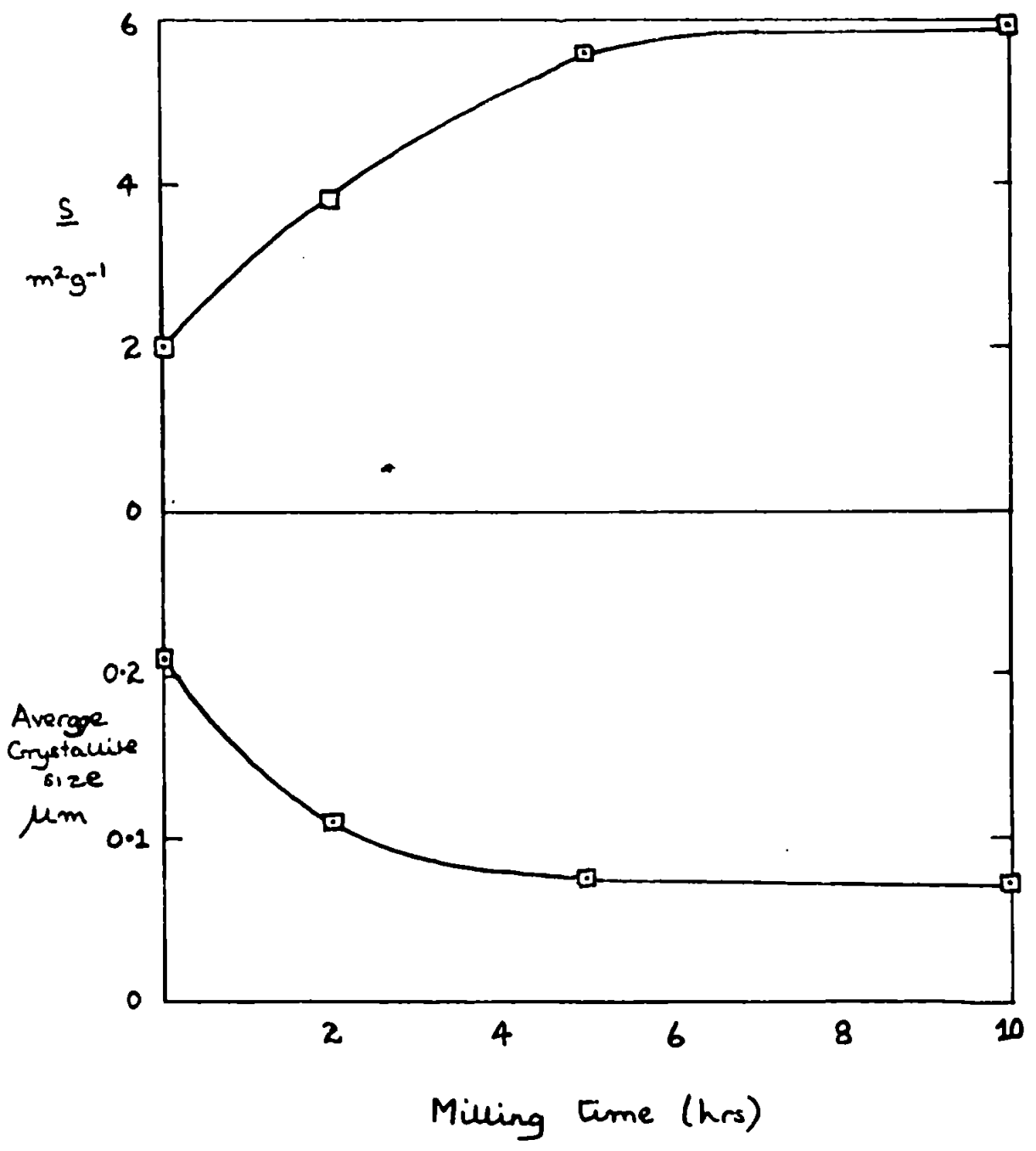
#### 4.3.2. Milling of Tantalum Nitride

When a 6g - sample of tantalum nitride was milled under conditions described in Chapter II, section 2.6, the specific surface progressively increased as shown in Figure 4.11(a). After about 5 h. the specific surface and average crystallite size remained practically constant on further milling (Figure 4.11 (a) and (b)). This is the hardest of the nitrides presently investigated, since there was less X-ray line (or peak)-broadening (Figure 4.12).

The initial nitride consisted of a mixture of about equal parts of  $\xi$  -  $TaN_{0.9-1.0}$  and  $\delta$  -  $TaN_{0.8-0.9}$  giving an overall empirical composition  $TaN_{0.93 \pm 0.03}$  (from analysis and oxidation). During the 10h- milling, the  $\xi$ -form is progressively converted to the  $\delta$ -form as shown by the X-ray diffractometer traces in Figure 4.12. This involves a transformation from a hexagonal  $CoSn$  ( $B_{35}$ ) type-lattice

FIG. 4.11

MILLING OF TANTALUM NITRIDE



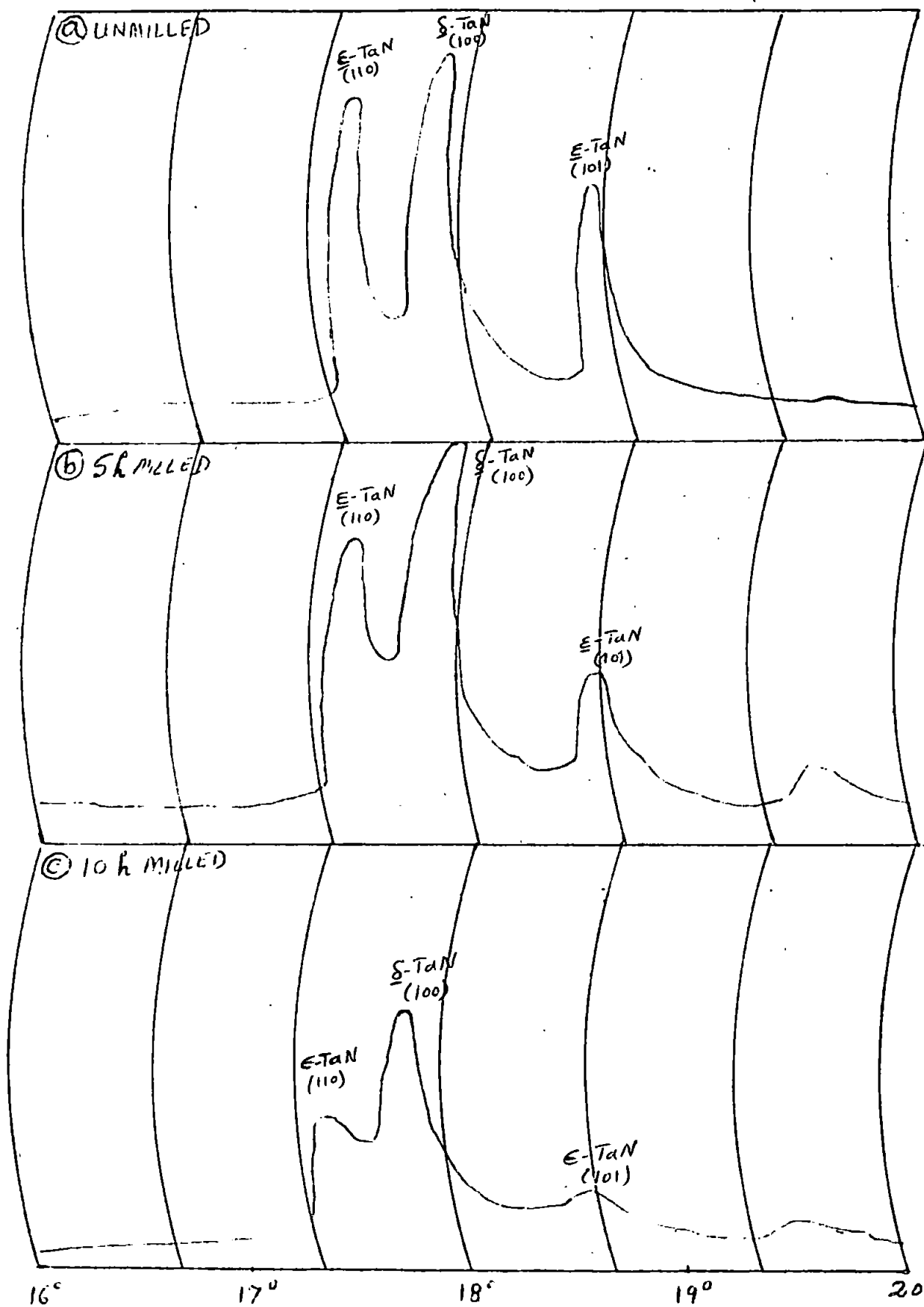


FIGURE 4.12:- X-ray Diffractometer Traces of TaN Samples.

1  $\mu$ m



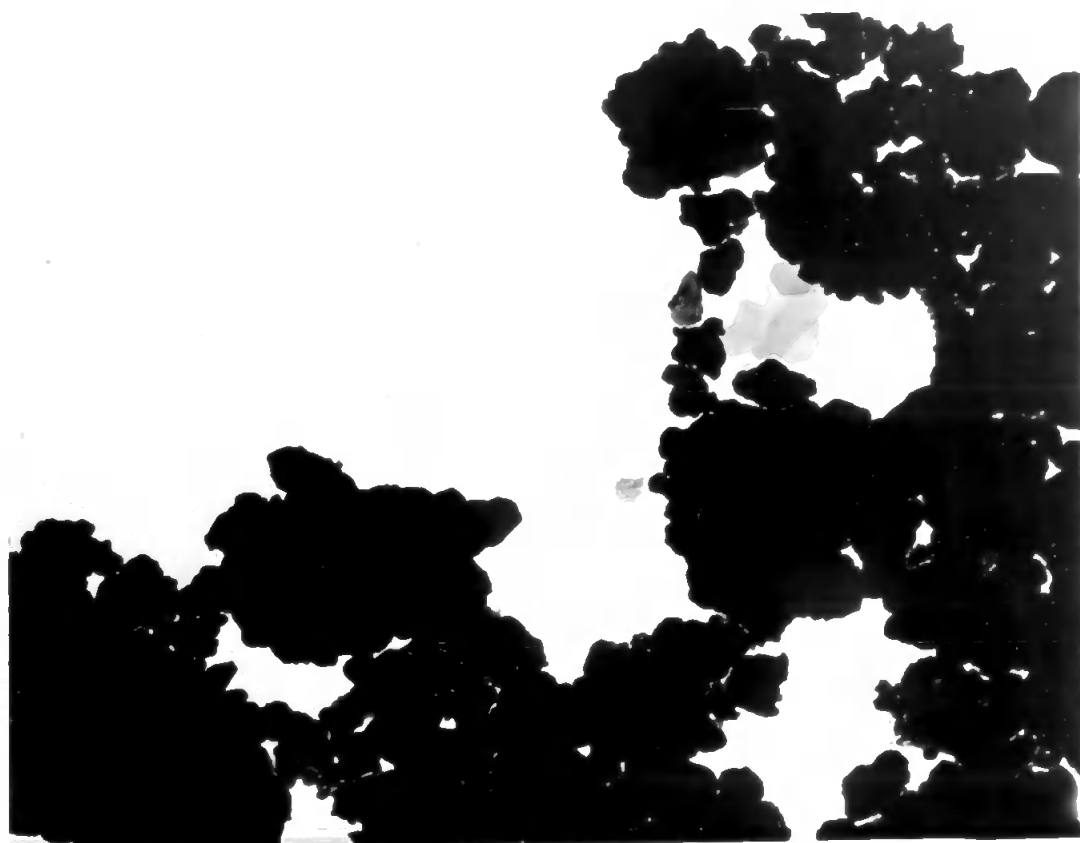
PLATE 4.9 Tantalum Nitride, Untreated

Magnification x 20,000

Page (174)

PLATE 4.10 Tantalum Nitride, Oxidised in Air at 400°C for 5 hours

1  $\mu$ m



1  $\mu$ m

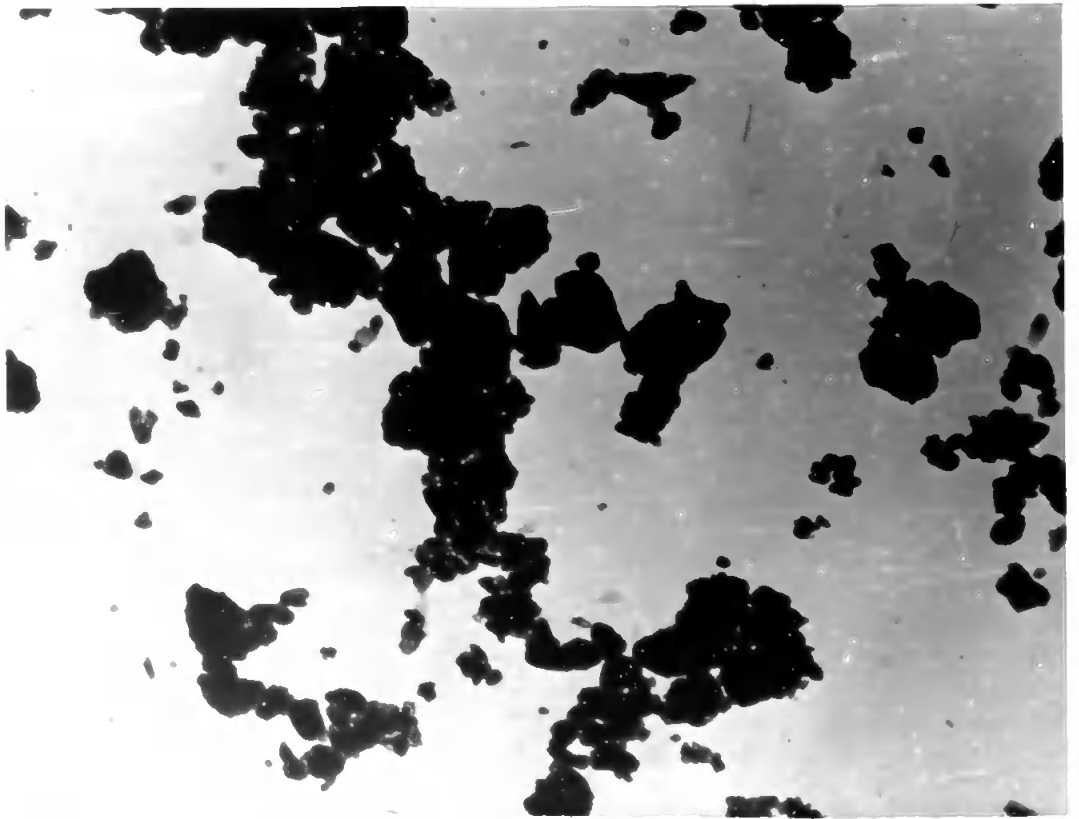


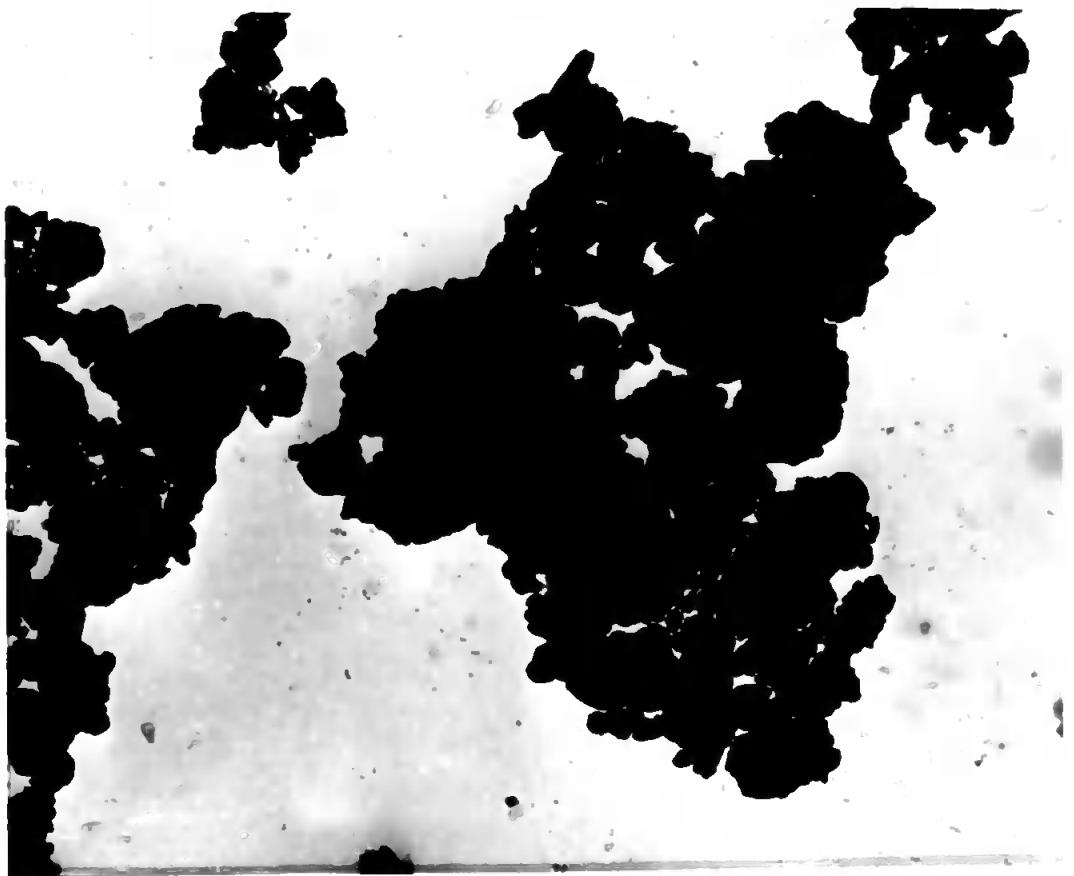
PLATE 4.11 Tantalum Nitride, Ball-milled for 10 hours

Magnification x 20,000

Page (175)

PLATE 4.12 Tantalum Nitride, Oxidised in Air at 550°C for 5 hours

1  $\mu$ m



to another hexagonal WC ( $B_h$ ) type-lattice. The true homogeneity range of the  $\underline{\alpha}$ -TaN structure is nearer 1 than 0.9 atom nitrogen per tantalum atom, viz., 0.99-1.00, and that of the  $\underline{\delta}$ - structure is nearer 0.9 rather than 0.8 atomic nitrogen per tantalum atom, viz., 0.87-0.90, cf., Schönberg (1954). The crystal lattice transformation evidently adjusts the distribution of nitrogen to approach these homogeneity ranges favourable to the  $\underline{\delta}$ - and  $\underline{\alpha}$ - structures. It involves reducing the  $\underline{c}$ -axis lattice constant from 2.91 $\overset{\circ}{\text{A}}$  for  $\underline{\alpha}$ -TaN to 2.88 $\overset{\circ}{\text{A}}$  for the  $\underline{\delta}$ - form and rearrangement of the layers so that the  $\underline{a}$ -axis lattice constant of 5.19 $\overset{\circ}{\text{A}}$  for the  $\underline{\alpha}$ - unit cell with 3 molecules becomes 2.94 $\overset{\circ}{\text{A}}$  for the simpler  $\underline{\delta}$ - unit cell with 1 molecule. This is equivalent to an increase of about 2% in the  $\underline{a}$  dimensions within the layers accompanied by a decrease of about 1% in the  $\underline{c}$ - distance between the layers. Electron micrographs of the unmilled and 10h-milled nitride give no indication of any well-defined hexagonal structures (Plates 4.9 & 4.11).

#### 4.3.3 Oxidation of Tantalum Nitride:

The tantalum nitride is converted to  $\beta$ - tantalum pentoxide,  $\text{Ta}_2\text{O}_5$ , at 400-600°C in air. X-ray diffractometer traces give no indications of any oxynitrides or lower oxides of tantalum being formed at these temperatures.

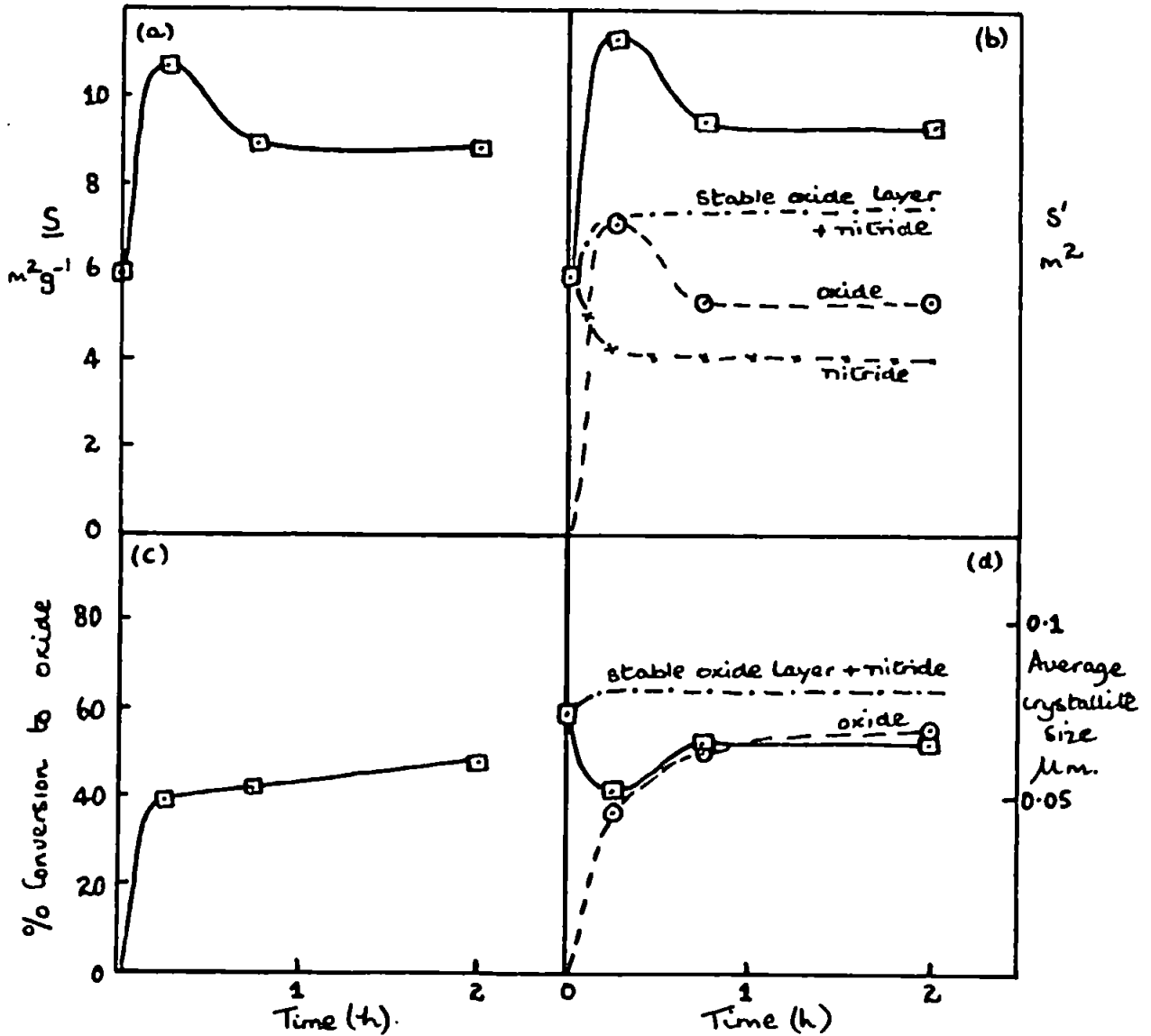
Variations in specific surface,  $\underline{S}$  actual surface area (for 1 g-initial sample),  $\underline{S}^1$  and average crystallite size are shown in Figure 4.13 for the atmospheric oxidation of 10h-milled tantalum nitride. These are compared with similar changes for the oxidation of tantalum metal in Figure 4.14.

When the milled nitride is oxidised at 500°C in air (Figure 4.13a),  $\underline{S}$  increases rapidly to a maximum value and then decreases to an almost constant value after about 1 hour. Thus, when the



FIGURE 4.13

OXIDATION OF MILLED TANTALUM NITRIDE AT 500° IN AIR



KEY:-  $\square$  whole material;  $\circ$  oxide only;  
 $-x-x$  nitride only;  $- \cdot - \cdot -$  theoretical for an initially stable oxide layer.

tantalum pentoxide crystallites out from the nitride matrix, it evidently splits off to give smaller crystallites. Any additional spalling at the oxide-nitride interface, when the samples were cooled for surface area determination was negligible by comparison since reheated samples proceeded to give oxidation rates similar to those of samples which had been continuously heated. Hence, the crystallite splitting results mainly from changes in type of crystal structure (hexagonal CoSn (B35) and WC ( $B_H$ ) to  $\beta$ - orthorhombic) and a volume increase of 0.97 of the original volume as the nitride is converted to the less dense oxide.

Changes in the actual surface area,  $S''$ , and the average crystallite size of the remaining tantalum nitride (assuming no appreciable sintering) and the tantalum oxide,  $\beta$ -  $Ta_2O_5$ , are deduced from the surface area data and volume changes. These are illustrated in Figure 4.13(b) and (d), confirming the ultimate sintering of the oxide. When there is sufficient oxide of rational crystallite size composition, it tends to form a stable coating around the remaining nitride particles. Therefore, the surface area  $S''$  in the earlier stages of the oxidation, increased much more rapidly than it would if a stable oxide layer had been formed throughout the oxidation (Figure 4.13(b)). The experimental results lie above the theoretical curve and are calculated from the formula for a continually stable oxide layer (Glasson, 1958), viz.,

$$S''/S = (1 + 0.97x)^{2/3}$$

where,  $S''$  = surface area of product (i.e. oxide + remaining nitride).

$S$  = specific surface of original 1 g nitride.

and  $x$  = fraction of nitride oxidised.

Accordingly, increases in the number of crystallites of up to 1.8-fold are calculated from  $(S_1/S)^3$ , where  $S_1 = S'/1.57$ , i.e.,  $S_1 = S'/(1.97)^{2/3}$ , to allow for volume changes on oxidation.

#### 4.3.3(a) Comparison with Oxidation of Tantalum Metal

Similar behaviour to that of milled tantalum nitride is shown by tantalum powder on oxidation in air at the same temperature, viz., 500°C (Figure 4.14). The surface areas fluctuate somewhat during the earlier and more rapid part of the metal oxidation. The heat generated by the high oxidation enthalpy of the finely-divided metal is not conducted away sufficiently rapidly and increases the temperature of parts of the sample, giving non-isothermal oxidation and non-uniform sintering. The mixed black, grey and white colours of the products indicate very uneven distribution of the metal and the oxide. This is analogous to the observations of other workers (Gulbransen & Andrew, 1949; Schmahl et al., 1956, 1958; Caplan, 1960) on rapid oxidation of finely-divided metals, where effects of ageing and of overheating may account for some of the difficulties in interpreting the earlier oxidation behaviour for film thicknesses between about 100-3000Å.

The surface heterogeneity of the milled tantalum nitride initially causes almost linear rather than parabolic oxidation rates (as found for niobium nitride). Further oxidation isotherms are compared in Figure 4.15 for unmilled tantalum nitride. The oxidation rates ultimately become almost linear with the formation of thicker oxide layers which are subject to cracking and partial detachment from the underlying metal or nitride. This is more prevalent with the metal since the volume increase on oxidation (1.50 of the original metal volume)

is much larger than that for the nitride (0.97 of the original volume.). In the case of the milled nitride a stable oxide layer is established at an earlier stage in the oxidation at 500°C, after which the reaction is impeded considerably and the surface area becomes practically constant (Figure 4.13(a) & (c)).

The Tammann temperature of the oxide (m.p. 1870°C) is about 800°C, so that crystal lattice diffusion is minimal although surface diffusion can be appreciable at 500°C ( $\frac{1}{3}$  m.p. of  $Ta_2O_5 = 440^\circ C$ ) to promote sintering.

The smaller initial TaN crystallites compared with those of the metal ultimately produce smaller oxide crystallites (Figures 4.13(d) and 4.14 (d)). The initial milled TaN crystallites are smaller than those of the metal and eventually also produce smaller oxide crystallites (ca. 0.07  $\mu m$  compared with 0.28  $\mu m$  from the metal at 500°C). A similar difference in oxide crystallite sizes was found for the oxidations of niobium nitride and metal, even when the initial materials were of similar crystallite size. Again, the fractional volume increase is greater for the metal oxidation (1.50 compared with 0.97 for the nitride oxidation), and the metal is comparatively high melting (ca., 3000°C). Hence, removal of nitrogen again seems to inhibit sintering of the oxide from the nitrided metal. In both cases, the porosity of the resulting oxides is low at the temperature studied (500°C), and adsorption hysteresis was not detected even in the most active samples.

Increases in the number of crystallites for the milled nitride oxidation are rather less than those in the metal oxidation (up to about 2-fold compared with 4-fold respectively). Nevertheless, the average crystallite size of the initial nitride is much less than that of the metal (0.07  $\mu m$  compared with 0.30  $\mu m$  respectively).

Electron micrographs (Plates 4.10 and 4.12) do not show such rounding of the edges of the aggregates of the oxide formed from the nitride or the metal as found with the lower-melting niobium oxide at similar temperatures, viz., 550-600°C.

#### 4.3.3.(b) Oxidation of Tantalum and its Nitride at Higher Temperatures

At higher temperatures crystal lattice diffusion becomes more important in the oxidation of larger niobium and tantalum metal samples (sheets). Niobium pentoxide and tantalum pentoxides are n-type oxides in which diffusion is inward via vacant anion sites (Cathcart et.al., 1958; Cathcart et.al., 1960). In addition, as mentioned earlier niobium and tantalum form the respective pentoxides involving large volume increases. These conditions typically produce the following oxidation mechanism; oxygen ions diffuse from the surface to the metal-oxide interface where they form new oxide which, owing to its large volume increase (1.68 and 1.50 for  $Nb_2O_5$  and  $Ta_2O_5$  respectively), expands against the resistance of the existing oxide layer. As a result of this expansion, severe stresses develop which eventually rupture the film. In the case of tantalum, its conversion into oxide has been shown to occur by the nucleation and growth of little plates along the (100) planes of the body-centred cube metal (Cathcart et.al., 1960). Simultaneously, oxygen dissolves in the metal. Ideally, an initial parabolic growth turning into a linear one has been observed by various investigators at temperatures between 500 and 700°C (Peterson et.al., 1954; Gebhardt & Seghezzi, 1959; Cathcart et.al., 1960). The mechanism is, however, likely to involve some self-healing so that there may be considerable deviations from linear oxidation and the relationship between the gas pressure and oxidation rate is not simple. These types of irregularities

have been observed by Hurlen et.al., (1960-61) in the case of niobium. On the other hand, the oxidation of tantalum depends essentially on the square root of the oxygen pressure (Cowgill & Stringer, 1960). The structure change of tantalum on heating in air and oxygen has been studied by Terao, (1967), using X-ray diffraction technique. He has identified numerous forms of tantalum oxides, e.g., Ta-O (solid solution), TaOy, TaOz,  $\delta$ -form (TaO<sub>2</sub>) and  $\beta$ -Ta<sub>2</sub>O<sub>5</sub>, which are formed in air at either atmospheric pressure or reduced pressure. The nitrogen in the air is believed to be important for high temperature oxidation of tantalum, since nitrides such as Ta<sub>2</sub>N and  $\delta$ -Ta<sub>2</sub>N were observed. Heating of tantalum powder in oxygen causes violent ignition and the  $\alpha$ -Ta<sub>2</sub>O<sub>5</sub>, which has hitherto been considered to be the high temperature form of Ta<sub>2</sub>O<sub>5</sub>, is obtained. The transformation  $\alpha \rightarrow \beta$  occurs on heating in oxygen and the inverse transformation  $\beta \rightarrow \alpha$  occurs on heating in vacuum at a temperature higher than 1300°C. The Helium (Terao, 1967) method of density measurement showed that the  $\alpha$ -form is an oxide lower than Ta<sub>2</sub>O<sub>5</sub>. In the present work, oxidation of tantalum nitride at temperatures of 600-1000°C gave products consisting mainly of  $\beta$ -Ta<sub>2</sub>O<sub>5</sub> with small amounts of  $\alpha$ -Ta<sub>2</sub>O<sub>5</sub>, detected from X-ray diffractometer traces.

Industrially, a study of the thermal oxidation of tantalum nitride thin films has led to the development of a thermal processing technique by which these metal films can be made to exhibit superior resistor characteristics (Rao et.al., 1965). The thermal process simply involves heating the tantalum nitride (Ta<sub>2</sub>N) film resistors in air at some temperature between 450 and 700°C. Radiant heating was found to be most convenient for this purpose. While the resistor is maintained at the elevated temperature, its resistance is monitored and when it reaches the desired value, the heat source is quickly removed.

## CHAPTER V

### CHROMIUM AND MOLYBDENUM NITRIDES

#### 5.1 CHROMIUM NITRIDE

##### 5.1.1 Nitridation of Chromium

The chromium-nitrogen system and its thermodynamics have been described in Chapter I, Neumann et.al., (1934), Sato, (1938a), Maier, (1942) and Brewer et. al., (1950) have also given thermodynamic data for chromium nitrides. Nitrogen has a marked effect on the melting point of chromium due to solid solutions being formed. In the present work, X-ray analysis of high nitrogen specimens indicates the presence of two phases: (i) a  $\text{Cr}_2\text{N}$ - phase with a close-packed hexagonal superlattice ( $L_3$ ) structure with  $a = 4.76\text{\AA}$  and  $c = 4.44\text{\AA}$  (usually found at the N-poor boundary) and (ii) a  $\text{CrN}$ -phase having a cubic  $\text{NaCl}$  ( $B_1$ ) lattice structure with  $a = 4.15\text{\AA}$ . The latter is difficult to prepare pure. According to Neumann et.al., (1931), the formation of mixed crystals makes it difficult to determine the heat of formation of  $\text{CrN}$  from dissociation pressures. Thus, the nitride sample used for milling and oxidation contained 79.9%  $\text{CrN}$  and 20.3%  $\text{Cr}_2\text{N}$  (from analysis and oxidation data).

Kinetics of the nitridation of chromium and ferrochrome alloys of iron and the solubility of nitrogen in chromium have been studied by (Kazielski, 1966). X-ray examination indicated phases  $\text{Cr}$ ,  $\text{CrFe}$  and  $\text{Cr}_2\text{N}$  but not  $\text{CrN}$  present during the nitridation. The whole process can be divided into three stages:

- (i) adsorption of  $N_2$  on the surface of the metal and breaking up of  $N_2$  molecule into N- atoms;
- (ii) diffusion of nitrogen atoms into the metal (slowest, i.e. rate-controlling stage), and
- (iii) chemical reaction for  $Cr_2N$  formation.

The nitriding rate and the solubility of nitrogen increased with temperature. The nitride  $Cr_2N$  was formed on the surface and diffused slowly into the specimen. Diffusion studies in chromium-nitrogen system have been carried out also by Arkharov et.al., (1959).

The conditions of formation and decomposition of chromium nitrides are reported by (Zak, 1962), who has also shown by thermodynamic calculations the following:

- (i) the reaction,  $2 Cr + \frac{1}{2} N_2 \rightleftharpoons Cr_2N$  predominates above  $400^\circ C$ ,
- (ii) at  $400-1032^\circ C$ ,  $Cr_2N$  is formed first, then CrN according to the reaction,  $Cr_2N + \frac{1}{2} N_2 \rightleftharpoons 2 CrN$ ,
- (iii) above  $1032^\circ C$  CrN is dissociated to form  $Cr_2N$ , the latter dissociating above  $1477^\circ C$ , and
- (iv) as pressure drops the dissociation temperature of nitrides is lowered.

Measurement of nitridation kinetics for nitrogen-chromium surface reactions during the early stage of the nitride film growth has been investigated by Johnson (1966) using Ellipsometry. The film is assumed to be  $Cr_2N$ , which is optically isotropic. The kinetic behaviour obeys a parabolic law, with the rate constant of  $4.4 \times 10^{-16} \text{ cm}^2 \text{ s}^{-1}$ . The reactions of chromium with nitrogen + hydrogen gas mixtures at elevated temperatures ( $1100-1310^\circ C$ ) have



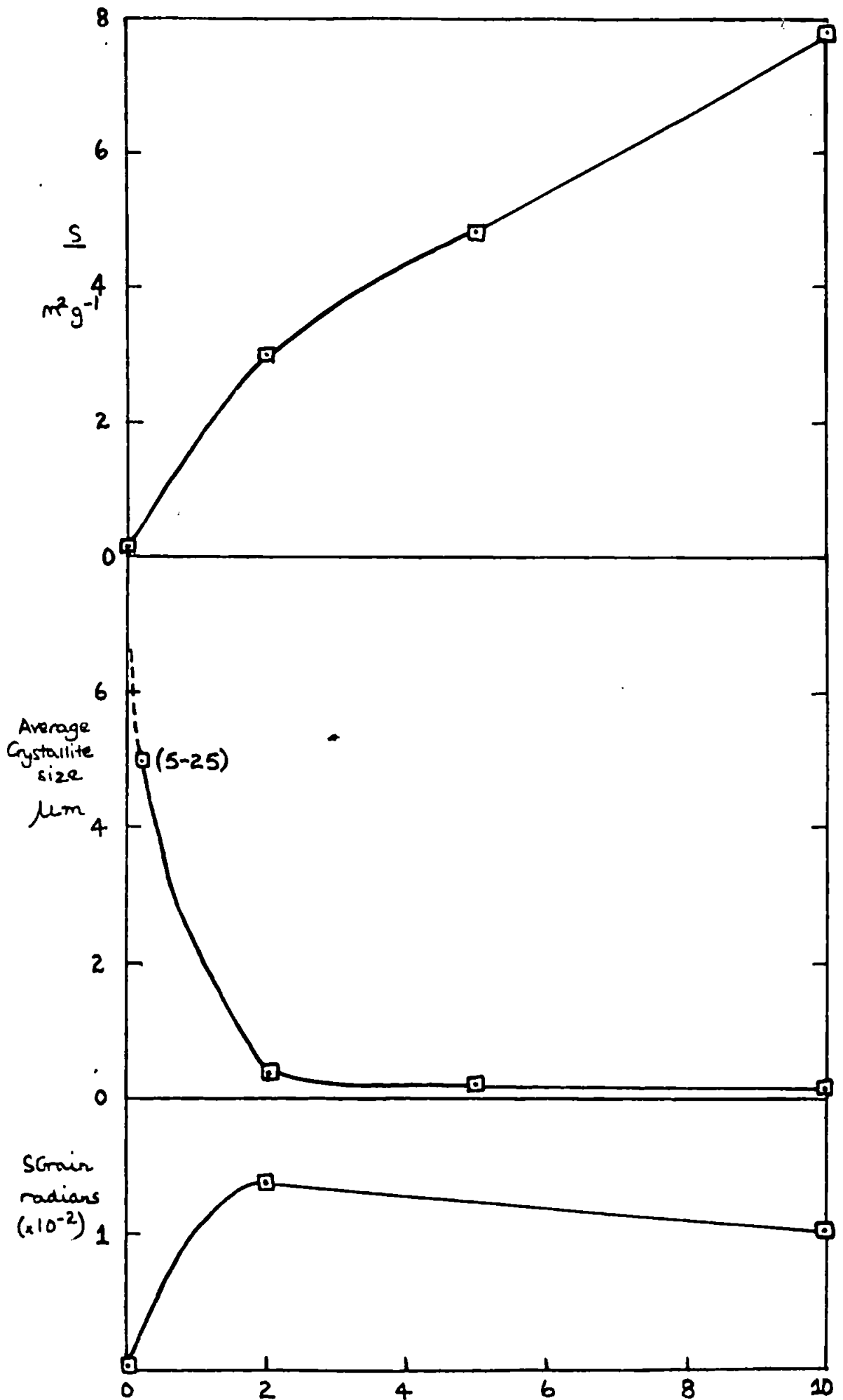
been investigated by Schwerdtfeger (1967).

Using a thermogravimetric technique, Mills (1967) has studied the reaction,  $2 \text{Cr}_2\text{N} + \text{N}_2 \rightleftharpoons 4\text{CrN}$ . The formation and decomposition of this higher nitride of chromium is not sharply defined and the reaction exhibits irreversibility, and there is a temperature region, at constant nitrogen pressure, of about  $25^\circ\text{C}$  in which the stable composition is a mixture of  $\text{Cr}_2\text{N}$  and  $\text{CrN}$ . The stability of these mixtures is difficult to account for at present. An average value of 11.32 wt.% N has been obtained as the upper limiting composition of  $\text{Cr}_2\text{N}$ . The latter was found to have a homogeneity range of approximately 3 wt.% nitrogen (Mills, 1967a). Mills (1967) found  $\text{CrN}$  to be nitrogen-deficient with a homogeneity range. At one atmosphere pressure of nitrogen the upper limiting composition of  $\text{CrN}$  contained 20.80 wt.% N compared with the stoichiometric composition of 21.22 wt.% N. The chromium nitride sample used in the present work contained 19.3 wt.% N.

#### 5.1.2 Milling of Chromium Nitride

When 6 g- samples of the chromium nitride were milled (under conditions described in Chapter II, Section 2.6), the specific surface progressively increased as shown in Figure 5.1(a). Optical observations indicated that the original nitride consisted mainly of single crystals or large aggregates of 5-25  $\mu\text{m}$  size with some more finely divided material shown in the electron micrograph (Plate 5.1). The single crystals were fractured during the earlier stages of the milling and the fragments were incorporated into the aggregates which remained approximately the same size throughout the milling. Thus, the average crystallite size (Fig. 5.1(b))

FIG. 5.1: MILLING OF CHROMIUM NITRIDE



1  $\mu$ m



PLATE 5.1 Chromium Nitride, Untreated

Magnification x 20,000

Page (109)

PLATE 5.2 Chromium Nitride, Oxidised in air at 1000°C for 5 hours

1  $\mu$ m



decreased rapidly at first and later slowly when the crystallites became of sub-micron size. This behaviour is similar to that found for the milling of nitrides of groups IVA and VA described in Chapters III and IV. Electron micrographs of 2 h and 10 h milled samples are presented in Plates 5.3 and 5.4 respectively.

Again, the milling caused strain to be set up within the crystallites, so that there was X-ray line (or peak)-broadening. Table 5.1 shows the half peak widths of the (111) and (200) reflections. The strain was calculated from the half-peak width of the (200) X-ray reflection, after allowing for broadening due to crystallite size. Figure 5.1(c) illustrates the development of strain, which occurred mainly during the first two hours milling

TABLE 5.1

Lattice Strain in Milled Cr-Nitride Samples

Chromium Nitride	Half-Peak widths (2 $\theta$ ) in Minutes for Reflection		Strain (radians) (using (200) reflections)
	CrN (111)	CrN(200)	
Unmilled	12	12	-
Milled, 2 h	38	28	$1.37 \times 10^{-2}$
Milled, 10h	36	26	$1.02 \times 10^{-2}$

when the single crystals were fractured and incorporated into the aggregates. Subsequently, the strain remained almost constant. Slight decreases may have resulted from possible redistribution of N to within homogeneity ranges more favourable to the Cr<sub>2</sub>N and CrN structure; cf., behaviour of  $\xi$ - and  $\delta$ -tantalum nitrides.

1  $\mu$ m

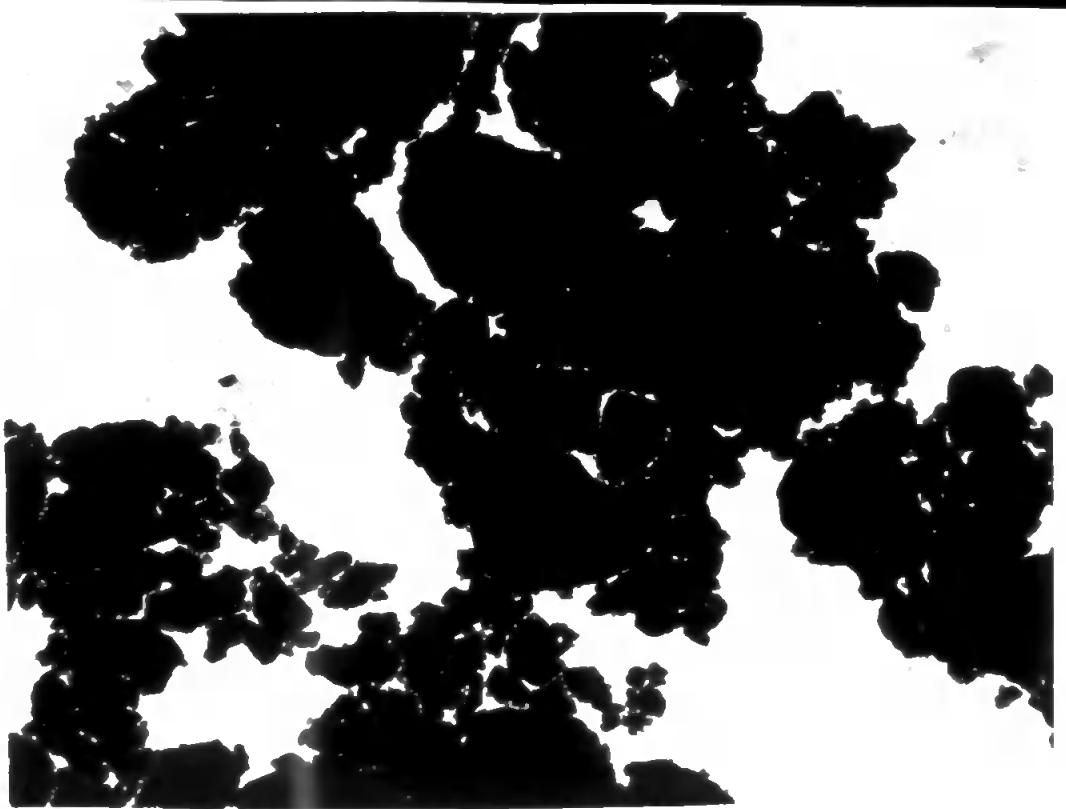


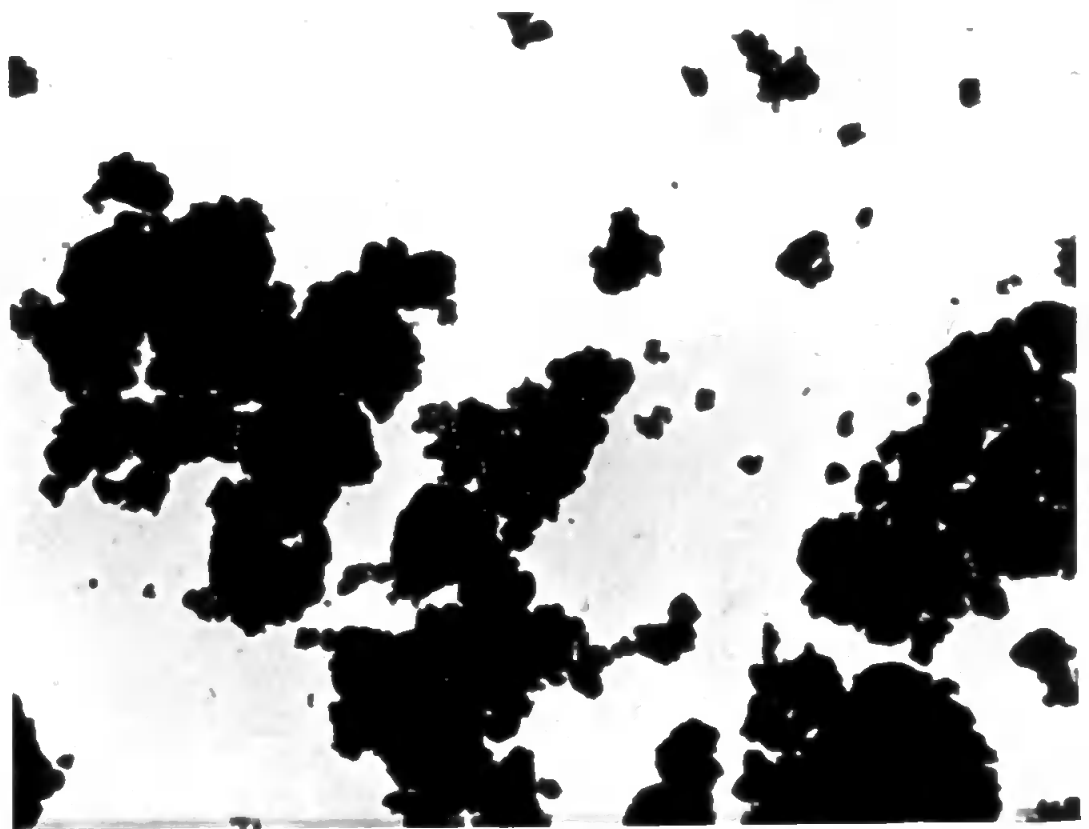
PLATE 5.3 Chromium Nitride, Ball-Milled for 2 hours

Magnification x 20,000

Page (191)

PLATE 5.4 Chromium Nitride, Ball-Milled for 10 hours

1  $\mu$ m



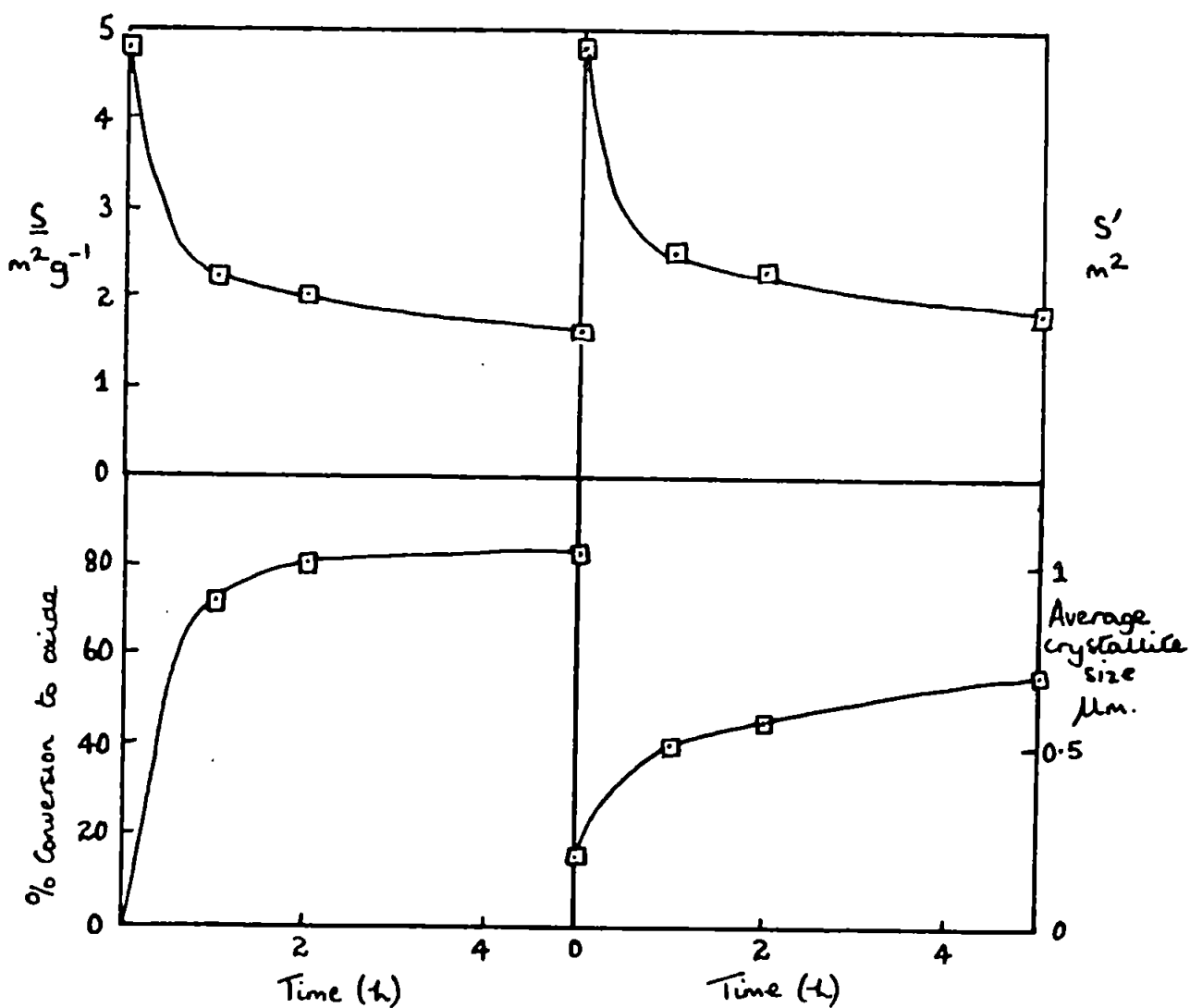
### 5.1.3 Oxidation of Chromium Nitride

Chromium nitride is converted to chromium sesquioxide (chromic oxide),  $\text{Cr}_2\text{O}_3$ , at 750-1200°C in air. X-ray diffractometer traces give no indications of any oxynitride or other oxides of chromium being formed at these temperatures. Variations in specific surface,  $\underline{S}$ , actual surface area (for 1g initial sample),  $\underline{S}'$  and average crystallite size (equivalent spherical diameter) are shown in Fig. 5.2., for 5 h-milled chromium nitride oxidised at 1000°C in air. About  $\frac{2}{3}$  of the material oxidises comparatively rapidly (Figure 5.2(c)), while  $\underline{S}$  and  $\underline{S}'$  decrease and the average crystallite size increases to about 0.5  $\mu\text{m}$ . Subsequently the oxidation proceeds much more slowly with correspondingly smaller changes in the surface areas and average crystallite sizes.

When the oxide crystallises out from the nitride matrix, the change in type of crystal lattice (cubic F-CrN and hexagonal superlattice  $\text{Cr}_2\text{N}$  to (hexagonal) rhombohedral  $\text{Cr}_2\text{O}_3$ ) and fractional volume increases (0.354 and 0.597 of the original nitride volumes) would be expected to produce splitting away of oxide crystallites. However the surface areas decrease since chromium oxide sinters readily at 1000°C, which is near the Tammann temperature (about  $\frac{1}{2}$  m.p. in K for  $\text{Cr}_2\text{O}_3$  is 1060°C), so that lattice diffusion can be appreciable as well as extensive surface diffusion (above  $\frac{1}{3}$  m.p.  $\equiv$  620°C). When sufficient oxide of rational crystallite size composition is formed, the remaining nitride particles are surrounded by oxide layers impermeable to normal gaseous diffusion. Thus, the initial approximately linear kinetics become parabolic

FIGURE 5.2

OXIDATION OF MILLED CHROMIUM NITRIDE AT 1000° IN AIR



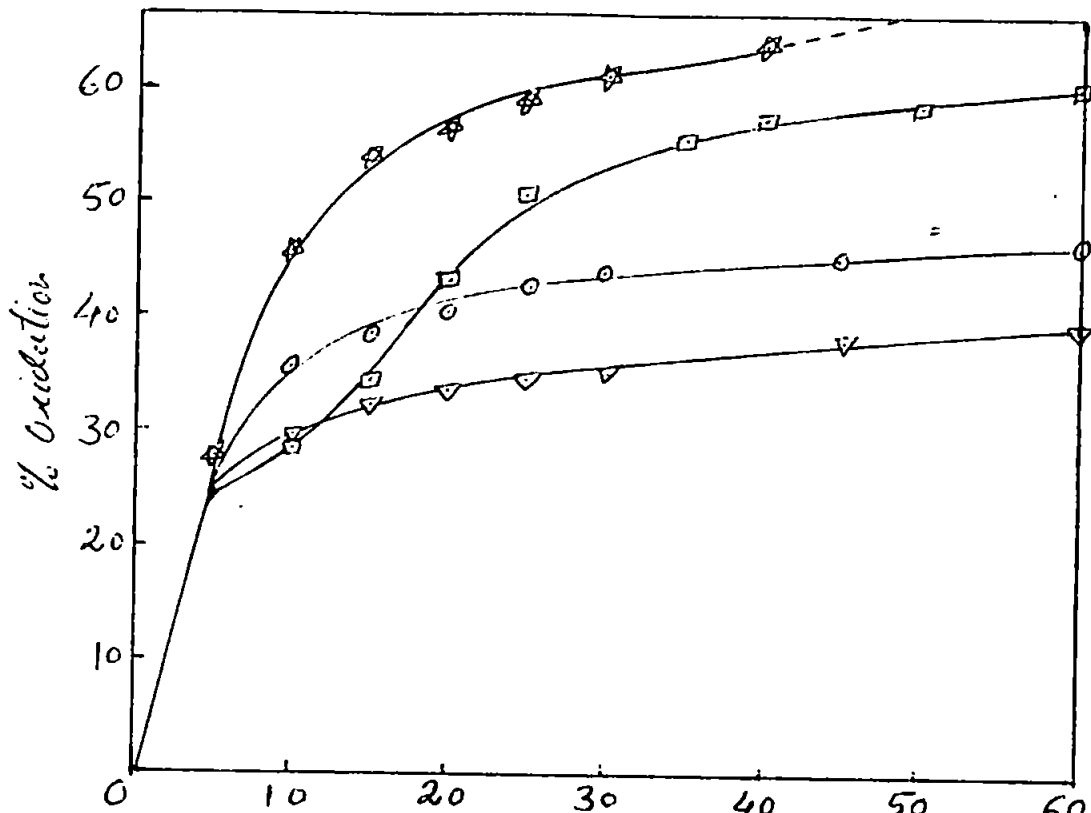
being controlled by lattice diffusion through the oxide layer. This is demonstrated further by oxidation isotherms on 1 g-samples of milled and unmilled chromium nitride shown in Figures 5.3 and 5.4. The greater surface heterogeneity of the milled samples tends initially to give linear rather than parabolic oxidation rates (as generally found for the nitrides of groups IVA and VA and discussed in section 3.1.3). The oxidation rates become almost linear with the formation of thicker oxide layers, so that complete oxidation is not achieved within a reasonable time at temperatures below 1100°C (cf., Figs. 5.3 and 5.5). Electron micrograph of an oxidised nitride sample is presented in Plate 5.4.

#### 5.1.3 (a) Comparison with Oxidation of Chromium Metal

As in the oxidation of the nitride, the main oxide formed on heating chromium metal in air at various temperatures up to 1200°C is the sesquioxide,  $\text{Cr}_2\text{O}_3$ . Electron diffraction rings are sharp when the oxide is formed at 500°C but diffuse for lower temperatures (cf. Plates 5.5 and 5.6). Research on the oxidation of vapour-deposited chromium films by Glasson & Maude (1970) shows that oxidation first becomes appreciable above 300°C with the sizes of the oxide particles increasing at higher temperatures and being comparable with those of chromium oxide obtained by decomposition of the hydroxide at similar temperatures. In the newly formed  $\text{Cr}_2\text{O}_3$ , the 2.48 Å (110) spacing is the most prominent (Glasson and Leach, 1964).

The sintering of chromium sesquioxide was studied further by calcining separate portions of chromium hydroxide for 2 hours at a series of fixed temperatures in air on a thermal balance (Gregg & Winsor, 1945). The weight losses showed that the chromium





KEY: ▽ 2 h milled, 750°C. : Time, Minutes : ○ 10 h milled, 750°C  
 □ 2 h milled, 890°C. : ⊠ 10 h milled, 890°C

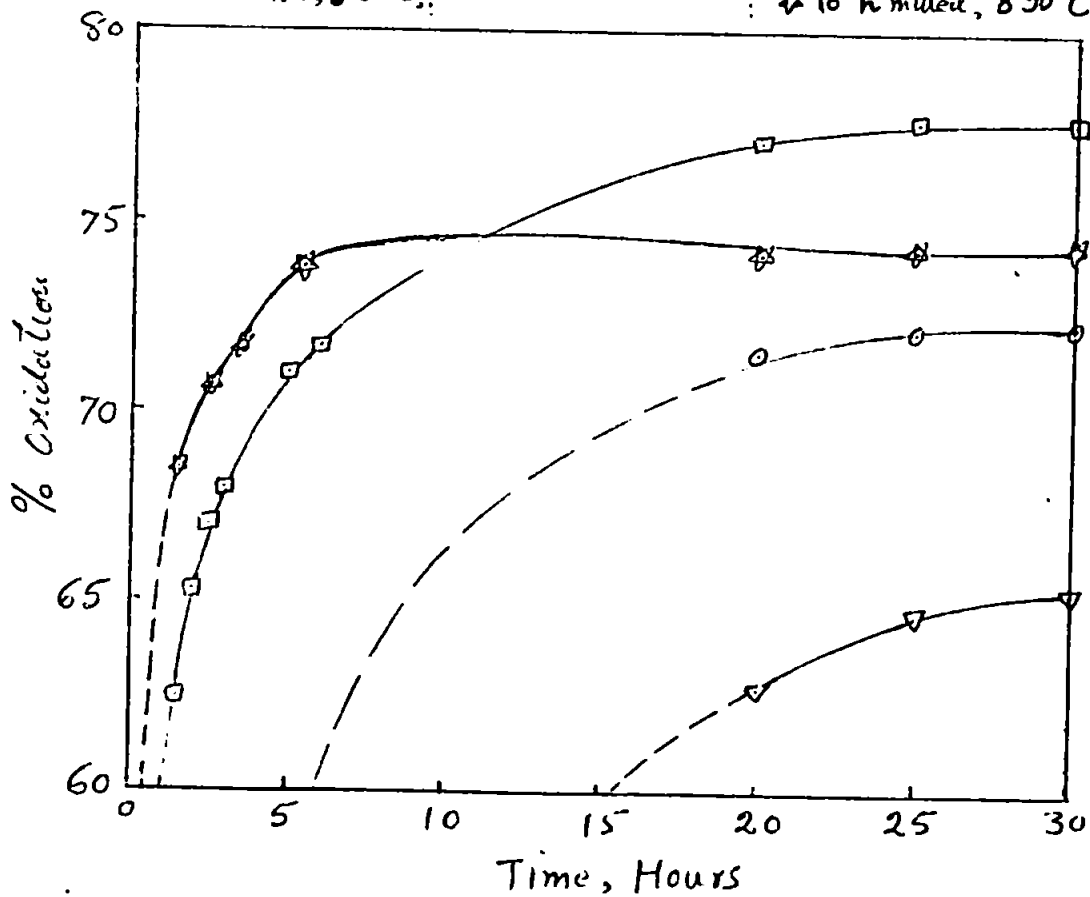


Figure 5.3:--Oxidation Isotherms for CrN at different temps.in air.

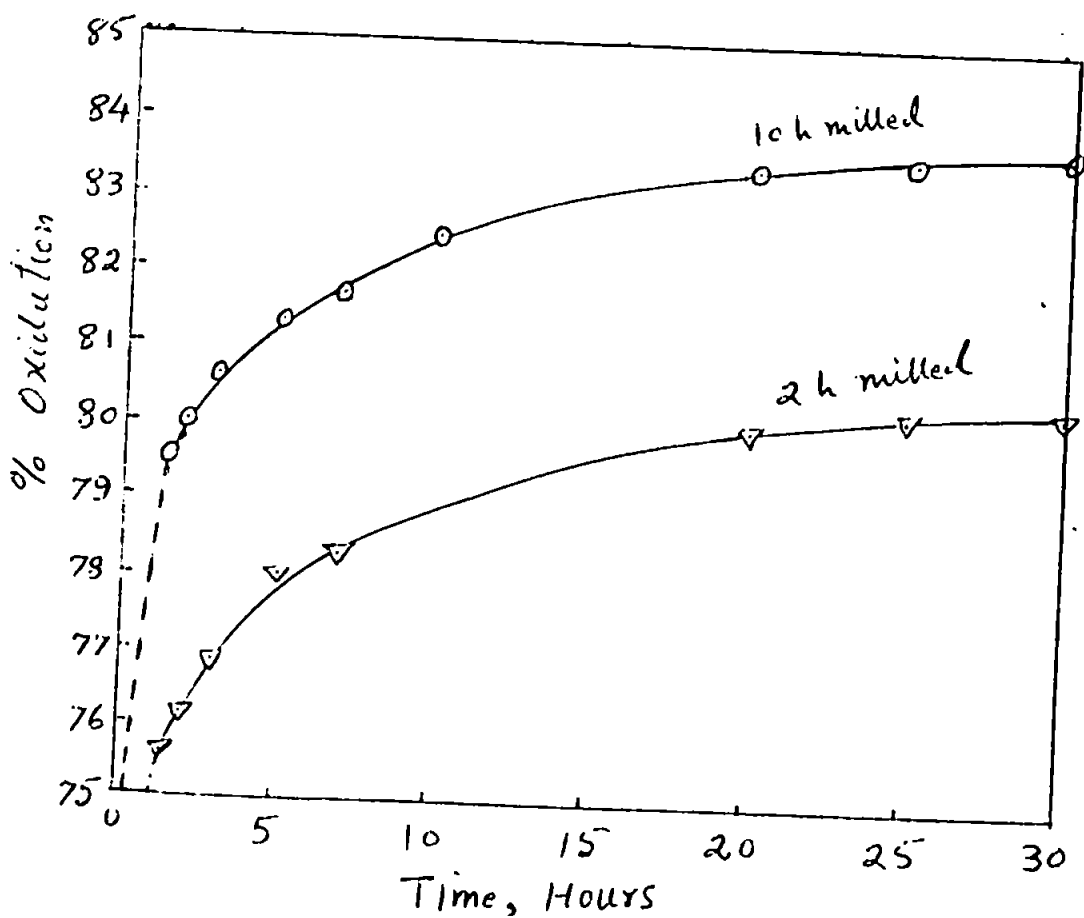
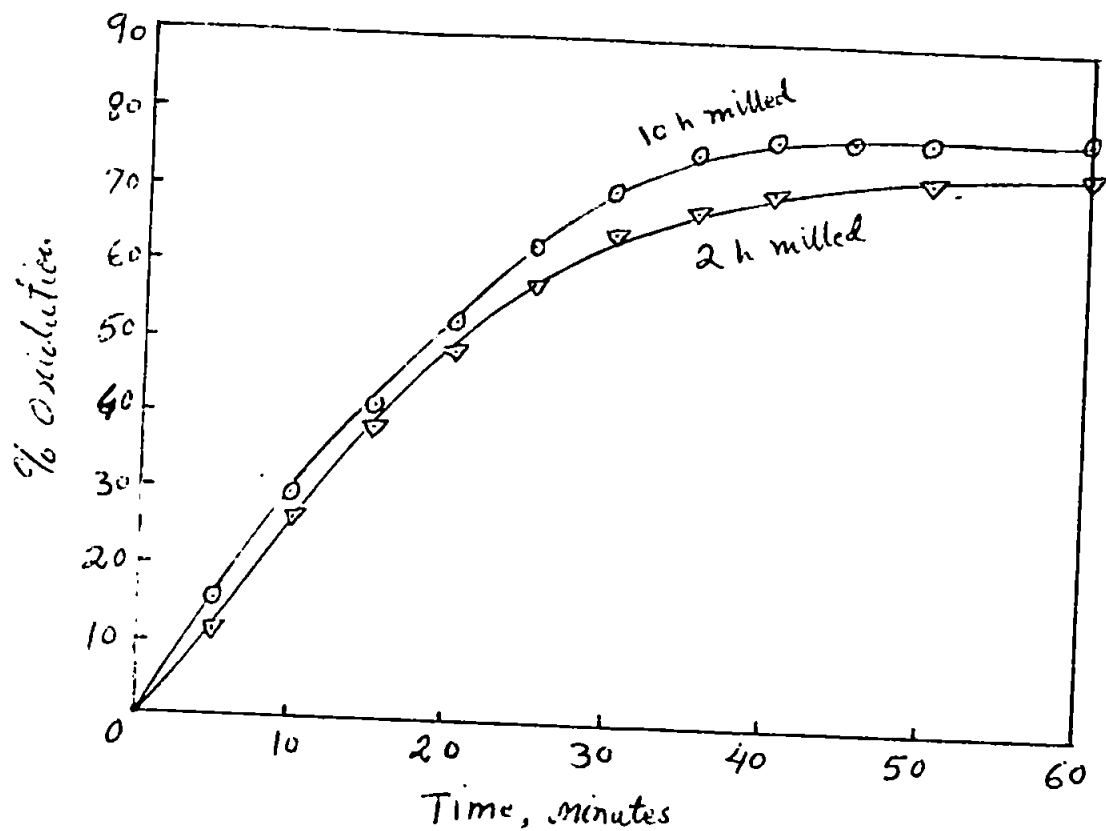


Figure 5.4:-Oxidation Isotherms for milled Chromium Nitride in air at 1000°C. (196)

1  $\mu$ m

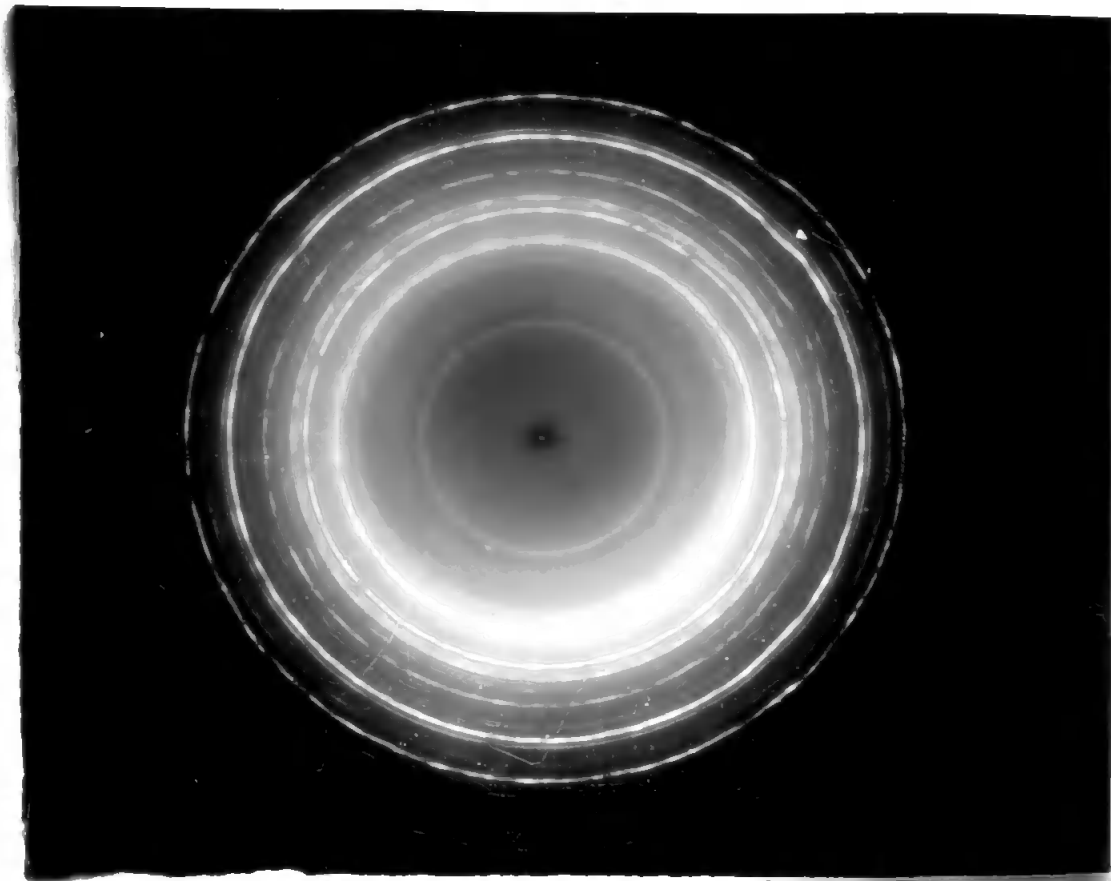


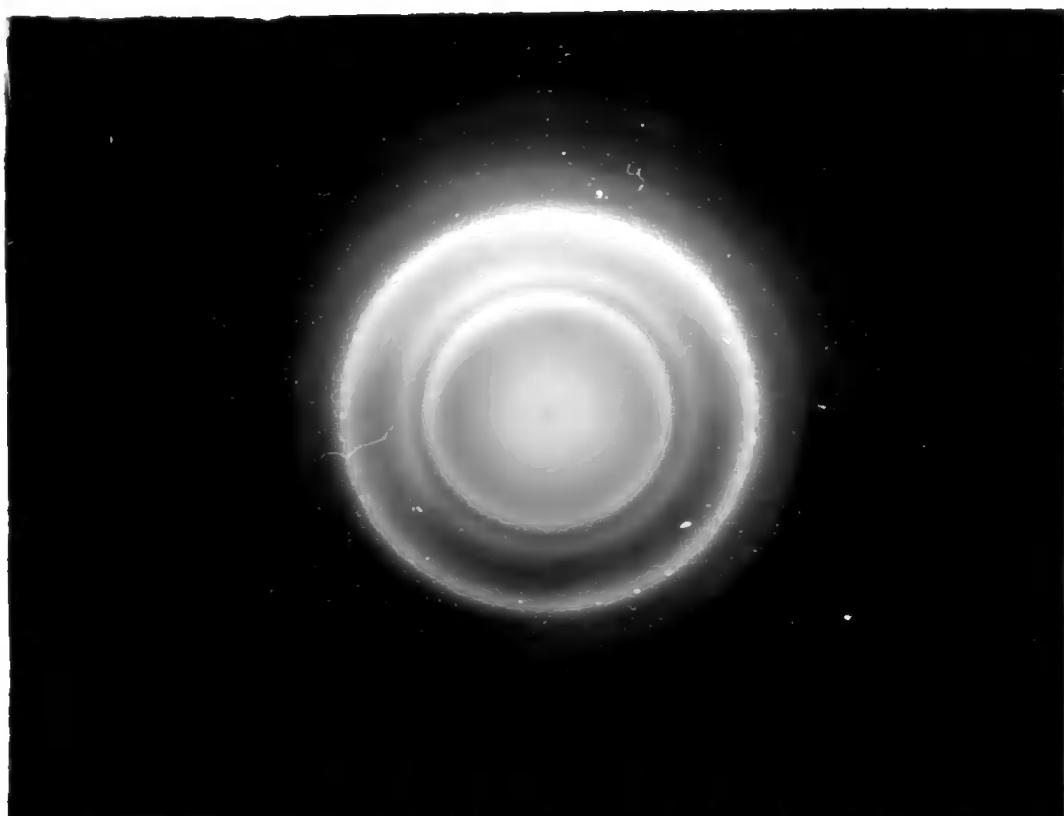
PLATE 5.5 Electron Diffraction Pattern of Chromium Metal Powder Oxidised in Air at 500°C for 10 hours.

Magnification x 20,000

Page (190)

PLATE 5.6 Electron Diffraction Pattern of Chromium Metal Powder oxidised in Air at 500°C for 3 hours

1  $\mu$ m



hydroxide had lost adsorbed water at 200°C when its formula was approximately  $\text{Cr}(\text{OH})_3$  or  $\text{Cr}_2\text{O}_3 \cdot 3\text{H}_2\text{O}$ . The decomposition to chromic sesquioxide,  $\text{Cr}_2\text{O}_3$ , was practically complete within 2 hours at 400°C. Samples obtained in two hours at 300-400°C had lost most of their water of crystallisation but contained some oxygen in excess of  $\text{CrO}_{1.50}$  (according to Rode (1965) up to  $\text{CrO}_{1.93}$  0.06  $\text{H}_2\text{O}$  at about 350°C) from atmospheric oxidation.

The samples were outgassed at 200°C (Glasson, 1964) and their specific surfaces measured from nitrogen isotherms recorded on the sorption balance. No adsorption hysteresis was shown at 500°C and over. Nevertheless, slight hysteresis was observed for the more active oxide samples prepared at 300-400°C and the "adsorption" points (Figure 5.6) were used for calculations.

The variations in specific surface,  $S_p$ , and the corresponding crystallite sizes of the oxide products are shown in Figs. 5.7 & 5.8. The oxide samples of largest specific surface and smallest average crystallite size are obtained when decomposition of the hydroxide is practically complete within the given time, i.e., 2 hours (cf. decomposition rates in Fig. 5.9). This behaviour is similar to that found for nickel hydroxide (Glasson & Maude, 1970).

The increase in surface area constitutes an activation ascribed to an increase in the number of microregions in the decomposition product as compared with the initial substance (Glasson, 1956), and the decrease in area to sintering of the product.

Crystallite splitting results from the changes in type of crystal structure (hexagonal to rhombohedral) and volume decreases (0.394 of the original volume) as the hydroxide (density = 4.3 approx) is

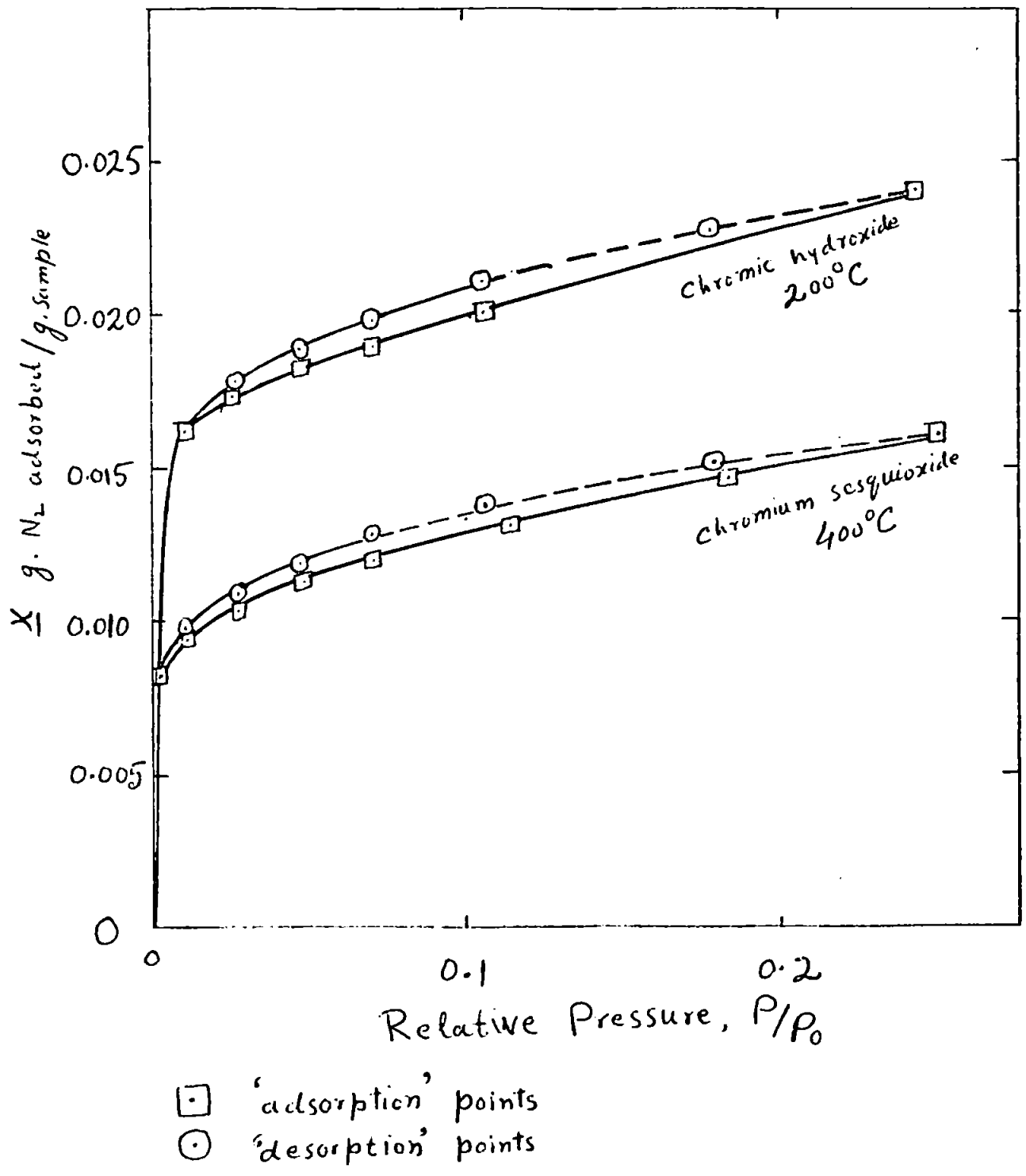


Figure 5.6: Adsorption of Nitrogen on  $Cr_2O_3$  obtained from  $Cr(OH)_3$ , Calcined 2h in air at different temperatures.

converted to the more dense oxide (density = 5.23). Decomposition of  $x$  gram in a 1 g-sample of chromic hydroxide would cause a proportionate volume change of  $\{(1-x)+0.606x = 1 - 0.394x\}$ . If the development is approximately the same in each direction, the corresponding change in surface is  $(1 - 0.394x)^2$  which amounts to  $(0.606)^2$ , i.e., 0.716 for complete decomposition. In general if  $S$  and  $S'$  are the actual surface areas of the original chromic hydroxide and its partly decomposed product, then, assuming no crystallite splitting,

$$S'/S = (1 - 0.394x)^2$$

Changes in the number of crystallites (Figure 5.10) can be estimated from the ratio  $(S_1/S)^3$ , where  $S_1$  is the value of the surface area of the chromic oxide, i.e.,  $S'/0.716$  and  $S$  the specific surface of the original chromic hydroxide. Thus, allowance being made for the change in crystal lattice (Glasson, 1958b), (See Fig. 5.10).

Sintering of the chromium sesquioxide,  $Cr_2O_3$ , is found to be enhanced by increased temperatures. This is illustrated by the decreases in specific surfaces and the number of crystallites and also the increases observed in the average crystallite sizes of the oxide prepared at higher temperatures (Figs. 5.7, 5.8 & 5.10). Longer calcination also increases sintering as shown by decreases in specific surface and increases in average crystallite size (Fig. 5.11). Since the chromic hydroxide decomposes more rapidly at the higher temperatures, the newly-formed oxide will have progressively more time to sinter, causing further decreases in specific surface and increases in average crystallite size.

The aggregate sizes of the chromium sesquioxide products at various temperatures are shown by electron micrographs (Eaude, 1970).

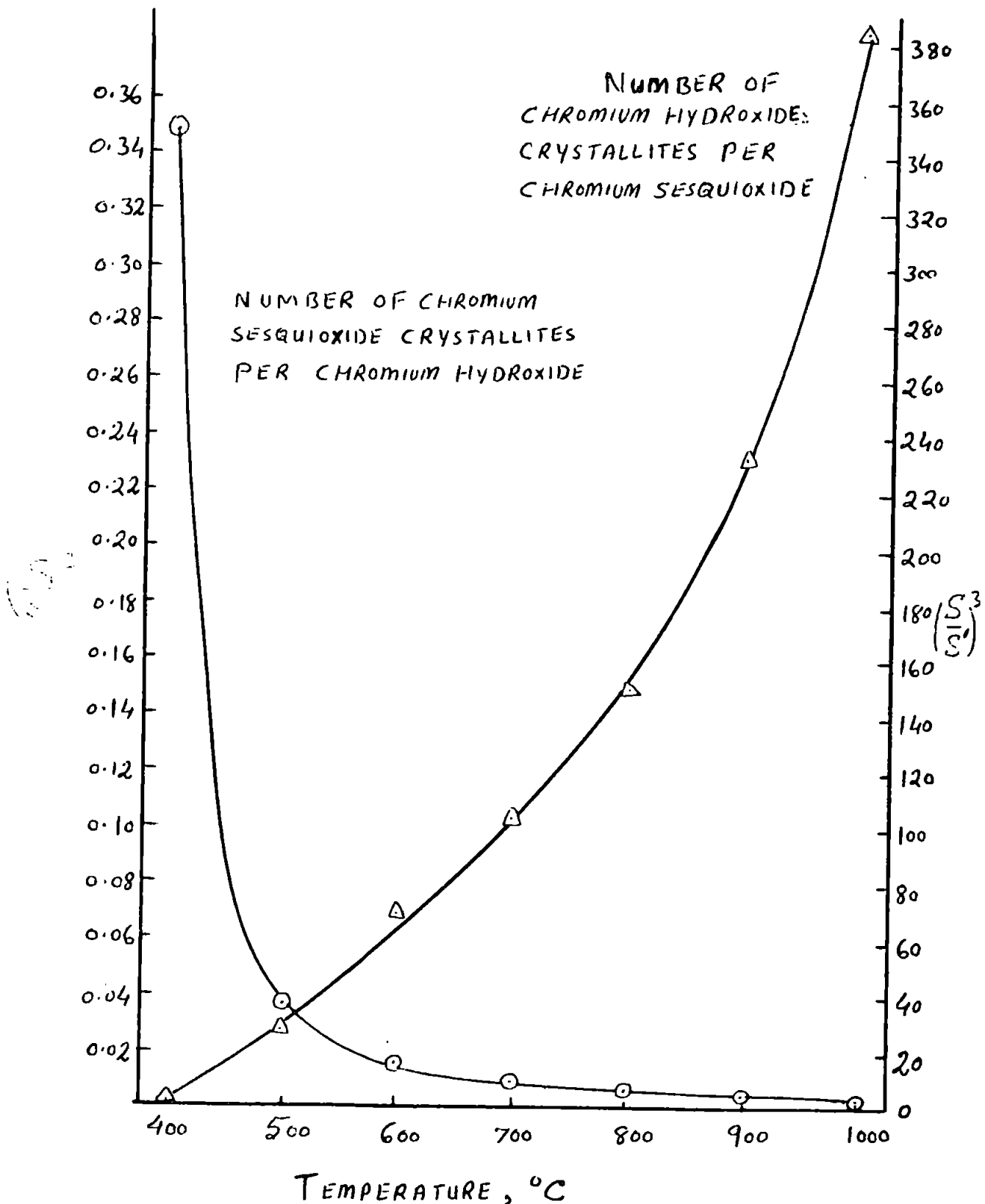


FIGURE 5.10

The aggregates increase in size with higher temperatures and becoming more rounded at the edges at 1000°C, illustrating extensive sintering. They are found to be similar to those of chromium sesquioxide formed by oxidising the nitride at 1000°C (Plate 5.2). However, the oxide formed by oxidising chromium powder at 1000°C in air consisted of much larger crystallites and aggregates observed optically to be mainly above 5µm. Yet, any splitting away of the oxide crystallites cannot be extensive since the specific surfaces of the oxidised metal samples are below 0.2 m<sup>2</sup>g<sup>-1</sup>. The oxidation generally obeys a parabolic rate law consistent with the formation of a stable oxide layer and a diffusion mechanism (Figure 5.12). In the absence of sintering, the average crystallite size should increase by (2.00)<sup>1/2</sup> i.e., 1.26-fold, for complete oxidation of every chromium crystallite. As found for zirconium and niobium metal powder oxidation, the sintering of Cr<sub>2</sub>O<sub>3</sub> is probably accelerated by the remaining chromium metal. In contrast, the finely divided, Cr<sub>2</sub>O<sub>3</sub>, prepared from the hydroxide sinters only slowly at 1000°C in air, like the oxide obtained from the nitride. In the latter case, sintering is inhibited probably by the removal of nitrogen.

It would be expected that at temperatures higher than 1000°C, oxidation by outward metal migration predominates. Gulbransen & Andrew (1957) claim that at about 1000°C, the rate of evaporation of chromium becomes equal to the rate of oxidation, in terms of the number of chromium atoms evaporating or reacting with oxygen (Pilling-Bedworth rule becomes less significant). Ultimately, the removal of the chromium at the metal-oxide interface leaves behind vacancies which reduce the adhesion. This causes detachment of the thicker



PERCENTAGE WEIGHT CHANGE FOR CHROMIUM  
POWDER HEATED AT DIFFERENT TEMPERATURES  
USING A THERMOBALANCE.

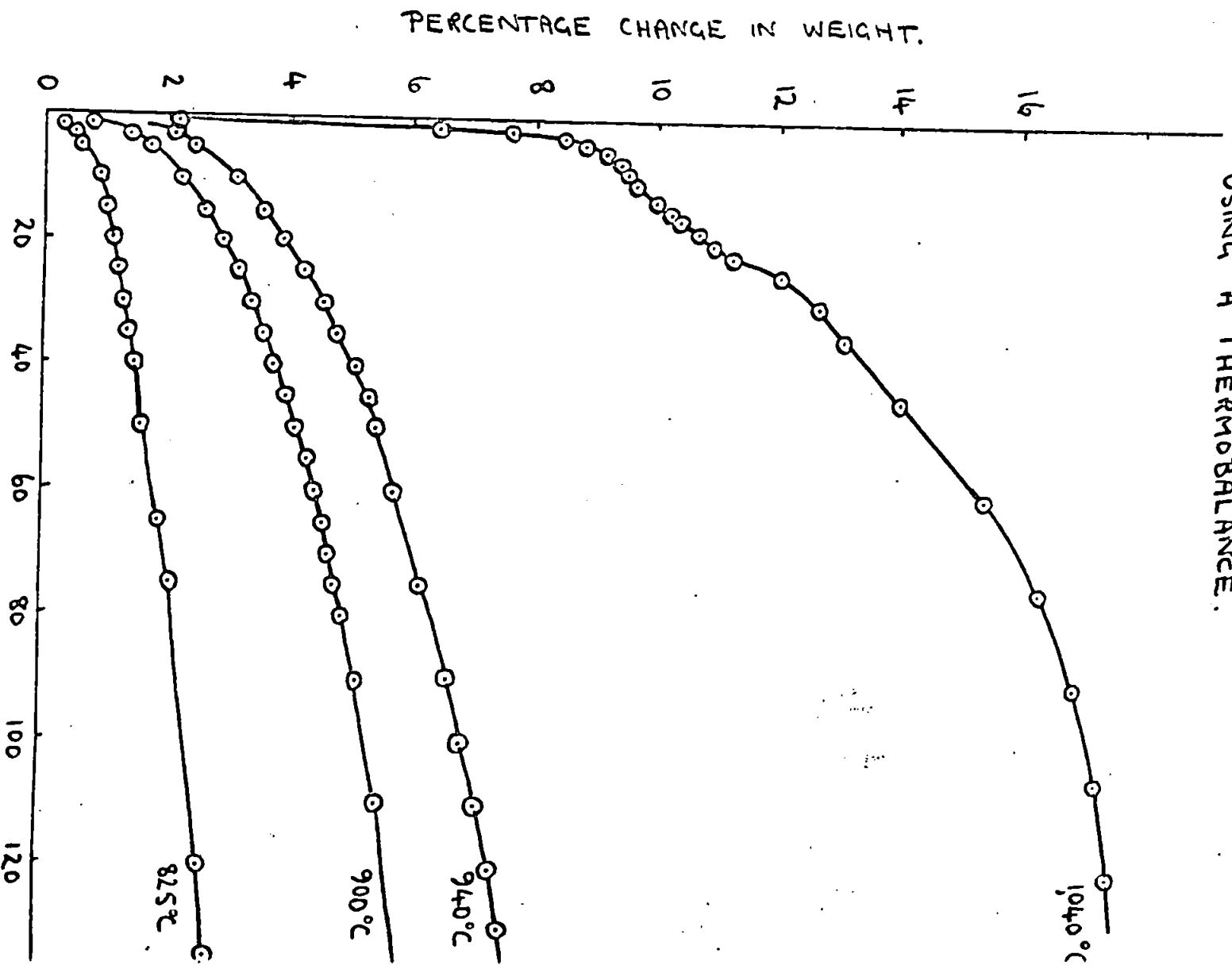


FIGURE 5.12

(208)

and appreciably-strained oxide films, e.f., analogous behaviour of iron on oxidation (Bauklon & Thiel, 1940).

This type of oxidation mechanism at higher temperatures would assist further the oxidation of the metal nitride, the former was found to be complete within a few hours at 1100°C in contrast to incomplete oxidation over a much longer period at 1000°C (Fig. 55).

## 5.2 Molybdenum Nitride

### 5.2.1 Nitridation of Molybdenum

The molybdenum-nitrogen system and its thermodynamics have been described in Chapter I. Neumann et al., (1934), Sato (1938 b), and Brewer et al., (1950) have also compiled thermodynamic data on molybdenum nitrides. Since there is little or no nitride formation by direct action between the metal and nitrogen in the temperature range 400-1000°C (see Section 1.14, Chapter I), kinetic measurements mainly concern the rate of diffusion of nitrogen through molybdenum at various temperatures (Smithells and Ransley, 1934, 1935). The equation concerned is:

$$D = K \sqrt{P} \left[ \frac{aP}{1 + aP} \right]$$

where, D = Diffusion coeff., k and a are constants, P = pressure of nitrogen gas which allows for the fraction of surface covered by the adsorbed layer, according to Langmuir's isotherm.

Conditions for nitride formation from the metal and ammonia and the thermal stabilities of the crystalline phases Mo<sub>2</sub>N and MoN have been discussed previously in Section 1.14. The nitriding of the almost pure Mo-alloy TsM=2A (C 0.003, Ti 0.09 and Zr 0.14 wt-%) by ammonia (Lakhtin & Kogan, 1968) produces a maximum surface hardness at 900-1400°C due to the formation of Mo<sub>2</sub>N and MoN.

Nitridation at temperatures above  $1400^{\circ}\text{C}$  resulted in a decrease in hardness due to recrystallisation of molybdenum and lack of nitride formation. Optimum nitriding conditions were  $900\text{--}1000^{\circ}\text{C}$  for 1 hour. Nitrided molybdenum showed increased resistance (by 60-90%) to plastic deformation at  $1000\text{--}1400^{\circ}\text{C}$ . The nitrided layer was brittle.

In the present work, the nitride used for milling and oxidation studies had a composition of 72.6 wt-%  $\text{Mo}_2\text{N}$  and 27.4 wt-% Mo (4.93%N compared with 6.80 % for  $\text{Mo}_2\text{N}$ )

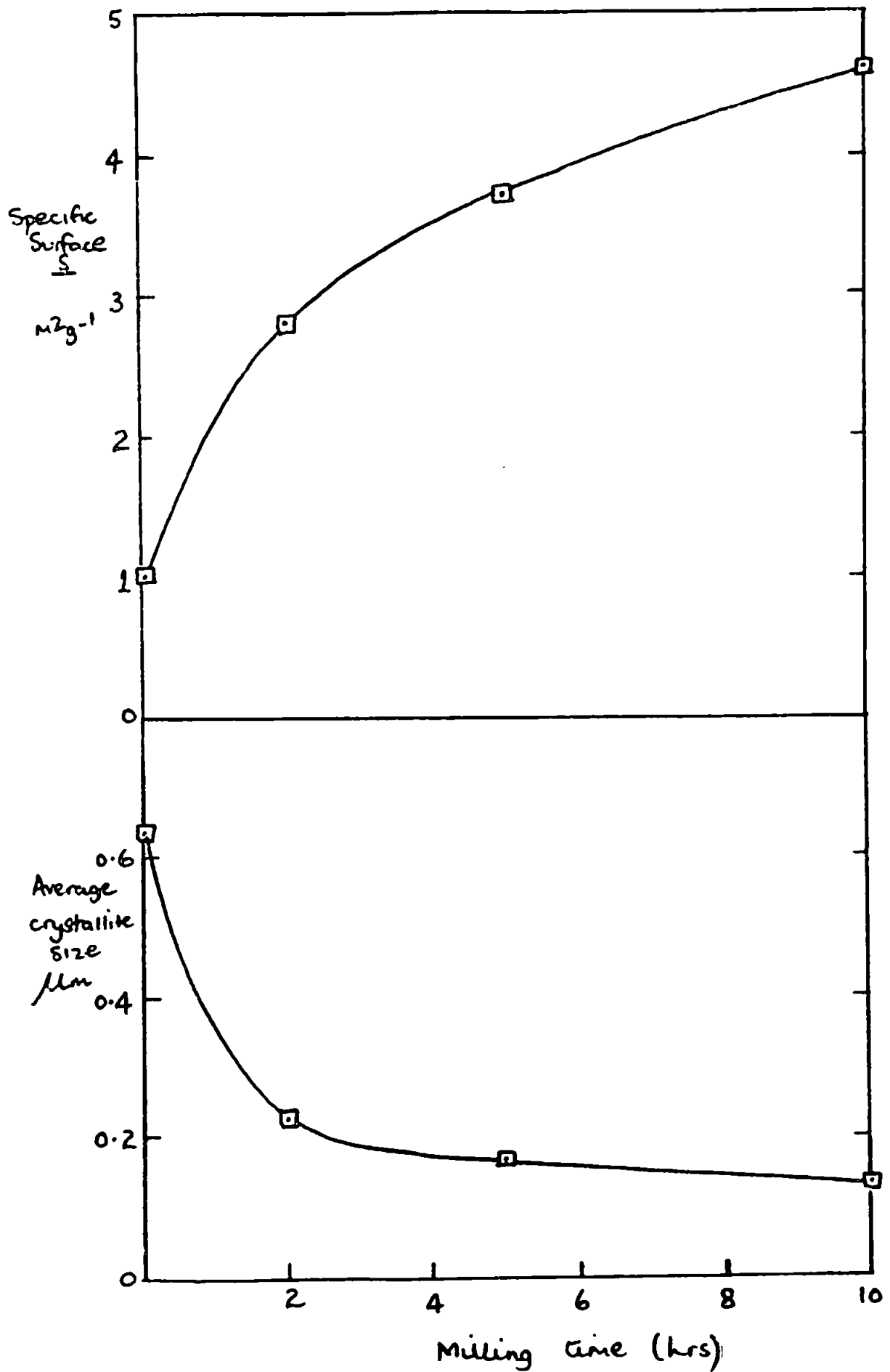
### 5.2.2. Milling of Molybdenum Nitride

6 g-portions of the Molybdenum nitride were milled under standard conditions described in Section 2.6 Chapter I. The specific surface progressively increased and the average crystallite size decreased during milling times of up to 10 hours (Figure, 5.13).

The milling caused strain to be set up within the crystallites, so that there was X-ray line (or peak)-broadening as shown in Figure 5.14. These X-ray diffractometer traces reveal that the nitride present (in the initial sample) has been more extensively milled than the metal, in contrast to the behaviour found in the case of zirconium nitride and the metal, as reported in Section 3.2.2 Chapter III. The main Mo and  $\text{Mo}_2\text{N}$  X-ray peaks were too close to determine accurately the changes in half-peak widths for estimating the crystal lattice strains.

The initial aggregates and single crystals are reduced considerably in size during the first 2 h milling, cf. change in average crystallite size illustrated in Figure 5.13(b) and electron micrographs, Plates 5.8 & 5.12. This probably represents also

FIG. 5.13:- MILLING OF MOLYBDENUM NITRIDE



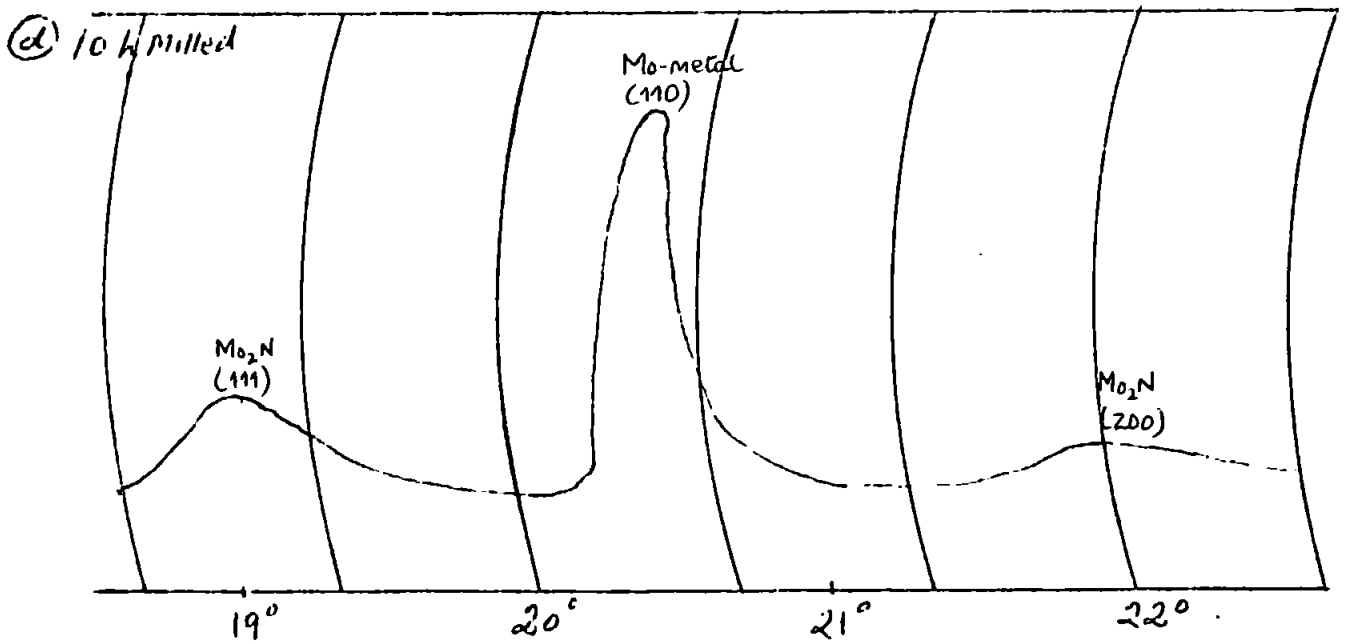
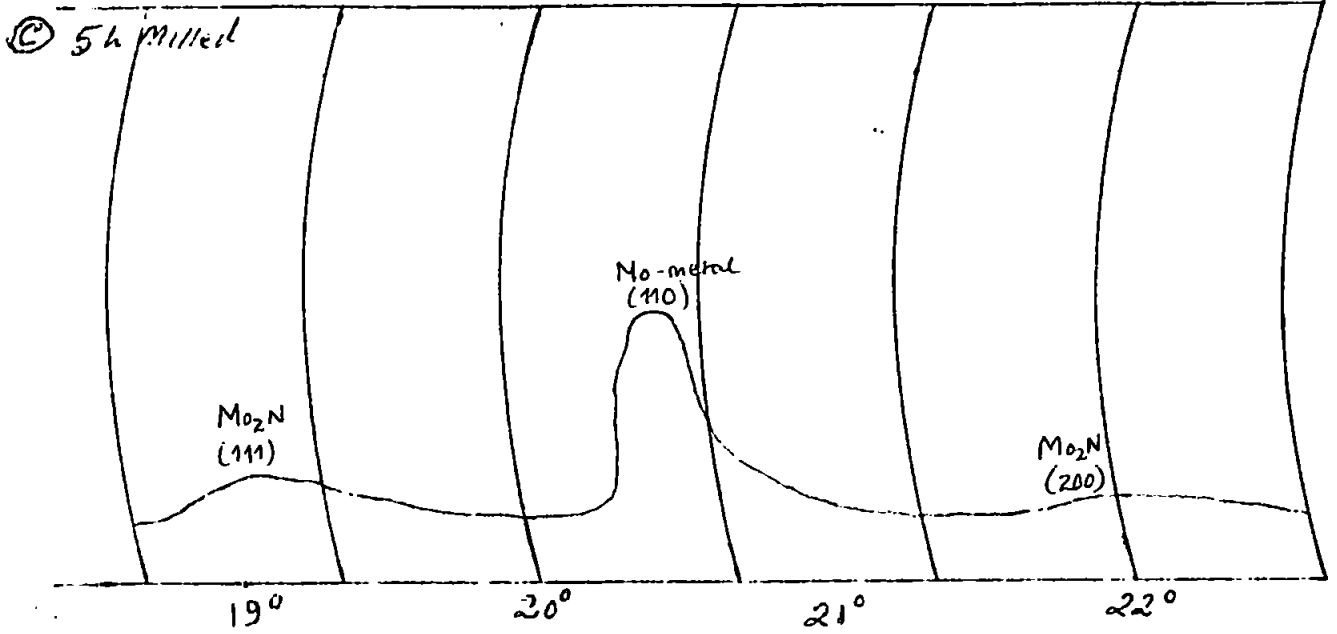


FIGURE 5.141 (CONT.)

1  $\mu$ m

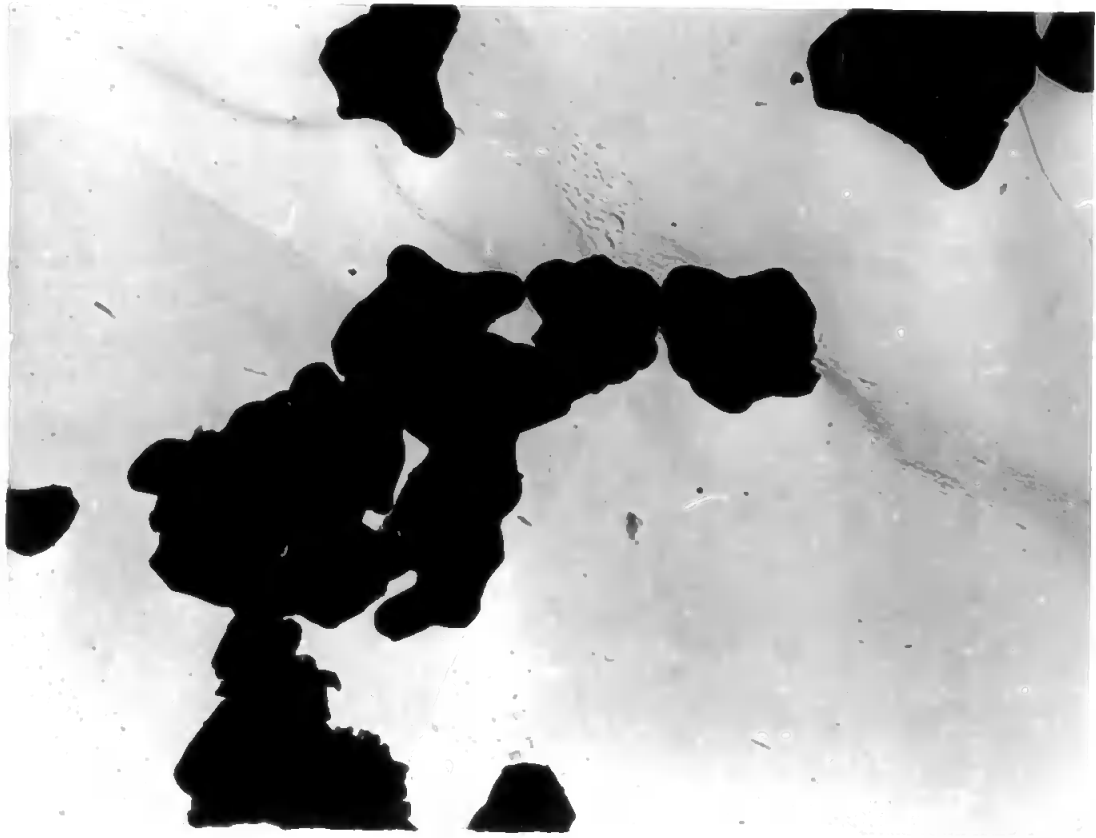


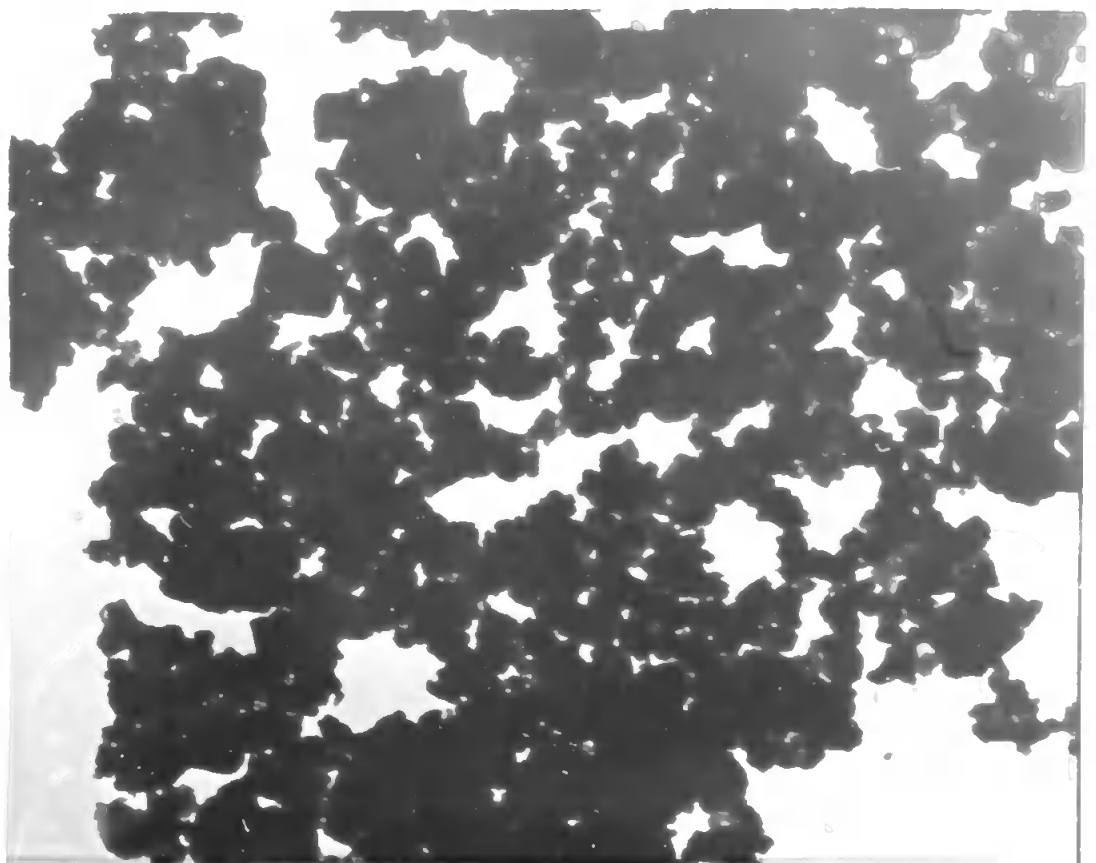
PLATE 5.7 Molybdenum Nitride, Untreated

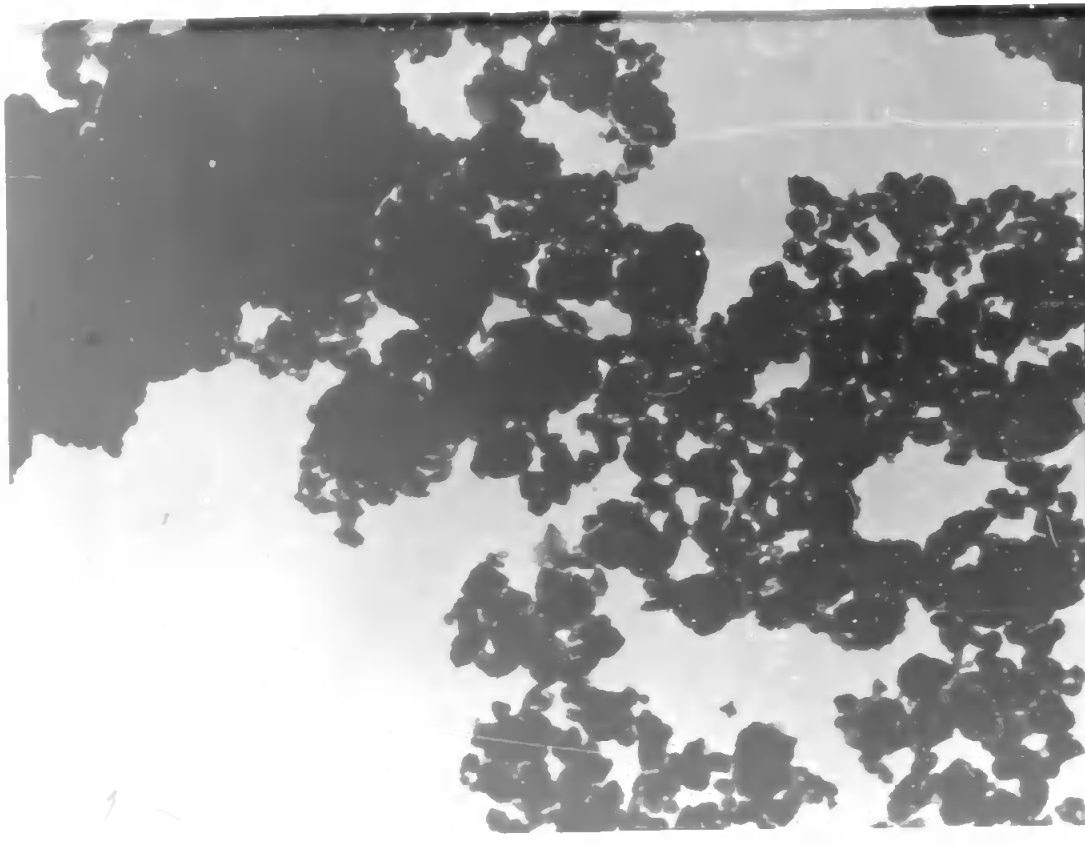
Magnification x 20,000

Fe<sub>3</sub>O<sub>4</sub> (12A)

PLATE 5.8 Molybdenum Nitride, Ball-Milled for 1 Hour

1  $\mu$ m





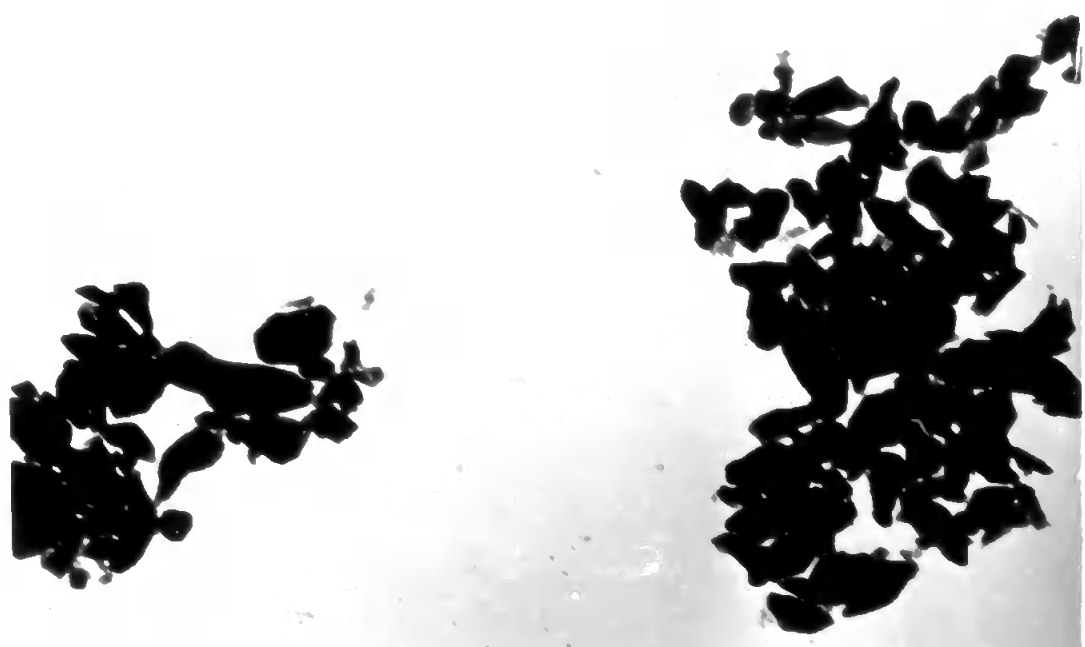
1 μm

PLATE 8.10 Polydioxane Nitride, Treated for 10 hours


Page (110)

Magnification x 20,000

PLATE 8.9 Polydioxane Nitride, Oxidized in air at 400°C for 5 hours



1 μm



1  $\mu$ m

PLATE 5.11 Molybdenum Nitride, Oxidised in Air at 550°C for 5 hours

Magnification x 20,000

Page (21C)



removal and comminution of more brittle nitride from the outside of the partly nitrated metal particles. On further milling (2-10 hours) there was comparatively less change in the average crystallite sizes and the aggregate sizes of the material.

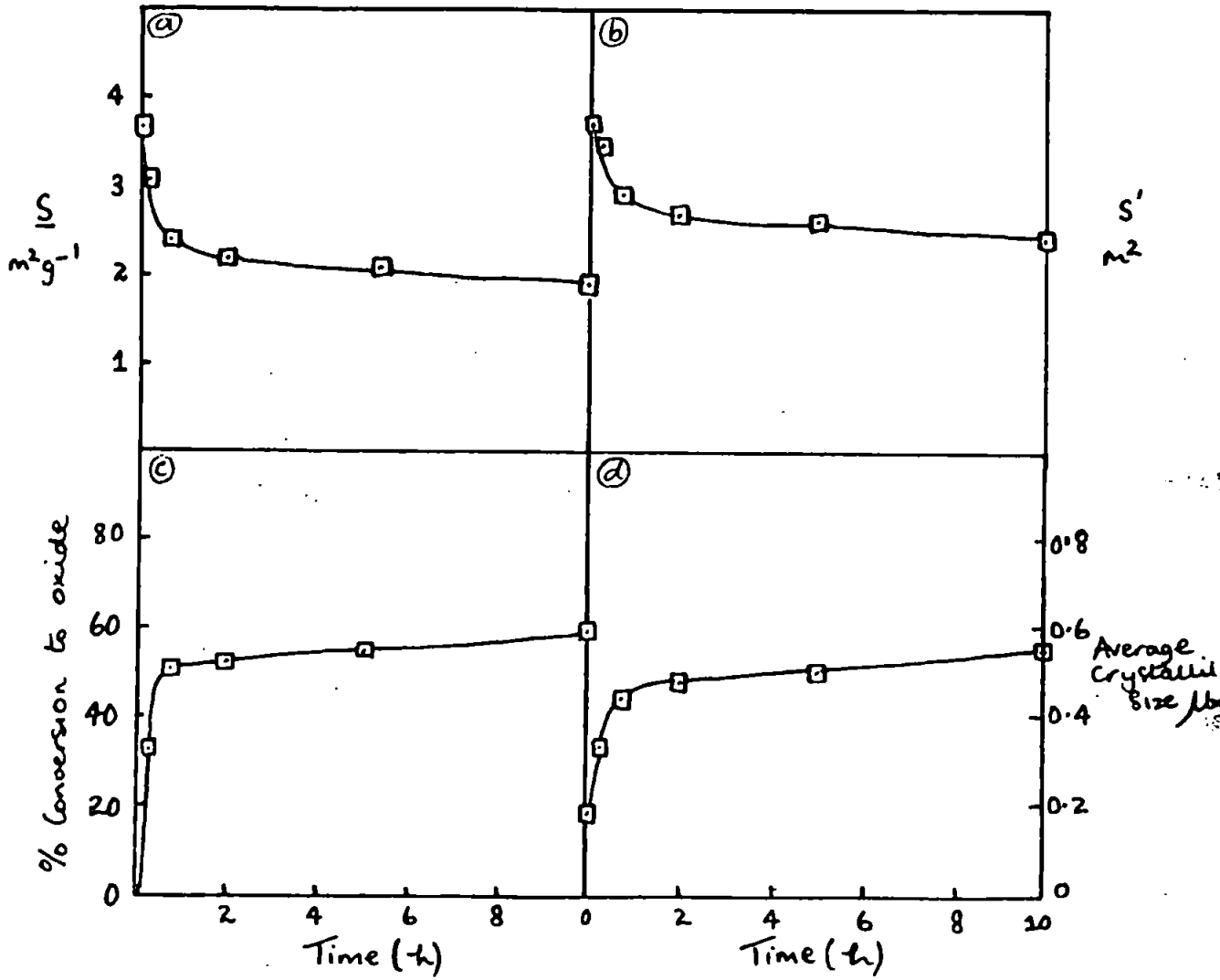
### 5.2.3 Oxidation of Molybdenum Nitride

Molybdenum nitride is converted to molybdic oxide,  $\text{MoO}_3$ , at temperatures between  $350-600^\circ\text{C}$  in air. X-ray diffractometer traces give no indications of any oxynitrides or lower oxides of molybdenum being formed at these temperatures. Variations in specific surface,  $S_s$ , actual surface area (for 1 g initial sample)  $S_s^0$ , and average crystallite size (equivalent spherical diameter) are shown in Figure 5.15, for 5 h-milled molybdenum nitride subjected to atmospheric oxidation at  $400^\circ\text{C}$ . About  $\frac{1}{2}$  of the material oxidises comparatively rapidly, while  $S_s$  and  $S_s^0$  values decrease and the average crystallite size increase to about  $0.5\mu\text{m}$ .

When the oxide crystallises out from the nitride matrix, the changes in types of crystal lattice (cubic NaCl ( $B_1$ ) of  $\text{Mo}_2\text{N}$  or cubic b.c. ( $A_2$ ) of Mo to orthorhombic  $\text{MoO}_3$ ) and large fractional volume increases (1.84 and 2.3 of the original  $\text{Mo}_2\text{N}$  and Mo volumes respectively) would be expected to produce considerable splitting away of oxide crystallites. However, the surface areas decrease since molybdic oxide ( $\text{MoO}_3$ ) sinters very readily at  $400^\circ\text{C}$ . This temperature is well above the Tammann temperature (about  $\frac{1}{2}$  m.p. in K) of about  $260^\circ\text{C}$  for molybdic oxide, so that crystal lattice diffusion can be extensive. Hence, in the later stages of the oxidation the remaining nitride particles are surrounded by layers of oxide impermeable to normal gaseous diffusion. The initial approximately

FIGURE 5.15

OXIDATION OF MILLED MOLYBDENUM NITRIDE AT 400° IN AIR



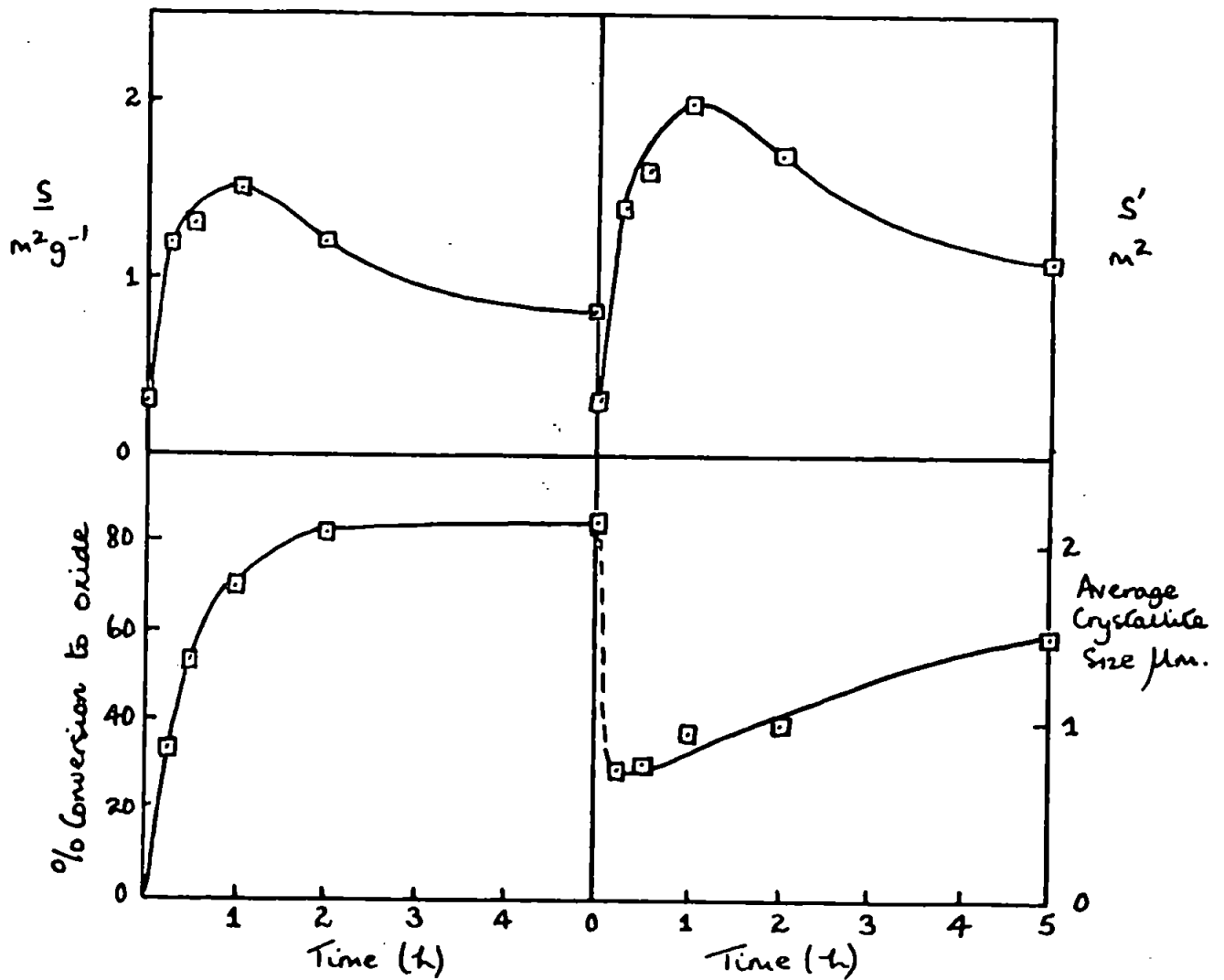
linear kinetics become parabolic being controlled by lattice diffusion through the oxide layer. This is shown also for oxidation of milled and unmilled nitride samples in Figures 5.15(c), 5.16 and 5.17 at temperatures ranging between 350-450°C. As found for other nitrides, the milled material apparently has the greater surface heterogeneity and has more tendency to give initial linear rather than parabolic oxidation rates (as discussed in Section 3.1.3). The oxidation rates increase comparatively little between 450° and 600°C, cf., Fig. 5.18(a) and (b), most probably caused by more extensive sintering of the oxide impeding the reaction at the higher temperature (cf. vanadium nitride, Section 4.1.3), and similarly impeding the final oxidation of the 10 h-compared with the 2 h-milled samples. Accordingly electron micrographs show that the initial irregular particles of unmilled or milled nitride ultimately give regular shaped MoO<sub>3</sub> particles on oxidation at 400° and especially at 550°C (Plates 5.9 & 5.11). The unmilled nitride shows some crystallite splitting in the earlier oxidation stages at the lower temperature, viz., 400°C, but more extensive sintering predominates at the higher temperature, 550°C, when less finely-divided material is given.

#### 5.2.3(a) Comparison with oxidation of Molybdenum metal

The main oxide formed on oxidation of molybdenum powder in air at 500°C is molybdic oxide MoO<sub>3</sub>, as found for the oxidised nitride. About  $\frac{2}{3}$  of the metal is oxidised rapidly, accompanied by some splitting away of the oxide crystallites from the metal matrix as evidenced by increases in specific surface,  $\underline{S}$  and actual surface area,  $\underline{S}^0$  (for a 1 g -initial metal sample) and decreases in average crystallite size (Figure 5.19). This behaviour is ascribed to the

FIGURE 5.19

OXIDATION OF MOLYBDENUM POWDER AT 500° IN AIR



1  $\mu$ m

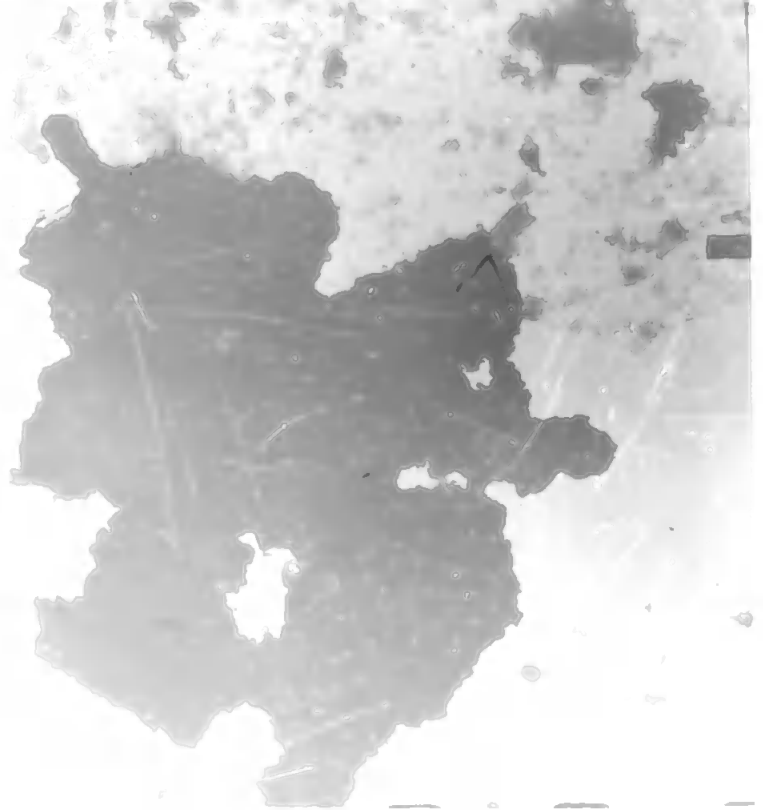


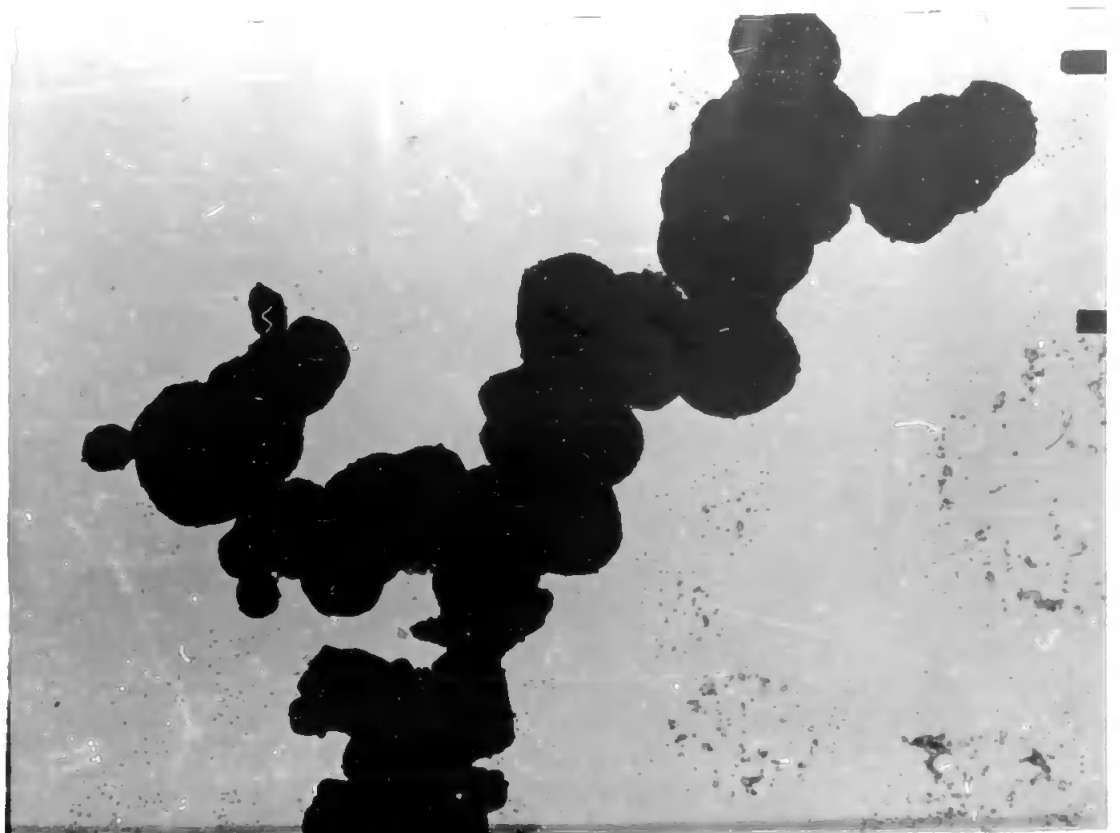
PLATE 5.12 Molybdenum Metal Powder, Oxidized in Air at 500°C for 1 hour

Magnification  $\times 20,000$

Page (23)

PLATE 5.13 Molybdenum Metal Powder, Oxidized in Air at 400°C for 5 hours.

1  $\mu$ m



change in type of crystal lattice and large fractional volume increase (viz., 2.3 of the original volume described in the preceding section) when the metal is oxidised to the less dense oxide. Subsequently, oxide sintering predominates so that  $\bar{S}$  and  $\bar{S}^0$  diminish and the average crystallite size increases. This stable oxide film like that obtained from the nitride again considerably impedes the oxidation. Similarly, electron micrographs show that the original rounded (sintered) particles of Molybdenum powder are large'v unaffected by limited (11%) oxidation at 400°C in 5 hours (Plate 5. 3 ) but more extensive oxidation at 500°C in air (about 70% oxidation in 1h) produces some finer material with less rounded aggregates. This part of the oxidised specimen is shown electron-micrographically in Plate 5.12, but together with coarser remainder of the material, it sinters extensively on further heating to above one micron in size.

## CHAPTER VI

### CONCLUDING SUMMARY

The present research reported in Chapters III - V demonstrates the general principles presented in Chapter I. The kinetics and products of oxidation of the nitrides of transition metals, viz., Ti, Zr, V, Nb, Ta, Cr and Mo, depend mainly on the intrinsic reactivity of the material and the available surface at which oxidation can occur.

The temperatures for the formation of the nitrides are sufficiently high to cause extensive sintering so that the products usually have specific surfaces below  $1 \text{ m}^2 \text{ g}^{-1}$  and average crystallite sizes above  $0.5 \mu\text{m}$ . When the nitrides are milled the specific surface progressively increases. Electron micrographs show that the original nitrides consist of single crystals and aggregates. The single crystals are fractured in the earlier stages of the milling and the fragments are incorporated into the aggregates. The average crystallite sizes decrease rapidly at first and later slowly when the crystallites become of submicron size.

The milled nitrides apparently have greater surface heterogeneity and tend initially to give linear rather than parabolic oxidation rates, until sufficient oxide of rational crystallite-size composition is formed to give stable oxide layers. The kinetics and oxidation rates are influenced also by differences in type of crystal structure and in molecular volume of the nitrides and their oxide products. This leads to splitting away of newly-formed oxide crystallites from the remaining nitride matrix.

particularly in the earlier stages of many of the oxidations. Thus, there are initial increases in specific surface and decreases in average crystallite size.

In contrast, oxide sintering decreases the surface area, being enhanced by longer calcination and higher temperatures. The sintering is controlled by surface diffusion promoting grain-boundary penetration at lower temperatures (above about  $\frac{1}{2}$  m.p. in K) and crystal lattice diffusion at higher temperatures (above the Tammann temperature, about  $\frac{1}{2}$  m.p. in K). Comparison of the oxidation of nitrated and free metals indicates that oxide sintering is inhibited sometimes by removal of nitrogen but accelerated occasionally by the remaining metal.

In the formation of titanium nitride from  $\alpha$ -,  $\beta$ -, and mixed  $\alpha/\beta$ - titanium alloys, the nitride layers adhere strongly to the metal substrate. X-ray analysis indicates that there is some dissolution of nitrogen in the original  $\alpha$ - or  $\beta$ - titanium to slightly distort their lattices to that of the so-called  $\beta$ -TiN, before further nitridation and formation of well-defined crystalline TiN. There are only small volume increases (0.05 to 0.08 of the original metal volume) during the nitridations, facilitating good adhesion of the nitride layer. At lower temperatures (800-1300°C) lattice diffusion is also operative. However, the scaling resistance of titanium nitride in air is poor, since it oxidises appreciably at temperatures above only 400°C.

In the oxidation of titanium nitride, crystallites of rutile split off from the remaining nitride before they sinter and inhibit further oxidation. Zirconium nitride oxidation is complicated by formation of tetragonal ZrO<sub>2</sub> at higher temperatures, particularly



above  $1200^{\circ}\text{C}$ , and monoclinic  $\text{ZrO}_2$  at lower temperatures. The nitride initially forms the so-called 'amorphous' cubic  $\text{ZrO}_2$  notably between  $400\text{-}600^{\circ}\text{C}$ , which may be stabilised somewhat by the remaining cubic  $\text{ZrN}$ . Subsequently, there is a further fractional volume increase while formation of monoclinic  $\text{ZrO}_2$  is being completed.

The atmospheric oxidation of vanadium nitride,  $\text{VN}$ , at  $450\text{-}650^{\circ}\text{C}$  produces vanadium pentoxide,  $\text{V}_2\text{O}_5$ , which is comparatively low melting (m.p.  $674^{\circ}\text{C}$ ) and sinters extensively. Hence, oxide sintering predominates over possible surface activation caused by any crystallite splitting through change in type of crystal lattice and large fractional volume increase (1.27 of the original volume), as the nitride is converted to the less dense oxide. The maximum oxidation rate is given at about  $500^{\circ}\text{C}$ . Lower rates at  $500\text{-}650^{\circ}\text{C}$  are ascribed to more extensive oxide sintering impeding the oxidation.

Niobium nitride ( $\alpha\text{-NbN}$ ) and tantalum nitride ( $\alpha\text{-}$  and  $\delta\text{-TaN}$ ) are converted in air to niobium pentoxide,  $\beta\text{-Nb}_2\text{O}_5$  at  $300\text{-}800^{\circ}\text{C}$  and tantalum pentoxide,  $\beta\text{-Ta}_2\text{O}_5$  at  $400\text{-}600^{\circ}\text{C}$  respectively. There are considerable increases in specific surface and decreases in average crystallite size in the earlier stages of the oxidations when the oxides crystallise out from the remaining nitride matrices. Similar behaviour is shown when the metals are oxidised in air. In all cases, there are large volume increases resulting in extensive crystallite splitting. Subsequently, the newly-formed oxides sinter causing the oxidation to be impeded. The sintering of the niobium pentoxide between  $400\text{-}600^{\circ}\text{C}$  is extensive enough to reverse the temperature coefficient to negative values for the oxidation rates of

the nitride as well as those previously found for the metal. At temperatures, above  $600^{\circ}\text{C}$ , the oxidation rates increase again with temperature as the crystal lattice diffusion increases. Production of correspondingly smaller oxide crystallites from the nitride compared with the metal oxidations suggests that removal of nitrogen inhibits oxide sintering; the comparatively high melting metal is not expected to accelerate sintering in the metal oxidation.

Chromium nitrides,  $\text{CrN}$  and  $\text{Cr}_2\text{N}$ , are the most oxidation-resistant of the nitrides studied. Both oxidised to give chromium-sesquioxide,  $\text{Cr}_2\text{O}_3$ , at temperatures between  $750$ - $1200^{\circ}\text{C}$ . The chromic oxide sinters extensively at temperatures above  $1000^{\circ}\text{C}$  (i.e. above about its Tammann temperature) so that oxidation of the nitrides is impeded. Nevertheless, sintering is less extensive than that found in the oxidation of the metal at corresponding temperatures. It is more comparable with that of chromic sesquioxide formed by thermally decomposing chromic hydroxide. The comparatively lower melting chromium metal apparently accelerates oxide sintering.

When molybdenum nitride,  $\text{Mo}_2\text{N}$ , oxidises in air between  $350$ - $550^{\circ}\text{C}$ , mainly molybdic oxide,  $\text{MoO}_3$ , is formed. Since, this oxide is comparatively low-melting ( $795^{\circ}\text{C}$ ) it sinters readily and hinders oxidation of both the nitride and the metal.

These studies are being extended to other transition metal nitrides, notably of tungsten. Further investigations have been carried out in this Department on the formation and reactivity of ionic and covalent nitrides (Glasson & Jayawera, 1968-69 and Coles, 1969-70) and also on other refractory hard metal and non-metal borides, carbides and silicides (Glasson & Jones, 1969-70).

## REFERENCES

- Agte, C., & Moers, K.: Z.Anorg.Chem., 1931, 198, 243.
- Aivazov, M.I., & Melekhin, V.F.: Izv.Akad.Navk. SSSR, Neorg.Mater., 1967, 3(11), 2109-10.
- Alexander, P.P.: U.S.Patent, 2,461,018, 8/2/1949.
- Alexander, P.P.: U.S.Patent, 2,461,019, 8/2/1949b.
- Alexander, L.E., & Klug, H.P.: "X-ray Diffraction Procedures", 1954, Chapter 9, (N.Y.: Wiley).
- Ang, C.Y.: Acta Metall., 1953, 1, 123.
- Arai, Z., Hayashi, H., Nakamura, S., & Azuma, U.N.: Rept.Govt.Ind.Res. Inst., Nagoya, 1962, 11, 119.
- Argent, B.B., & Phelps, B.: J.Less-Common Metals, 1960, 2, 181.
- Arkharov, V.I., Konev, V.N., & Men'shikov, A.Z.: Fiz.Metal.i.Metalloved., Akad.Nauk.S.S.R., 1959, 7, 64-71.
- Armstrong, C.I.: J.Am.Chem.Soc., 1949, 71, 3583.
- Aylmore, D.W., Gregg, S.J., & Jepson, W.B.: J.Electrochem.Soc., 1960, 107, 495.
- Bagnall, K.W.: "Chemistry of Rare Radioelements", 1957, (London: Cambridge Univ. Press).
- Bakish, R.: J.Electrochem.Soc., 1958, 105, 574-7.
- Barrer, R.M.: "Diffusion in the through Solids", 1941 (London: Cambridge Univ. Press).
- Barrer, R.M.: "Diffusion in and through Solids", 1941, (Cambridge: Univ. Press).
- Baughan, E.C.: Trans.Farad.Soc., 1959, 55, 2025.
- Baukloh, W., & Thiel, G.: Korros Metallschutz, 1940, 16, 121.
- Becker, K.: Phy.Z., 1933, 34, 185.
- Beisswenger, H.: Hätterie-Tech. Wärmebehandl., 1958, 4, 40.
- Bennett, H., & Lindop, E.H.: "The Determination of Nitrogen in Boron N<sup>4</sup>tride", Research Paper No. 425, The Brit.Ceram.Res.Assoon., Stoke-on-Trent, 1958.
- Bernhard Berghaus (Elektrophysikalische Anstalt): British Patent 877,675, 20/9/61.
- Berry, R.W., Jackson, W.H., Parisi, G.I., & Shafer, A.H.: Trans.Compt.Pts., 1964, 11(2), 86-96.
- Bickley, R.I.: Ph.D. Thesis, Exeter Univ., 1965.
- Bilz, H.Z.: Phys.Chem., 1958, 153, 338.

- Blix, R.: Z.Phys.Chem., 1929, E3, 229.
- Blum, A.: Planseeber Pulv. Metall., 1962, 10, 72.
- Bradford, C.I., Catlin, J.P. & Wemple, E.L.: Metal Progr. 1949, 55, 348.
- Bradshaw, B.C.: J.Chem.Phys., 1951, 19, 1057.
- Bradshaw, W. G. & Matthews, C.O.: "Properties of Refractory Materials; Collected Data and References", 1958, LMSD-2466.
- Brager, A.: Acta Physicochimica URSS, 1939, 11, 607.
- Brager, A.: Acta Physicochimica URSS, 1939a, 10, 887.
- Brauer, G. & Jander, J.Z.: Anorg.Chem., 1952, 270, 160.
- Brauer, G., & Jander, J.: Z.Anorg.Chem., 1952, 270, 160-78.
- Brauer, G., Jander, J. & Rogener, H.Z.: Phys., 1953, 134, 432-4.
- Brauer, G., & Kirner, Z.: Z.Anorg.Allgem.Chem., 1964, 328, 34.
- Brauer, G. & Schmel, W.D.: J.Len-Common Metals, 1964, 6(4), 326-32.
- Brauer, G. & Weidlein, J.R.: Angew.Chem., 1965, 77(5), 218-19.
- Brauer, G. & Zapp, K.H.: Naturwissenschaften, 1953, 40, 604.
- Brewer, L., Bromley, L.A., Gilles, P.W., & Lofgren, N.L.: "The Chemistry and Metallurgy of Miscellaneous Materials - Thermodynamics", 1950, pp.40 ff Edit.Quill, L.L. (New York : McGraw Hill).
- British Standards 3406, Part IV, 1963: Particle Size of Powders by Optical Microscope.
- British Standards 4359, Part I, 1969.
- Britton, H.T.S.: "Hydrogen Ions", 2nd Edn., 1955 (London: Chapman & Hall).
- Brown, B.R., in "Comprehensive Treatise on Inorganic and Theoretical Chemistry", Supplement to Vol. VIII, Part I, 1969, pp.150-239 (London: Longmans).
- Brunauer, S., Emmett, P.H., & Teller, E.: J.Am.Chem.Soc., 1938, 60, 309.
- Cabrera, N., & Mott, N.F.: Rept.Prog.Phy., 1948, 12, 163.
- Campbell, I.E., & Powell, C.F.: Iron Age, 1952, 169, No. 15, 113.
- Campbell, I.E., Powell, C.F., Nowicki, D.H., & Gonser, B.W.: J.Electrochem.Soc., 1949, 96, 318.
- Caplan, D.: J.Electrochem.Soc., 1960, 107, 359.
- Carpenter, L.G. & Reavell, F.R.: Metallurgia, 1948, 39, 63.
- Cathcart, J.V., Bakish, R., Norton, D.R.: J.Electrochem.Soc., 1960, 107, 668.
- Chilton, J.P.: "Principles of Metallic Corrosion", 2nd edn., 1968; Monograph for Teachers, No. 4 (London: R.I.C.).

- C.I.B.A. Ltd. Neth.Appl. 6,516,039 (Cl.C.016), June, 13, 1966, 10 pp.
- Chiotti, P.: J.Am.Ceram.Soc., 1952, 35, 123.
- Clair, J.: French Patent 1,215, 862, 21/4/60.
- Clarke, J. & Jack, K.H.: Chemy.Ind., 1951, 1004.
- Clausing, P.: Z.Anorg.Allgem.Chem., 1932, 208, 407.
- Coble, R.L.: J.Appl.Phys., 1961, 32, 707-77.
- Coble, R.L.: "Fundamental Phenomena in the Material Sciences", 1964, Vol. 1 (New York: Plenum).
- Cochet, A.: Z.Angew.Chem., 1931, 44, 367.
- Coles, N.G., Glasson, D.R., & Jayaweera, S.A.A.: J.Appl.Chem., 1969, 19, 178-181.
- Cooper, C.F.: Proc.Brit.Ceram.Soc., 1969, No. 12, 1.
- Cosgrove, J.D., & Shears, E.C.: Analyst, 1960, 85, 448.
- Cowgill, M.G., & Stringer, J.: J.Less-Common Metals, 1960, 2, 233.
- Coyne, H.J., Jr. & Tauber, R.N.: J.Appl.Phys., 1968, 39(12), 5585-93.
- Croato, U., Genta, V., & Maltese, P.: Gazz.Chim.Ital., 1951, 81, 827.
- Crossley, F.A., & Kessler, H.D.: J.Metals, N.Y., 195h, 6, 119.
- Cuthill, J.R., Hayes, W.D., & Seebold, R.E.: J.Res.Natl.Bur.Stds., 1960, 64A, No. 1, 119.
- de Boer, J.H.: Proceedings of the International Symp. on Surface Area Detn., Bristol, July, 1969, SCI Monograph (in press).
- de Boer, J.H., & East, J.D.: Rec.Trav.Chim., 1936, 55, 459.
- de Gelis, P.: Rev.Chim.Minerale, 1966, 3(1), 75-96.
- Dell, R.M., Wheeler, V.J., & McIver, E.J.: Chem.Soc.Symp., Aberdeen, 1966, Paper 3-3; Trans.Farad.Soc., 1966, 62, 3591.
- Denker, S.P.: J.Less-Common Metals, 1968, 14(1), 1-22.
- Domagala, R.F., McPherson, D.J., & Hansen, M.: J.Metals, 1956, 8, AIME Trans., 206, 98
- Dravnieks, A.: J.Am.Chem.Soc., 1950, 72, 3568.
- Duparc, L., Weuger, P., & Schussele, W.: Helv.Chim.Actu., 1930, 13, 917.
- Duwez, P., & Odell, F.: J.Electrochem.Soc., 1950, 97, 299.
- Ehrlich, P.: Z.Anorg.Chem., 1949, 259, 1.
- Ellingham, H.J.T.: J.Soc.Chem.Ind., 1944, 63, 125.

- Elliot, N.: Phys.Rev., 19 129, 1120.
- Elliot, R.P., & Komjathy, . . . : U.S.At.Energy Comm., ARF-2120 (5 through 8), 1960, 74 pp.
- Elwall, W.T., & Wood, D.F.: "The Analysis of Titanium Zirconium and their Alloys", 1961, pp. 65-69 (Birmingham: Wiley).
- Epelbaum, V.A., & Brager, A.K.: Acta Physikochim., U.S.S.R., 1940, 13, 595-600.
- Epelbaum, V.A., & Ormont, B.F.: J.Phys.Chem., U.S.S.R., 1946, 20 459.
- Epelbaum, V.A., & Ormont, B.F.: J.Phys.Chem., SSSR, 1947, 21, 3.
- Eriksson, S.: Jern-kont. Annlr., 1934, 118, 530.
- Evans, U.R.: Trans.Electrochem.Soc., 1924, 46, 247.
- Evans, U.R.: "The Corrosion & Oxidation of Metals", First Supplementary volume, 1968 (London: Edward Arnold).
- Farr, J.D. in: "Fundamentals of Refractory Compounds", 1968, p.42; Editors, Hausner & Bowman, (New York: Plenum Press).
- Federchenko, I.M. & Skorokhod, V.V.: Izv.Akad.Nauk.SSSR, 1967, 58, (10), 29; "Progress in Inorganic Materials", 50th Anniversary Publication, Akud.Nauk SSSR, Oct., 1967.
- Fischbeck, K.: Z.Elektrochem, 1933, 39, 316.
- Foster, L.S.: Met.Prog., 1952, 62(2), 160.
- Frank, H.H., & Heimann, H.: Z.Angew.Chem., 1931, 44, 372.
- Frenkel, J.: J.Phys. U.S.S.R., 1945, 2, 385.
- Friederich, E., & Sittig, L.Z.: Anorg.Allgem.Chem., 1925, 143, 293.
- Fujiwara, S.: J.Chem.Soc.Japan, Pure Chem.Sect., 1950, 71, 580.
- Fulrath, R.M., & Rice, R.W.: "Science of Ceramics", Proc.Brit.Ceram.Society, 1969, No.12, p.92.
- Gaydon, F.P.: Vacuum, 1967, 17(6), 325-7.
- Gebhart, E., & Seghezzi, H.D.: Z.Metallk., 1959, 50, 248.
- Gerschbacher, H.: Wien.Chem.Ztg., 1947, 48, 30-36.
- Gerschbacher, H.: Chim et Ind., 1947, 58, 352.
- Gerstanberg, D., & Hall, P.M.: J.Electrochem.Soc., 1964, 111, No. 8, 936-42.
- Ghosh, S.P.: J.Ind.Chem.Soc., 1952, 29, 484.
- Gill, R.M., & Spence, G.: Refractory J., 1962, p.92.
- Glasson, D.R.: Ph.D. Thesis, London Univ., 1949.

- Glasson, D.R.: J.Chem.Soc., 1956, 1506.
- Glasson, D.R.: J.Appl.Chem., 1958a, 8, 793.
- Glasson, D.R.: J.Appl.Chem., 1958b, 8, 798.
- Glasson, D.R.: J.Appl.Chem., 1960, 10, 38.
- Glasson, D.R.: J.Appl.Chem., 1961a, 11, 24.
- Glasson, D.R.: J.Appl.Chem., 1961b, 11, 201.
- Glasson, D.R.: J.Appl.Chem., 1963a, 13, 111.
- Glasson, D.R.: J.Appl.Chem., 1963b, 13, 119.
- Glasson, D.R.: J.Appl.Chem., 1967, 17, 91.
- Glasson, D.R.: J.Appl.Chem., 1964, 14, 121.
- Glasson, D.R.: S.C.I. Monographs, 1964a, No. 18, 401.
- Glasson, D.R., & Jayaweera, S.A.A.: J.Appl.Chem., 1968, 18, 67.
- Glasson, D.R., & Sheppard, M.A.: J.Appl.Chem., 1968, 18, 327.
- Goodenough, J.B.: "Magnetism and the Chemical Bond", 1963, (New York: Wiley-Interscience).
- Goodenough, J.B.: Phys.Rev., 1960, 120, 67.
- Goodenough, J.B.: Phys.Rev., 1960, 117, p.1442.
- Goodeve, C., & Jack, K.H.: Discuss.Faraday Soc., 1948, No.4, 82.
- Gooding, R.W., Parratt, N.J.: T.I.(Group Services) Ltd. Brit.Pat. 1,010,651 (cl.C.01b), Nov. 24, 1965, 4pp.
- Goon, E.J.: U.S.Pat. 3,427,132 (Cl. 23-204), 11/2/1969, 3pp.
- Gregg, S.J.: "Surface Chemistry of Solids", 1st edn., 1951, Ch.4, pp.63-79; ibid, 2nd edn., 1961, Ch.7, pp.300-328 (London: Chapman & Hall).
- Gregg, S.J. in: "Surface Phenomena in Chemistry and Biology", (Edts.: J.F. Danielli, K.G.A. Pankhurst & A.C. Riddiford), 1958, Ch.15, pp.195-213 (London: Pergamon Press).
- Gregg, S.J.: J.Chem.Soc., 1946, 561.
- Gregg, S.J.: J.Chem.Soc., 1955, 1438.
- Gregg, S.J., & Sing, K.S.W.: "Adsorption, Surface Area and Porosity", 1967 (London: Academic Press).
- Gregg, S.J., & Sing, K.S.W.: J.Phys.Coll.Chem., 1952, 56, 388.
- Gregg, S.J., & Bickley, R.I.: J.Chem.Soc.(A), 1966, p1849.
- Gregg, S.J., & Facker, R.K.: J.Chem.Soc., 1955, 51.

- Gregg, S.J., Parker, T.W., & Stephens, M.J.: *J. Appl. Chem.*, 1954, 4, 633.
- Gregg, S.J., & Wheatley, K.H.: *J. Chem. Soc.*, 1955, 3804.
- Gregg, S.J., & Winsor, G.W.: *Analyst, London*, 1945, 70, 336.
- Griffiths, R., & Pryde, J.A.: *Trans. Farad. Soc.*, 1967, 63(11), 2599-604.
- Guard, R.G., Savage, J.W., & Swarthout, D.G.: *Trans. Metal. Soc., AIME (Amer. Inst. Mining, Met., Petrol. Engrg.)*, 1967, 239(5), 643-9.
- Gulland, C., & Wyart, J.: *J. Rech. Cent. Natn. Rech. Scient.*, 1947, 3, 123.
- Gulbransen, E.A., & Andrew, K.F.: *J. Metals, N.Y.*, 1949a, 1, No. 8, 515.
- Gulbransen, E.A., & Andrew, K.F.: *J. Metals., New York*, 1949b, 1, No. 10, 741.
- Gulbransen, E.A., & Andrew, K.F.: *J. Electrochem. Soc.*, 1949c, 96, 354.
- Gulbransen, E.A., & Andrew, K.F.: *J. Metals, N.Y.*, 1950, 188, 586.
- Gulbransen, E.A., & Andrew, K.F.: *Trans. Amer. Inst. Min. (Metall). Engrs.*, 1949, 185, 741.
- Gulbransen, E.A., & Andrew, K.F.: *J. Electrochem. Soc.*, 1950, 97, 383 and 396.
- Gulbransen, E.A., & Andrew, K.F.: *J. Electrochem. Soc.*, 1951, 98, 241.
- Gulbransen, E.A., & Andrew, K.F.: *J. Electrochem. Soc.*, 1957, 104, 334.
- Guldner, W.G., & Wooten, L.A.: *J. Electrochem. Soc.*, 1948, 93, 223.
- Hag, G.: *Z. Phys. Chem.*, 1930, (B), 7, 339.
- Hag, G.: *Z. Phys. Chem. (B)*, 1930, 6, 221; *ibid*, 1931a, 12, 33.
- Hag, G.: *Metallwirt.*, 1931b, 10, 387.
- Hag, G.: *Iva*, 1953, 24, 345.
- Hahn, H.: *Z. Anorg. Chem.*, 1949, 258, 58.
- Hahn, H., & Konrad, A.: *Z. Anorg. Allgem. Chem.*, 1951, 264, 174.
- Hardie, D., & Jack, K.H.: *Nature, Lond.*, 1957, 180, 332.
- Hayes, E.T., & Roberson, A.H.: *J. Electrochem. Soc.*, 1949, 96, 142.
- Henderson, G.G., & Galletly, J.C.: *J. Soc. Chem. Ind.*, 1908, 27, 387.
- Herring, C.: *J. Appl. Phys.*, 1950, 21, 437.
- Hickman, J.: Ph.D. Thesis, Exeter (1959).
- Hirsch, P.B., Howie, A., Nicholson, R.B., Pashley, D.W., & Whelan, M.J.: "Electron Microscopy of Thin Crystals", 1965 (London: Butterworth).
- Holmberg, B.: *Acta. Chem. Scand.*, 1962, 16, 1255.



- Hosoya, S., Yamagishi, J., & Tokonami, M.: J.Phy. Japan, 1968, 24(12), 363-7.
- Hough, R.L.: "Refractory Reinforcements for Ablative Plastics, Part I, Synthesis & Reaction Mechanisms of Fibrous Zirconium Nitride", 1962, ASD-TDR-GL-260, AD291903 (Ohio: Wright-Patterson AFB).
- Hume-Rothery, W.: Ann.Rept.Prog.Chem., 1949, 46, 42.
- Hume-Rothery, W.: Phil.Mag., 1953, 44, 1154.
- Hurlen, T.: J.Inst.Metals, 1960-61, 89, 273-80.
- Hughes, W., & Harris, B.: British Patent, 787,516; 11/12/1957.
- Hurlen, T., Kjollesdal, H., Markali, J., & Norman, N.: Publ.Cent.Inst.Ind. Res., Oslo-Blindern, April, 1959.
- Huttig, G.F.: Kolloidzeitschrift, 1941, 97 281.
- Huttig, G.F.: Z.Metallkunde, 1957, 48, 352.
- Ishii, R.: Papers Inst.Phy.Chem.Res., Tokyo, 1943, 41, 1.
- Ishii, R., & Wada, I.: Bull.Inst.Phy.Chem.Res., Tokyo, 1943, 22, 112.
- Jack, K.H.: Proc.Royal Society(A), 1948, 195, 41.
- Jacobson, A.E.: U.S.Patent, 2,672,400, 16/3/1954.
- James, J.A.: Metall.Review, 1964, 9, No. 33, pp.93-120.
- Jandell, A.Z.: Anorg.Chem., 1956, 288, 81.
- Jayaweera, S.A.A.: Ph.D.Thesis, London Univ., 1969.
- Jeffe, R.I., & Campbell, I.E.: U.S.A.E.C., 1948, No. NP-266,285,300.
- Jenkins, A.E.: J.Inst.Metals, 1955, 84, 1.
- Joncich, M.J., Vaughn, J.W., & Knutsen, B.F.: Canad.J.Chem., 1966, 44, 137.
- Jones, J.A.: Ph.D.Thesis, C.N.A.A., 1970.
- Jones, F.W.: Proc.Roy.Soc.(Lond.), 1938, 166A, 16.
- Jones, F.W.: J.Appl.Phys., 1950, 21, 126.
- Johnson, D.L.: Trans.Met.Soc. AIME (Amer.Inst.Mining Met., Petrol.Eng.), 1966, 236(12), 1755-56.
- Joy, A.S.: Proceedings of the International Symposium on Surface Area Detn., Bristol, July, 1969, SCI-Monograph (in press).
- Juza, R.: "Advances in Inorganic Chemistry & Radiochemistry", (Editors: Emsleus & Sharp), 1966, Vol. 9, p.81.
- Juza, R.: Chemio, 1945, 58, 25-30.
- Juza, R., Anschutz, E., & Puff, H.: Angew.Chem., 1959, 71, 16'.

- Juza, R.: "Advances in Inorganic Chemistry & Radiochemistry", (Editors: Emeleus & Sharp), 1966, Vol. 9, p.81.
- Karal'nik, S.M., Nikolayeva, L. G., & Korolenko, Y.I.: Ukr.Fiz.Zh., 1959, 4, 404.
- Kay, D.H.: "Techniques for Electron Microscopy", 1965 (Oxford: Blackwell).
- Kempton, C.P., Krikorian, N. H., & McGuire, J. C.: J.Phys.Chem., 1957, 61, 1237.
- Kiessling, R.: Acta.Chem.Scand., 1950, 4, 209.
- Kiessling, R.: Fortschr.Chem.Forsch., 1954, 3, 41.
- Kiessling, R.: Met.Rev., 1957, 2(5), 77.
- Kiessling, R.: Powder Met., 1959, No. 3, 177.
- Kiessling, R., & Liu, Y.H.: J.Metals, N.Y., 1951, 3, Trans. p.639.
- Kiessling, R., & Peterson, L.: Acta Metall., 1954, 2, 675.
- King, E.G.: J.Am.Chem.Soc., 1949, 71, 316.
- Kingery, W.D.: J.Am.Ceram.Soc., 1955, 38, 3.
- Kingery, W.D.: "Introduction to Ceramics", 1960, p.353, (New York: Wiley).
- Kirchevskii, I.R., & Khazanova, N.E. (1950): Zh.Fiz.Khim., 1950, 24, 1188.
- Klemm, W. & Winkelmann, G. Z.: Anorg.Chem., 1956, 288, 87.
- Kofstad, P., Private communication to Kubaschewski, O., & Hopkins, B.E., "Oxidation of Metals and Alloys", 1962, p.96, (London: Butterworth).
- Korolev, M.L.: Izv.Akad.Nauk. SSSR, Otdel.Tekh.Nauk., 1953, p.1465.
- Korsunskiy, M.I., & Genkin, Y.Y.: "Heat Resisting Materials Seminar", 1958, Bull.No.5 (Kiev: Izdvo Akad.Nauk. SSSR).
- Kozielski, J.: Zeszyty Nauk Akad., Gorniczo-Hutniczej Krakowie, Rozprawy No. 66, 1966, 84 p.p.
- Kriege, O.H.: "The Analysis of Refractory Borides, Carbides, Nitrides and Silicides", U.S.At.Energy Comm.Rept. No. LA-2306, Los Alamos, New Mexico, 1959.
- Kroll, W.J. & Bacon, F.E.: U.S.Pat. 2,427,360; 16/9/1947.
- Kubaschewski, O. & Hopkins, B.E.: "Oxidation of Metals and Alloys", 1962 (London: Butterworth).
- Kubaschewski, O., & Schneider, A.: J.Inst.Metals, 1949, 72, 403.
- Kuczynski, G.C.: "Theory of Solid State Sintering", 1961 (New York: Wiley, Interscience).
- Kume, K., & Yamagishi, H.: J.Phys.Soc.Jap., 1964, 19, 414.

- Kuo, C.Y., Fisher, J.S., & King, J.C.: I.E.E.E. (Inst. Elect. Electron. Engrs.), Trans. Pt., Mater Packaging, 1965, 1, No. 1, 123-28.
- Kuriyama, M., Hosoya, S., & Suzuki, T.: Phys. Rev., 1963, 130, 898.
- Laffitte, P., & Grandadam, P.: C.r. hebdom. Seanc. Acad. Sci., Paris, 1935, 200, 1039.
- Lakhtin, Yu.M., & Kogan, Yd.D.: Metalloved. Term. Obrab. Metal., 1968, No. 1, 24-9.
- Laplanche, H.: Met. Constr. Mec., 1963, 95(10), 849; *ibid.*, (11), 937.
- Leeming, W.: Metal Prog., 1964, 85, 86-87.
- Lohberg, K., Sagel, K., & Ruppert, W.: German Patent 1,028,542; 24/4/1958.
- Lorenz, M.R., & Binkowski, B.B.: J. Electrochem. Soc., 1962, 109, 24.
- Lorentz, M.R., & Binkowski, B.B.: J. Electrochem. Soc., 1962, 109, 24.
- Lyntaya, M.D., & Samsonov, G.V.: Redkie Redkozem. Elementy. Tekhn., Akad. Nauk. Ukr. SSR, Inst. Probl. Material o ved., 1964, 118.
- Maier, C.G.: U.S. Bur. Mines Bull. No. 436, 1942.
- Mallet, M.W., Belle, J., & Cleland, B.B.: J. Electrochem. Soc., 1954, 101, 1.
- Mallet, M.W., & Gerds, A.F.: J. Electrochem. Soc., 1955, 102, 292.
- Mallet, M.W., Baroody, E.M., Nelson, H.R., & Papp, C.A.: J. Electrochem. Soc., 1953, 100, 103.
- Margrave, J.L., & Sthapitdnonda, P.: J. Phys. Chem., Ithaca, 1955, 59, 1231.
- Maude, R.: Ph.D. Thesis, London Univ., 1970.
- Matsumoto, O., & Hayakawa, Y.: Denki Kagaku, 1966, 34, 775-9.
- Matsumoto, O.: Denki Kagaku, 1955, 34(11), 872-7.
- McQuillan, A.D., & McQuillan, M.D.: "Metallurgy of the rarer metals, No. 4, Titanium", 1956, (London: Butterworths).
- Meerson, G.A., Rakitskaya, E.M., Bulgakov, V.N., & Ladygo, A.S.: Izv. Akad. Nauk. SSSR, Neorgan. Materialy, 1966, 2(8), 1429-33.
- Mekata, M.: J. Phys. Soc. Japan, 1962, 17, 796.
- Mellor, J.W.: "Comprehensive Treatise on Inorganic and Theoretical Chemistry", Vol. VIII, 1927, pp. 97-144 (London: Longmans); Brown, B.R.: Supplement to Vol. VIII, Part I, 1969, pp. 150-239, (London: Longmans).
- Meyer, R.A., Parry, E.P., & Davis, J.H.: Anal. Chem., 1967, 39(11), 1321-3.
- Mills, T.: "Thermogravimetric study of the Higher Nitride of Chromium (CrN)", Australian Dep. Supply, Aeronaut. Res. Lab., 1967, ARL MNT-69, 8 pp.

Mills, T.: "Thermogravimetric Study of the Lower Nitride of Chromium ( $\text{Cr}_2\text{N}$ )", 1967d, ARL MET-66, 10 pp.

Mills, T.: Aust. Commonwealth Dept. Supply, Aeronaut. Res. Lab., Rept. MET 1967, ARL Met. 68, 7 pp.

Minkevich, A.N., Taimer, A.D., & Zot'ev, Yu.A.: Metalloved. Obrabot Ka Metallov, 1956, No. 7, 39.

Mitchell, D.W., & Dawes, C.: Metal Treat., 1964, 31(220), 3; *ibid*, (221), 49; *ibid*, (222), 88; *ibid*, (224), 195.

Moers, K.: Z. Anorg. Allgem. Chem., 1931, 198, 243.

Moore, C.H.: Ceramic Age, 1948, 52, 281.

Moreau, C., & Phillippot, J.: Bull. Soc. Chim., France, 1963, 283.

Mott, N.F.: Nuovo Cim., 1958, 7(10), Suppl. 312.

Munster, A.: Angew. Chem., 1957, 69, 281.

Munster, A.: Z. Elektrochem., 1959, 63, 807.

Munster, A., & Ruppert, W.: Z. Elektrochem., 1953, 57, 564.

Munster, A., & Ruppert, W.: Z. Elektrochem., 1953a, 57, 558.

Munster, A., & Sagel, K.: Z. Elektrochem. 1953, 57, 571.

Munster, A., Rinck, G., & Ruppert, W.: Z. Phy. Chem., Frankf. Ausg., 1956, 2, 228.

Munster, A., & Schlamp, G.: Proc. 16th Int. Congr. Pure and Appl. Chem., Paris, 1957, Min. Chem. Section, p.691, (London: Butterworth).

Munster, A., & Schlamp, G.: Z. Phy. Chem., 1957, (N.F.), 13, 59; *ibid*, 1958, 15, 176.

Munster, A., & Weber, R.: U.S. Patent 2,836,514; 27/5/1958.

Muthmann, W., Weiss, L., & Riedelbauch, R.: Liebigs Ann., 1907, 355, 92.

Nabarro, F.R.N.: "The Strength of Solids", Physical Society, 1948.

Nemchenko, V.F., L'vov, S.M., & Samsonov, G.V.: Ukr. Fiz. Zh., 1962, 7, 331.

National Lead Co.: Brit. Patent 745,468, 29/2/1956.

Nemnonov, S.N., & Men'shikov, A.Z.: Izv. Akad. Nauk SSSR (Ser. Fiz.), 1959, 23, 587.

Nechpor, V.S.: "Refractory Transition Metal Compounds", (Ed. G.V. Samsonov), 1964, Chapter 7, pp.62-106 (New York: Academic Press).

Neugebauer, J., Hegedus, A.J., & Millner, T.: Z. Anorg. Allgem. Chem., 1959, 302, 50.

Newkirk, A.E.: Anal. Chem., 1960, 32, No. 12, 1558.

- Neumann, B., Kroger, C., & Haebler, H.: Z.Anorg.Chem., 1931, 196, 65.
- Neumann, B., Kroger, C., & Kunz, H.: Z.Anorg.Allgem.Chem., 1934, 218 & 379.
- Niederhause, D.O.: U.S. Patent 2,865,791; 23/12/1958.
- Noldge, H.: Phys.Z., 1938, 39, 546.
- Olette, M., & Ancey-Moret, M.F.: Rev.Metall., 1963, 60, 569.
- Olson, C.M.: U.S. Patent No. 2,413,778.
- Opfermann, W.: Mber.Dt.Akad,Wiss., Berl., 1964, 6, 92.
- Orsage, R. in "The Science and Technology of W, Ta, Mo, Nb and Their Alloys", 1964, p.398; Proc. of an AGARD (Advisory Group for Aeronautical Development, NATO) Conference on Refractory Metals held at Oslo, 23-26 June, 1963 (AGARDograph 82); Ed. N. E. Promisel, Pergamon Press.
- Osthagen, K., & Kofstad, P.: J.Less-Common Metals, 1963, 5, No. 1, 7-25.
- Oswald, M.: U.S.Pat. 2,509,838; 30th May, 1950.
- Palty, A., Margolin, H., & Nielson, J.: Trans.Amer.Soc.Metals., 1954, 46, 312.
- Passer, R.G., Hart, A., & Juliette, R.J.: Analyst, 1962, 87, 501-3.
- Pauling, L.: Phy.Rev., 1938, 54, 899.
- Pauling, L.: "The Nature of the Chemical Bond", 2nd Edn., 1940, pp.401-422; ibid, 3rd Edn., 1960, pp.393-448 (Ithaca, New York: Cornell Univ. Press).
- Pauling, L.: J.Am.Chem.Soc., 1947, 69, 542.
- Pauling, L.: J.Chem.Soc., 1948, 1461.
- Pauling, L.: Proc.Roy.Soc.(A), 1949, 196, 343.
- Pauling, L. in "Molybdenum Compounds", Edts: Killefer D.H., & Linz, A., 1952, p.105 (New York: Interscience).
- Pauling, L., & Ewing, F.J.: Rev.Mod.Phy., 1948, 20, 112.
- Pearson, J., & Ende, U.J.C.: J.Iron & Steel Inst., 1953, 175, 52.
- Peiser, H.S., Rooksby, H.P., & Wilson, A.J.C.(Edts.), "X-ray Diffraction of Polycrystalline Materials", 1955, p.413 (Institute of Physics).
- Pensler, J.P.: Trans.Electrochem.Soc., 1958, 105, 315
- Peterson, R.C., Fassell, W. M., & Wadsworth, M.E.: Trans.Am.Inst.Min.Metall. Engrs., 1954, 200, 1038.
- Phalnikar, C.A., & Baldwin, W.M. Jr.: Proc.Soc.Am.Test.Mater., 1952, 51, 1038.
- Pilling, N.B., & Bedworth, R.E.: J.Inst.Metals, 1923, 29, 529.
- Pollard, F.H., & Fowles, G.W.A.: J.Chem.Soc., 1952, 2444-5.

- Pollard, F.H., & Woodward, P.: J.Chem.Soc., 1948, p.1709; *ibid*; Trans. Farad.Soc., 1950, 46, 190.
- Popper, P., & Ruddlesden, S.N.: Nature, Lond., 1957, 179, 1129.
- Popova, C.I., & Kabbanik, G.T.: Zhur.Neorg.Khim., 1960, 5, 930-34.
- Portnoi, K.I., & Levinskii, Yu.V.: Issled.Splavov.Tsvetn.Metal., Akad. Nauk SSSR, Inst.Met., 1963, No.4, 279.
- Powell, C.F., Oxley, J.H., & Blocker, J.M.: "Vapour Deposition", 1966 (New York: Wiley).
- Prosvirin, B.I.: Vest.Metalloprom., 1937, 17(12), 102.
- Rairden, J.R.: Electrochem.Technol., 1968, 6(7-8), 269-72.
- Rice, R.W.,: Proc. 3rd Int.Mater.Symp., 1966, p.579.
- Richardson, L.S., & Grant, N.J.: Trans.Metall.Soc., A.I.M.E., 1954, 200, 69.
- Riviere, J.C.: "Surface Phenomena of Metals", Soc.Chem.Ind., Monography, No. 28, 1968 (London: The Society).
- Robins, D.A.: Powder Metall., 1958, No.1-2, 172.
- Rode, T.V.: "Thermal Analysis", 1965, 1st Internat.Conf., p.122 (London: MacMillan).
- Rostoker, W., & Yamamoto, A.: Trans.Am.Soc.Metals, 1953, Prepr. No. 29.
- Ruddlesden, S.N.: "Special Ceramics", Proc.Symp.Br.Ceram.Res.Assocn., 1962, p.341 (London: Academic Press).
- Rundle, R.E.: Acta. Cryst., 1948, 1, 180.
- Rundle, R.E., Baenziger, N.C., Wilson, A.S., & McDonald, R.A.: J.Am.Chem. Soc., 1948, 70, 99.
- Ruppert, W., & Schwedler, G.: U.S.Patent 2,865,791; 23/12/1958.
- Ruppert, W., & Schwedler, G.: German Patent 1,056,450; 30/4/1959.
- Sabroff, A.M., Boulger, F.W., & Henning, M. J.: "Forging Materials and Practices", 1968, pp.230-52, (N.Y.: Reinhold).
- Salibekov, S.E., Levinskii, Yu.V., Khvostikov, V.D., & Levinskaya, M.Kh.: Fiz Metal.Metalloved., 1948, 18(6), 856.
- Samsonov, G.V.: Dokl.Akad.Nauk. S.S.S.R., 1953a, 93, 689.
- Samsonov, G.V.: Izg.Sek.Fiz.Khim.Anal., 1956a, 27, 97.
- Samsonov, G.V.: Zh.Takh.Fiz, 1956c, 26, 716.
- Samsonov, G.V.: Soviet Phy., Tech.Phy., 1957, 1, 695.
- Samsonov, G.V.: "Refractory Transition Metal Compounds", 1964. (London: Academic Press).

- Samsonov, G.V.: "Handbook of High Temperature Materials", No. 2, Properties Index, 1964 (N.Y.: Plenum).
- Samsonov, G.V.: Ukr.Khim.Zh., 1965, 31(10), 1005 (N.L.L. Translation, RTS 4233; Dec. 1967); Summarised in Izv.Akad.Nauk S.S.S.R., 1967, 58(10), 76.
- Samsonov, G.V., & Neshpor, V.S.: Dokl.Akad.Nauk. SSSR., 1958, 122, 1021.
- Samsonov, G.V., & Neshpor, V.S.: "Powder Metallurgy and Strength of Materials", 1959, No. 7, pp. 7 & 99, (Kiev: Izdvo Akad.Nauk S.S.S.R.).
- Samsonov, G.V., & Golubeva, N.K.: J.Phys.Chem., Moscow, 1956, 30, 1258.
- Samsonov, G.V., & Petrash, E.V.: Metalloved Obrabotka Met., 1955, No. 4, 19.
- Samsonov, G.V., Verkhoglyadova, T.S., & Dubovik, T.V.: Pporosh Metal.Akad. Nauk. Ukr. SSSR., 1961a, 1, No. 4, 9.
- Samsonov, G.V., & Verkhoglyadova, T.S.: Dokl.Akad.Nauk. SSSR., 1962, 142, 608.
- Sato, S.: Sci.Pap.Inst.Phy.Chem., Tokyo, 1938, 34, 241.
- Sato, S.: Sci.Pap.Inst.Phy.Chem., Tokyo, 1938a, 34, 1001.
- Sato, S.: Sci.Pap.Inst.Phy.Chem.Res.Tokyo, 1938b, 34, 362.
- Sato, S., & Yamane, K.: Rept.Sci.Res.Inst.Jap., 31, 418; J.Sci.Res.Inst., Tokyo, 1955, 49, 325.
- Shaler, A.J., & Wulff, J.: Ind. & Engg. Chem., 1948.
- Schaffer, P.T.B.: "Handbook of Higher Temperature Materials", No. 1, Materials Index, 1964 (N.Y.: Plenum).
- Schaffer, P.T.B., & Samsonov, G.V.: "High Temperature Materials", 1964, Handbooks 1 and 2 (New York: Plenum).
- Scherrer, P.: Gottinger Nachrichten, 1918, 2, p.98.
- Schmahl, N.G., Baumann, H., & Schenck, H.: Arch.Eisenhüttenw., 1956, 27, 707.
- Schmahl, N.G., Baumann, H., & Schenck, H.: Arch. Eisenhüttenw., 1958, 29, 41.
- Schmitz-Dumont, O.: Z.Elektrochem., 1956, 60, 866.
- Schneider, A., Heymer, G., & Klotz, H.: German Patent, No. 1,160,189; 12/12/63.
- Schonberg, N.: Acta.Chem.Scand., 1954, 8, 199 and 208.
- Schonberg, N.: Acta.Chem.Scand., 1954a, 8, 204.
- Schwarzkopf, P.: Powder Met.Bull., 1950, 5, 68.
- Schwarzkopf, P., & Kieffer, R.: "Refractory Hard Metals: Borides, Carbides, Nitrides and Silicides", 1953, (New York: MacMillan).
- Seith, W., & Kubaschewski, O.: Z.Elektrochem., 1935, 41, 551.
- Schwerdtfeger, K.: Trans.Met.Soc. AIME, 1967, 239(9), 1432-8.

- Septier, A., Gauzit, M., & Baruch: Compt.Rend., 1952, 234, 105-7.
- Shulishova, O.I.: "High Temperature Cermet Materials", 1962 (Kiev: Izd.Akad.Nauk. S.S.S.R.).
- Sieverts, A., & Zupf, G.: Z.Anorg.Chem., 1936, 229, 161-174.
- Sloman, H.A., Harvey, C.A., & Kubachewski, O: J.Inst.Metals, 1951, 80, 391.
- Smithells, C.J., & Ransley, C.E.: Nature, 1934, 134, 814.
- Smithells, C.J., & Ransley, C.E.: Proc.Roy.Soc., 1935, A150, 172-97.
- Soliman, A.: J.Appl.Chem., London, 1951, 1, 98.
- Spriggs, R.M., & Atteraaas, L.: Proc. 3rd Int.Materials Symposium, Berkeley, California, 1966, p.701.
- Stadelmaier, H.H., & Tong, S.Y.: Z.Mettalk., 1961, 52, 477.
- Sterling, H.F., & Swann, R.C.G.: Solid State Electronics, 1956, 8, 653.
- Sterling, H.F., Alexander, J.H., & Joyce, R.J.: Le Vide, 1966, No. Special AVI Sem., 80.
- Sterling, H.F., & Swann, R.C.G.: Solid State Electronics, 1965, 8, 653.
- Stokes, C.S., & Knipe, W.W.: Ind.Engg.Chem., 1960, 52, 287.
- Straumanis, M.E., Faunce, A.A., & James, W.J.: Acta Met., 1967, 15(1), 65-71.
- Straumanis, M.E., Faunce, C.A., & James, W.J.: Inorg.Chem., 1966, 5, 2027.
- Stringer, J.: Acta Metall., 1960, 8, 758 and 810.
- Suchet, J.: U.S.Patent 2,952,599; 13/9/1960.
- Taylor, A., & Kagle, B.J.: "Crystallographic Data on Metal and Alloy Structures", 1963 (New York: Dover).
- Taylor, A., & Doyle, N.J.: J.Less-Common Metals, 1967, 13(4), 399-412.
- Terao, N.: Jap.J.Appl.Phy., 1967, 6(11), 21-34.
- Thompson, R., & Wood, A.A.R.: Chem.Engr., 1963, p. CE 51.
- Tsuchiya, M.: Bunski Kagaku, 1959, 8, 723.
- Tylecote, R.F.: J.Iron & Steel Inst., 1960, 196, 135.
- Tylecote, R.F., & Mitchell, T.E.: J.Iron & Steel Inst., 1960, 196 445.
- Ubbelohde, A.R.: Trans.Farad.Soc., 1932, 28, 275.
- Ubbelohde, A.R.: Proc.Roy.Soc.(A), 1937, 159, 295.
- Umanski, Ya.S.: Izv.Sek.Fiz.Khim.Anal., 1943, 16, 127.



- Umezu, S.: Proc.Imp.Acad.Tokyo, 1931, 7, 353.
- U.S. Air Force Syst.Command, Res. & Technol.Div., Tech.Rept.No. AFML-TR-65-299, 1966, 57 pp.
- van Arkel, A.E.: Metallwirt.Metallwiss.Metalltech., 1934, 13, 511.
- van Arkel A.E.: "Molecules and Crystals", 1956, p.63 (London: Butterworths).
- van Arkel, A.E., & de Boer, J.H.: Z.Anorg.Chem., 1925, 148, 345.
- Van Torne, L.I., & Thomas, G.: Acta Met., 1964, 12(5), 601-15.
- Vasyutinskii, B.M., Kogan, V.S., Kartmazov, G.N.,
- Vaughan, D.A.: J.Metals, N.Y., 1956, 8, 78.
- Vanyshiteyn, E.Y., & Vasili'yev, Y.N.: Dokl.Akad.Nauk. SSSR., 1957, 114, 53.
- Vanyshiteyn, E.Y., & Zhurakovskiy, Y.A.: Dokl.Akad.Nauk.SSSR, 1958, 122, 365; ibid, 1959, 127, 534; ibid, 1959, 128, 595; ibid, 1959, 129, 6.
- Vermilyea, D.A.: Acta Metall., 1957, 5, 492.
- Wagner, C.: Z.Phy.Chem.(13), 1933, 21, 25.
- Wallwork, G.R., & Jenkins, A.E.: J.Electrochem.Soc., 1959, 106, 10.
- Wasilewski, R.J., & Kehl, G.L.: J.Inst.Metals, 1954, 83, 94.
- Watt, G.W., & Davies, D.D.: J.Am.Chem.Soc., 1948, 70, 3753.
- Weaver, C.W.: Nature, Lond., 1957, 180, 806.
- Weiner, G.W., & Berger, A.J.: J.Metals, N.Y., 1955, 7, 360.
- White, J.: "Science of Ceramics", Proceed.Br.Ceram.Soc., 1962, 1, 305; ibid., 1965, 3, 155 (London: Academic Press).
- Whittemore, O.J., Jr.: The Trend in Engr.(Univ.Washington), 1968, 20, No. 2, p.28.
- Wicks, C.E., & Block, F.E.: "Thermodynamic Properties of 65 Elements - their Oxides, Halides, Carbides and Nitrides", 1963, Bulletin 605 of the U.S. Bureau of Mines (Washington: U.S. Department of the Interior).
- Wyatt, J.L., & Grant, N.J.: Trans.Amer.Soc.Metals, 1954, 46, 540.
- Wyatt, J.L., & Grant, N.J.: U.S. Patent 2,804, 410, 27/8/1957.
- Yakimenko, L.F.: Fiz.Metall.i.Metalloved, 1962, 13, 310-311.
- Zak, H.: Prace Inst.Hutniczych, 1962, 14, No. 4, 169-174.
- Zelikman, A.N., & Govorits, N.N.: Zh.Prikl.Khim, 1950, 23, 689; Chem.Coll. No.2, Soviet Res.Glass.Ceram.Refractories, 1949-1955, 15.
- Zworykin, V.K., Morton, G.A., Ramberg, E.G., Hillier, J., & Vance, A.W.: "Electron Optics and the Electron Microscope", 1945 (N.Y.: Wiley).

Additional References

Albrecht, C., & Mueller, J.: German Patent, 1,149,035, 22/5/1963.

Anselin, F., & Pascard, R.: French Patent, 1,335,556, 23/8/1963.

Deeley, G.G.: British Patent 970,639, 23/9/1964.

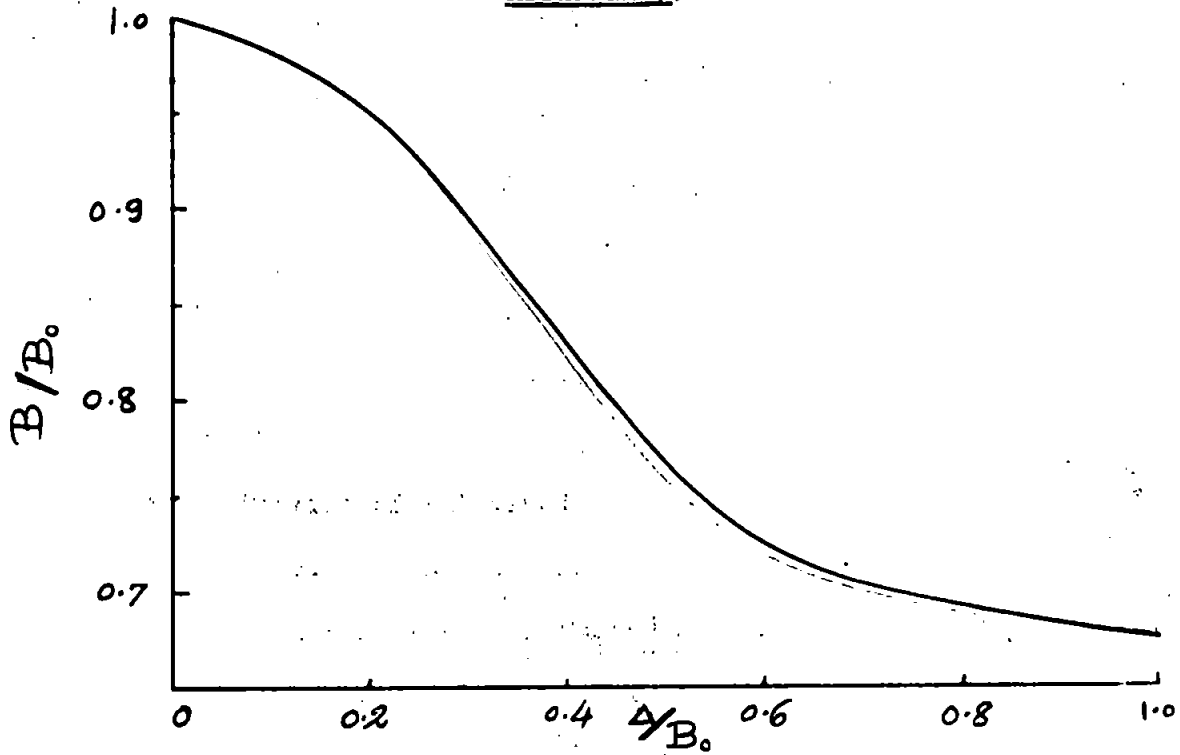
Evans, E.B.: J.Less-Common Metals, 1965, 2, 465.

Funk, H., & Boehland, H.: Z.Anorg.Allgem.Chem., 1964, 334(3-4), 155.

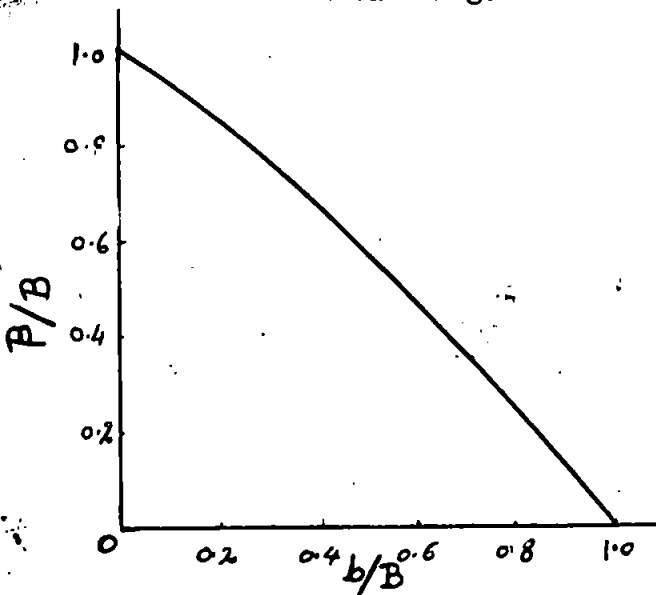
## APPENDICES

1. Curves for correcting line breadths for K - doublet and instrumental broadening in the method by Jones for determining intrinsic X-ray line (or peak) broadening.
2. Calculation of the angular separation of the  $\alpha_1$  and  $\alpha_2$  components of K radiation.
3. IBM 1130 Computer programme for B.E.T. gas sorption data.
4. Reprint of published paper  
Formation and reactivity of nitrides.  
IV Titanium and zirconium nitrides.  
J. appl. Chem., 1969, 19, 182-4

APPENDIX 1.



Curve for correcting line breadths for K -doublet broadening.



Curve for correcting line breadths for instrumental broadening

## Appendix 2

### Calculation of the angular separation of the 1 and 2 components of K radiation

Data for angular separation of the two components of various K radiations are given in the Internationale Tabellen\* accurate to two significant figures. A direct calculation using the Bragg relationship

$$\sin \theta_1 = \frac{\lambda_{\alpha_1}}{2d} \qquad \sin \theta_2 = \frac{\lambda_{\alpha_2}}{2d}$$

wherein  $d$  is the crystal spacing and  $\lambda$  is the wavelength in Angstrom units, is tedious and gives only two or three significant figures, because the two  $\theta$  angles must be subtracted to obtain angular separation.

An equation for small values of  $\theta$  was developed as follows: subtracting the above equations,

$$\frac{\lambda_{\alpha_2} - \lambda_{\alpha_1}}{2d} = \sin \theta_2 - \sin \theta_1 = 2 \sin \frac{1}{2} (\theta_2 - \theta_1) \cos \frac{1}{2} (\theta_2 + \theta_1)$$
$$2 \sin \frac{1}{2} (\theta_2 - \theta_1) = \frac{\lambda_{\alpha_2} - \lambda_{\alpha_1}}{2d \cos \theta_{av}}$$

Substituting

$$d = \frac{\lambda_{av}}{2 \sin \theta_{av}}$$
$$2 \sin \frac{1}{2} (\theta_2 - \theta_1) = \frac{\lambda_{\alpha_2} - \lambda_{\alpha_1}}{\lambda_{av}} \tan \theta_{av}$$

For very small angles, the sin is very nearly equal to the angle in radians, i.e.,

$$2 \sin \frac{1}{2} (\theta_2 - \theta_1) = \theta_2 - \theta_1$$

Thus,

$$\begin{aligned} \Delta &= \frac{360}{\pi} \frac{\lambda_{\alpha_2} - \lambda_{\alpha_1}}{\lambda_{av.}} \tan \theta_{av.} \\ &= C \tan \theta_{av.} \end{aligned}$$

Various values of C for different X-ray tube targets are given below:

K-	Radiation	C
	Cr	0.195
	Fe	0.233
	Co	0.249
	Ni	0.266
	Cu	0.285
	Mo	0.690
	Ag	0.899

Example: Cu K- $\alpha$  radiation,

Bragg angle  $\theta = 14^\circ 43'$ ;

$$\begin{aligned} \Delta &= 0.285 \tan 14^\circ 43' \\ &= 0.0746 \end{aligned}$$

\* Internationale Tabellen zur Bestimmung von Kristallstrukturen, vol. 2., 1935, Gebrüder, Borntraeger, Berlin.

APPENDIX 3

I.B.M. 1130 Computer Programme for the determination of Specific Surfaces by the B.E.T. Method using least squares method to determine the intercept and slope of the isotherm.

PAGE 1

77 JOB

COPIES OF REPORT MADE FOR THE DIRECTOR AND THE CHIEF OF BUREAU

M2 406 ACTUAL 28 0 13 10 0

77  
1937

	ACTUAL	ESTIMATE	DIFFERENCE	PERCENTAGE
1.0000	100	100	0	100
0.9900	100	100	0	100
0.9800	100	100	0	100
0.9700	100	100	0	100
0.9600	100	100	0	100
0.9500	100	100	0	100
0.9400	100	100	0	100
0.9300	100	100	0	100
0.9200	100	100	0	100
0.9100	100	100	0	100
0.9000	100	100	0	100
0.8900	100	100	0	100
0.8800	100	100	0	100
0.8700	100	100	0	100
0.8600	100	100	0	100
0.8500	100	100	0	100
0.8400	100	100	0	100
0.8300	100	100	0	100
0.8200	100	100	0	100
0.8100	100	100	0	100
0.8000	100	100	0	100
0.7900	100	100	0	100
0.7800	100	100	0	100
0.7700	100	100	0	100
0.7600	100	100	0	100
0.7500	100	100	0	100
0.7400	100	100	0	100
0.7300	100	100	0	100
0.7200	100	100	0	100
0.7100	100	100	0	100
0.7000	100	100	0	100
0.6900	100	100	0	100
0.6800	100	100	0	100
0.6700	100	100	0	100
0.6600	100	100	0	100
0.6500	100	100	0	100
0.6400	100	100	0	100
0.6300	100	100	0	100
0.6200	100	100	0	100
0.6100	100	100	0	100
0.6000	100	100	0	100
0.5900	100	100	0	100
0.5800	100	100	0	100
0.5700	100	100	0	100
0.5600	100	100	0	100
0.5500	100	100	0	100
0.5400	100	100	0	100
0.5300	100	100	0	100
0.5200	100	100	0	100
0.5100	100	100	0	100
0.5000	100	100	0	100
0.4900	100	100	0	100
0.4800	100	100	0	100
0.4700	100	100	0	100
0.4600	100	100	0	100
0.4500	100	100	0	100
0.4400	100	100	0	100
0.4300	100	100	0	100
0.4200	100	100	0	100
0.4100	100	100	0	100
0.4000	100	100	0	100
0.3900	100	100	0	100
0.3800	100	100	0	100
0.3700	100	100	0	100
0.3600	100	100	0	100
0.3500	100	100	0	100
0.3400	100	100	0	100
0.3300	100	100	0	100
0.3200	100	100	0	100
0.3100	100	100	0	100
0.3000	100	100	0	100
0.2900	100	100	0	100
0.2800	100	100	0	100
0.2700	100	100	0	100
0.2600	100	100	0	100
0.2500	100	100	0	100
0.2400	100	100	0	100
0.2300	100	100	0	100
0.2200	100	100	0	100
0.2100	100	100	0	100
0.2000	100	100	0	100
0.1900	100	100	0	100
0.1800	100	100	0	100
0.1700	100	100	0	100
0.1600	100	100	0	100
0.1500	100	100	0	100
0.1400	100	100	0	100
0.1300	100	100	0	100
0.1200	100	100	0	100
0.1100	100	100	0	100
0.1000	100	100	0	100
0.0900	100	100	0	100
0.0800	100	100	0	100
0.0700	100	100	0	100
0.0600	100	100	0	100
0.0500	100	100	0	100
0.0400	100	100	0	100
0.0300	100	100	0	100
0.0200	100	100	0	100
0.0100	100	100	0	100
0.0000	100	100	0	100

1.0000 100.00  
0.9900 100.00  
0.9800 100.00  
0.9700 100.00  
0.9600 100.00  
0.9500 100.00  
0.9400 100.00  
0.9300 100.00  
0.9200 100.00  
0.9100 100.00  
0.9000 100.00  
0.8900 100.00  
0.8800 100.00  
0.8700 100.00  
0.8600 100.00  
0.8500 100.00  
0.8400 100.00  
0.8300 100.00  
0.8200 100.00  
0.8100 100.00  
0.8000 100.00  
0.7900 100.00  
0.7800 100.00  
0.7700 100.00  
0.7600 100.00  
0.7500 100.00  
0.7400 100.00  
0.7300 100.00  
0.7200 100.00  
0.7100 100.00  
0.7000 100.00  
0.6900 100.00  
0.6800 100.00  
0.6700 100.00  
0.6600 100.00  
0.6500 100.00  
0.6400 100.00  
0.6300 100.00  
0.6200 100.00  
0.6100 100.00  
0.6000 100.00  
0.5900 100.00  
0.5800 100.00  
0.5700 100.00  
0.5600 100.00  
0.5500 100.00  
0.5400 100.00  
0.5300 100.00  
0.5200 100.00  
0.5100 100.00  
0.5000 100.00  
0.4900 100.00  
0.4800 100.00  
0.4700 100.00  
0.4600 100.00  
0.4500 100.00  
0.4400 100.00  
0.4300 100.00  
0.4200 100.00  
0.4100 100.00  
0.4000 100.00  
0.3900 100.00  
0.3800 100.00  
0.3700 100.00  
0.3600 100.00  
0.3500 100.00  
0.3400 100.00  
0.3300 100.00  
0.3200 100.00  
0.3100 100.00  
0.3000 100.00  
0.2900 100.00  
0.2800 100.00  
0.2700 100.00  
0.2600 100.00  
0.2500 100.00  
0.2400 100.00  
0.2300 100.00  
0.2200 100.00  
0.2100 100.00  
0.2000 100.00  
0.1900 100.00  
0.1800 100.00  
0.1700 100.00  
0.1600 100.00  
0.1500 100.00  
0.1400 100.00  
0.1300 100.00  
0.1200 100.00  
0.1100 100.00  
0.1000 100.00  
0.0900 100.00  
0.0800 100.00  
0.0700 100.00  
0.0600 100.00  
0.0500 100.00  
0.0400 100.00  
0.0300 100.00  
0.0200 100.00  
0.0100 100.00  
0.0000 100.00

COPIES OF REPORT MADE FOR THE DIRECTOR AND THE CHIEF OF BUREAU

COPIES OF REPORT MADE FOR THE DIRECTOR AND THE CHIEF OF BUREAU



```

1 DIMENSION X(10),Y(10)
2 FORMAT(11,4,F12.2,F12.4)
3 FORMAT(11,4,F10.2,17,8,MS,1,F12.4,10MS,10,F10.2,17MS,10)
4
5 FORMAT(F12.5,F12.2)
6 DO 10 I=1,N
7   READ(2,100) X(I),Y(I)
100 READ(2,100) X(I),Y(I)
101 IF(N)9,9,6
102 DO 10 I=1,N
103   READ(2,100) X(I),Y(I)
104   IF(N)9,9,6
105   WRITE(3,2)AT,W,DO
106   DO 10 I=1,N
107     READ(2,3)G,P
108     GR=G/W
109     Y(I)=D/(GG*(DO-D))
110     X(I)=D/DO
111     WRITE(3,4)X(I),Y(I)
112 CONTINUE
C
C X=D/DO AND Y=D/X(DO-D). SLOPE=A AND INTERCEPT=C
21 FORMAT(1/1X,10HOLAYER? CAPACITY IS',F9.6,10H NITROGEN/G.SAMPLE')
22 FORMAT(1/1X,10HSPECIFIC SURFACE IS',F10.3,10H /G.')
C
C OBTAIN TWO EQUATIONS IN A AND C
SY=C
SY=C
SXX=0
SYY=0
DO 23 K=1,N
SX=SX+X(K)
SY=SY+Y(K)
SXX=SXX+X(K)*X(K)
23 SXY=SXY+X(K)*Y(K)
SX=N
C
C SOLVE EQUATIONS
CALL SOLV(SY,AN,SY,SXY,SYY,A,C)
XM=1./(A+C)
WRITE(3,21)XV
S=XM*3650.0
WRITE(3,22)S
CALL SCFOR(1,2,2,1,0)
CALL SCFOR(3,0,0,32,8,C)
CALL SCFOR(4,YMIN,YMAX,2,0)
DO 10 I=1,N
10 CALL SCFOR(5,X(I),Y(I),235,0)

```

10  
10  
2

APPENDIX 4

Reprint of published paper covering preliminary research  
during M.Sc. Crystallography course.

# FORMATION AND REACTIVITY OF NITRIDES

## IV.\* TITANIUM AND ZIRCONIUM NITRIDES

By D. R. GLASSON and S. A. A. JAYAWEERA

The reactivities of the interstitial titanium and zirconium nitrides have been compared. Samples of these nitrides have been converted to oxides by being calcined in air. Changes in phase composition, surface area, crystallite and aggregate sizes have been correlated with oxidation time and temperature.

Crystallites of rutile,  $\text{TiO}_2$ , split off from the remaining titanium nitride before they sinter, and inhibit further oxidation. Zirconium nitride oxidation is complicated by formation of tetragonal  $\text{ZrO}_2$  at higher temperatures, particularly over  $1200^\circ$ , and monoclinic  $\text{ZrO}_2$  at lower temperatures. The nitride initially forms the so-called 'amorphous' cubic  $\text{ZrO}_2$ , notably between  $400$ – $600^\circ$ , which may be stabilised somewhat by the remaining cubic  $\text{ZrN}$ . Subsequently, there is a further fractional volume increase while formation of monoclinic  $\text{ZrO}_2$  is being completed.

### Introduction

The formation, hydrolysis and oxidation of the more ionic and covalent nitrides have been described in earlier papers.<sup>1-4</sup> This research is extended now to a further study of titanium and zirconium nitrides which are regarded generally as interstitial nitrides.<sup>1</sup> The thermodynamics of their formation and the relation between bonding and crystal structure have been discussed in Part I.<sup>1</sup> Their preparation has been described previously by the authors.<sup>4</sup> The titanium nitride was found to be stable up to  $1000^\circ$ , but the zirconium nitride showed a range of homogeneity from nearly stoichiometric  $\text{ZrN}$  (13.3 wt.-%, 50 atom-% N) at  $600^\circ$  to lower nitrogen contents at temperatures up to  $1800^\circ$ . Thus, a typical sample of nitrified zirconium contained only 10.32 wt.-%, 42.8 atom-% N.

Most interstitial nitrides are hydrolysed less readily than the ionic and covalent nitrides, but are converted to oxides on calcining in air.<sup>1</sup> Hence, although the corrosion resistance of layers of titanium or zirconium nitrides on the metal surfaces is excellent, the scaling resistance in air (or oxygen) is not very good. Preliminary investigations<sup>4</sup> have indicated that the conversion of nitride to oxide involves splitting of the newly formed oxide layers. Changes in molecular volume and type of crystal lattice are important (cf. Pilling-Bedworth rule for oxidised metals<sup>5</sup>), and also the rate of oxide sintering. These variations are examined now more closely at different temperatures and calcination times.

### Experimental

#### Procedure

Separate portions of finely divided titanium and zirconium nitrides were calcined in air for various times at each of a series of fixed temperatures. Oxidation rates were estimated from weight changes in the samples during calcination.<sup>4</sup> The cooled products were outgassed at  $200^\circ$  *in vacuo* before their specific surfaces were determined by B.E.T. procedure<sup>6</sup> from nitrogen isotherms recorded at  $-183^\circ$  on an electrical sorption balance.<sup>7,8</sup> The deduced average crystallite sizes (equivalent spherical diameters) were compared with particle size ranges determined by optical or electron microscopy.

#### Phase composition identification

Samples were examined for phase composition and crystallinity using an X-ray powder camera and a Solus-Schall X-ray diffractometer with Geiger counter and Panax rate-

meter. Certain samples were examined further by optical- and electron-microscopes (Philips EM-100).

### Results

Fig. 1 (a), (b) and (d) shows the overall variations in specific surface,  $S$ , and average crystallite size during the conversion of titanium nitride to titanium dioxide (rutile) at  $600^\circ$  in air. These are compared with oxidation rates in Fig. 1(c). Electron-micrographs of the titanium and zirconium nitride samples and their oxidation products are presented in Fig. 2.

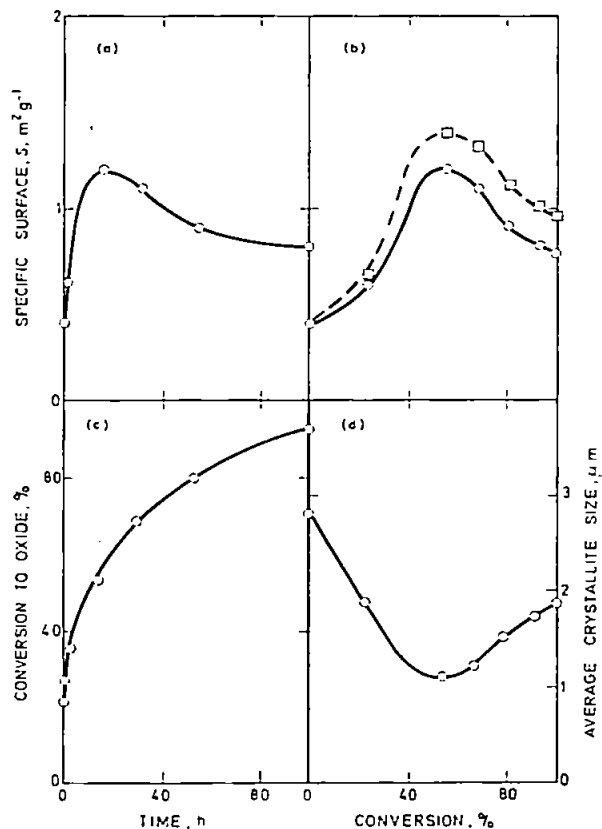


Fig. 1. Calcination of titanium nitride in air at  $600^\circ\text{C}$ . In (b), broken curve represents actual surface area ( $S'$ ), for an initial one-gramme sample of titanium nitride

\*Part III: preceding paper

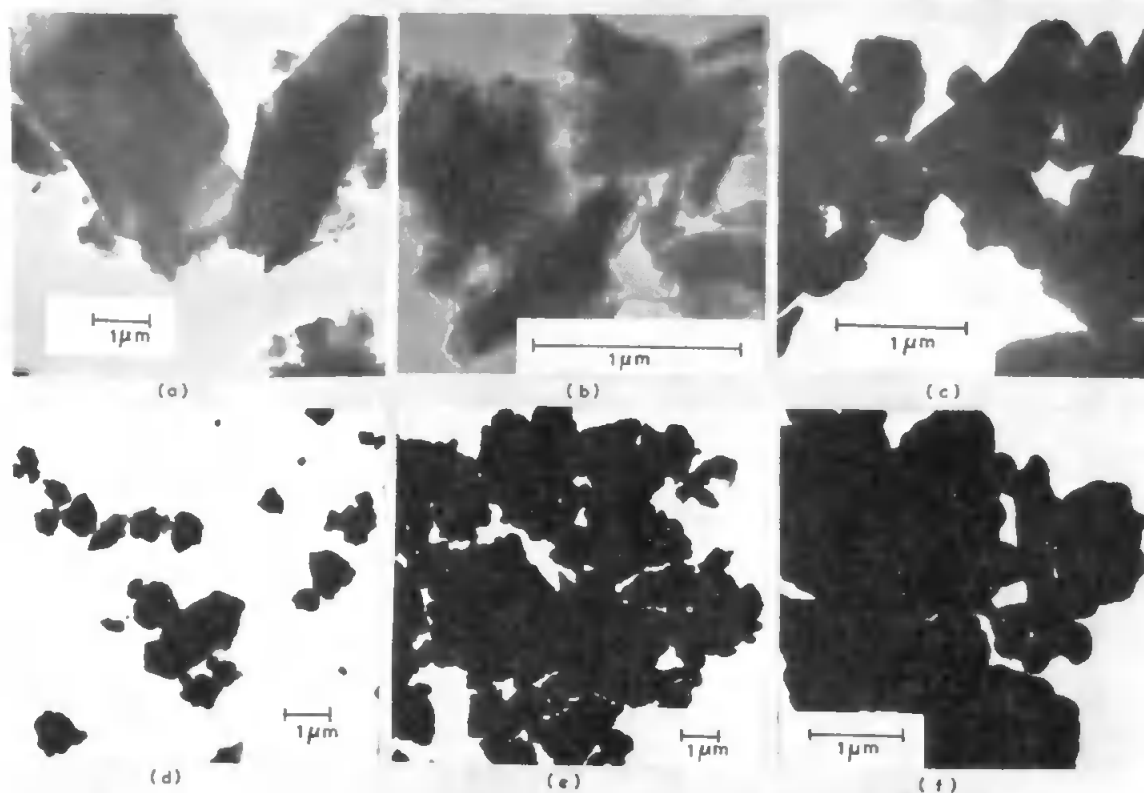


Fig. 2. Electron micrographs of titanium and zirconium nitrides calcined in air at 600°C and 1000°C respectively

Titanium nitride: (a) original sample; (b) after 15 h calcination; (c) after 200 h calcination  
 Zirconium nitride: (d) original sample; (e) after 2 h calcination; (f) after 20 h calcination

### Discussion

#### Oxidation of titanium nitride

Titanium nitride, TiN, is converted to tetragonal TiO<sub>2</sub> (rutile) at 600° in air. X-ray powder photographs and diffractometer traces give no indications of any oxynitrides being formed at temperatures between 400–1000°. In the oxidation at 600°, Fig. 1 (c), the initial weight increase is comparatively rapid, accelerating during the first half hour before becoming approximately linear and then parabolic,<sup>9</sup> as found for aluminium nitride.<sup>3</sup> The titanium dioxide X-ray patterns are given only after about a quarter of the total weight increases are recorded at 600°, but rutile patterns are detected after only 7% oxidation at 500°. The longer calcination time (5 h) at the lower temperature evidently permits crystallisation of the rutile, while at higher temperatures, TiN has a limited solubility in TiO as discussed in Part I.<sup>1</sup> The lattice constant of TiN can remain unchanged from TiN to TiN<sub>0.6</sub>O<sub>0.4</sub> when the binary compounds are sintered at 1700°, and this may retard crystallisation of rutile at higher temperatures.

The variations in rate of titanium nitride oxidation at 600° are accompanied by corresponding increases and decreases in specific surface, *S*, in Fig. 1 (a) and (b) and in actual surface area, *S'*, for an initial 1 g-sample of titanium nitride,

illustrated by the broken-lined curve in Fig. 1 (b). Consequently, the average crystallite size of the material at first decreases and later increases, Fig. 1 (d). Factors contributing to the detailed shape of the initial oxidation rate curves have been summarised in the previous paper<sup>3</sup> and apply similarly to aluminium and titanium nitrides. When there is sufficient titanium dioxide of rational crystallite size composition, it sinters to form surface films through which normal gaseous diffusion cannot easily occur. The reaction becomes controlled by solid-state diffusion, with the kinetics becoming parabolic and the surface area decreasing, as observed after about 50% conversion in Fig. 1 (a), (b) and (c).

When the titania crystallises out from the nitride matrix, during the acceleratory and approximately linear stages of the oxidation, it evidently splits off to give smaller crystallites as *S* and *S'* increase more rapidly in Fig. 1 (b). Any additional spalling at the nitride-oxide interface when the samples were cooled for surface area determination was negligible by comparison, since the reheated samples proceeded to give oxidation rates similar to those of samples which had been continuously heated. Thus, the crystallite splitting results mainly from changes in type of crystal structure (cubic F-type to tetragonal) and a volume increase (0.630 of the original volume) as the nitride is converted to the less dense oxide.

The maximum increase in the number of crystallites, calculated from  $(S'/S)^3$  and allowing for molecular volume changes,<sup>10</sup> is about twenty-fold, similar to that found for the aluminium nitride oxidation at 1000°. The splitting apparently facilitates release of nitrogen, since the material ultimately (after 200 h) reaches constant weight corresponding to the calculated weight-loss for complete conversion of nitride to TiO<sub>2</sub>.

The m.p. of TiN (2930°) and TiO<sub>2</sub> (1920°) give Tammann temperatures (half m.p. in °K) of 1600°K and 1096°K, indicating very little crystal lattice diffusion at 600°, but limited sintering promoted by surface diffusion should be possible for TiO<sub>2</sub> but not TiN at this temperature, cf. one-third m.p. = 460°C and 800°C respectively. This is confirmed by decreases in surface area and increases in average crystallite size during the later stages of the titanium nitride oxidation (Fig. 1 (a), (b) and (d)), i.e., as TiN is consumed by oxidation, its crystallite size must decrease while that of the oxide increases. Longer calcination (up to 200 h) causes very little additional sintering. In contrast, there is extensive sintering during the oxidation of titanium nitride at 1000° in air, giving a solid mass of TiO<sub>2</sub>, mainly formed within 2 h.<sup>4</sup> It is even greater than sintering of TiO<sub>2</sub>, promoted by crystal lattice diffusion at temperatures above 1000°, which has been reported recently by one of the authors for samples from other sources.<sup>11</sup> The titania from the TiN must be produced in a more compact form, possibly also giving a more suitable grain size composition for sintering. Electron micrographs also indicate fragmentation and subsequent sintering of material during the oxidation of titanium nitride, cf. Fig. 2 (a), (b) and (c).

#### Oxidation of zirconium nitride

Zirconium nitride, Fig. 2 (d), is converted to zirconium dioxide, Fig. 2 (e), which subsequently sinters at 1000° in air, Fig. 2 (f); at this temperature, any initial crystallite splitting is hidden by the more extensive oxide sintering which gives

denser and more rounded aggregates. The oxidation of this nitride is complicated by the formation of tetragonal ZrO<sub>2</sub><sup>12</sup> at higher temperatures, particularly over 1200°, and monoclinic ZrO<sub>2</sub><sup>12,13</sup> at lower temperatures.

When samples of zirconium nitride containing some free zirconium metal are calcined in air, the metal oxidises rapidly at temperatures of 350–400°. The nitride requires correspondingly higher oxidising temperatures, and initially forms the so-called 'amorphous' cubic ZrO<sub>2</sub>,<sup>14</sup> notably between 400° and 600° (cf. cubic ZrO<sub>2</sub> from Zr alkoxides decomposed in nitrogen at 300–400°,<sup>14</sup> which may be stabilised somewhat by the remaining cubic ZrN in the present work). X-ray diffractometer traces show an additional reflection at 2.94–5 Å, some reinforcement of the 2.54 Å spacing and displacement and broadening of the 1.81 and 1.54 Å spacings of monoclinic ZrO<sub>2</sub> towards the shorter distances of 1.80 and 1.53 Å of the cubic form. At higher temperatures, 700–1000°, the additional reflection disappears and the main monoclinic ZrO<sub>2</sub> reflections at 3.16 and 2.84 Å develop more rapidly. The conversion of the cubic F-ZrN ( $a = 4.56$  Å) to cubic F-ZrO<sub>2</sub> ( $a = 5.09$  Å) involves a fractional volume increase of 0.367 (of the initial volume) which further increases to 0.521 when formation of monoclinic ZrO<sub>2</sub> is completed.

#### Acknowledgments

The authors thank Mr. I. Ali and Mrs. M. A. Sheppard for their assistance in the analytical work; the University of London, Imperial Chemical Industries Ltd., and the Science Council for grants for apparatus and a S.R.C. Research Technicianship (for M.A.S.); the College Governors for a Research Assistantship (for I.A.).

John Graymore Chemistry Laboratories,  
College of Technology,  
Plymouth

cf. also S. A. A. Jayaweera,  
Ph.D. thesis, London, 1969.

#### References

- Glasson, D. R., & Jayaweera, S. A. A., *J. appl. Chem., Lond.*, 1968, 18, 65
- Glasson, D. R., & Jayaweera, S. A. A., *J. appl. Chem. Lond.*, 1968, 18, 77
- Coles, N. G., Glasson, D. R., & Jayaweera, S. A. A., *J. appl. Chem., Lond.*, 1969, 19, 178
- Glasson, D. R., & Jayaweera, S. A. A., 'Surface phenomena of metals', *Soc. chem. Ind. Monogr.*, 1968, No. 28, p. 353 (London: The Society)
- Pilling, N. B., & Bedworth, R. E., *J. Inst. Metals*, 1923, 29, 529
- Brunauer, S., Emmett, P. H., & Teller, E., *J. Am. chem. Soc.*, 1938, 60, 309
- Gregg, S. J., *J. chem. Soc.*, 1946, p. 561
- Sartorius-Werke, 'Electrono-vacuum balances', 1963 (Göttingen: Sartorius-Werke, A.-G.)
- Münster, A., *Z. elektrochem.*, 63, 807
- Glasson, D. R., *J. appl. Chem., Lond.*, 1958, 8, 798
- Glasson, D. R., Johnson, J. S., & Sheppard, M. A., *J. appl. Chem., Lond.*, 1969, 19, 46
- Lynch, C. T., Vahldiek, F. W., & Robinson, L. B., *J. Am. ceram. Soc.*, 1961, 44, 147
- McCullough, J. D., & Trueblood, K. N., *Acta crystallogr.*, 1959, 12, 507
- Mazdiyasi, K. S., & Lynch, C. T., 'Special ceramics', *Proc. symp. Br. ceram. Res. Ass.*, 1964, p. 115 (London: Academic Press)

#### ERRATUM

In the paper by Marson, *J. appl. Chem.*, 1969, 19, page 97, left hand column, line 12:

$$\text{for } 'S(\mu\text{g/ml of Cu}^+) = 6.357 \times 10^4 \log_{10} (4.03 - \text{pH})'$$

$$\text{read } 'S(\mu\text{g/ml of Cu}^+) = 6.357 \times 10^{4.03 - \text{pH}}'$$